Supramolecular biomaterials based on ureido-pyrimidinones : development of a synthetic basement membrane for a bioartificial kidney

Mollet, B.B.

Published: 29/01/2015

Document Version
Publisher's PDF, also known as Version of Record (includes final page, issue and volume numbers)

Supramolecular biomaterials based on ureido-pyrimidinones

Development of a synthetic basement membrane for a bioartificial kidney

Mollet, B.B. ©
Supramolecular biomaterials based on ureido-pyrimidinones - Development of a synthetic basement membrane for a bioartificial kidney

Cover design: Björne Mollet
Cover description: A kidney shaped fractal represents how non-covalent biomaterial building blocks can be combined in virtually infinite ways, with the potential to aid the formation of a bioartificial kidney - an artist's impression

Printed by: Gildeprint Drukkerijen, Enschede

A catalogue record is available from the Eindhoven University of Technology Library
ISBN: 978-90-386-3769-3

Supramolecular biomaterials based on ureido-pyrimidinones

Development of a synthetic basement membrane for a bioartificial kidney

PROEFSCHRIFT

ter verkrijging van de graad van doctor aan de Technische Universiteit Eindhoven, op gezag van de rector magnificus prof.dr.ir. C.J. van Duijn, voor een commissie aangewezen door het College voor Promoties, in het openbaar te verdedigen op donderdag 29 januari 2015 om 16:00 uur

door

Björne Bernadette Mollet

geboren te Oirschot

Dit proefschrift is goedgekeurd door de promotor en de samenstelling
van de promotiecommissie is als volgt:

voorzitter:	prof.dr. P.A.J. Hilbers
promotor:	prof.dr. E.W. Meijer
copromotor:	dr.dr. P.Y.W. Dankers
leden:	prof.dr. C.V.C Bouten
	prof.dr.ir. R.P Sijbesma
	prof.dr. M.C. Verhaar (Universitair Medisch Centrum Utrecht)
	dr. R. Masereeuw (Radboud Universiteit Nijmegen)
adviseur:	dr. A.W. Bosman (SupraPolix BV)

Voor Michael

Intelligentie is niet veel studeren.
Het is weten hoe je in alle omstandigheden kunt groeien.

CONTENTS

Chapter 1 ..... **1**
The kidney, renal replacement therapies and material advances towards the formation of a bioartificial kidney

Chapter 2 ..... **27**
Design and synthesis of ureido-pyrimidinone based biomaterial building blocks and model compounds

Chapter 3 ..... **45**
UPy-PCL based basement membrane mimics: electrospinning and characterization

Chapter 4 ..... **57**
The effect of UV irradiation on UPy-based biomaterials

Chapter 5 ..... **81**
UPy-biomaterial screening: towards a materiomics approach

Chapter 6 ..... **99**
Modular supramolecular bilayered scaffolds

Chapter 7 ..... **121**
Elastic microfibrous 2D and 3D hybrid hydrogel scaffolds composed of chain-extended UPy-modified PEG and gelatin

Chapter 8 ..... **149**
Renal organotypical culture environments

Summary **173**

Epilogue **177**

List of publications **185**

Curriculum Vitae **186**

Samenvatting voor leken **187**

Dankwoord **191**

Chapter 1

The kidney, renal replacement therapies and material advances towards the formation of a bioartificial kidney

Abstract: *Current renal replacement therapies as hemodialysis and hemofiltration still fail to provide a sustained solution for patients suffering from renal failure. These patients face decreased quality of life, and high morbidity and mortality rates. The therapies are incapable of complete replacement of kidney function and could potentially benefit from supplementation with the active functions of renal tubule epithelial cells. Initial attempts have been undertaken to implement such an approach in the clinic, in the form of tissue engineered living bioartificial kidneys. These consisted of conventional hemofilters treated with a cell adhesive coating which are seeded with the relevant cells. The desired clinical benefits were however not achieved as a consequence of insufficient understanding and control over the function of renal epithelial cells outside their natural environment. The importance of the biomaterial applied to support cells is now generally acknowledged in tissue engineering approaches. Instead of applying inert materials a general awareness has evolved that a biomaterial can (and should) play an active role in gaining control over cellular behavior. In this chapter an overview is given of the work that has been done in the formation of living bioartificial kidney membranes with a focus on the materials used, and discuss opportunities towards future improvements. The formation of synthetic materials that provide a high degree of control and which can mimic natural extracellular matrices, both in structure and function, is actively pursued. Materials based on supramolecular interactions have received particular interest because of their potential to embody the dynamic, responsive behavior of the natural extracellular matrix. In this thesis supramolecular biomaterials based on ureido-pyrimidinone (UPy) are explored for application as basement membrane mimics to support renal tubular epithelial cells in the formation of living bioartificial renal membranes.*

1. Renal function and failure

With common Western diseases such as cardiovascular disease, obesity, high blood pressure and diabetes being associated with renal failure, there is a rising prevalence of renal failure. Nearly half a million people in the United States alone suffer from end-stage renal disease while the incidence rate has been steadily increasing for over 25 years.[1] The future predicts poor outcomes and high medical costs. Although the kidney was the first organ to be successfully transplanted [2] and also the first organ to be mimicked by an artificial device,[3] these therapies still come short in availability or in meeting the desired improvement for renal patients, respectively. To understand the latter and gain insight into possible improvements for current therapies, we first need to understand renal function.

1.1 Kidney anatomy and function

The kidneys are responsible for blood clearance and several homeostatic functions, which they fulfill via impressive regulatory pathways. Body volume and acid-base balance is maintained as a result of the excreting function of the kidneys. Excess water and electrolytes leave the body via controlled formation of urine, together with water-soluble waste products which are actively removed from the blood by the kidneys. The kidneys furthermore exert metabolic and endocrine functions. They are responsible for the production of active vitamin D, prostaglandins, renin and erythropoietin. The kidneys are highly perfused organs; ~20-25% of cardiac output flows through the kidneys and is filtered. Each of both kidneys contains approximately one million functional units: nephrons. A nephron is composed of an initial filtering component, the renal corpuscle, followed by the renal tubule, a structure specialized in reabsorption and secretion. The renal corpuscle consists of a fenestrated capillary tuft, the glomerulus (G), which is encapsulated by Bowman's capsule (Figure 1). The ultrafiltration of plasma through the glomerular capillary wall into Bowman's capsule is the first stage of urine production. This is a passive process and involves the flow of water and solutes through a semi-permeable filter as the result of a pressure gradient. The glomerular filtration barrier consists of four elements;[4] a layer of negatively charged glycosaminoglycans, i.e. the glycocalyx (1) which covers the capillary endothelial cells (2), a basement membrane (3) and epithelial podocytes (4). The endothelial cells have fenestrations of 70 nm that circumvent passage of blood cells. The basement membrane (BM) is a thin sheet of specialized extracellular matrix (ECM), which consists of fibrous network forming proteins such as collagen IV and laminin, and negatively charged glycoproteins such as heparin sulphate proteoglycans. The BM makes an important contribution to the total filtration characteristics of the glomerular filter. It blocks the passage of large solutes (molecular weight > 1 kDa) and restricts passage of negatively charged solutes from the plasma, in particular negatively

charged intermediate sized compounds. The podocytes (4) have long foot processes that cover the BM (3) and wrap around the glomerular capillary in an interdigitating structure. Filtration slits between interdigitations are connected by the slit diaphragm with pores ranging from 4 to 14 nm in size. The ultrafiltrate, consisting of water and solutes that could pass all layers of the glomerular filter, is collected in Bowman's capsule (BC) from where it enters the renal tubule. In total, approximately 180 liters of ultrafiltrate is formed in the kidneys each day. This is severely reduced in volume and altered in composition while it travels down the renal tubular system. The renal tubule consists of several segments, which roughly can be divided in the proximal tubule (PT), loop of Henle (LH), distal tubule (DT) and collecting duct (CD) (Figure 1). These tubule segments, further sub-divided in components, are each formed by a different type of specialized epithelial cells that perform very specific functions in reabsorption and secretion. Over fifteen different epithelial cell types have been identified to form the renal tubular structure. The tubule is closely surrounded by a microvascular network so that water and solutes can be actively interchanged between blood and pre-urine by the epithelial cells. The active reabsorption and secretion processes are mediated by transporters located specifically at the apical (lumen side) or basolateral (side facing the underlying BM or neighboring cells) part of the renal tubule epithelial cell's membrane. Transport can take place along a chemical gradient or against a chemical gradient. Via an intricate organization of a diversity of transporter functions in the different segments of the renal tubule, a remarkable control over final urine composition and hence body homeostasis is achieved. Useful compounds such as glucose and amino acids are reabsorbed, as well as approximately 99% of the filtered water. Water-soluble substances that are harmful to the body are actively secreted to the urine. This function of the renal tubule is in particular important for compounds that are not removed from the blood by glomerular filtration, such as protein bound uremic toxins.

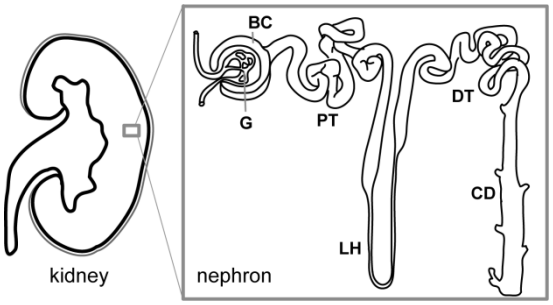

Figure 1. The nephron. A schematic representation of a kidney and a nephron, representing the main structurally and functionally distinctive components: glomerulus (G), Bowmans' capsule (BC), proximal tubule (PT), Loop of Henle (LH), distal tubule (DT) and collecting duct (CD). Figure adapted from Dankers *et al.*[5]

1.2 Renal failure

When renal function is greatly diminished, metabolic waste products and uremic toxins will accumulate in the blood. Depending on the severity and duration of the renal dysfunction, this accumulation is accompanied by metabolic disturbances such as acidification of the blood, elevated potassium levels, imbalance of body fluids and effects on many other organ systems. In acute kidney injury (AKI) the renal function is rapidly lost. The cause can be found in the blood supply (pre-renal), in the kidney itself (intrinsic) or in the urinary tract (post-renal). AKI can be reversed when treatment is successful. However, available treatments are often inadequate leading to a high AKI related mortality rate (pooled data of 11 studies revealed an AKI-associated all-cause mortality rate of 23 %).[6] The high mortality is caused by multiorgan dysfunction as a result of systemic inflammatory response.[7] This has been correlated with altered plasma cytokine levels observed in sepsis.[8] Chronic kidney disease (CKD) is a slow and progressive loss of renal function over a period of months to years. The severity of CKD is graded in five stages. CKD often remains unnoticed during the first stages of development as a consequence of the compensatory capacity of remaining functional kidney tissue and resultant lack of symptoms. There is no specific treatment which has unequivocally shown to slow the worsening of CKD. End stage renal disease (ESRD) is a severe illness which requires renal replacement therapy to prolong the life of the patient.

2. Current renal replacement therapies

2.1 Kidney transplantation

Different forms of renal replacement therapy are available. Kidney transplantation is the ideal treatment for end stage renal failure. It restores near-normal renal function and improves quality of life tremendously. However, donor shortage is still the limiting factor; many patients never make it to the top of a waiting list. Provided that there is a donor kidney available that matches the patient's blood and human leukocyte antigen type, there are still short and long term complications to overcome. Short term complications are operative failure and acute rejection of the donor kidney. Possible long term complications comprise infection or recurrence of the original disease. Another drawback of this treatment, even after successful transplantation, is the need for continuing immunosuppressive medication. The alternative, artificial renal replacement therapies comprise peritoneal dialysis, hemodialysis and hemofiltration.

2.2 Peritoneal dialysis

In peritoneal dialysis, dialysis fluid is administered into the abdominal cavity via a permanent tube through the abdomen. The dialysis fluid is a mimic of clean plasma. It consists of purified water with a balanced solute composition. The peritoneal membrane functions as the filtration membrane over which solutes diffuse along their compositional gradient between blood and dialysis fluid. This treatment provides a continuous and gradual blood clearance and does not require the patient to visit a hospital of dialysis center. This provides the patient with a somewhat better quality of life compared to patients treated with hemodialysis or hemofiltration. The net rate of clearance that can be reached is however lower than with hemodialysis and is dependent on the permeability of the peritoneal membrane. The latter complicates the effectiveness of the treatment in the long run. The dialysate inevitably evokes inflammation reactions in the peritoneal membrane. The resultant fibrosis thickens the membrane and slows down exchange via diffusion. This forces many patients to switch to an alternative treatment after a few years of peritoneal dialysis.

2.3 Hemodialysis and hemofiltration

The kidney was the first organ which function was replaced by an artificial device. In 1943 Kolff, a Dutch pioneer in the development of artificial organs, described the first successful dialysis treatment. Using cellophane as dialysis membrane, a bathtub as container for dialysis fluid and a pump driven by a Ford motor Kolff *et al.* were able to maintain urea concentrations in a 27 years old female uremic patient for 26 days.[3] The technique was commercialized in 1956.[9] Both hemodialysis and hemofiltration are still performed using an extracorporeal machine through which the patient's blood is pumped along or over synthetic, porous membranes. In hemofiltration blood clearance is based on convection over a semi-permeable membrane. Hence this treatment more or less mimics glomerular filtration. Hemodialysis is the most commonly applied therapy in most countries. During hemodialysis the blood is pumped along a semi-permeable membrane, while dialysis fluid passes the other side of the membrane in countercurrent direction. Waste products from the blood can diffuse along their concentration gradient into the dialysis fluid. Dialysis dose can be adjusted by altering the blood flow, the area of the semi-permeable membrane or the duration of the treatment. The average adult patient with minimal residual renal function requires approximately four hours of treatment three times a week either in a dedicated dialysis center or at home during the night. The intermittent nature of these treatments forms a major drawback. As clearance of the blood is discontinuous, metabolites will accumulate between treatments and homeostatic balance is disrupted. Patients often feel fatigue and face additional complications such as hypotension, hemolysis, air embolism and reactions to the dialysis membrane. Furthermore, this treatment is associated with very high expenses.

2.4 The need for improved renal replacement therapies

Although artificial renal replacement therapies prolong the life of patients, renal function is never fully replaced.[10] These techniques only rely on convection or diffusion, which at most mimicks part of the glomerular filtration function and passive tubular transport functions of the kidney. In the kidneys, the size and charge selective glomerular filtration is supplemented with active transport in the tubular system, which is not accounted for by artificial renal replacement therapies. This severely limits the blood clearance effect of these techniques. The clearance of uremic retention solutes, or uremic toxins, remains unsatisfactory. Uremic toxins represent a heterogeneous group of organic compounds. In particular the 'middle molecules', with molecular weights between 500 and 6000 Da, and protein bound uremic toxins accumulate in the blood of renal patients with insufficient residual kidney function as clearance by renal replacement therapies is absent or insufficient.[11] Although increase in permeability and pore size of artificial membranes has improved the clearance of 'middle molecules' to some extent, the limits of current techniques have almost been reached. Advanced high-flux dialysis membranes could not provide enhanced removal of protein bound toxins.[12] In addition, artificial therapies do not substitute at all for metabolic and endocrine functions normally fulfilled by the kidneys. As a result of these shortcomings, current artificial renal replacement therapies are still related with high morbidity and mortality rates.

3. Development of improved alternative renal treatments

3.1 Wearable and implantable therapies

A diversity of endeavors to improve the artificial treatments for renal patients is undertaken. An interesting approach is to downsize the dialysis device to allow a wearable or even implantable alternative.[13,14] This would enable improved continuous clearance and increase not only the patients' health but also quality of life by providing more freedom. Amongst the many challenges[15] this requires downscaling to either eliminate the need of dialysis fluid or enable regeneration of the dialysate to limit the volume needed. Research focusses mainly on membrane technology and sorbent development,[16] but also other technologies are explored. A recent example is the removal of urea from the dialysate by electro-oxidation.[17] Despite all efforts, artificial kidney devices are deemed to never perform as well as their biological counterparts. The wide and unaccountable range of compounds that are cleared from the blood and the highly adaptive capacity of the kidneys to maintain homeostasis, combined with the kidneys endocrine and metabolic function make it impossible to capture the kidneys functions in a non-living device. Alternative approaches based on living renal tissue on the other hand provide possibilities

to further aid the health of renal patients. For this reason, a diversity of regenerative medicine and tissue engineering approaches have been explored.

3.2 Alternative renal therapies based regenerative medicine and tissue engineering

Regenerative medicine and tissue engineering

Regenerative medicine is a broad field that focusses on replacement or regeneration of human cells, tissue or organs, to restore or establish normal function.[18] Ideally the body's own regenerative capacity is stimulated to achieve this. Tissue engineering, a subfield of regenerative medicine was defined in 1993 by Langer and Vacanti as an interdisciplinary field of research that applies both the principles of engineering and the processes and phenomenon of the life science towards the development of biological substitutes that restore, maintain or improve tissue function.[19] Engineering of a specific tissue, e.g. skin, bone, blood vessels, cartilage, etc, involves specific cell types, biomaterial needs and stimulating factors. Most cell types apart from blood cells are adherent and display anchorage dependent behaviour. In natural tissues, these cells reside in close interaction with an ECM. In tissue engineering structural support for cell attachment and subsequent tissue formation is provided by biomaterial scaffolds. Typically polymeric materials are used either from natural or synthetic origin. Stimulating factors such as growth factors, but for example also mechanical stimuli, are additionally applied to stimulate certain cellular behaviour and gain control over tissue formation. Hence, generally a combination of the three components is employed in tissue engineering; cells, a biomaterial scaffolds and stimulating factors, referred to as the tissue engineering triad (Figure 2).

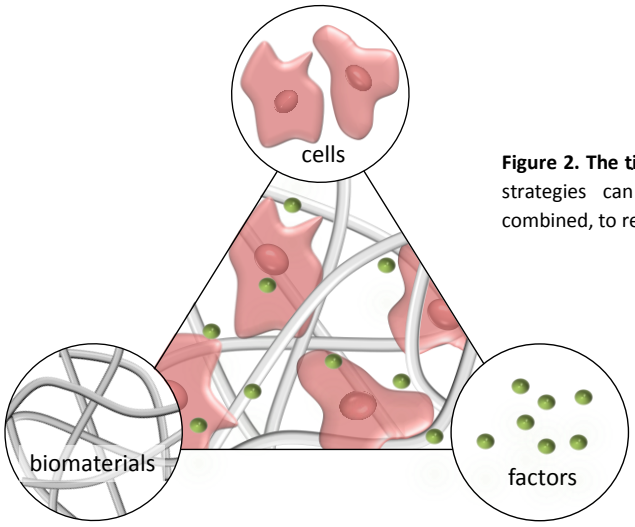

Figure 2. The tissue engineering triad. Three possible strategies can be employed, either separate or combined, to regenerate or engineer tissues

During the past 20 years, mayor advances have been made in the fields of each separate component of the triad. Stimulated and guided differentiation of stem cells towards a diversity of specified cell lineages has been established, as well as the induction of pluripotent stem cells from differentiated cell sources. In biomaterials a wide variety of new synthetic materials has been developed, but also naturally derived materials are engineered towards specific needs. New stimulating factors have been identified and working mechanisms were unravelled. A deepened understanding of the complex interplay of the triads components has strengthened the overall field of tissue engineering. Nevertheless, the number of FDA approved, commercially available tissue engineered therapies that are applied in the clinic is still scarce. This limited number reflects the complexity of the field and difficulty to achieve the degree of control needed to gain approval for clinical application.

Renal regeneration and tissue engineering

Natural regeneration of adult renal tissue is limited. Maintenance of renal tissue comprises slow turnover of cells and the natural adaptive capacity of the kidneys is a result of hypertrophy of the remaining functional tissue. Although in response to injury the number of proliferating cells in the kidney have been observed to rapidly increase, no new nephrons are formed post-embryogenesis. The origin of proliferating renal cells responsible for repair in adult human kidneys is still under debate. Different mechanisms have been hypothesized and investigated. Small populations of stem cells might reside in adult kidney tissue. These remain in a dormant state in healthy kidneys, but are activated upon injury. Researchers have identified such cell populations in adult kidneys of small mammals[20-22] and the existence of multipotent progenitor cells in human adult glomeruli was demonstrated.[23] An alternative mechanism involves dedifferentiation of tubular epithelial cells towards a more stem-cell like lineage.[24] Either way, intrarenal cells are considered responsible for tubular regeneration, rather than bone-marrow derived stem cells.[25-27] Nonetheless, indications of the involvement of bone marrow derived cells provided rationale for cellular therapy of acute renal failure.[28] Hence, employment of stem cell therapy to benefit renal tissue regeneration is explored. For example, injected bone marrow derived cells in rats were shown to participate in glomerular endothelial and mesangial cell turnover and contribute to microvascular repair.[29] More recently, administration of human MSC conditioned medium resulted in long-lasting therapeutic function by decreased progression of CKD in a rat model and reduced hypertension and glomerular injury.[30] This indicated that beneficial effects of mesenchymal stem cells (MSC) were mediated by soluble factors and cytokines secreted by these cells. Renal regenerative medicine is thought to be in particular helpful to intervene and cure early stages of CKD.

When the kidneys natural or induced regenerative capacity is not sufficient to prevent deterioration of kidney tissue and function, tissue engineering might provide solutions. In the ultimate, perhaps even utopic case, tissue engineering would enable the formation of

whole kidneys or completely functional kidney tissue to circumvent the problem of donor shortage. Adult kidneys are arguably too large and anatomically complex for direct construction via *in-vitro* tissue engineering. However, engineering immature kidneys, transplanting them and allowing them to mature within the host has been hypothesized as feasible approach.[31] Recent advances have been made by directing human embryonic stem cell differentiation towards a renal lineage, which generates self-organizing structures *in vitro*, including nephron formation.[32] These results seem very promising towards establishment of renal regeneration or engineering, but the use of embryonic stem cells in clinical applications is restricted by ethical and safety issues. Hence, this recent development is still far from providing solutions beneficial to patients. In the meantime, controlled tissue engineering of simplified bioartificial renal structures might provide opportunities to both improve current artificial renal replacement therapies and to gain insight into the pathogenesis of specific kidney tissues.

3.3 The potential use of tissue engineered tubular membranes

More than a quarter century ago, Aebischer *et al.* suggested that renal patients could potentially benefit from the incorporation of renal tubular epithelial cells in hemodialysis and hemofiltration treatments.[33,34] These cells could supplement the passive blood clearance processes with active transport and in addition provide metabolic and endocrine functions. Tissue engineered living bioartificial kidney tubular membranes furthermore hold potential to facilitate *in-vitro* nephrotoxicity tests.[35,36] In their role of eliminating many toxic xenobiotics and/or their metabolites from the body, the kidneys are often exposed to higher levels of toxic substances than most organs. This makes the kidneys frequently a primary target of toxic injury by xenobiotics.[37] Such injuries involve disruption of normal cell-cell interactions, alterations in membrane permeability and/or epithelial polarity in various regions of the kidney. However, the ability for early detection and monitoring of kidney damage in humans is inadequate. Thorough screening of nephrotoxic effects, of for example new drugs, is of high importance. Results from animal toxicology studies are specific for the tested species and are not necessarily relevant for humans.[38] *In-vitro* studies using human cells or tissues might offer results that are more predictive for humans and in addition animal friendly and more cost effective. For this approach it is important to realize that, unlike the *in-vivo* situation in animal organisms, cells *in vitro* are not able to perform all the stages of development, differentiation and ageing. As described by Pfaller and Gstraunthaler, *in vitro* highly differentiated renal cells with markedly extended life spans and near *in-vivo* characteristics may facilitate the use of renal cell culture for routine screening of nephrotoxins.[35,36] In this thesis we will focus on the use or engineered renal tubular tissues for the aim of improvement of renal replacement therapies, although the work could be translated for the aim of nephrotoxin screening.

3.4 Proximal renal tubule cells

Proximal tubule epithelial cells (PTC) have been considered as the prime cell type of interest for both the incorporation in clinical blood purifying applications and nephrotoxicity tests.[36,39] These cells, located in the first segment of the tubular system, perform a wide variety of functions, including transport, metabolic and endocrine functions and probably immunomodulatory functions as well.[38] With respect to transport functions, PTC are for example responsible for glucose and amino acid resorption. For incorporation in clinical blood purifying applications, their active function in secreting protein bound uremic toxins from the blood to the urine is of particular interest. As discussed before, retention of protein bound uremic toxins forms a major complication for renal patients.[40] PTC furthermore handle a wide range of drugs and are as a consequence of their secreting functions a frequent target for nephrotoxin induced damage. This raises the interest for their use in nephrotoxicity tests for new drugs. To fulfill their active transport functions, these cells have a specific differentiated phenotype. The high density of microvilli on their apical cell surface provides the cells with a large active cell membrane, while the many mitochondria in the cells cytoplasm provide the energy needed for the active transport of compounds over the membrane. The transport functions are facilitated by a rich representation of transporters, all with specific functions and located specifically at either basolateral or apicical cell membrane. For example, basolateral uptake of most organic anions is mediated by organic anion transporter 1 and 3 (OAT1 and 3), while multidrug resistance proteins 2 and 4 (MRP2 and MRP4) at the apical cell membrane are responsible for their urinary efflux. Most organic cations on the other hand are taken up by PTC basolaterally via organic cation transporter 2 (OCT2), whereas multidrug and toxin extrusion proteins 1 and 2 (MATE1 and MATE2) or P-glycoprotein (P-gp, also termed MDR1 or ABCB1) handle their urinary efflux.[41] For successful implementation in an *in-vitro* clinical application these cells are required to retain viability, a highly differentiated phenotype and characteristic functionality outside of their natural environment.

3.5 Humes' Bioartificial kidney and cell-based renal assist device

Endeavors by Humes *et al.* to apply renal epithelial cells for improved hemodialysis or hemofiltration treatments comprise renal epithelial cells in a renal assist device (RAD). This RAD was placed in series behind a conventional hemofilter to form an extracorporeal bioartificial kidney (BAK), mimicking both tubular and glomerular function, respectively (Figure 3). For the formation of this RAD cells were cultured on the inside of hollow fibers of commercial hemodialysis filters. To improve cell adhesion the inside of the filters hollow fibers was coated with a biomatrix consisting of pronectin-L. This is a synthetic protein with multiple cell attachment sites found in laminin. In initial tests, primary porcine PTC were seeded and shown to successfully form a near-confluent layer at the inside of the coated fibers. The cells displayed differentiated transport, metabolic and

endocrine functions.[42] In later animal studies, RAD containing human PTC (HPTC) were applied in the treatment of uremic dogs. The RAD maintained excellent performance and durability characteristics for 24 hours of continuous use in the uremic animals. Although active transport was virtually absent, metabolic and endocrine functions were observed in increased ammonia excretion, glutathione metabolism, and active vitamin D production.[43] These results led to the implementation of the RAD in clinical trials. RAD with approximately 10^9 HPTC were applied to treat patients with acute renal and multiorgan failure. The experimental treatment was delivered safely up to 24 hours and demonstrated metabolic activity with systemic effects in patients. Reduced cytokine levels, as previously observed in porcine animal models with induced septic shock,[44] was speculated to improve patients' prognosis.[45] However, a clinical phase II trial was discontinued since interim analysis of the results did not yield the desired significant positive effect of the RAD compared to the control group in the improvement of 28-day survival rate of acute kidney injury patients with multiorgan failure.[45,46]

After this result the research group of Humes pursued a potentially interesting lead focusing on the unforeseen positive effect of the control, a bare membrane without cells, on amelioration of cytokines. Nevertheless, continuation in the pursue to apply renal epithelial cells for improvement of current therapies was carried out by others.

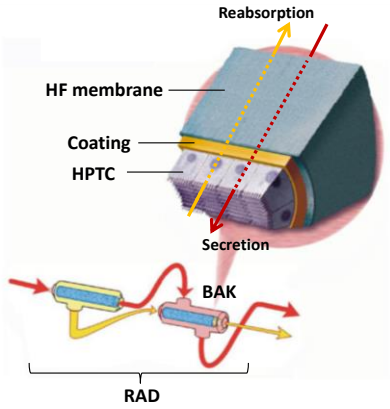

Figure 3: Humes' bioartificial kidney (BAK). A schematic representation of the extracorporeal circuit of a BAK. The first cartridge, a hemofilter, is placed in series with a renal tubular cell-assist device (RAD). The ultrafiltrate of the hemofilter is delivered to the luminal compartment of the RAD, which contains the cells. The post-filtered blood is pumped into the extracapillary space of the RAD. The processed luminal ultrafiltrate from the RAD is discarded to waste and the processed blood is returned to the patient. This figure was adapted from Humes *et al. 2014.*[47]

3.6 Approaches to improve renal epithelial cell performance in vitro

Tubular epithelial cells in vitro, both primary cells and cell lines, have been indicated to be susceptible to lose their characteristics. The confluent monolayer morphology, is either not achieved or overgrown by loss of natural contact inhibition. Furthermore, specific transport functions are lost when cultured *in vitro*.[48-50] This is likely the cause of limited clinical results achieved by the implementation of HPTC in treatments with the BAK. Ventures to improve renal epithelial cell performance in bioartificial renal tubule devices have been performed, varying from soluble factors in the media to the search for better hollow fiber membrane materials and cell adhesive coatings (Table 1).

Table 1: Overview of applied hollow fiber material and coatings for bioartificial kidneys

Membrane material	Coating or treatment	Cells (location)	Main result	Ref.
PSF/PVP	ECM (Col IV, laminin based Pronectin-L)	LLC-PK1, MDCK, HPTC (ID)	In vitro: Animal study: Clinical trial: Promising functional results, but no proof of differentiated epithelia.	[42] [43, 51-54] [45, 46] Described in [55] Ni 2011
PC	Nothing, fibronectin, laminin	MDCK	Prolonged culture after confluence: morphology changes, decreased active Na^+ transport.	[48] Saito 2002
PSF	Pronectin-F	LLC-PK_1 (ID)	Cell reduced UN and Cr leakage over membrane. Cell overgrowth obstructs hollow fiber.	[49] Saito 2004
PI, PSF, EVAL		HK-2 (ID)	Confluent on PI and EVAL, not on PSF.	[56] Siato 2006
EVAL	Attachin	RPTEC (ID)	Confluent cell layer.	[57] Saito 2011
		LE-RPTEC	In vitro: Characteristic genes of RPTEC recovered on porous membranes. Transport + metabolic functions	[58]Sanechika 2011
		LE-RPTEC	Animal study: less damage from endotoxin shock, increased life span in AKI goat.	[59] Saito 2012
PSF or CA	Col I, Col IV, Pronectin-F	LLC-PK_1 (ID)	Cell proliferation (day7): CA < CA+coat ≤ PSF < PSF+coat Expressions of sGLT-1 and GLUT-1 mRNA maintained for 3 weeks in confluent cultures, independent of membrane of coating.	[60] Sato 2005
PSF, PSM (flat assymetric membrane)	Nothing, fibronectin	RPTEC, MDCK, LLC-PK_1	In PSM, MPC rich hemocompatible sponge layer and MPC poor, cytocompatible skin layer.MDCK and LLC-PK1 cells adhere and proliferate on skin layers of PSF and PSM. RPTEC require coating.	[61] Ueda 2006
PSF, PSF/PVP, PES/PVP, RC,		HPTC (ID)	No coating: improper cell adhesion on all membranes.	[55] Ni 2011
PES/PVP and PET Transwell®	Col I, Col IV, Col IV+ laminin	HPTC (ID)	Non-HPTC-compatiblePES/PVP membranes could not be significantly improved by ECM coatings: membrane material has superior impact on performance, not coating.	[55]
PES/PVP	Oxygen plasma, H_2O_2, DOPA, poly-L-lysine, PA-18	HK-2 (ID)	After 1h DOPA coating induced highest cell adhesion.	[55]
PES/PVP	Nothing, DOPA, DOPA+Col IV	HPTC (ID)	Cell performance: no coating<<DOPA<DOPA+Col IV	[55]
PES, PES/PVP, PSF, PSF/PVP	-	HPTC (ID)	Cell growth, survival and differentiation improved in absence of PVP.	[55]
PSF-FC	Nothing, Col IV, DOPA+Col IV	HPTC (ID)	HPTC form differentiated epithelium on membrane with porous sponge-like microstructure. Coating does not improve HPTC performance.	[54]
PAES, PSF** (smooth skin ID, rough sponge OD)	Nothing or DOPA + Col IV	HPTC (OD)	No coating is needed when cells are seeded on the rough sponge OD of commercial hollow fibers. Expression levels marker genes are largely similar in PEAS without and with coating.	[62] Oo 2013
PES/PVP	Fibrin hydrogel	HPTEC*	Formation of a tight confluent monolayer with active glucose transport.	[63] Teo 2012)

Polysulfone (PSF), polyvinylpyrrolidone (PVP), polycarbonate (PC), ethylene vinyl alcohol copolymer (EVAL), PSM = PSF + 1wt% phospholipid copolymer (PMBU) prepared from 20/80 mol% 2-methacryloyloxyethyl phosphorylcholine polymer (MPC) and 2-methacryloyloxyethyl butylurethane (MEBU), cellulose acetate (CA), Fullcure™ 720 (FC), polyimide (PI), polyarylethersulfone (PAES), extracellular matrix (ECM), collagen I (Col I), collagen IV (Col IV), hydrogen peroxide (H_2O_2), 3,4-dihydroxyl-L-phenylalanine (DOPA), poly(maleic anhydridealt-1-actadecene (PA-18), inner diameter (ID), outer diameter (OD), Lewis-lung cancer porcine kidney 1 cells (LLC-PK1, a proximal tubule cell line), Madin-Darby canine kidney cells (MDCK, a distal tubule cell line[64]), Human derived renal proximal tubule epithelial cells (RPTEC), lifespan extended RPTC (LE-RPTC) Human kidney-2 cells (HK-2, proximal tubule cell line), human primary renal proximal tubule epithelial cells (HPTC), urea nitrogen (UN), Creatinine (Cr), acute kidney injury (AKI), sodium-glucose cotransporter-1 (SGLT1), glucose transporter-1 (GLUT1), * RPTEC (Lonza), ** commercial, Fresenius Polysulfone®

In the group of Saito, overgrowth of LLC-PK1 (Lewis-lung cancer porcine kidney) cells in a bioartificial renal tubule device was prevented by the use of a MEK inhibitor, U0126, in the culture media.[65] The inhibitory effect was shown to be temporary and reversible; after removal of U0126 from the media reproliferation occurred within one week. They furthermore applied ethylene vinyl alcohol copolymer (EVAL) hollow-fiber modules, coated with attachin. This material induced cell adhesion and achieved a confluent monolayer of extended lifespan HPTC at the inner wall of the hollow fibers. This led to the formation of a bioartificial renal tubule device (BTD).[58] In goats with induced AKI this BTD showed to establish an increased life span and reduced damage from endotoxin shock.[59]

The group of Zink focused on optimization of the hollow fiber membranes and cell adhesive coatings.[66] Hollow fiber membranes applied in hemofiltration and hemodialysis treatments are commonly made of hydrophobic thermoplastic polymers like polysulfone (PSF) or polyethersulfone, (PES). To circumvent adverse adsorption of serum proteins and increase hemocompatibility, these hydrophobic polymers are mixed with a hydrophilic component, often polyvinylpyrrolidone (PVP). In particular commercial PSF/PVP hollow fiber membranes, coated with an ECM protein, have been applied to form the bioartificial kidneys employed in *in-vitro* studies,[42] animal studies[43,51-54] and clinical trials.[45,46] Although these tests provided initial promising functional results, no data had been published to show differentiated epithelial on the ECM-coated PSF/PVP. Therefore, Ni *et al.*[55] tested the suitability of a variety of membrane compositions comprising PSF/PVP, PSF, PES/PVP and regenerated cellulose. Primary HPTC poorly adhered to all these membrane materials and were unable to form a confluent monolayer over a timespan of three weeks. This seems logical since hemodialysis membranes were optimized for hemocompatibility, but not for the growth of complex primary cells. The non-HPTC-compatible membranes could not be significantly improved by applying an appropriate ECM coating, although this was the approach applied to induce cell adhesion in previous pre-clinical and clinical studies. The influence of other coatings including poly(maleic anhydride-alt-1-octadecene) (PA-18), poly-L-lysine (PLL) or 3,4-dihidroxy-L-phenylalanine (DOPA), and surface treatments with hydrogen peroxide or oxygen plasma were tested for PES/PVP membranes. Cells performed best on DOPA coated membranes and double coating with DOPA followed by collagen IV resulted in the formation of a confluent differentiated layer of HPTC. An alternative membrane was formed consisting of polysulfone and Fullcure™ 720 (FC, PolyJET acrylic-based monomer). The hollow fiber membrane had an internal sponge-like

porous structure and dense outer skin layer. No surface treatments or coatings were needed to achieve good HPTC attachment inside the hollow fiber and proper HPTC performance was sustained.[55] The positive effect of a porous sponge-like membrane structure, rather than the smooth skin-like structure, as seen at the hemocompatible inside of the commercial hollow fibers, was recently verified.[62]

3.7 Restrictions of the currently applied synthetic and natural biomaterials

The surface of the membrane material applied should not only be intended to support cell adhesion, but also to gain control over cell differentiation and performance. Advances have been made towards the improvement of renal epithelial cell behavior and performance via membrane polymer composition, coating and morphology. Nonetheless, all these approaches have focused on covalent polymers, bioactivated via simple adsorption of natural polymers. These approaches provide limited control over the exact surface that will be represented to the renal epithelial cells. Furthermore, there is a lack of knowledge on the exact mechanisms of interaction between cells and biomaterials. Therefore, the identification of optimal biomaterial candidates is still merely based on trial and error. Hence a screening type of approach is needed. Both the freedom and ease of accessibility that covalent polymers and natural biopolymers provide, limits opportunities for diversification. Lastly, the morphology of surfaces has been shown to severely influence cellular behavior.[62,67] A three-dimensional nanofibrillar organization resembling the natural ECM or BM could be key. For example a synthetic nanofibrillar polyamide matrix has been indicated to provide cues for stem cell proliferation and self-renewal.[68] Furthermore, normal rat kidney cells displayed the morphology and characteristics of their counterparts *in vivo* when grown on nanofibers in presence of serum.[69] The membranes applied in bioartificial kidneys so far, all have a porous structure, but were limited to morphologies at hand with commercial hemofilters. These do not display a nanofibrous structure. Any structure resulting from the adsorbed coating of ECM proteins has not been described or studied. Hence it is for example unclear whether adsorption to the synthetic polymer membranes enables natural proteins to form of maintain their higher order structure.

3.8 Further improvements from a synthetic biomaterial point of view

We envision that optimal cell function will be retained by a bioartificial *in-vitro* environment that is ideally indistinguishable from the cells' natural environment, as perceived by the cell. Hence, to form a functional living bioartificial kidney tubular membrane, there is need for better *in-vitro* mimicry of the natural environment of renal epithelial cells. The natural substrate of renal epithelial cells is formed by the BM, the thin sheet of specialized ECM that primarily consists of laminin, collagen IV, entactin/nidogen, and sulfated proteoglycans.[70] These components form a fibrous network that structurally

supports the cells and closely interacts with the cells. The influence of the BM on renal cellular behavior is witnessed during embryogenesis. ECM proteins are known to determine cell polarization in kidney development.[71] Laminin was suggested to be involved in the increased cell adhesiveness during the early aggregation of the nephrogenic mesenchyme,[72] whereas the laminin α-chain was indicated fundamental for initiation of cell polarity.[73] The exact composition of renal BM still remains elusive, but is known to display great heterogeneity along the different components of the glomerulus and tubular segments. This molecular heterogeneity in the BM is thought to contribute to the spatial functional specificity within the nephron.[70]

The use of natural (human) ECM proteins is restricted as a consequence of poor availability, processability and limited control over their composition and stability. Extracellular structures as ECM and BM induce cellular morphogenesis via specific interaction with transmembrane receptors at the cell membrane, such as integrins. Integrins recognize and bind to specific peptide sequences present in different ECM and BM proteins, such as GRGDS[74,75] present in laminin, collagen I and IV, and fibronectin; PHSRN derived from fibronectin[76] and DGEA present in collagen I and IV.[77] Synthetic biomaterial approaches apply such peptide sequences to induce specific bioactivity in a controlled manner. The synthetic approach should allow easy diversification to explore optimal composition and properties for a specific application. Hence, we are interested in a biomaterial system that allows a combinatorial approach including components that provide structural and mechanical stability and bioactive components to direct cellular behavior. The currently applied covalent polymers such as PSF, PES and PVP do not allow such approach.

4. Supramolecular biomaterials for bioartificial kidneys

4.1 Synthetic supramolecular biomaterials as BM mimic

Since two decades, supramolecular materials have gained a lot of interest. These materials possess many advantageous properties for tissue engineering applications. Supramolecular chemistry can be described as chemistry beyond the molecule and is based on non-covalent interactions between molecules.[78] These interactions include metal coordination, hydrophobic forces, hydrogen bonding, pi-pi interactions, electrostatic effects and van der Waals interactions. These non-covalent interactions provide supramolecular materials, which are merely based on small molecules, interesting properties. The bond energies of non-covalent interactions are lower compared to covalent interactions. Therefore, supramolecular chemistry gives rise to intrinsically dynamic materials which hold the ability to reversibly associate and dissociate, and thus to be deconstructed and reconstructed. This dynamic character enables supramolecular biomaterials to be responsive to environmental factors such as temperature and pH. Also

an interactive behavior with cells can be envisioned.[79] Furthermore chemical complementarity and structural compatibility can direct multiple weak, non-covalent interactions to participate in stronger, joint interactions leading to molecular self-assembly.[79] Self-assembly is thus based on information stored at the molecular level. This assembly process allows for the formation of structurally well-defined materials at the nanoscale as is beautifully exemplified in natural materials.[17,80] Hence, the accessibility of self-assembly in synthetic biomaterials introduces a rich variety of novel architectures and material properties, similar to natural materials.

Supramolecular polymers are polymers in which the monomeric components are joint by non-covalent interactions. These materials have demonstrated to poses similar or even improved mechanical properties compared to their macromolecular covalent counterparts. Furthermore these materials allow reversible accessibility to the beneficial behavior of the small molecular building blocks. As a result, supramolecular polymers allow for example easy processing, which enables the formation of desired morphologies. In addition, the dynamic rearrangement of the monomeric components and their self-assembling capacity allows for combinatorial approaches towards biomaterial diversification, and hence for tailoring and optimization towards specific application needs. For example the introduction of desired bioactivity can be established by functionalization of bioactive molecules, such as specific peptides, with the same supramolecular recognition unit as the supramolecular monomers. This has proven to be an effective and valuable tool to facilitate the incorporation of these bioactives in supramolecular polymer biomaterials.[81,82]

Altogether, supramolecular chemistry has opened new perspectives in biomaterial science towards mimicry of natural materials. All these properties make supramolecular materials eminently suitable to create multifunctional biomaterials for tissue engineering that more closely mimic their natural counterparts that they aim to substitute or interact with. Most examples of synthetic biomaterials that are based on self-assembling/supramolecular interactions form hydrogels or hydrogel-like materials. In general these soft, dynamic materials are considered appropriate materials for potential ECM mimics.[83-85] However, for the tissue engineering of a bioartificial renal tubular membrane, a gel-like supramolecular material might not offer the appropriate mechanical properties or structural features required. In general, the engineering of tissues that contain a BM or tough connective tissue, such as for example skin,[86] the bladder,[87] the pelvic floor,[88] or heart valves[89] would benefit from a relative tough freestanding sheet-like scaffold material with some elastic properties.

4.2 Our supramolecular biomaterial approach towards BM mimics

UPy-based supramolecular polymers

2-Ureido-4[1H]-pyrimidinones (UPy) form exceptionally stable homodimers via quadruple hydrogen bonding (Figure 4A). Dimerization constants were determined to exceed 10^6 M^{-1} (K_{dim} of $6 \cdot 10^7$ M^{-1} in chloroform, $1 \cdot 10^7$ M^{-1} in chloroform saturated with water, and $6 \cdot 10^8$ M^{-1} in toluene).[90,91] Such high dimerization constants facilitated the use of UPy-units towards the formation of linear supramolecular polymers. Hydrogen bonding units with lower dimerization constants failed to achieve sufficiently high degrees of polymerization,[92] whereas UPy-end-functionalization of a short carbon-spacer effectively led to an increase of virtual molecular weight resulting in polymer-like behaviour.[93] The ease of synthesis of the UPy-moiety furthermore stimulated its use for large scale formation of supramolecular polymers. This supramolecular polymerization strategy was successfully applied to macromolecular monomers as well (Figure 4B). This was initially demonstrated with telechelic UPy-functionalized polydimethylsiloxanes (PDMS),[93] followed by different oligomer and polymer backbone chemistries. Variations that were explored[94] included poly(ethylenebutylenes) (PEB),[95,96] polycarbonates,[97] polyethers[97-99] and polyesters.[100-103] UPy-functionalization induced impressive changes in material properties. For instance amorphous PEB, which is a highly viscous liquid, became strong and flexible when end-functionalized with UPy-moieties via a urethane linker.[94,96] The method of UPy-coupling to the polymer backbone was found to be of influence. Functionalization through the formation of a urethane (UT) or urea (U) linker was compared to direct UPy-coupling.[95,104] The UT and U linkers gave rise to directional single or double hydrogen bonding between supramolecular UPy-polymer chains, respectively. Combined with the ability of flat UPy-dimers to stack via dipole-dipole interactions, these lateral directional hydrogen bonding interactions stimulated 1D aggregation (Figure 4C). Atomic force microscopy (AFM) measurements on drop-cast films of these telechelic UPy-functional polymers revealed phase separated hard-segmented nanofibers (Figure 4D). These nanofibers were better defined and showed an increase in persistence length with increasing numbers of lateral hydrogen bonds in the linker (direct coupling (0) < UT (1) < U(2)). The combination of supramolecular polymerization and nanophase segregation gave rise to mechanically improved materials with thermoplastic elastomeric behavior.[95] Next to bifunctional UPy-polymer building blocks, which result in linear supramolecular polymers, variants with multiple UPy-units per macromolecular monomer were developed for the formation of supramolecular crosslinked polymer networks. Examples comprise telechelic trifunctional derivatives,[93,103,105,106] polymer chains grafted with UPy-units[107,108] and polymer chains with multiple UPy-units incorporated in the backbone (chain-extended macromolecular monomers).[98,102,109]

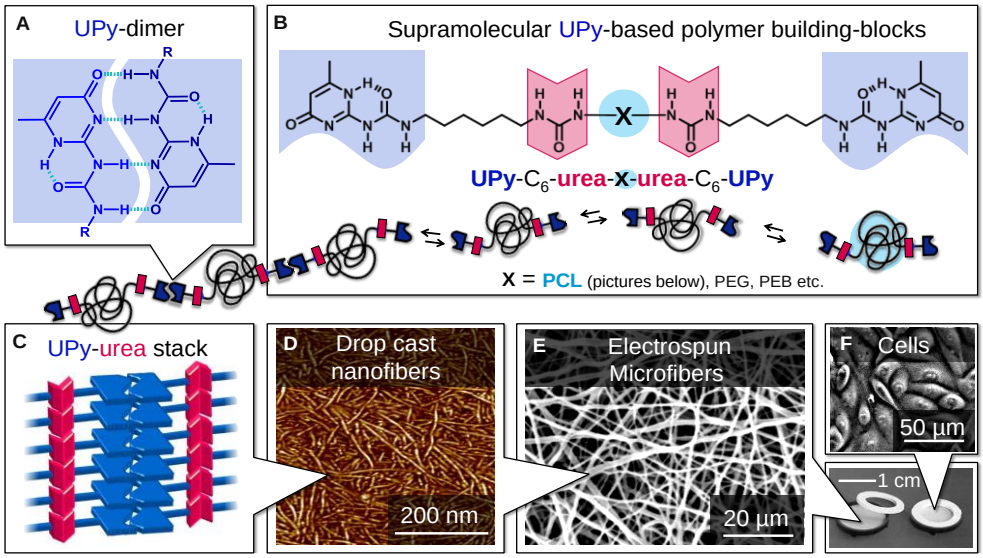

Figure 4. From UPy-dimerization mediated supramolecular polymer to biomaterial. A) A schematic representation of UPy-dimerization via four-fold hydrogen bonding. B) A telechelic UPy-modified macromolecular monomer with urea (U) linkers. UPy-telechelic monomers polymerize via UPy-dimerization to give rise to a supramolecular polymer chain. C) UPy-dimers stack, aided by hydrogen bonding between lateral urea (depicted) or urethane linkers. D) An atomic force micrograph of phase separated hard-segmented nanofibers at the surface of a drop-cast UPy-PCL (**2**, see chapter 2) film, which are constituted of aggregated self-assembled UPy-dimer stacks. E) A scanning electron micrograph of electrospun UPy-PCL. These microfibers are proposed to embody a self-assembled nanofibrous sub-structure. F) Electrospun meshes of biocompatible UPy-polymers such as UPy-PCL can be applied as biomaterial, e.g. as BM mimic for the culture of renal epithelial cells.

UPy-based supramolecular polymer biomaterials

Biocompatible prepolymers functionalized with UPy-units possess unique properties that were proposed to be highly attractive for application as biomaterials in tissue engineering. The reversible nature of the supramolecular interactions in UPy-polymer materials provides a responsive character. Self-assembly of UPy-dimer stacks furthermore gives rise to nanostructures, comparable with structures that are present in natural biomaterials. In addition, the UPy-functionalities allow unification of different UPy-building blocks and hence facilitate a modular approach towards the facile formation and exploration of new biomaterials. Telechelic UPy-functionalized PCL with a urethane linker (UPy-UT-PCL, referred to as **2(UT)** in chapter 2) was the first UPy-based supramolecular polymer that was applied as biomaterial.[110] In this work, described more than a decade ago, initial *in-vitro* cell-culture studies demonstrated good biocompatibility, fibroblast cell adhesion and interesting biodegradation behavior for **2(UT)** films.

Since the first proof of principle a diversity of UPy-based polymers, either bare or bioactivated with UPy-peptides, have been applied as biomaterial. Control over specific bioactivation is considered to be a key to successful creation of 'the next generation' of biomaterials. Therefore, also many different peptides, UPy-peptide-linker designs and

synthesis approaches of the latter have been explored.[111] UPy-biomaterial studies have focused on renal applications,[112,113] but also cardiovascular tissue engineering[114] and drug deliver applications have been explored.[98,99,115] For drug delivery applications, hydrogels based on UPy-modified high molecular weight poly(ethylene glycol) (PEG) were of interest. To function as scaffold in tissue engineering applications, primarily UPy-functionalized thermoplastic elastomers (TPE) based on PCL have been applied. Telechelic UPy-functionalized PCL has been processed by electrospinning (on which we will elaborate in chapter 3) to form microfibrous membranes (Figure 4F), on which adherent cells can be cultured.

5. Aim of this thesis

In principle, the UPy-biomaterial tool box can be expanded with virtually any UPy-functionalized building block, not solely limited to UPy-polymers and UPy-peptides. The true questions therefore are: *What biomaterial properties do we need for mimicry of natural BM? Can we achieve these properties using UPy-based biomaterials?* And hence the final question is: *What are the possibilities and current limitations, or challenges, of UPy-based biomaterials for this specific purpose?* The aim of this thesis is to investigate the potential of UPy-based biomaterials to mimic natural ECM. This research is performed specifically within the scope of the formation of an optimal BM mimic for a bioartificial kidney. In a broader sense, we explore and redefine the current status and future potential of UPy-based biomaterials in the field of tissue engineering and regenerative medicine.

6. Outline of this thesis

This journey will include both quests for answers on material-based questions, as well as inquiries from an application point of view. *Chapter 2* introduces the UPy-based molecules used for these purposes. In *chapter 3* electrospinning is applied as a method to produce microfibrous scaffolds out of UPy-based biomaterials. The hierarchical structure of these scaffolds is investigated as well as the performance of human kidney 2 (HK-2) cells on such electrospun structures. In the research described in *chapter 4* we explore the effect of UV sterilization on dynamic UPy-based materials. The ability to mix-and-match UPy-functionalized biomaterial building blocks is applied in both chapter 5 and 6. In *chapter* 5 this ability is applied to form a small biomaterial library, which is tested for cell-adhesive properties using two distinct analysis methods. Furthermore, the potential of UPy-biomaterial diversification and dynamics in relation to high-throughput screening is discussed. In *chapter 6* the UPy-building blocks are applied to form modular biomaterial scaffolds with tailorable properties. This is demonstrated by the formation of bilayered

membranes with distinct properties at each side. Chain-extended UPy-PEG, a new supramolecular hydrogelator, is studied in *chapter 7* for the formation of structurally defined BM or interstitial ECM mimicking 2D or 3D hydrogel scaffolds. In *chapter 8* the design of organotypical culture and assessment environments is described, which were designed to stimulate and test the formation of bioartificial renal tubular membranes on new biomaterial BM mimics. These environments comprise both static culture devices and flow culture bioreactors. Finally, the implications of the findings presented in this thesis are surveyed with respect to future biomaterial development and application as BM mimic in a bioartificial kidney.

7. References

(1) Unites States Renal Data System.

(2) Doyle, A. M.; Lechler, R. I.; Turka, L. A. Organ Transplantation: Halfway through the First Century. *J. Am. Soc. Nephrol.* **2004**, *15*, 2965–2971.

(3) Kolff, W. J. De Kunstmatige Nier: Een Dialysator Met Groot Oppervlak. *Ned Tijdschr Geneeskd* **1843**, *87*, 1984–1988.

(4) Boron, W. F.; Boulpaep, E. L. *Medical Physiology:a Cellular and Molecular Approach*; 2nd edition.; Saunders Elsevier, 2012.

(5) Dankers, P. Y. W.; Boomker, J. M.; Meijer, E. W.; Popa, E. R.; van Luyn, M. J. A. From Kidney Development to Drug Delivery and Tissue Engineering Strategies in Renal Regenerative Medicine. *J. Control. Release Off. J. Control. Release Soc.* **2011**, *152*, 177–185.

(6) Susantitaphong, P.; Cruz, D. N.; Cerda, J.; Abulfaraj, M.; Alqahtani, F.; Koulouridis, I.; Jaber, B. L. World Incidence of AKI: A Meta-Analysis. *Clin. J. Am. Soc. Nephrol.* **2013**, *8*, 1482–1493.

(7) Breen, D.; Bihari, D. Acute Renal Failure as a Part of Multiple Organ Failure: The Slippery Slope of Critical Illness. *Kidney Int. Suppl.* **1998**, *66*, S25–S33.

(8) M R Pinsky, J. L. V. Serum Cytokine Levels in Human Septic Shock. Relation to Multiple-System Organ Failure and Mortality. *Chest* **1993**, *103*, 565–575.

(9) Colton, C. K. Engineering a Bioartificial Kidney. *Nat. Biotechnol.* **1999**, *17*, 421–422.

(10) Perl, J.; Bargman, J. M. The Importance of Residual Kidney Function for Patients on Dialysis: A Critical Review. *Am. J. Kidney Dis.* **2009**, *53*, 1068–1081.

(11) Dhondt, A.; Vanholder, R.; Van Biesen, W.; Lameire, N. The Removal of Uremic Toxins. *Kidney Int.* **2000**, *58*, S47–S59.

(12) Krieter, D. H.; Hackl, A.; Rodriguez, A.; Chenine, L.; Moragues, H. L.; Lemke, H.-D.; Wanner, C.; Canaud, B. Protein-Bound Uraemic Toxin Removal in Haemodialysis and Post-Dilution Haemodiafiltration. *Nephrol. Dial. Transplant. Off. Publ. Eur. Dial. Transpl. Assoc. - Eur. Ren. Assoc.* **2010**, *25*, 212–218.

(13) Fissell, W. H.; Roy, S.; Davenport, A. Achieving More Frequent and Longer Dialysis for the Majority: Wearable Dialysis and Implantable Artificial Kidney Devices. *Kidney Int.* **2013**, *84*, 256–264.

(14) Ronco, C.; Davenport, A.; Gura, V. The Future of the Artificial Kidney: Moving towards Wearable and Miniaturized Devices. *Nefrol. Publ. Of. Soc. Esp. Nefrol.* **2011**, *31*, 9–16.

(15) Kim, J. C.; Garzotto, F.; Nalesso, F.; Cruz, D.; Kim, J. H.; Kang, E.; Kim, H. C.; Ronco, C. A Wearable Artificial Kidney: Technical Requirements and Potential Solutions. *Expert Rev. Med. Devices* **2011**, *8*, 567–579.

(16) Fissell, W. H.; Fleischman, A. J.; Humes, H. D.; Roy, S. Development of Continuous Implantable Renal Replacement: Past and Future. *Transl. Res.* **2007**, *150*, 327–336.

(17) Wester, M.; Simonis, F.; Lachkar, N.; Wodzig, W. K.; Meuwissen, F. J.; Kooman, J. P.; Boer, W. H.; Joles, J. A.; Gerritsen, K. G. Removal of Urea in a Wearable Dialysis Device: A Reappraisal of Electro-Oxidation. *Artif. Organs* **2014**, n/a – n/a.

(18) Mason, C.; Dunnill, P. A Brief Definition of Regenerative Medicine. *Regen. Med.* **2007**, *3*, 1–5.

(19) Langer, R.; Vacanti, J. P. Tissue Engineering. *Science* **1993**, *260*, 920–926.
(20) Oliver, J. A.; Maarouf, O.; Cheema, F. H.; Martens, T. P.; Al-Awqati, Q. The Renal Papilla Is a Niche for Adult Kidney Stem Cells. *J. Clin. Invest.* **2004**, *114*, 795–804.
(21) Gupta, S.; Verfaillie, C.; Chmielewski, D.; Kren, S.; Eidman, K.; Connaire, J.; Heremans, Y.; Lund, T.; Blackstad, M.; Jiang, Y.; Luttun, A.; Rosenberg, M. E. Isolation and Characterization of Kidney-Derived Stem Cells. *J. Am. Soc. Nephrol. JASN* **2006**, *17*, 3028–3040.
(22) Dekel, B.; Zangi, L.; Shezen, E.; Reich-Zeliger, S.; Eventov-Friedman, S.; Katchman, H.; Jacob-Hirsch, J.; Amariglio, N.; Rechavi, G.; Margalit, R.; Reisner, Y. Isolation and Characterization of Nontubular Sca-1+lin- Multipotent Stem/progenitor Cells from Adult Mouse Kidney. *J. Am. Soc. Nephrol. JASN* **2006**, *17*, 3300–3314.
(23) Sagrinati, C.; Netti, G. S.; Mazzinghi, B.; Lazzeri, E.; Liotta, F.; Frosali, F.; Ronconi, E.; Meini, C.; Gacci, M.; Squecco, R.; Carini, M.; Gesualdo, L.; Francini, F.; Maggi, E.; Annunziato, F.; Lasagni, L.; Serio, M.; Romagnani, S.; Romagnani, P. Isolation and Characterization of Multipotent Progenitor Cells from the Bowman's Capsule of Adult Human Kidneys. *J. Am. Soc. Nephrol. JASN* **2006**, *17*, 2443–2456.
(24) Humphreys, B. D.; Valerius, M. T.; Kobayashi, A.; Mugford, J. W.; Soeung, S.; Duffield, J. S.; McMahon, A. P.; Bonventre, J. V. Intrinsic Epithelial Cells Repair the Kidney after Injury. *Cell Stem Cell* **2008**, *2*, 284–291.
(25) Duffield, J. S.; Park, K. M.; Hsiao, L.-L.; Kelley, V. R.; Scadden, D. T.; Ichimura, T.; Bonventre, J. V. Restoration of Tubular Epithelial Cells during Repair of the Postischemic Kidney Occurs Independently of Bone Marrow-Derived Stem Cells. *J. Clin. Invest.* **2005**, *115*, 1743–1755.
(26) Duffield, J. S.; Bonventre, J. V. Kidney Tubular Epithelium Is Restored without Replacement with Bone Marrow-Derived Cells during Repair after Ischemic Injury. *Kidney Int.* **2005**, *68*, 1956–1961.
(27) Lin, F.; Moran, A.; Igarashi, P. Intrarenal Cells, Not Bone Marrow-Derived Cells, Are the Major Source for Regeneration in Postischemic Kidney. *J. Clin. Invest.* **2005**, *115*, 1756–1764.
(28) Gupta, S.; Verfaillie, C.; Chmielewski, D.; Kim, Y.; Rosenberg, M. E. A Role for Extrarenal Cells in the Regeneration Following Acute Renal Failure. *Kidney Int.* **2002**, *62*, 1285–1290.
(29) Rookmaaker, M. B.; Smits, A. M.; Tolboom, H.; Van 't Wout, K.; Martens, A. C.; Goldschmeding, R.; Joles, J. A.; Van Zonneveld, A. J.; Gröne, H.-J.; Rabelink, T. J.; Verhaar, M. C. Bone-Marrow-Derived Cells Contribute to Glomerular Endothelial Repair in Experimental Glomerulonephritis. *Am. J. Pathol.* **2003**, *163*, 553–562.
(30) Van Koppen, A.; Joles, J. A.; van Balkom, B. W. M.; Lim, S. K.; de Kleijn, D.; Giles, R. H.; Verhaar, M. C. Human Embryonic Mesenchymal Stem Cell-Derived Conditioned Medium Rescues Kidney Function in Rats with Established Chronic Kidney Disease. *PLoS ONE* **2012**, *7*, e38746.
(31) Davies, J. A.; Chang, C.-H. Engineering Kidneys from Simple Cell Suspensions: An Exercise in Self-Organization. *Pediatr. Nephrol. Berl. Ger.* **2014**, *29*, 519–524.
(32) Takasato, M.; Er, P. X.; Becroft, M.; Vanslambrouck, J. M.; Stanley, E. G.; Elefanty, A. G.; Little, M. H. Directing Human Embryonic Stem Cell Differentiation towards a Renal Lineage Generates a Self-Organizing Kidney. *Nat. Cell Biol.* **2014**, *16*, 118–126.
(33) Aebischer, P.; Ip, T. K.; Panol, G.; Galletti, P. M. The Bioartificial Kidney: Progress towards an Ultrafiltration Device with Renal Epithelial Cells Processing. *Life Support Syst.* **1987**, *5*, 159–168.
(34) Ip, T. K.; Aebischer, P. Renal Epithelial-Cell-Controlled Solute Transport across Permeable Membranes as the Foundation for a Bioartificial Kidney. *Artif. Organs* **1989**, *13*, 58–65.
(35) Pfaller, W.; Gstraunthaler, G. Nephrotoxicity Testing in Vitro--What We Know and What We Need to Know. *Environ. Health Perspect.* **1998**, *106*, 559–569.
(36) Tiong, H. Y.; Huang, P.; Xiong, S.; Li, Y.; Vathsala, A.; Zink, D. Drug-Induced Nephrotoxicity: Clinical Impact and Preclinical in Vitro Models. *Mol. Pharm.* **2014**, *11*, 1933–1948.
(37) Prozialeck, W. C.; Edwards, J. R. Cell Adhesion Molecules in Chemically-Induced Renal Injury. *Pharmacol. Ther.* **2007**, *114*, 74–93.
(38) Knight, A. Systematic Reviews of Animal Experiments Demonstrate Poor Contributions toward Human Healthcare. *Rev. Recent Clin. Trials* **2008**, *3*, 89–96.
(39) Tasnim, F.; Deng, R.; Hu, M.; Liour, S.; Li, Y.; Ni, M.; Ying, J. Y.; Zink, D. Achievements and Challenges in Bioartificial Kidney Development. *Fibrogenesis Tissue Repair* **2010**, *3*, 14.
(40) Vanholder, R.; De Smet, R.; Lameire, N. Protein-Bound Uremic Solutes: The Forgotten Toxins. *Kidney Int.* **2001**, *59*, S266–S270.
(41) Masereeuw, R.; Mutsaers, H. A. M.; Toyohara, T.; Abe, T.; Jhawar, S.; Sweet, D. H.; Lowenstein, J. The Kidney and Uremic Toxin Removal: Glomerulus or Tubule? *Semin. Nephrol.* **2014**, *34*, 191–208.

(42) Humes, H. D.; Mackay, S. M.; Funke, A. J.; Buffington, D. A. Tissue Engineering of a Bioartificial Renal Tubule Assist Device: In Vitro Transport and Metabolic Characteristics. *Kidney Int.* **1999**, *55*, 2502–2514.

(43) Humes, H. D.; Fissell, W. H.; Weitzel, W. F.; Buffington, D. A.; Westover, A. J.; MacKay, S. M.; Gutierrez, J. M. Metabolic Replacement of Kidney Function in Uremic Animals with a Bioartificial Kidney Containing Human Cells. *Am. J. Kidney Dis.* **2002**, *39*, 1078–1087.

(44) Humes, H. D.; Buffington, D. A.; Lou, L.; Abrishami, S.; Wang, M.; Xia, J.; Fissell, W. H. Cell Therapy with a Tissue-Engineered Kidney Reduces the Multiple-Organ Consequences of Septic Shock. *Crit. Care Med.* **2003**, *31*, 2421–2428.

(45) Humes, H. D.; Weitzel, W. F.; Bartlett, R. H.; Swaniker, F. C.; Paganini, E. P.; Luderer, J. R.; Sobota, J. Initial Clinical Results of the Bioartificial Kidney Containing Human Cells in ICU Patients with Acute Renal Failure. *Kidney Int.* **2004**, *66*, 1578–1588.

(46) Tumlin, J.; Wali, R.; Williams, W.; Murray, P.; Tolwani, A. J.; Vinnikova, A. K.; Szerlip, H. M.; Ye, J.; Paganini, E. P.; Dworkin, L.; Finkel, K. W.; Kraus, M. A.; Humes, H. D. Efficacy and Safety of Renal Tubule Cell Therapy for Acute Renal Failure. *J. Am. Soc. Nephrol. JASN* **2008**, *19*, 1034–1040.

(47) Humes, H. D.; Buffington, D.; Westover, A. J.; Roy, S.; Fissell, W. H. The Bioartificial Kidney: Current Status and Future Promise. *Pediatr. Nephrol.* **2014**, *29*, 343–351.

(48) Fujita, Y.; Kakuta, T.; Asano, M.; Itoh, J.; Sakabe, K.; Tokimasa, T.; Saito, A. Evaluation of Na+ Active Transport and Morphological Changes for Bioartificial Renal Tubule Cell Device Using Madin-Darby Canine Kidney Cells. *Tissue Eng.* **2002**, *8*, 13–24.

(49) Ozgen, N.; Terashima, M.; Aung, T.; Sato, Y.; Isoe, C.; Kakuta, T.; Saito, A. Evaluation of Long-Term Transport Ability of a Bioartificial Renal Tubule Device Using LLC-PK1 Cells. *Nephrol. Dial. Transplant.* **2004**, *19*, 2198–2207.

(50) Miller, J. H. Sodium-Sensitive, Probenecid-Insensitive P-Aminohippuric Acid Uptake in Cultured Renal Proximal Tubule Cells of the Rabbit. *Proc. Soc. Exp. Biol. Med. Soc. Exp. Biol. Med. N. Y. N* **1992**, *199*, 298–304.

(51) Fissell, W. H.; Dyke, D. B.; Weitzel, W. F.; Buffington, D. A.; Westover, A. J.; MacKay, S. M.; Gutierrez, J. M.; Humes, H. D. Bioartificial Kidney Alters Cytokine Response and Hemodynamics in Endotoxin-Challenged Uremic Animals. *Blood Purif.* **2002**, *20*, 55–60.

(52) Fissell, W. H.; Lou, L.; Abrishami, S.; Buffington, D. A.; Humes, H. D. Bioartificial Kidney Ameliorates Gram-Negative Bacteria-Induced Septic Shock in Uremic Animals. *J. Am. Soc. Nephrol. JASN* **2003**, *14*, 454–461.

(53) Huijuan, M.; Xiaoyun, W.; Xumin, Y.; Hengjin, W.; Xia, S. Effect of Continuous Bioartificial Kidney Therapy on Porcine Multiple Organ Dysfunction Syndrome With Acute Renal Failure: *ASAIO J.* **2007**, *53*, 329–334.

(54) Humes, H. D.; Buffington, D. A.; MacKay, S. M.; Funke, A. J.; Weitzel, W. F. Replacement of Renal Function in Uremic Animals with a Tissue-Engineered Kidney. *Nat Biotech* **1999**, *17*, 451–455.

(55) Ni, M.; Teo, J.; Ibrahim, M. S.; Zhang, K.; Tasnim, F.; Chow, P. Y.; Zink, D.; Ying, J. Y. Characterization of Membrane Materials and Membrane Coatings for Bioreactor Units of Bioartificial Kidneys. *Biomaterials* **2011**, *32*, 1465–1476.

(56) Akira Saito MD, P.; Tun Aung MD, P.; Ms, K. S.; Md, Y. S.; Md, D. M. V.; Md, M. I.; Md, G. K.; Reika Tanaka MD, P.; Md, H. S.; Takatoshi Kakuta MD, P. Present Status and Perspectives of Bioartificial Kidneys. *J. Artif. Organs* **2006**, *9*, 130–135.

(57) Saito, A.; Sawada, K.; Fujimura, S. Present Status and Future Perspectives on the Development of Bioartificial Kidneys for the Treatment of Acute and Chronic Renal Failure Patients. *Hemodial. Int.* **2011**, *15*, 183–192.

(58) Sanechika, N.; Sawada, K.; Usui, Y.; Hanai, K.; Kakuta, T.; Suzuki, H.; Kanai, G.; Fujimura, S.; Yokoyama, T. A.; Fukagawa, M.; Terachi, T.; Saito, A. Development of Bioartificial Renal Tubule Devices with Lifespan-Extended Human Renal Proximal Tubular Epithelial Cells. *Nephrol. Dial. Transplant.* **2011**, *26*, 2761–2769.

(59) Saito, A.; Sawada, K.; Fujimura, S.; Suzuki, H.; Hirukawa, T.; Tatsumi, R.; Kanai, G.; Takahashi, H.; Miyakogawa, T.; Sanechika, N.; Fukagawa, M.; Kakuta, T. Evaluation of Bioartificial Renal Tubule Device Prepared with Lifespan-Extended Human Renal Proximal Tubular Epithelial Cells. *Nephrol. Dial. Transplant.* **2012**, *27*, 3091–3099.

(60) Sato, Y.; Terashima, M.; Kagiwada, N.; Aung, T.; Inagaki, M.; Kakuta, T.; Saito, A. Evaluation of Proliferation and Functional Differentiation of LLC-PK1 Cells on Porous Polymer Membranes for the Development of a Bioartificial Renal Tubule Device. *Tissue Eng.* **2005**, *11*, 1506–1515.

(61) Ueda, H.; Watanabe, J.; Konno, T.; Takai, M.; Saito, A.; Ishihara, K. Asymmetrically Functional Surface Properties on Biocompatible Phospholipid Polymer Membrane for Bioartificial Kidney. *J. Biomed. Mater. Res. A* **2006**, *77A*, 19–27.

(62) Oo, Z. Y.; Kandasamy, K.; Tasnim, F.; Zink, D. A Novel Design of Bioartificial Kidneys with Improved Cell Performance and Haemocompatibility. *J. Cell. Mol. Med.* **2013**, *17*, 497–507.

(63) Ng, C. P.; Zhuang, Y.; Lin, A. W. H.; Teo, J. C. M. A Fibrin-Based Tissue-Engineered Renal Proximal Tubule for Bioartificial Kidney Devices: Development, Characterization and *In Vitro* Transport Study. *Int. J. Tissue Eng.* **2012**, *2013*, e319476.

(64) Herzlinger, D. A.; Easton, T. G.; Ojakian, G. K. The MDCK Epithelial Cell Line Expresses a Cell Surface Antigen of the Kidney Distal Tubule. *J. Cell Biol.* **1982**, *93*, 269–277.

(65) Inagaki, M.; Yokoyama, T. A.; Sawada, K.; Duc, V. M.; Kanai, G.; Lu, J.; Kakuta, T.; Saito, A. Prevention of LLC-PK1 Cell Overgrowth in a Bioartificial Renal Tubule Device Using a MEK Inhibitor, U0126. *J. Biotechnol.* **2007**, *132*, 57–64.

(66) Zhang, H.; Tasnim, F.; Ying, J. Y.; Zink, D. The Impact of Extracellular Matrix Coatings on the Performance of Human Renal Cells Applied in Bioartificial Kidneys. *Biomaterials* **2009**, *30*, 2899–2911.

(67) Unadkat, H. V.; Hulsman, M.; Cornelissen, K.; Papenburg, B. J.; Truckenmüller, R. K.; Carpenter, A. E.; Wessling, M.; Post, G. F.; Uetz, M.; Reinders, M. J. T.; Stamatialis, D.; Blitterswijk, C. A. van; Boer, J. de. An Algorithm-Based Topographical Biomaterials Library to Instruct Cell Fate. *Proc. Natl. Acad. Sci.* **2011**, *108*, 16565–16570.

(68) Nur-E-Kamal, A.; Ahmed, I.; Kamal, J.; Schindler, M.; Meiners, S. Three-Dimensional Nanofibrillar Surfaces Promote Self-Renewal in Mouse Embryonic Stem Cells. *Stem Cells Dayt. Ohio* **2006**, *24*, 426–433.

(69) Schindler, M.; Ahmed, I.; Kamal, J.; Nur-E-Kamal, A.; Grafe, T. H.; Young Chung, H.; Meiners, S. A Synthetic Nanofibrillar Matrix Promotes in Vivo-like Organization and Morphogenesis for Cells in Culture. *Biomaterials* **2005**, *26*, 5624–5631.

(70) Miner, J. H. Renal Basement Membrane Components. *Kidney Int.* **1999**, *56*, 2016–2024.

(71) Lelongt, B.; Ronco, P. Role of Extracellular Matrix in Kidney Development and Repair. *Pediatr. Nephrol. Berl. Ger.* **2003**, *18*, 731–742.

(72) Ekblom, P.; Alitalo, K.; Vaheri, A.; Timpl, R.; Saxén, L. Induction of a Basement Membrane Glycoprotein in Embryonic Kidney: Possible Role of Laminin in Morphogenesis. *Proc. Natl. Acad. Sci. U. S. A.* **1980**, *77*, 485–489.

(73) Klein, G.; Langegger, M.; Timpl, R.; Ekblom, P. Role of Laminin A Chain in the Development of Epithelial Cell Polarity. *Cell* **1988**, *55*, 331–341.

(74) Pierschbacher, M. D.; Ruoslahti, E. Cell Attachment Activity of Fibronectin Can Be Duplicated by Small Synthetic Fragments of the Molecule. *Nature* **1984**, *309*, 30–33.

(75) Hersel, U.; Dahmen, C.; Kessler, H. RGD Modified Polymers: Biomaterials for Stimulated Cell Adhesion and beyond. *Biomaterials* **2003**, *24*, 4385–4415.

(76) Aota, S.-I.; Nomizu, M.; Yamada, K. M. The Short Amino Acid Sequence Pro-His-Ser-Arg-Asn in Human Fibronectin Enhances Cell-Adhesive Function. *J. Biol. Chem.* **1994**, *269*, 24756–24761.

(77) Staatz, W. D.; Fok, K. F.; Zutter, M. M.; Adams, S. P.; Rodriguez, B. A.; Santoro, S. A. Identification of a Tetrapeptide Recognition Sequence for the α2β1 Integrin in Collagen. *J. Biol. Chem.* **1991**, *266*, 7363–7367.

(78) Lehn, J.-M. *Supramolecular Chemistry: Concepts and Perspectives*; VCH, 1995.

(79) Lehn, J.-M. From Supramolecular Chemistry towards Constitutional Dynamic Chemistry and Adaptive Chemistry. *Chem. Soc. Rev.* **2007**, *36*, 151–160.

(80) Viney, C. Processing and Microstructural Control: Lessons from Natural Materials. *Mater. Sci. Rep.* **1993**, *10*, 187–236.

(81) Silva, G. A. Selective Differentiation of Neural Progenitor Cells by High-Epitope Density Nanofibers. *Science* **2004**, *303*, 1352–1355.

(82) Dankers, P. Y. W.; Harmsen, M. C.; Brouwer, L. A.; Van Luyn, M. J. A.; Meijer, E. W. A Modular and Supramolecular Approach to Bioactive Scaffolds for Tissue Engineering. *Nat. Mater.* **2005**, *4*, 568–574.

(83) Cui, H.; Webber, M. J.; Stupp, S. I. Self-Assembly of Peptide Amphiphiles: From Molecules to Nanostructures to Biomaterials. *Pept. Sci.* **2010**, *94*, 1–18.

(84) Collier, J. H.; Rudra, J. S.; Gasiorowski, J. Z.; Jung, J. P. Multi-Component Extracellular Matrices Based on Peptide Self-Assembly. *Chem. Soc. Rev.* **2010**, *39*, 3413–3424.

(85) Kouwer, P. H. J.; Koepf, M.; Le Sage, V. A. A.; Jaspers, M.; van Buul, A. M.; Eksteen-Akeroyd, Z. H.; Woltinge, T.; Schwartz, E.; Kitto, H. J.; Hoogenboom, R.; Picken, S. J.; Nolte, R. J. M.; Mendes, E.; Rowan, A. E. Responsive Biomimetic Networks from Polyisocyanopeptide Hydrogels. *Nature* **2013**, *493*, 651–655.

(86) MacNeil, S. Biomaterials for Tissue Engineering of Skin. *Mater. Today* **2008**, *11*, 26–35.

(87) Korossis, S.; Bolland, F.; Ingham, E.; Fisher, J.; Kearney, J.; Southgate, J. Review: Tissue Engineering of the Urinary Bladder: Considering Structure-Function Relationships and the Role of Mechanotransduction. *Tissue Eng.* **2006**, *12*, 635–644.

(88) Mangera, A.; Bullock, A. J.; Chapple, C. R.; MacNeil, S. Are Biomechanical Properties Predictive of the Success of Prostheses Used in Stress Urinary Incontinence and Pelvic Organ Prolapse? A Systematic Review. *Neurourol. Urodyn.* **2012**, *31*, 13–21.

(89) Mol, A.; Smits, A. I. P. M.; Bouten, C. V. C.; Baaijens, F. P. T. Tissue Engineering of Heart Valves: Advances and Current Challenges. *Expert Rev Med Devices* **2009**, *6*, 259–275.

(90) Beijer, F. H.; Sijbesma, R. P.; Kooijman, H.; Spek, A. L.; Meijer, E. W. Strong Dimerization of Ureidopyrimidones via Quadruple Hydrogen Bonding. *J. Am. Chem. Soc.* **1998**, *120*, 6761–6769.

(91) Söntjens, S. H. M.; Sijbesma, R. P.; van Genderen, M. H. P.; Meijer, E. W. Stability and Lifetime of Quadruply Hydrogen Bonded 2-Ureido-4[1H]-Pyrimidinone Dimers. *J. Am. Chem. Soc.* **2000**, *122*, 7487–7493.

(92) Brunsveld, L.; Folmer, B. J. B.; Meijer, E. W.; Sijbesma, R. P. Supramolecular Polymers. *Chem. Rev.* **2001**, *101*, 4071–4098.

(93) Sijbesma, R. P.; Beijer, F. H.; Brunsveld, L.; Folmer, B. J. B. Reversible Polymers Formed from Self-Complementary Monomers Using Quadruple Hydrogen Bonding. *Science* **1997**, *278*, 1601–1604.

(94) Folmer, B. J. B.; Sijbesma, R. P.; Versteegen, R. M.; van der Rijt, J. a. J.; Meijer, E. W. Supramolecular Polymer Materials: Chain Extension of Telechelic Polymers Using a Reactive Hydrogen-Bonding Synthon. *Adv. Mater.* **2000**, *12*, 874–878.

(95) Kautz, H.; van Beek, D. J. M.; Sijbesma, R. P.; Meijer, E. W. Cooperative End-to-End and Lateral Hydrogen-Bonding Motifs in Supramolecular Thermoplastic Elastomers. *Macromolecules* **2006**, *39*, 4265–4267.

(96) Keizer, H. M.; van Kessel, R.; Sijbesma, R. P.; Meijer, E. W. Scale-up of the Synthesis of Ureidopyrimidinone Functionalized Telechelic Poly(ethylenebutylene). *Polymer* **2003**, *44*, 5505–5511.

(97) Keizer, H. M.; Sijbesma, R. P.; Jansen, J. F. G. A.; Pasternack, G.; Meijer, E. W. Polymerization-Induced Phase Separation Using Hydrogen-Bonded Supramolecular Polymers. *Macromolecules* **2003**, *36*, 5602–5606.

(98) Dankers, P. Y. W.; van Luyn, M. J. A.; Huizinga-van der Vlag, A.; van Gemert, G. M. L.; Petersen, A. H.; Meijer, E. W.; Janssen, H. M.; Bosman, A. W.; Popa, E. R. Development and in-Vivo Characterization of Supramolecular Hydrogels for Intrarenal Drug Delivery. *Biomaterials* **2012**, *33*, 5144–5155.

(99) Dankers, P. Y. W.; Hermans, T. M.; Baughman, T. W.; Kamikawa, Y.; Kieltyka, R. E.; Bastings, M. M. C.; Janssen, H. M.; Sommerdijk, N. A. J. M.; Larsen, A.; van Luyn, M. J. A.; Bosman, A. W.; Popa, E. R.; Fytas, G.; Meijer, E. W. Hierarchical Formation of Supramolecular Transient Networks in Water: A Modular Injectable Delivery System. *Adv. Mater.* **2012**, *24*, 2703–2709.

(100) Yamauchi, K.; Kanomata, A.; Inoue, T.; Long, T. E. Thermoreversible Polyesters Consisting of Multiple Hydrogen Bonding (MHB). *Macromolecules* **2004**, *37*, 3519–3522.

(101) Van Beek, D. J. M.; Spiering, A. J. H.; Peters, G. W. M.; te Nijenhuis, K.; Sijbesma, R. P. Unidirectional Dimerization and Stacking of Ureidopyrimidinone End Groups in Polycaprolactone Supramolecular Polymers. *Macromolecules* **2007**, *40*, 8464–8475.

(102) Dankers, P. Y. W.; van Leeuwen, E. N. M.; van Gemert, G. M. L.; Spiering, A. J. H.; Harmsen, M. C.; Brouwer, L. A.; Janssen, H. M.; Bosman, A. W.; van Luyn, M. J. A.; Meijer, E. W. Chemical and Biological Properties of Supramolecular Polymer Systems Based on Oligocaprolactones. *Biomaterials* **2006**, *27*, 5490–5501.

(103) Dankers, P. Y. W.; Zhang, Z.; Wisse, E.; Grijpma, D. W.; Sijbesma, R. P.; Feijen, J.; Meijer, E. W. Oligo(trimethylene Carbonate)-Based Supramolecular Biomaterials. *Macromolecules* **2006**, *39*, 8763–8771.

(104) Botterhuis, N. E.; van Beek, D. J. M.; van Gemert, G. M. L.; Bosman, A. W.; Sijbesma, R. P. Self-Assembly and Morphology of Polydimethylsiloxane Supramolecular Thermoplastic Elastomers. *J. Polym. Sci. Part Polym. Chem.* **2008**, *46*, 3877–3885.

(105) Lange, R. F. M.; Van Gurp, M.; Meijer, E. W. Hydrogen-Bonded Supramolecular Polymer Networks. *J. Polym. Sci. Part Polym. Chem.* **1999**, *37*, 3657–3670.

(106) Wietor, J.-L.; van Beek, D. J. M.; Peters, G. W.; Mendes, E.; Sijbesma, R. P. Effects of Branching and Crystallization on Rheology of Polycaprolactone Supramolecular Polymers with Ureidopyrimidinone End Groups. *Macromolecules* **2011**, *44*, 1211–1219.

(107) Yamauchi, K.; Lizotte, J. R.; Long, T. E. Thermoreversible Poly(alkyl Acrylates) Consisting of Self-Complementary Multiple Hydrogen Bonding. *Macromolecules* **2003**, *36*, 1083–1088.

(108) McKee, M. G.; Elkins, C. L.; Long, T. E. Influence of Self-Complementary Hydrogen Bonding on Solution Rheology/electrospinning Relationships. *Polymer* **2004**, *45*, 8705–8715.

(109) Guo, M.; Pitet, L. M.; Wyss, H. M.; Vos, M.; Dankers, P. Y. W.; Meijer, E. W. Tough Stimuli-Responsive Supramolecular Hydrogels with Hydrogen-Bonding Network Junctions. *J. Am. Chem. Soc.* **2014**, *136*, 6969–6977.

(110) Dankers, P. Y. W.; van Beek, D. J. M.; ten Cate, A. T.; Sijbesma, R. P.; Meijer, E. W. Novel Biocompatible Supramolecular Materials for Tissue Engineering. *Polym. Mater. Sci. Eng.* **2003**, *88*, 52.

(111) Feijter, I. de; Goor, O. J. G. M.; Hendrikse, S. I. S.; Comellas-Aragonès, M.; Bastings, M. M. C.; Sijbesma, E.; Söntjens, S. H. M.; Peeters, J. W.; Milroy, L.-G.; Dankers, P. Y. W. A Convergent Solid-Phase Based Synthesis of Ureido-Pyrimidinone-Peptide Conjugates for Biomaterials. *(in preparation)*

(112) Dankers, P. Y. W.; Boomker, J. M.; Huizinga-van der Vlag, A.; Smedts, F. M. M.; Harmsen, M. C.; van Luyn, M. J. A. The Use of Fibrous, Supramolecular Membranes and Human Tubular Cells for Renal Epithelial Tissue Engineering: Towards a Suitable Membrane for a Bioartificial Kidney. *Macromol. Biosci.* **2010**, *10*, 1345–1354.

(113) Dankers, P. Y. W.; Boomker, J. M.; Huizinga-van der Vlag, A.; Wisse, E.; Appel, W. P. J.; Smedts, F. M. M.; Harmsen, M. C.; Bosman, A. W.; Meijer, E. W.; van Luyn, M. J. A. Bioengineering of Living Renal Membranes Consisting of Hierarchical, Bioactive Supramolecular Meshes and Human Tubular Cells. *Biomaterials* **2011**, *32*, 723–733.

(114) Almen, G. C.; Talacua, H.; Ramaekers, M.; Mollet, B. B.; Simonet, M.; Smits, A. I. P. M.; Kluin, J.; Dankers, P. Y. W. Development of Non-Cell Adhesive Vascular Grafts: From Supramolecular Building Blocks towards in Situ Vascular Tissue Engineering. *(submitted)*.

(115) Bastings, M. M. C.; Koudstaal, S.; Kieltyka, R. E.; Nakano, Y.; Pape, A. C. H.; Feyen, D. A. M.; van Slochteren, F. J.; Doevendans, P. A.; Sluijter, J. P. G.; Meijer, E. W.; Chamuleau, S. A. J.; Dankers, P. Y. W. A Fast pH-Switchable and Self-Healing Supramolecular Hydrogel Carrier for Guided, Local Catheter Injection in the Infarcted Myocardium. *Adv. Healthc. Mater.* **2014**, *3*, 70–78.

Chapter 2

Design and synthesis of ureido-pyrimidinone based biomaterial building blocks and model compounds

Abstract: *This chapter introduces the ureido-pyrimidinone functionalized compounds that are used in this thesis, discussing their design, synthesis and application. These compounds comprise both UPy-polymer and UPy-peptide biomaterial building blocks which are used in the formation of basement membrane mimics, and UPy-model compounds and additional UPy-polymers for the study towards the effect of sterilization of UPy-based biomaterials by UV irradiation.*

Part of this chapter was published in: B.B. Mollet, M. Comellas-Aragonès, A.J.H. Spiering, S.H.M. Söntjens, E.W. Meijer, P.Y.W. Dankers, *A modular approach to easily processable supramolecular bilayered scaffolds with tailorable properties*, J. Mater. Chem. B., 2014, 2, 2483-2493.

1. Introduction

Supramolecular building blocks based on ureido-pyrimidinone (UPy) allow the formation of new biomaterials via a modular approach.[1] In the past, many UPy-compounds have been synthesized. Those that have been explored as biomaterial or biomaterial component comprise UPy-polymers and UPy-peptides. The UPy-polymers include both telechelic building blocks, such as those based on polycaprolactone (i.e. PCLdiUPy, referred to as UPy-PCL in this thesis) and chain-extended (CE) macromolecular monomer designs, such as CE-UPy-PCL.[2,3] UPy-peptides are primarily intended to mix in small quantities into UPy-polymers, to introduce specific bioactive cues.[1,4-6,]

Dankers *et al.* postulated that UPy-based supramolecular biomaterials allow for modular bioactivation.[7] Functionalization of peptides with a UPy-moiety would facilitate bioactive cues to be built-in the supramolecular UPy-polymer biomaterial (Figure 2). The successful incorporation of UPy-modified peptides into UPy-modified polymer biomaterial was confirmed by work of Wisse *et al.*[5], who furthermore demonstrated that the strength of peptide incorporation is enhanced by matching the supramolecular motifs. When comparing UPy-urethane (UPy-UT) and UPy-urea (UPy-U) functionalized peptides and polymers, the combination in which both peptide and polymer were UPy-U-functionalized, showed least peptide leakage from the material.[8] To functionalize peptides with a UPy-moiety, convenient solid-phase synthesis strategies were developed, in which the UPy-moiety could be attached either to the N-terminus of the peptide or selectively on the ε-position of a C-terminal lysine.[6] Also a chemo-selective strategy in solution, based on oxime ligation was successfully demonstrated.[4] Bioactivation of UPy-UT-PCL via the introduction of UPy-peptides was verified *in vitro* in cell-culture studies and the positive biological effect was demonstrated *in vivo* by subcutaneous implantation of the bioactivated supramolecular biomaterial in rats.[1]

As described in chapter 1, in this thesis we further explore the use of UPy-based biomaterials as scaffolding material in tissue engineering, with a focus on the formation of a renal basement membrane (BM) mimick. UPy-polymer building blocks with very distinct properties, each having their own strength and weaknesses as separate biomaterial, are combined with the aim to create a new biomaterial which embodies the combined favourable properties (chapter 6). To this extent low molecular weight (M_n = 2 kg · mol^{-1}) polycaprolactone and poly(ethylene glycol) are applied, both end-functionalized with a UPy-moiety via a urea-linker.

Scheme 1: Overview of UPy-modified compounds applied in this thesis. I) UPy-polymers, both telechelic with a PCL or PEG backbone with Mn of 2 kg·mol^{-1} (a) and chain-extended UPy-PEG with an average Mn of each PEG segment of 10 kg·mol^{-1} (n=~227, m is not well defined, but estimated at ~ 50, PDI>3) (b). II) First generation UPy-peptides (a), functionalized with UPy-NCO linker **1**, which was also used for the functionalization of telechelic UPy-polymers, and b) a second generation UPy-RGD peptide functionalized with UPy-OEG-linker **15** for imp roved surface representation of the peptide in aqueous environment. III) UPy-model compounds, both polymer (a) and small molecules (b), applied in studies to elucidate the effect of UV-irradiation on UPy-materials.

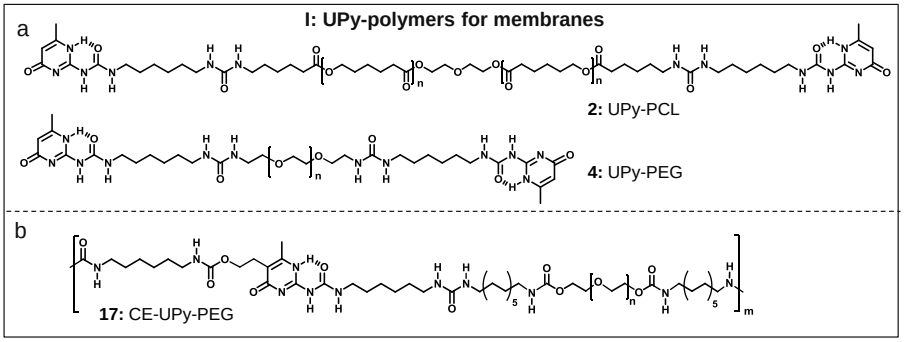
a
I: UPy-polymers for membranes
2: UPy-PCL
4: UPy-PEG
b
17: CE-UPy-PEG

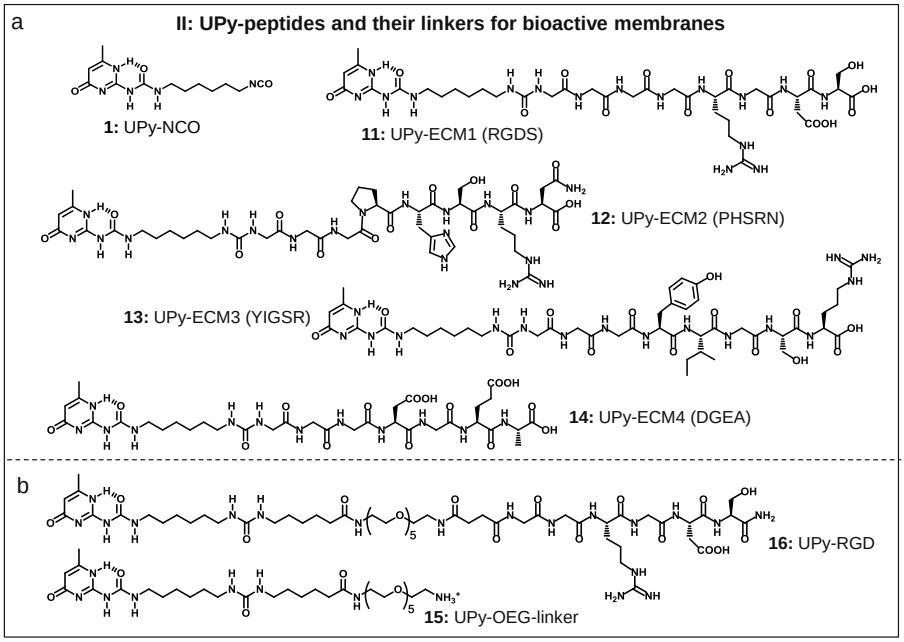
a
II: UPy-peptides and their linkers for bioactive membranes
1: UPy-NCO
11: UPy-ECM1 (RGDS)
12: UPy-ECM2 (PHSRN)
13: UPy-ECM3 (YIGSR)
14: UPy-ECM4 (DGEA)
b
16: UPy-RGD
15: UPy-OEG-linker

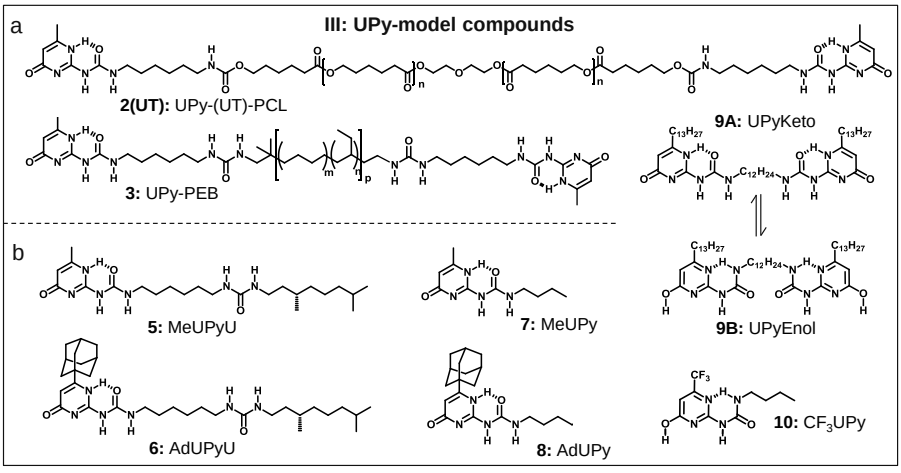
a
III: UPy-model compounds
2(UT): UPy-(UT)-PCL
3: UPy-PEB
9A: UPyKeto
9B: UPyEnol
b
5: MeUPyU
7: MeUPy
6: AdUPyU
8: AdUPy
10: CF3UPy

In this chapter the supramolecular polymer biomaterial components UPy-PCL **2** and UPy-PEG **4** (Scheme 1-Ia) are presented along with their synthesis, as well as a UPy-peptide-linker designed to be compatible with PEG containing UPy-biomaterials (UPy-OEG-linker, **16,** Scheme 1-IIb). Furthermore, the supramolecular hydrogelator chain-extended UPy-PEG (CE-UPy-PEG, **17**, Scheme 1-Ib), which is explored for application as hydrogel scaffold material in chapter 7, is introduced here. Finally, the new UPy-model compounds, **5** and **6** (Scheme 1-III) are presented. These are applied in chapter 4 together with other UPy-model compounds in a study towards the effect of UPy-biomaterial sterilization by UV-irradiation.

2. Results

2.1 UPy-polymer design and synthesis

Two telechelic UPy-polymer compounds, UPy-PCL **1** and UPy-PEG **2**, were synthesized. Both supramolecular polymers are similar in design; a short covalent polymer backbone (M_n= ~2.0 kg/mol) end-functionalized with UPy-moieties via a urea-C_6-spacer. The chemical composition of each backbone gives very distinct properties to supramolecular polymers made from either compound. This will be discussed in more detail later.

UPy-PCL has been described, synthesized[9] and applied[10,11] before. A new synthesis route employed at a larger scale (developed and performed by S. Söntjens) is depicted in Scheme 2. In both the prior and new synthetic approach, an amine-terminated oligocaprolactone is functionalized with the UPy-hexyl-isocyanate synthon (UPy-NCO, **1**)[12] to yield a urea-linker between the UPy-moiety and polymer. However, the conversion to obtain the amine-terminated polymer backbone starting from the diol was adjusted. This conversion, here performed at large lab-scale with 100 gram starting material, was achieved via a tert-butyloxycarbonyl (Boc) protected amine instead of carboxybenzyl (Cbz) protection. Furthermore, work-up was performed without precipitation. Both UPy-PCL obtained by the new synthesis route (**2-II**)[13] and the old synthesis route (**2-I**)[9] are used in the work presented in this thesis.

UPy-PEG was synthesized (Scheme 3) at a smaller scale, starting with 20 g commercial poly(ethylene glycol)diol (synthesis design and execution by A.J.H. Spiering). Conversion to amine-terminated PEG was performed via yet another route, employing tosylation, subsequent azide-functionalization and reduction. The hydrophilic mechanically weak UPy-PEG material is applied in conjunction with UPy-PCL in chapter 6 in the formation of freestanding hydrophilic electrospun membranes to mimic the BM.

Chain-extended UPy-PEG (CE-UPy-PEG **17**) is studied as hydrogel biomaterial for the formation of microfibrous scaffolds to mimic the BM or extracellular matrix (See chapter 7). The synthesis, physical and chemical characterization of this polymer was described before.[14]

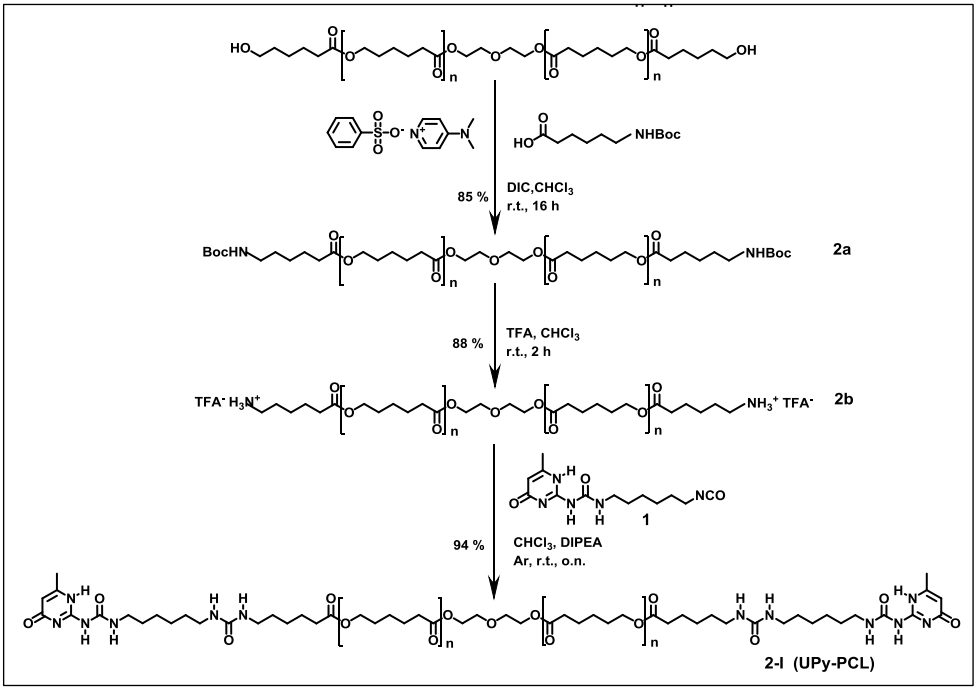

Scheme 2. Synthesis of UPy-PCL via Boc-protected amine.

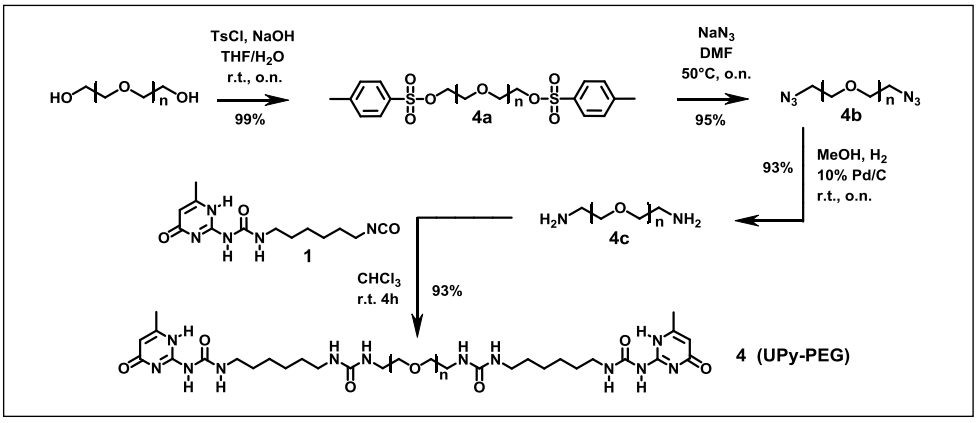

Scheme 3. Synthesis of UPy-PEG 4.

2.2 UPy-peptide design and synthesis

In the work performed by Dankers *et al.*, UPy-functionalized peptides were successfully applied in the biofunctionalization of UPy-PCL (**2-I**), to form improved basement membrane mimics for bioartificial kidney membrane tissue engineering. The peptides applied represented four cell-binding epitopes derived from ECM proteins; RGDS,[15] PHSRN,[16] DGEA[17] and YIGSR.[18] These UPy-ECM-peptides, with linkers consisting of UPy-C_6-U were synthesized as described before.[6,9]

A new UPy-linker was designed (Scheme 4), containing a short OEG segment, separated from the UPy-moiety by short carbon spacers, linked together via a urea and urethane functionality. The rationale behind this newly designed UPy-OEG-linker **15** is optimized presentation of the linked bioactive peptide at the biomaterial surface, available for interaction with cells. It was hypothesized that the OEG-functionality would stimulate presentation of the peptide at the surface of the biomaterial in aqueous environment and in particular when the UPy-biomaterial contains PEG which may form a highly hydrophilic layer at the surface of the material. The UPy-unit, short hydrophobic carbon spacer and urea functionality facilitate incorporation in the UPy-urea stacks, anchoring the peptide to the UPy-polymer material. The UPy-OEG-linker was synthesized via ten steps (synthesis design and performance by A.J.H. Spiering) starting from monodisperse hexa(ethylene glycol) (Scheme 4). This symmetric starting compound was desymmetrized to facilitate controlled monofunctionalization with a UPy-moiety. This was achieved via controlled monotosylation,[19] subsequent azide-functionalization, reduction and Boc-protection of the resultant amine. This amine was intended for reaction with the peptide. Then, selectively the remaining hydroxy-terminus of the OEG was aminated for sequential coupling. First a protected aminohexanoic acid was coupled to yield a short carbon spacer, which was then reacted with UPy-NCO resulting in a urea-linker. The product was Boc-deprotected to yield the UPy-linker as TFA-salt, ready for coupling to a peptide.

A peptide based on the potent cell-binding epitope, the RGD sequence,[20] was chosen to couple to the new UPy-OEG-linker. This UPy-RGD was applied to assess the representation of the peptide at the surface of a PEG containing UPy-biomaterial (see chapter 6). Peptide synthesis was performed according to standard solid phase peptide synthesis by hand in a syringe (performed by M. Comellas-Aragonès). The Fmoc-protected Gly-Gly-Arg-Gly-Asp-Ser-$CONH_2$ peptide (**16a**) was synthesized on a Rink amide MBHA resin. UPy-functionalization via reaction with UPy-OEG-linker **15** was successfully performed on the resin (Scheme 5).

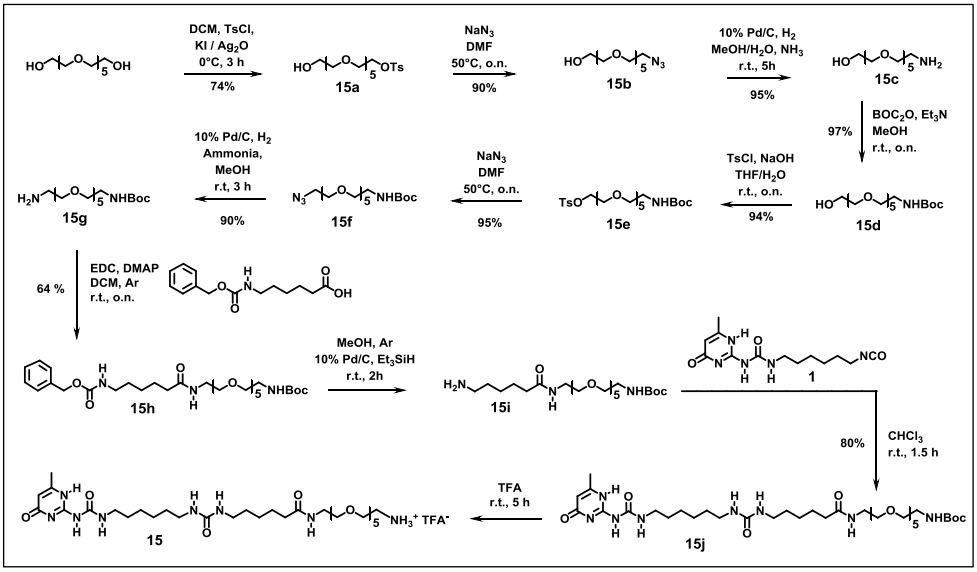

Scheme 4. Synthesis of UPy-U-OEG-linker.

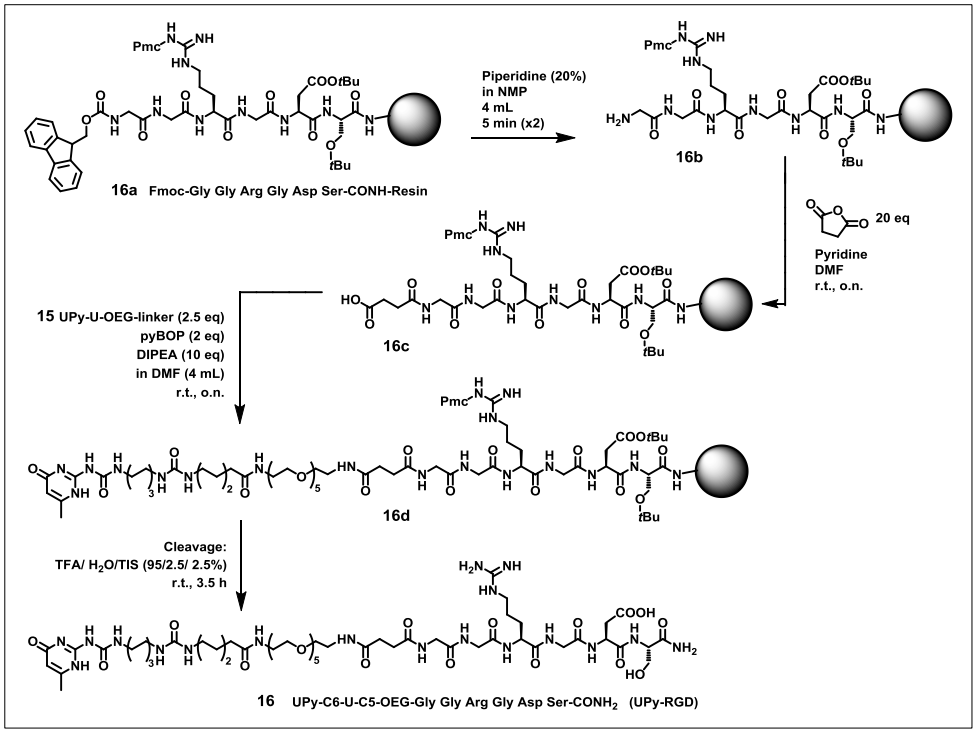

Scheme 5. Synthesis of UPy-RGD.

2.3 UPy-model compounds design and synthesis

UPy-model compounds, both polymers and small molecules (Scheme 1-III), were applied to study the effect of UV irradiation (chapter 4), which is commonly applied for sterilization of the UPy-based biomaterials prior to cell-culture studies. A diversity of available telechelic UPy-polymers with different backbone chemistries were used, including the hydrophilic, crystalline UPy-PEG **4**, the hydrophobic, semi-crystalline UPy-PCL **2**, and a highly hydrophobic, amorphous UPy-PEB with M_n= ~3.5 kg/mol polyethylene butylene backbone.[21] Additionally a urethane linked polymer, UPy-(UT)-PCL **2(UT)** was included in the study.[2] The latter two polymers were synthesized similarly as described before.

The small molecule UPy-model compounds comprise a set of four UPy-compounds **5**-**8** with varying ability to form UPy-dimer stacks. Stacking is improved in the presence of the urea-functionality (U),[22] and is suppressed by steric hindrance of a bulky adamantly (Ad) substituent at the 6-position of the pyrimidinone ring[23], where commonly a small methyl (Me) is situated. MeUPy[24] and AdUPy were synthesized and described before. MeUPyU and AdUPyU were synthesized by reaction of UPy-NCO[12] or AdUPy-NCO[23] with an amine-terminated carbon-tail, 1-amine-3,7dimethyloctane. Furthermore, previously described tautomer switchable compound **9** and UPy-enol compound **10** are employed. [24,25]

3. Conclusions

The UPy-toolbox applied in the present work is defined, consisting of biomaterial building blocks, both UPy-polymers and UPy-peptides, and UPy-model compounds. A new synthetic route for UPy-PCL polymer **2** was established, which allows the production of this routinely used biomaterial building block at large scale. The synthesis of UPy-PEG **4** was established at a smaller scale. However, intended applications require considerable smaller amounts of UPy-PEG compared to UPy-PCL. For example the supramolecular co-polymerization of UPy-PCL with small quantities of UPy-PEG to induce hydrophilicity and possibly anti-cell-adhesive behaviour, as described in chapter 6. The new UPy-U-OEG-linker **15** was designed for bioactivation of such UPy-PEG containing materials via functionalized UPy-peptides. Due to the desymmetrized design and resultant ten-step synthesis route, only small overall yields were achieved. Nonetheless, the acquired quantity matches the scale at which peptides are routinely synthesized in our lab and the very small amounts of UPy-peptide needed (few milligrams) to bioactivate our UPy-polymer materials at gram scale.

4. Acknowledgements

Jolanda Spiering is acknowledged for synthesis of UPy-NCO synthon **1**, UPy-(UT)-PCL **2(UT)**, UPy-PEG **4,** UPy-U-OEG linker **15**, UPy-model compounds **5**-**8** and help with synthesis of UPy-PCL **2-I**. Joris Peeters is acknowledged for synthesis of UPy-PEB **3**, Serge Söntjens for synthesis of UPy-PCL **2-II** and UPy-model compound **9**, Felix Beijer for synthesis of UPy-model compound **10**, Eva Wisse for the synthesis of the UPy-ECM peptides **11**-**14**, Marta Comellas-Aragonès for synthesis of UPy-RGD peptide **16**, Mingyu Guo and Louis Pitet for synthesis of CE-UPy-PEG **17**.

5. Experimental section

Materials

Poly(ethylene glycol)diol (M_n = 2 kg · mol^{-1}; PEG), polycaprolactonediol (M_n = 2 kg · mol^{-1}; PCL), hexa(ethylene glycol) (OEG_6), N-(3-dimethyla-minopropyl)-N-ethylcarbodiimide (EDC), triethylsilane (Et_3SiH), p-toluenesulfonyl chloride (TsCl), succinic anhydride, dibutyltin dilaurate (DBTDL), diisopropylcarbodiimide (DIC), Boc-6-aminohexanoic acid (BOC_2O) and di-tert-butyldicarbonate were purchased from Sigma Aldrich and used as received, unless stated otherwise. Pd/C was purchased from Merck and triethylamine (Et_3N) was purchased from Acros. Benzotriazol-1-yl-oxytripyrrolidinophosphonium hexafluorophosphate (PyBOP) and amino acids for solid phase peptide synthesis were purchased from Novabiochem. The solvents chloroform ($CHCl_3$), dichloromethane (DCM), tetrahydrofuran (THF), dimethylformamide (DMF), methanol (MeOH), hexane, and ethyl acetate (EtOAc), N-methylpyrrolidone (NMP), N,N-diisopropylethylamine (DIPEA) were purchased from Biosolve and used as received, unless stated otherwise. Deuterated chloroform ($CDCl_3$) was obtained from Cambridge Isotope Laboratories, Inc. The compounds 4-(dimethylamino)pyridinium-4-toluenesulfonate (DPTS),[26] 2(6-Isocyanatohexyl-aminocarbonyl-amino)-6-methyl-4[1H]pyrimidinone (UPy-NCO synthon **1**),[12] (s)-3,7dimethyloctylamine[27] and 6-Isocyanatohexylaminocarbonylamino)-6-adamantyl-4[1H]pyrimidinone (AdUPy-NCO synthon)[23] were synthesized as described before.

General methods

^{1}H-NMR and ^{13}C-NMR spectra were recorded in $CDCl_3$, unless indicated otherwise, on a Varian Mercury (400 MHz for 1H-NMR, 100 MHz for 13C-NMR) spectrometer at 298 K. Chemical shifts (δ) are reported in ppm downfield from tetramethylsilane (TMS). Abbreviations used for splitting patterns are s = singlet, d = doublet, t = triplet, q = quartet, m = multiplet and br = broad.

Attenuated total reflectance Fourier transform infrared spectroscopy (ATR-FTIR) spectra were recorded on a Perkin Elmer Spectrum One FT-IR spectrometer with a Universal ATR Sampling Accessory for solids.

SEC was performed on a Shimadzu LC–10ADVP system with a Shimadzu RID–10A refractive index detector, a Shimadzu SPD-M10AVP UV-Vis detector at 254 nm, and a serial configuration of a PLgel 5-µm mixed-C column and a PLgel 5-µm mixed-D column, using chloroform as eluent. The apparent number averaged molecular weights (Mn) and polydispersity indices (PDI) are reported relative to polystyrene standards.

Preparative reversed phase liquid chromatography (prep-RPLC) was performed on a system consisting of the following components: Shimadzu LC-8A preperative liquid chromatography pumps (with an Alltima C18 5u (125 x 20 mm) preparative reversed phase column and gradients of water-acetonitrile, supplemented with 0.1% trifluoro acetic acid), a Shimadzu CBM-20A prominence communications bus module and Shimadzu DGU 20A3 prominence degasser, Thermo Finnigan Surveyor PDA detector, Finigan LCQ Deca XP and Thermo Finnigan surveyor autosampler.

Reversed phase liquid chromatography–mass spectrometry (RPLC-MS) was performed on a system consisting of the following components: Shimadzu SCL-10A VP system controller with Shimadzu LC-10AD VP liquid chromatography pumps (with an Alltima C18 3u (50 mm x 2.1 mm) reversed phase column and gradients of water-acetonitrile supplemented with 0.1% formic acid, a Shimadzu DGU 20A3 prominence degasser, a Thermo Finnigan surveyor autosampler, a Thermo Finnigan surveyor PDA detector and a Thermo Scientific LCQ Fleet.

Synthesis of UPy-compounds

UPy-PCL 2

*Synthesis of compound **2a***

Boc-6-aminohexanoic acid (25 g, 110 mmol), DPTS (0.7 g, 2.5 mmol) and DIC (16.3 g, 125 mmol) at 0 ºC was added to a stirring solution of PCL_{2000}diol (100 g, 50 mmol) in chloroform (150 mL). For 16 h the reaction mixture was stirred while it was allowed to heat to r.t. Then the reaction mixture was filtered over celite and concentrated resulting in a viscous, yellowish oil. This oil was subsequently stirred with 200 mL diisopropyl ether, cooled to 4 ºC and decanted, giving a waxy solid. This solid was dried *in vacuo*, and was subsequently dissolved in 200 mL toluene leaving undissolved precipitate. The suspension was filtered over celite, and concentrated to again obtain a viscous, yellowish oil. This oil was precipitated with 200 mL diisopropyl ether, yielding a white to off-white waxy solid, which was collected by filtration and dried *in vacuo* to obtain product **2a** (yield = 103 g, 85%). ^{1}H-NMR ($CDCl_3$): δ (ppm) = 4.55 (br.s, 2H), 4.20 (t, 4H), 4.05 (t, 2(2n)H), 3.85 (t, 4H), 3.05 (br.t, 4H), 2.25 (m, 2(2n+2)H), 1.7–1.2 (br.m, 6(2n+2)H + 2*9H) ppm. IR (ATR): ν = 3396, 2939, 2865, 1730, 1515, 1459, 1419, 1390, 1364, 1236, 1161 cm^{-1}.

*Synthesis of compound **2b***

TFA (70 mL) was added to a solution of compound **2a** (50 g) in chloroform (70 mL). The reaction mixture was stirred for 2 h, after which the complete deprotection of the terminal amine group was confirmed by both IR and ^{1}H-NMR. Concentration *in vacuo* to remove most of the solvent resulted in a viscous oil that was stirred with diethyl ether and decanted (3x200 mL) to extract residual TFA and chloroform. During the last extraction the product precipitated as an off-white solid. This solid was stirred with diethyl ether and was collected by filtration, yielding product **2b** as the TFA salt, as a white, waxy solid (44 g, 88%). ^{1}H-NMR ($CDCl_3$): δ = 7.95 (br.s, 3H), 4.20 (t, 4H), 4.05 (t, 2(2n)H), 3.85 (t, 4H), 2.95 (br.t, 4H), 2.25 (m, 2(2n+2)H), 1.7–1.2 (br.m, 6(2n+2)H) ppm. IR (ATR): ν = 2944, 2865, 1722, 1471, 1419, 1397, 1366, 1294, 1240, 1172 cm^{-1}.

*Synthesis of compound **2***

The TFA-salt of compound **2b** (100.7 g, 28.9 mmol) was mixed with UPy-NCO synthon **1** (18.3 g, 62.4 mmol) in dry chloroform (300 mL). The mixture was kept under argon at r.t., and a mechanical stirrer was used to stir the viscous, thick white suspension. DIPEA N,N-diisopropylethylamine (29 mL, 0.17 mol) was added dropwise to the stirred reaction mixture over a 30 min period. After overnight stirring, IR spectroscopy indicated the absence of isocyanate reactant, and a ninhydrin test showed the presence of amines. So additional portions of UPy-synthon **1** (3 portions of in total 4.8 g, 16.4 mmol) were added, and stirring was continued until IR spectroscopy showed the presence of isocyanates in the reaction mixture. This indicated that all amines were converted into urea. The

viscosity of the reaction mixture increased during reaction. The mixture was transferred to a 1 L flask and the solvent was removed by using a rotary evaporator yielding a white residue. This crude product was stirred in methanol (0.5 L), filtered and washed with two portions of methanol (100 mL). This procedure was repeated two times. Then, the residue was mixed with methanol (0.5 L), refluxed for 1.5 h, allowed to reach r.t., filtered and washed with methanol (100 mL). This procedure was repeated also two times. The white residue was finally dissolved by stirring in chloroform (600 mL) and methanol (50 mL) and the beige, hazy solution was filtered over celite in a glass filter yielding a clear filtrate. Concentration of the filtrate *in vacuo* gave a white solid that was dried *in vacuo* at r.t. overnight (yield = 108 g, 94%). ^{1}H-NMR ($CDCl_3$): δ = 13.16 (s, 2H), 11.83 (s, 2H), 10.08 (s, 2H), 5.83 (s, 2H), 4.73 (br, 2H), 4.57 (bs, 2H), 4.23 (t, 4H), 4.06 (t, 2(2n)H), 3.69 (t, 4H), 3.24 (q, 4H), 3.19-3.13 (m, 8H), 2.37-2.27 (m, 2(2n)H+4H), 2.24 (s, 6H), 1.71-1.59 (2n*4H + 4H), 1.53-1.46 (12H), 1.42-1.31 (2(2n)H + 12H) ppm. ^{13}C-NMR ($CDCl_3$): δ = 173.7, 173.6, 173.4, 173.3,158.4, 156.5, 154.8, 148.5, 106.6, 69.1, 64.4, 64.2, 63.3, 40.2, 40.2, 39.6, 34.1, 34.0, 30.0, 29.8, 28.4, 26.4, 26.2, 26.1, 25.5, 25.5, 24.6, 24.5, 19.0 ppm. FT-IR (ATR): ν = 3333, 2938, 2863, 1728, 1701, 1668, 1620, 1585, 1527, 1462, 1417, 1391, 1361, 1257, 1236, 1160, 1100, 1066, 1043, 1016, 994, 964, 942, 879, 814, 799, 785, 768, 742 cm^{-1}. SEC ($CHCl_3$, UV at 254 nm): M_n = 1.05 kg/mol and PDI = 3.6. SEC ($CHCl_3$, RI): M_n = 3.5 kg/mol, PDI = 1.4.

UPy-PEG 4

*Synthesis of compound **4a***

Poly(ethylene glycol)diol (M_n = 2000 g/mol; 20 g, 10 mmol) was dissolved in 100 mL THF. NaOH (1.6 g, 40 mmol) dissolved in 10 mL H_2O was added. The mixture was cooled to 0 °C, and p-toluenesulfonyl chloride (TsCl, 4.96 g, 26 mmol) dissolved in 20 mL THF was added dropwise. The reaction mixture was allowed to warm up to r.t., and was stirred overnight. The reaction was checked with IR and ^{1}H NMR showing complete conversion. The mixture was supplemented with 100 mL H_2O, extracted twice with $CHCl_3$ and washed once with brine. The resulting product **4a** in chloroform was dried over $MgSO_4$, and the chloroform was evaporated to yield a white solid. The product was immediately used for the subsequent reaction (yield = 26 g, quantitatively, with residual THF). M_n = ~2310 g/mol (calculated from ^{1}H-NMR). ^{1}H-NMR ($CDCl_3$): δ = 7.80 (d, 2H), 7.35 (d, 4H), 4.16 (q, 4H), 3.69-3.60 (2t, 4nH) 2.45 (s, 6H) ppm. ^{13}C-NMR ($CDCl_3$): δ = 162.4, 77.3, 77.2, 77.0, 76.7, 70.6, 70.6, 70.5, 70.0, 50.6, 36.4, 31.4 ppm.

*Synthesis of compound **4b***

Compound **4a** was dissolved in 100 mL DMF and NaN_3 (2.6 g, 40 mmol) was added. The reaction mixture was stirred overnight at 50 °C. The reaction was checked with ^{1}H NMR, showing complete conversion. Then 1 L water was added, followed by 6 extractions with 100 mL DCM. The resulting product in DCM was dried over $MgSO_4$, and DCM was evaporated. The product was obtained as white solid. Apart from traces of solvent the product was pure as detected with ^{1}H NMR. The total amount of product was immediately used for the subsequent reaction (yield = 20.1 g, ~98%). M_n = ~2242 g/mol, n=49, (calculated from ^{1}H-NMR). ^{1}H-NMR ($CDCl_3$): δ = 3.69-3.64 (2t, 4nH), 3.39 (t, 4H) ppm. ^{13}C-NMR ($CDCl_3$): δ = 162.4, 77.3, 77.2, 77.0, 76.7, 70.6, 70.5, 70.0, 50.6, 36.4, 31.4 ppm.

*Synthesis of compound **4c***

Compound **4b** (20.1 g, 9.8 mmol) was dissolved in 100 mL MeOH and hydrogenated in a Parr reactor with H_2 in the presence of Pd/C (10%, 2 g) overnight. Disappearance of the peak at 3.39 ppm ($C\underline{H_2}N_3$) in ^{1}H-NMR indicated complete conversion. The product was filtered over hyflo, and the solvent was evaporated. The resulting light gray solid was immediately used for the subsequent reaction (yield = 18.4 g, 94%). ^{1}H-NMR ($CDCl_3$): δ = 3.65 (t, 4nH), 3.56 (t, 4H), 2.90 (t, 4H), 2.33 (s, br, 4H) ppm.

*Synthesis of compound **4** (**UPy-PEG**)*

Compound **4c** (18.4 g, 9.2 mmol) was dissolved in 300 mL dry $CHCl_3$ (molsieves). UPy-NCO synthon **1** (6.4 g, 21.8 mmol) was added and stirred at r.t. under argon for 4 h. Unreacted **1** was removed by reaction with an amine-resin (Sigma Aldrich) and stirred at r.t. for 2 h. The mixture was filtered over hyflo and 15 mL MeOH was added. UPy-PEG was precipitated in 2.5 L ether, filtered and dried in vacuo. The product was obtained as white powder (yield = 22.25 g, 93%). M_n = 2585 g/mol, M_n = 2763 g/mol, with n = ~49, calculated from ^{1}H-NMR). ^{1}H-NMR ($CDCl_3$): δ = 13.12 (s, 2H), 11.84 (s, 2H), 10.11 (s, 2H), 5.83 (s, 2H), 5.32 (s, 2H), 5.14 (s, 2H), 3.64 (t, 4nH), 3.54 (t, 4H), 3.35 (q, 4H), 3.24 (q, 4H), 3.14 (q, 4H), 2.24 (s, 6H), 1.59-1.35 (3m, 16H) ppm. ^{13}C-NMR ($CDCl_3$): δ = 173.0, 158.6, 156.4, 154.6, 148.3, 106.6, 70.6, 70.5, 70.4, 70.2, 70.0, 69.9, 42.8, 40.1, 40.0, 39.7, 31.1, 30.1, 29.3, 29.2, 26.5, 26.4, 26.1, 18.9 ppm. IR (ATR): ν= 3320, 2876, 1701 (UPy), 1667 (UPy), 1620 (urea), 1585 (UPy), 1527 (UPy), 1412, 1348, 1281, 1257, 1091, 1039, 943, 844, 810, 768, 742 cm^{-1}

UPy-ECM1-4 peptides

The synthesis of UPy-ECM peptides was performed in a similar manner as described before.[6]

UPy-OEG-linker 15

*Synthesis of compound **15a***

Hexa(ethylene glycol) (10.0 g, 35.4 mmol) was dissolved in 120 mL DCM and the solution was cooled to 0 °C and stirred before addition of Ag_2O (12.4 g, 53.5 mmol), TsCl (7.4 g, 38.8 mmol), and KI (1.2 g, 7.23 mmol). After stirring under argon at r.t. for 3 h, the silver salt precipitates were removed by filtration over hyflo. The hyflo was thoroughly washed with EtOAc. The combined filtrates were evaporated, and the residue was purified using SiO_2 column chromatography with 4% isopropanol in DCM as eluent. The pure product was obtained as clear oil (yield = 11.5 g, 74%). RPLC-MS: In the chromatogram one peak with m/z = 437.25 $[M+H]^+$, 459.33 $[M+Na]^+$ was measured. Calculated MW = 436.53 g/mol. ^{1}H-NMR ($CDCl_3$): δ = 7.80 (d, 2H), 7.34 (d, 2H), 4.16 (t, 2H), 3.74-3.59 (m, 22H), 2.45 (s, 3H) ppm. ^{13}C-NMR ($CDCl_3$): δ = 144.8, 133.0, 129.8, 128.0, 77.3, 77.2, 77.0, 76.7, 72.4, 70.7, 70.6, 70.5, 70.3, 69.2, 68.7, 64.4, 61.7, 25.3, 21.6 ppm.

*Synthesis of compound **15b***

Compound **15a** (10 g, 23 mmol) was dissolved in 50 mL DMF. Subsequently NaN_3 (2.24 g, 34.5 mmol) was added. The reaction mixture was stirred at 50 °C overnight. Then 1 L water was added, followed by 6 extractions with 100 mL DCM. The product was dried over $NaSO_4$ and solvent was evaporated under reduced pressure. The product was obtained as clear oil (yield = 6.38 g, 91%). RPLC-MS: In the chromatogram the product peak m/z = 308.08 $[M+H]^+$, 330.25 $[M+Na]^+$ was present. Calculated MW = 306.39 g/mol. ^{1}H-NMR ($CDCl_3$): δ = 3.70 (q, 2H), 3.67 (t, 18H), 3.61 (t, 2H), 3.39 (t, 2H), 2.51 (t, 1H) ppm. ^{13}C-NMR ($CDCl_3$): δ = 77.3, 77.0, 76.7, 72.5, 70.7, 70.6, 70.5, 70.3, 70.0, 61.7, 50.7 ppm.

*Synthesis of compound **15c***

Compound **15b** (6 g, 19.6 mmol) was dissolved in 80 mL MeOH and 20 mL 25% ammonia solution, and reacted with H_2 in presence of Pd/C (10%, 0.6 g) in a Parr reactor for 5 h. The reaction mixture was filtered over hyflo and solvent was evaporated. The product was dissolved in THF/EtOAc, dried over Na_2SO_4, filtered, and the solvent was evaporated. The product was obtained as clear oil (yield = 5.26 g, 96%). RPLC-MS: In the chromatogram one peak was observed with m/z = 282.33 $[M+H]^+$. Calculated MW = 281.35 g/mol. ^{1}H-NMR ($CDCl_3$): δ = 3.73-3.52 (m, 22H), 2.87 (t, 2H), 2.36 (s, broad, 3H) ppm. ^{13}C-NMR ($CDCl_3$, 100 MHz): δ = 77.3, 77.2, 77.0, 7607, 73.1, 72.8, 70.5, 70.2, 61.4, 41.6 ppm.

*Synthesis of compound **15d***

Compound ***15c*** (5.0 g, 17.8 mmol) was mono-Boc-protected by dissolution in 50 mL MeOH, addition of BOC_2O (4.27 g, 19.5 mmol) and Et_3N (3 mL, 21.3 mmol) under constant stirring at r.t. under argon

overnight. Solvent was evaporated and the product was obtained as clear oil (yield = 6.64 g, 97%). RPLC-MS: In the chromatogram the product was primarily observed in one peak with m/z = 382.17 $[M+H]^+$, 404.33 $[M+Na]^+$. Also m/z = 282.33 (M-Boc); Partial deprotection happened during RPLC-MS analysis because of the presence of formic acid in the eluent. Calculated MW = 381.47 g/mol. ^{1}H-NMR ($CDCl_3$): δ = 5.12 (s, br, 1H), 3.72-3.60 (m, 22H), 3.54 (t, 2H), 3.31 (q, 2H), 2.64 (s, br, 1H), 1.44 (s, 9H) ppm. ^{13}C-NMR ($CDCl_3$): δ = 156.0, 79.1, 77.3, 77.0, 76.7, 72.5, 70.6, 70.5, 70.3, 70.2, 61.7, 40.3, 31.2, 28.4 ppm.

*Synthesis of compound **15e***

Compound **15d** (6.5 g, 17 mmol) was dissolved in 70 mL THF. NaOH (1.36 g, 34 mmol) dissolved in 15 mL H_2O was added. The mixture was cooled to 0 °C and TsCl (3.9 g, 20 mmol) dissolved in 30 mL THF was added dropwise. The reaction mixture was allowed to warm to r.t. and was stirred overnight. THF was evaporated, 100 mL H_2O was added, followed by two extractions with 50 mL $CHCl_3$ and washing with 50 mL brine. The product was dried over $MgSO_4$, concentrated by solvent evaporation and purified using SiO_2 column chromatography with 5% isopropanol in $CHCl_3$ as eluent. The product was obtained as a clear oil (yield = 8.6 g, 94%). Calculated MW = 535.7 g/mol. ^{1}H-NMR ($CDCl_3$): δ =7.80 (d, 2H), 7.34 (d, 2H), 5.01 (s, br, 1H), 4.16 (t, 2H), 3.70 (t, 2H), 3.65-3.58 (m, 16H), 3.55 (t, 2H), 3.31 (q, 2H), 2.45 (s, 3H), 1.44 (s, 1H) ppm. ^{13}C-NMR ($CDCl_3$): δ = 156.0, 144.6, 133.0, 129.8, 128.0, 79.1, 77.3, 77.2, 77.0, 76.7, 70.7, 70.6, 70.5, 70.2, 69.2, 68.7, 40.3, 28.4, 21.6 ppm.

*Synthesis of compound **15f***

Compound **15e** (8.4 g, 15.7 mmol) and NaN_3 (1.52 g, 23.5 mmol) dissolved in 50 mL DMF was stirred overnight at 50 °C. The reaction mixture was cooled to r.t. Then, 1L H_2O was added, followed by 8 extractions with 100 mL DCM. The product was dried over $MgSO_4$ and solvent was evaporated under reduced pressure. The product was obtained as a clear oil (yield = 6.1 g, 95%). Calculated MW = 406.5 g/mol. ^{1}H-NMR ($CDCl_3$): δ = 5.03 (s, br, 1H), 3.69-3.61 (m, 18H), 3.54 (t, 2H), 3.39 (t, 2H), 3.31 (q, 2H), 1.44 (s, 9H) ppm. ^{13}C-NMR ($CDCl_3$): δ =77.3, 77.0, 76.7, 70.7, 70.6, 70.5, 70.2, 70.0, 50.7, 40.3, 36.4, 31.4, 28.4 ppm.

*Synthesis of compound **15g***

Compound **15f** (5.9 g, 14.5 mmol) was dissolved in 80 mL MeOH and 20 mL 25% ammonia solution and reacted with H_2 in presence of Pd/C (10%, 0.56 g) in a Parr reactor for 3 h. Complete reduction was confirmed with FTIR. The reaction mixture was filtered over hyflo and solvent was evaporated. The product was then dissolved in THF/EtOAc, dried over $MgSO_4$, filtered, and the solvent was evaporated. The product was obtained as clear oil (yield = 4.95 g, 90%). Calculated MW = 391.5 g/mol. ^{1}H NMR ($CDCl_3$): δ = 5.18 (s, 1H), 3.66-3.50 (m, 20H), 3.31 (q, 2H), 2.86 (t, 2H), 1.44 (s, 1H) ppm. ^{13}C-NMR ($CDCl_3$): δ =109.9, 79.1, 77.3, 77.0, 76.7, 73.4, 70.6, 70.5, 70.3, 41.8, 40.3, 28.4 ppm.

*Synthesis of compound **15h***

CBz-protected aminohexanoic acid (604 mg, 2.38 mmol), EDC (548 mg, 2.86 mmol) and few crystals of DMAP were stirred in 20 mL DCM for 30 min. Compound **15g** (1.0 g, 2.6 mmol) dissolved in 5 mL DCM was added dropwise and the reaction mixture was stirred at r.t. under argon overnight. An isocyanate-functionalized resin (Sigma Aldrich) was added, and the mixture was stirred for 2 h. The mixture was filtered, washed with 10% citric acid and washed with brine. Then the organic phase was dried over $MgSO_4$ and the solvent was evaporated. The product was purified by SiO_2 column chromatography with 10% isopropanol in $CHCl_3$ as eluent. The product was obtained as a clear oil (yield = 950 mg, 64%). ^{1}H-NMR ($CDCl_3$): δ = 7.35-7.27 (m, 5H), 6.29 (s, br, 1H), 5.09 (s, br, 2H), 4.94 (s, br, 1H), 3.65-3.62 (t, 18H), 3.53 (q, 2H), 3.43 (q, 2H), 3.30 (q, 2H), 3.18 (q, 2H), 2.18 (t, 2H), 1.65 (m, 2H), 1.52 (m, 2H), 1.44 (s, 9H) 1.34 (m, 2H) ppm. ^{13}C-NMR ($CDCl_3$): δ =172.9, 136.7,

128.5, 128.0, 79.2, 77.3, 77.0, 76.7, 70.5, 70.2, 70.1, 69.9, 40.8, 40.3, 39.1, 36.3, 29.6, 28.4, 26.3, 25.3, 25.2 ppm.

*Synthesis of compound **15j***

Compound **15h** (850 mg, 1.35 mmol) was dissolved in 5 mL MeOH and perfused with argon. Then Pd/C (10%, 60 mg) was added. To the stirred mixture under argon, Et_3SiH (680 uL, 4.25 mmol) was added dropwise. The mixture was stirred at r.t. for 2 h and then filtered over hyflo, and the solvent was evaporated. The residue (**15i**) was added to the UPy-NCO synthon **1** (475 mg, 1.62 mmol) dissolved in 100 mL $CHCl_3$. The mixture was stirred for 1.5 h. An amine-functionalized resin (Sigma Aldrich) was added, and the mixture was stirred over weekend. The mixture was filtered and solvent was evaporated. The residue was dissolved in approximately 10 mL $CHCl_3$ and 5 mL MeOH. Ether was added dropwise until a gel-like state was reached. The product was precipitated in hexane (yield = 800 mg, 80%). MW = 786.97 g/mol. ^{1}H-NMR ($CDCl_3$): δ = 13.14 (s, br, 1H), 11.82 (s, br, 1H), 10.06 (s, br, 1H), 6.43 (s, br, 1H), 5.82 (s, 1H), 5.15 (s, br, 1H), 4.90 (d, 2H), 3.66-3.52 (m, 20H) 3.43 (q, 2H), 3.31 (q, 2H), 3.23 (q, 2H), 3.14 (q, 4H), 2.19 (t, 2H), 2.08 (s, 3H), 1.49-1.26 (m, 14H), 1.44 (s, 9H) ppm. ^{13}C-NMR ($CDCl_3$): δ =173.2, 148.5, 106.6, 79.2, 77.3, 77.2, 77.0, 76.7, 70.5, 70.2, 70.1, 69.9, 40.4, 40.1, 40.0, 39.6, 39.1, 36.2, 31.9, 29.9, 29.8, 29.30, 28.4, 26.3, 25.1, 22.7, 18.9 ppm. IR (ATR): ν= 3332, 2931, 2858, 2160, 1701 (UPy), 1666 (UPy), 1642, 1620 (urea), 1578 (UPy), 1524 (UPy), 1461, 1364, 1254, 1172, 1101, 1039, 943, 870, 807, 783, 767, 740 cm^{-1}.

*Synthesis of UPy-U-OEG-linker **15***

Compound **15j** (780 mg) in 30 mL DCM was heated until completely dissolved. Then, 15 mL TFA was added and stirred at r.t. for 5 h. Solvent was evaporated and the residue was dissolved in DCM and precipitated in ether. After decantation of the ether, the residue was again dissolved in DCM (5 mL) and precipitated in 40 mL ether. The product was obtained as a white powder (yield = 700 mg). This TFA salt was stored at -20 °C until further use. ^{1}H-NMR (d7-DMF): δ= 8.27 (s, br, 3H), 7.84 (s, br, 1H), 5.95 (s, br, 1H), 5.80 (s, 1H) 3.80 (t, 2H), 3.66-3.49 (m, 20H), 3.32 (q, 4H), 3.23(q, 2H), 3.09 (q, 4H), 2.16 (m, 5H), 1.57-1.33 (m, 14H) ppm. IR (ATR): ν= 3332, 2932, 2858, 1700, 1665 (UPy), 1644 (UPy), 1620 (urea), 1578 (UPy), 1526 (UPy), 1480, 1462, 1447, 1414, 1379, 1350, 1303, 1277, 1256, 1200, 1176, 1119, 1039, 943, 870, 830, 798, 784, 766, 739, 720 cm^{-1}.

UPy-RGD peptide 16

*RGD-peptide synthesis **16c***

Peptide synthesis was performed according to standard solid phase peptide synthesis by hand in a syringe. The Fmoc-protected Gly-Gly-Arg-Gly-Asp-Ser-$CONH_2$ peptide (**16a**) was synthesized on a Rink amide MBHA resin (Nova Biochem) on 200 µmol scale, and was stored on the resin at -30 °C until further use. Before Fmoc-deprotection the peptide on the resin **16a** (154 mg, 200 µmol) was set to swell in NMP (4 mL) for 30 min, followed by deprotection with 20% piperidine in NMP (4 mL, 8.3 mmol) while shaken for 5 min 2 times, yielding compound **16b** on the resin. The resin was washed 5 times with 3 mL NMP and 5 times with 3 mL DMF. Succinic anhydride (400 mg, 4 mmol) and pyridine (2 mL) were dissolved in 3 mL DMF. The resultant solution was added to the peptide resin and shaken at r.t. overnight. The product **16c** was washed 6 times with 3 mL DMF, and 6 times with 3 mL DCM. Then the peptide on the resin was dried *in vacuo*, and stored at -30 °C.

*Peptide **16c** coupling to linker **15***

Compound **16c** (0.1 mmol) on the resin was set to swell in DMF (5 mL) for 2 h. A stock solution of linker **15** was prepared by dissolution (200 mg, 0.25 mmol) in 4 mL DMF with DIPEA (174 µL, 1 mmol) and PyBOP (104 mg, 0.2 mmol). This mixture was added to the peptide on the resin and shaken at r.t. overnight. The product **16d** was washed 6 times with DMF, and 6 times with 3 mL

DCM. Then the UPy-peptide on the resin was allowed to dry *in vacuo*, and stored at -30 °C. Cleavage of the UPy-functionalized peptide and deprotection of the amino acid protecting groups was performed using a cleavage cocktail consisting of TFA (95%, 4.75 mL), H_2O (2.5%, 0.125 mL) and TIS (2.5%, 0.125 mL). This mixture was added to the syringe and shaken at r.t. for 3.5 h, followed by precipitation of the product in ice-cold diethylether (20 mL). The precipitate was pelleted by centrifugation at 2000 rpm for 10 min, redissolved in 10% ACN in H_2O, and lyophilized. The product UPy-RGD **16** was purified with preparative RPLC-MS on a C18 column using a gradient of 18-22% ACN in H_2O, containing 0.1% TFA (yield = 18 mg, 13.7%). RPLC-MS: one peak in the chromatogram with m/z = 1315.5 $[M+H]^+$, 658.4 $[M+2H]^{2+}$, 439.3 $[M+3H]^{3+}$ was measured. Calculated = 1315.6 g/mol.

UPy-model compounds

Telechelic UPy-polymers UPy-(UT)-PCL **2(UT)**[2] and UPy-PEB **3**[21] were synthesized as described before, starting from commercially available PCL-diol with $M_n$of 2 kg/mol or PEB-diol with M_n of 3.5 kg/mol, respectively. Small molecular UPy-model compounds MeUPy **7**,[24] UPy-tautomer switchable **9** [25] and CF_3UPy **10**,[24] were synthesized as described before.

*MeUPyU **5***

UPy-isocyanate **1** (0,546 mmol, 160 mg) was dissolved in $CHCl_3$ by heating. (s)-3,7,dimethyloctylamine (1.2 eq, 0.655 mmol, 103 mg) was added and stirred overnight. MeOH was added until a clear solution was obtained. Isocyanate resin was added and the solution was stirred for 2 h. After filtration the solvent was evaporated. The product was dissolved in DCM+ MeOH and precipitated in ether. After filtration and drying *in vacuo* the product was obtained as white powder (yield = 173 mg, 72.4 %). MW = 450.63 g/mol. ^{1}H-NMR ($CDCl_3$ + MeOH): δ = 5.87 (s, 1H), 3.71 (s, 2H), 3.24 (t, 2H), 3.14 (t, 4H), 2.26 (s, 3H), 1.59-1.12 (m, 18H), 0.85 (q, 9H) ppm. ^{13}C-NMR ($CDCl_3$ + MeOH): δ =106.2, 49.7, 48.8, 39.8, 39.5, 39.2, 38.3, 37.1, 30.5, 29.6, 29.0, 27.9, 26.1, 24.6, 22.6, 22.5, 19.3 ppm. IR (ATR): ν= 3331, 2928, 2856, 1699 (UPy), 1667 (UPy), 1624 (urea), 1576 (UPy), 1523 (UPy), 1462, 1412, 1378, 1331, 1306, 1254, 1180, 1038, 1072, 1015, 940, 879, 799, 769, 741 cm^{-1}. MALDI calcd: M = 450.63 Da.; found: *m/z* 451.37 $[M+H]^+$, 473.35 $[M+Na]^+$, 489.31 $[M+K]^+$.

*AdUPyU **6***

AdUPy-isocyanate was synthesized as described before[23] and 0,546 mmol (160 mg) was dissolved in $CHCl_3$ by heating. (s)-3,7,dimethyloctylamine (1.2 eq, 0.655 mmol, 103 mg) was added and stirred overnight. MeOH was added until a clear solution was obtained. Isocyanate resin was added and the solution was stirred for 2 h. After filtration the solvent was evaporated. The product was dissolved in $CHCl_3$ and washed with water and brine. The mixture was dried over Na_2SO_4 and solvent was evaporated. The product was obtained as white powder (yield = 248 mg, 82.1 %). MW = 570.83 g/mol. ^{1}H-NMR ($CDCl_3$): δ = 13.44 (s, 1H), 11.91 (s. 1H), 10.09 (s, 1H), 5.87 (s, 1H), 4.83 (s, br, 2H), 3.37-3.02 (m, 6H), 2.13 -1.01 (s, m, 33H), 0.86 (2d, 9H) ppm. ^{13}C-NMR ($CDCl_3$): δ =174.0, 160.4, 102.7, 77.3, 77.2, 77.0, 76.7, 40.1, 39.6, 36.2, 38.6, 37.5, 37.2, 36.2, 36.1, 30.6, 29.7, 27.9, 26.2, 26.1, 24.7, 22.7, 22.6, 19.5 ppm.IR (ATR): ν= 2909, 2852, 1694 (UPy), 1633 (urea), 1571 (UPy), 1524 (UPy), 1451, 1365, 1345, 1315, 1246, 1138, 1104, 1075, 994, 973, 935, 849, 811, 749, 663 cm^{-1}. MALDI calcd: MW = 570.83 Da.; found: *m/z* 571.47 $[M+H]^+$, 593.45 $[M+Na]^+$, 609.42 $[M+K]^+$.

6. References

(1) Dankers, P. Y. W.; Harmsen, M. C.; Brouwer, L. A.; Van Luyn, M. J. A.; Meijer, E. W. A Modular and Supramolecular Approach to Bioactive Scaffolds for Tissue Engineering. *Nat. Mater.* **2005**, *4*, 568–574.

(2) Dankers, P. Y. W.; van Leeuwen, E. N. M.; van Gemert, G. M. L.; Spiering, A. J. H.; Harmsen, M. C.; Brouwer, L. A.; Janssen, H. M.; Bosman, A. W.; van Luyn, M. J. A.; Meijer, E. W. Chemical and Biological Properties of Supramolecular Polymer Systems Based on Oligocaprolactones. *Biomaterials* **2006**, *27*, 5490–5501.

(3) Söntjens, S. H. M.; Renken, R. A. E.; van Gemert, G. M. L.; Engels, T. A. P.; Bosman, A. W.; Janssen, H. M.; Govaert, L. E.; Baaijens, F. P. T. Thermoplastic Elastomers Based on Strong and Well-Defined Hydrogen-Bonding Interactions. *Macromolecules* **2008**, *41*, 5703–5708.

(4) Kieltyka, R. E.; Bastings, M. M. C.; van Almen, G. C.; Besenius, P.; Kemps, E. W. L.; Dankers, P. Y. W. Modular Synthesis of Supramolecular Ureidopyrimidinone–peptide Conjugates Using an Oxime Ligation Strategy. *Chem. Commun.* **2012**, *48*, 1452.

(5) Wisse, E.; Spiering, A. J. H.; Dankers, P. Y. W.; Mezari, B.; Magusin, P. C. M. M.; Meijer, E. W. Multicomponent Supramolecular Thermoplastic Elastomer with Peptide-Modified Nanofibers. *J. Polym. Sci. Part Polym. Chem.* **2011**, *49*, 1764–1771.

(6) Dankers, P. Y. W.; Adams, P. J. H. M.; Löwik, D. W. P. M.; van Hest, J. C. M.; Meijer, E. W. Convenient Solid-Phase Synthesis of Ureido-Pyrimidinone Modified Peptides. *Eur. J. Org. Chem.* **2007**, *22*, 3622–3632.

(7) Dankers, P. Y. W.; van Beek, D. J. M.; ten Cate, A. T.; Sijbesma, R. P.; Meijer, E. W. Novel Biocompatible Supramolecular Materials for Tissue Engineering. *Polym. Mater. Sci. Eng.* **2003**, *88*, 52.

(8) Wisse, E. Biomaterials by the Supramolecular Control of Nanofibers. Dissertation, Eindhoven University of Technology: Eindhoven, 2007.

(9) Dankers, P. Y. W. Supramolecular Biomaterials - Introducing a Modular Approach. Thesis, Eindhoven University of Technology: Eindhoven, The Netherlands, 2006.

(10) Dankers, P. Y. W.; Boomker, J. M.; Huizinga-van der Vlag, A.; Smedts, F. M. M.; Harmsen, M. C.; van Luyn, M. J. A. The Use of Fibrous, Supramolecular Membranes and Human Tubular Cells for Renal Epithelial Tissue Engineering: Towards a Suitable Membrane for a Bioartificial Kidney. *Macromol. Biosci.* **2010**, *10*, 1345–1354.

(11) Dankers, P. Y. W.; Boomker, J. M.; Huizinga-van der Vlag, A.; Wisse, E.; Appel, W. P. J.; Smedts, F. M. M.; Harmsen, M. C.; Bosman, A. W.; Meijer, E. W.; van Luyn, M. J. A. Bioengineering of Living Renal Membranes Consisting of Hierarchical, Bioactive Supramolecular Meshes and Human Tubular Cells. *Biomaterials* **2011**, *32*, 723–733.

(12) Folmer, B. J. B.; Sijbesma, R. P.; Versteegen, R. M.; van der Rijt, J. a. J.; Meijer, E. W. Supramolecular Polymer Materials: Chain Extension of Telechelic Polymers Using a Reactive Hydrogen-Bonding Synthon. *Adv. Mater.* **2000**, *12*, 874–878.

(13) Mollet, B. B.; Comellas-Aragonès, M.; Spiering, A. J. H.; Söntjens, S. H. M.; Meijer, E. W.; Dankers, P. Y. W. A Modular Approach to Easily Processable Supramolecular Bilayered Scaffolds with Tailorable Properties. *J. Mater. Chem. B* **2014**.

(14) Guo, M.; Pitet, L. M.; Wyss, H. M.; Vos, M.; Dankers, P. Y. W.; Meijer, E. W. Tough Stimuli-Responsive Supramolecular Hydrogels with Hydrogen-Bonding Network Junctions. *J. Am. Chem. Soc.* **2014**, *136*, 6969–6977.

(15) Pierschbacher, M. D.; Ruoslahti, E. Cell Attachment Activity of Fibronectin Can Be Duplicated by Small Synthetic Fragments of the Molecule. *Nature* **1984**, *309*, 30–33.

(16) Aota, S.-I.; Nomizu, M.; Yamada, K. M. The Short Amino Acid Sequence Pro-His-Ser-Arg-Asn in Human Fibronectin Enhances Cell-Adhesive Function. *J. Biol. Chem.* **1994**, *269*, 24756–24761.

(17) Staatz, W. D.; Fok, K. F.; Zutter, M. M.; Adams, S. P.; Rodriguez, B. A.; Santoro, S. A. Identification of a Tetrapeptide Recognition Sequence for the α2β1 Integrin in Collagen. *J. Biol. Chem.* **1991**, *266*, 7363–7367.

(18) Iwamoto, Y.; Robey, F. A.; Graf, J.; Sasaki, M.; Kleinman, H. K.; Yamada, Y.; Martin, G. R. YIGSR, a Synthetic Laminin Pentapeptide, Inhibits Experimental Metastasis Formation. *Science* **1987**, *238*, 1132–1134.

(19) Bouzide, A.; Sauvé, G. Silver(I) Oxide Mediated Highly Selective Monotosylation of Symmetrical Diols. Application to the Synthesis of Polysubstituted Cyclic Ethers. *Org. Lett.* **2002**, *4*, 2329–2332.

(20) Ruoslahti, E.; Pierschbacher, M. D. New Perspectives in Cell Adhesion: RGD and Integrins. *Science* **1987**, *238*, 491–497.

(21) Appel, W. P. J.; Portale, G.; Wisse, E.; Dankers, P. Y. W.; Meijer, E. W. Aggregation of Ureido-Pyrimidinone Supramolecular Thermoplastic Elastomers into Nanofibers: A Kinetic Analysis. *Macromolecules* **2011**, *44*, 6776–6784.

(22) Kautz, H.; van Beek, D. J. M.; Sijbesma, R. P.; Meijer, E. W. Cooperative End-to-End and Lateral Hydrogen-Bonding Motifs in Supramolecular Thermoplastic Elastomers. *Macromolecules* **2006**, *39*, 4265–4267.

(23) Van Beek, D. J. M.; Spiering, A. J. H.; Peters, G. W. M.; te Nijenhuis, K.; Sijbesma, R. P. Unidirectional Dimerization and Stacking of Ureidopyrimidinone End Groups in Polycaprolactone Supramolecular Polymers. *Macromolecules* **2007**, *40*, 8464–8475.

(24) Beijer, F. H.; Sijbesma, R. P.; Kooijman, H.; Spek, A. L.; Meijer, E. W. Strong Dimerization of Ureidopyrimidones via Quadruple Hydrogen Bonding. *J. Am. Chem. Soc.* **1998**, *120*, 6761–6769.

(25) Söntjens, S. H. M. Dynamics of Quadruply Hydrogen-Bonded Systems. Thesis, Eindhoven University of Technology: Eindhoven, The Netherlands, 2002.

(26) Moore, J. S.; Stupp, S. I. Room Temperature Polyesterification. *Macromolecules* **1990**, *23*, 65–70.

(27) Terashima, T.; Mes, T.; De Greef, T. F. A.; Gillissen, M. A. J.; Besenius, P.; Palmans, A. R. A.; Meijer, E. W. Single-Chain Folding of Polymers for Catalytic Systems in Water. *J. Am. Chem. Soc.* **2011**, *133*, 4742–4745.

Chapter 3

UPy-PCL based basement membrane mimics: electrospinning and characterization

Abstract: *This chapter describes the formation, structural characterisation and biofunctional validation of basement membrane (BM) mimicking scaffolds based on ureido-pyrimidinone (UPy) functionalized polycaprolactone (UPy-PCL). This is an end-functionalized supramolecular polymer. The processing of UPy-PCL into microfibrous scaffolds by electrospinning from a single solvent, in absence and presence of bioactive UPy-peptides, is demonstrated. Characterization of resultant membranes by atomic force microscopy (AFM) and wide angle x-ray scattering (WAXS) confirms the presence of self-assembled nanofibrous structures within the electrospun microfibers. These UPy-PCL based BM mimics demonstrate to facilitate adherence of human renal tubular epithelial cells. The formation of a confluent epithelial cell layer within three days indicates the usability of this biomaterial scaffold for the formation of a bioartificial renal membrane model.*

Part of the work described in this chapter has been submitted for publication: B.B. Mollet, I.L.J. Bogaerts, G.C. van Almen, P.Y.W. Dankers; *The development of a bioartificial environment for kidney epithelial cells through a supramolecular polymer basement membrane mimic and an organotypical culture system.*

1. Introduction

Natural basement membranes (BM) are porous hierarchical network structures consisting of fibrous proteins. Hence, for the application of biomaterials as BM mimic, a porous nano to microfibrous structure is considered relevant.[1] Electrospinning has been applied to form such structures. With this technique a very thin fiber is formed from a viscous polymer solution fed to the electrospun device by the application of high voltage. Charges built-up in the polymer solution until electrostatic repulsive forces counteract the surface tension. At that moment a jet of liquid ejects from the elongated droplet at the feeding tip and the so called 'Taylor cone'[2] is formed. When the molecular cohesion within the jet is sufficiently high, breakup does not occur and a continuous liquid stream is formed. Solvent evaporates quickly as a result of the high surface to volume ratio of the thin liquid stream, which upon drying becomes a polymer fiber. Charges accumulate at the surface of the stream and electrostatic repulsion causes instabilities. The resultant bending and whipping process further elongates the fiber and thus further reduces its diameter, until the fiber reaches the collector. If statically collected, random deposition of the fiber results. When sufficient layers of fibers are collected a dense non-woven fibrous mesh is obtained. The diameter of the fibers can vary from tens of nanometers to few micrometers, depending on the applied material and processing settings. In the electrospinning process there are many parameters that influence the resultant fiber and mesh morphology. These parameters involve polymer properties (e.g. molecular weight,[3] architecture), solvent properties (e.g. conductivity,[4] viscosity), 'hardware settings' (e.g. needle gauge, collector distance, type of collector), applied settings (e.g. voltage,[5] flow rate, concentration of solution[5]), and ambient parameters (e.g. temperature, humidity[3]).

Electrospinning of UPy-PCL (Scheme 1) was previously successfully performed from a solvent mixture of THF and water.[6] With an eye on a diversity of future multicomponent UPy-biomaterial mixtures, a robust single solvent system is preferred. This would circumvent solvent optimization every time a new UPy-biomaterial mixture is electrospun. Solvent composition can have a large influence on the electrospinning outcome and hence the opportunity to treat this as a fixed parameter will aid swift optimization of remaining electrospinning parameters to achieve desired mesh morphologies. Dissolving UPy-compounds, especially when functionalized via a urea-linker, requires a strong hydrogen bond-breaking solvent. Hexafluoroisopropanol (HFIP) is particularly effective in solubilizing a wide variety of polymers –both synthetic and natural– and has been successfully applied as solvent for electrospinning. The usability of this solvent for our UPy-biomaterial system is verified here, by electrospinning the earlier established UPy-PCL without and with bioactive UPy-peptides UPy-ECM1-4 (Scheme 1). The ability of renal epithelial cells to form a confluent monolayer on top of scaffolds prepared from HFIP is tested. The self-assembled nanofibrous structure,[7,8] as described in chapter 1 and identified in a diversity of UPy-functionalized polymer films, has earlier been postulated to be present within electrospun microfibers. This would resemble the hierarchical fibrous morphology of

natural biopolymer based materials such as the extracellular matrix (ECM) and BM. Here the actual presence of such substructures in electrospun UPy-PCL is assessed for the first time, using atomic force microscopy (AFM) and wide angle x-ray scattering (WAXS).

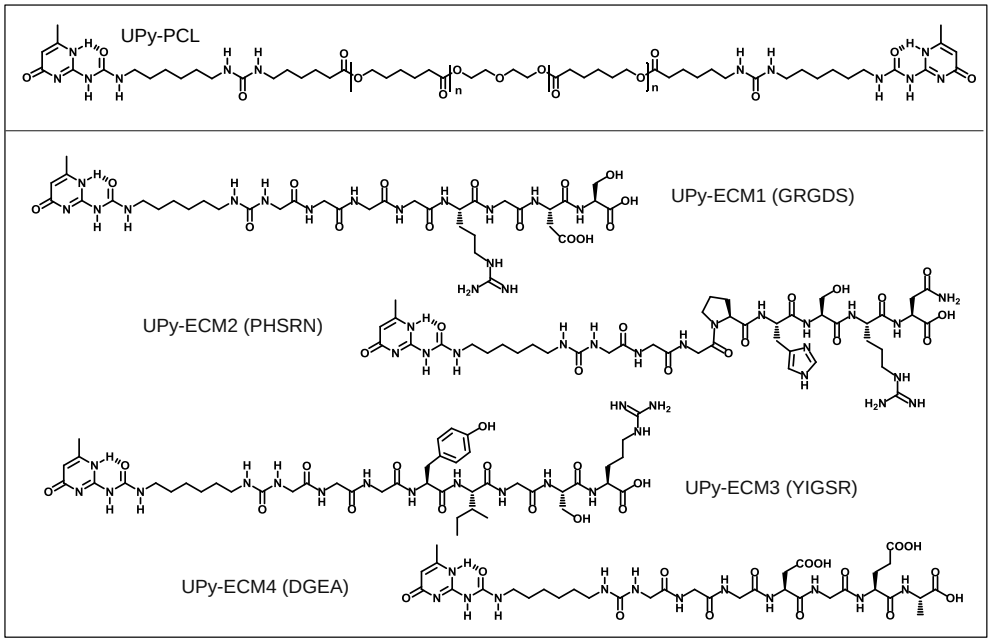

Scheme 1. UPy-based BM building blocks. Telechelic UPy-polymer UPy-PCL and mono-UPy-functional peptides, UPy-ECM1-4.

2. Results and discussion

2.1 Single solvent electrospinning of UPy-PCL and UPy-peptides

UPy-PCL and UPy-functionalized ECM-peptides (UPy-ECM1-4), all introduced in chapter 2 (as compound **2-I** and **11**-**14**), were successfully dissolved in HFIP. A viscous solution for electrospinning was obtained by dissolving 15 wt/v% UPy-PCL (**2-I**) in HFIP. This solution was processed by electrospinning to yield an opaque white, self-supporting non-bioactive membrane. The same solution with addition of a total of 4 mol% of UPy-ECM peptides (**11**-**14**, 1 mol% each) was successfully electrospun with the same settings, to yield a bioactive membrane.

The morphology of the membranes was studied by scanning electron microscopy (SEM) in low vacuum. SEM revealed similar homogeneous microfibrous morphologies for both membranes (Figure 1). The randomly oriented fibers had typical submicron diameters; 0.44 μm ± 0.22 μm for the bare UPy-PCL membrane and 0.34 ± 0.22 μm for the

bioactive UPy-PCL membrane. This is within the 0.1 - 1 µm fiber diameter range that was previously reported for these materials when electrospun from THF/water.[9] With apparent pore sizes smaller than 5 µm, these membranes were considered appropriate for application as BM mimic to allow adherent cells, such as renal epithelial cells, to grow on top rather than inside.

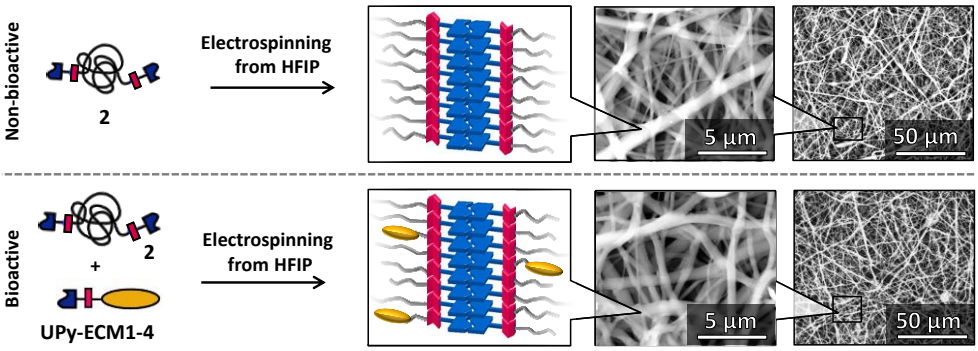

Figure 1. UPy-based biomaterial membranes electrospun from HFIP. UPy-PCL **2** was electrospun from HFIP without and with a mixture of UPy-ECM peptides **11-14** to make non-bioactive and bioactive microfibrous membranes, respectively. Scanning electron micrographs of the membranes show submicron fiber diameters, apparent pore sizes smaller than 5 µm and an overall homogeneous morphology.

Successful replacement of the water/THF co-solvent for HFIP in the electrospinning process of UPy-PCL, without and with UPy-peptides, provides potential opportunities towards facile processing of other, new UPy-biomaterials by electrospinning as well. However, electrospinnability of a compound is in the first place still highly dependent on properties of the compound. For example UPy-PEG (see chapter 2, compound **4**), with the same supramolecular design as UPy-PCL and same average molecular weight, did not result in a microfibrous mesh when 'electrospun' under similar conditions. A powdery deposit was formed instead, composed of polydisperse microparticles (Figure 2). This is the result of electrospraying rather than electrospinning, probably due to insufficient viscosity or cohesiveness of the UPy-PEG solution. However, having the UPy-moiety as unifying unit and HFIP as compatible solvent for most UPy-compounds, UPy-polymer biomaterial building blocks may well be mixed to make new biomaterials with combined properties. For example a mixture of hydrophobic, but electrospinnable UPy-PCL with hydrophilic UPy-PEG to acquire hydrophilic microfibrous membranes. This will be explored in chapter 6.

In previously reported work the UPy-PCL based membranes were visualized by SEM under application of high vacuum.[6,9] To prevent imaging artefacts as a result of built-up charges in the poor-conducting polymer material, the membranes were covered by a thin conducting layer of gold. Here, the membranes were visualized as-spun with a high voltage electron beam, without the application of a conducting layer. This was achieved by

performing visualization in low vacuum instead of high vacuum, to enable discharge of the sample via present water vapour. The direct imaging of electrospun polymer scaffolds with SEM by application of a high voltage electron beam enables the acquisition of more information than morphology of the mesh alone. The detection of both back scattering electrons (BSE) and secondary electrons (SE) from the mesh material might provide insight into the distribution of chemically varying components when different UPy-polymers are applied in one mesh (see chapter 6).

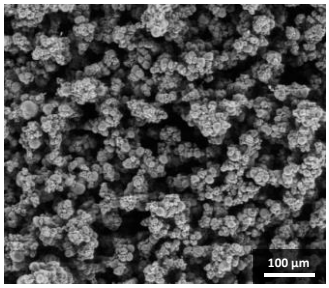

Figure 2. 'Electrospun' UPy-PEG. Scanning electron micrograph of UPy-PEG **4**, processed via 'electrospinning'. The settings as applied for the electrospinning of UPy-PCL **2** into fibrous scaffolds result in electrosprayed UPy-PEG deposition, without fibrous structure.

2.2 Analysis of hierarchical fibrous structures in electrospun UPy-PCL

Well-defined self-assembled nanofibers have been identified in drop-cast films of telechelic UPy-functionalized polymers. These structures were in particular well-defined when the UPy-moiety was linked to the polymer via a urea (U) linker.[7,8] These nanofibrous structures have been assumed to be present within electrospun microfibers of UPy-U-polymers. As such, these materials are postulated to enable resemblance of the hierarchical fibrous structure of native BM.[6,9] However, up to now empirical evidence for this hierarchical structure has not been provided. Here, electrospun UPy-PCL (which contains urea-linkers, see scheme 1) was studied by AFM and wide angle x-ray scattering (WAXS) in an attempt to identify nanostructures within the microfibers.

The identification of nanostructures by AFM on microfibers of electrospun UPy-PCL membranes proved to be challenging due to the irregular surface of these samples at the microscale. The irregularity was diminished by the collection of single electrospun fibers on a flat glass surface. The curvature of the single fiber still hampered the detection accuracy of the AFM tip. Nonetheless, features of distinct nanofibers were observed (Figure 3a). However, such features have also been observed by Lim *et al.* for electrospun high molecular weight PCL (M_n = 80 kg·mol^{-1}). Crystalline segments of the polymer were described to phase separate from the amorphous parts, resulting in formation of aligned nanofibrillar structures and even aligned lamellae.[10] Hence, the nanofibrous structures identified at the surface of electrospun UPy-PCL were not unequivocally the result of self-assembled UPy-urea stacks. Phase separation of the low molecular weight PCL segments might result in a similar observation. Therefore, X-ray scattering data was inquired to strengthen the ascribed identity of the nanofibrous structures. The presence of ordered

UPy-urea structures within electrospun UPy-PCL was confirmed. Similar diffraction patterns were observed for UPy-PCL before and after processing with electrospinning and in the presence of UPy-peptides (Figure 3b). These were compared to the diffraction pattern of non-functionalized PCL of similar molecular weight. It was observed that several small peaks were superimposed on the alkyl halo of the diffraction pattern. According to the diffraction pattern of the bare PCL, these could be related to crystalline PCL domains. However, also stacked UPy-dimers and hydrogen-bonded urea are known to cause diffraction peaks in this region.[11,12] Nevertheless, there was one specific peak only observed in the diffraction signal of all UPy-U-functionalized samples. The peak, which corresponds to a correlation distance of ~ 11 Å has previously been observed for multiple UPy-urea and UPy-urethane-functionalized polymers and has been attributed to the repeating distance between aligned UPy-dimer stacks.[11,12] These WAXS measurements thus confirm the presence of self-assembled, highly organized structures in electrospun UPy-PCL, also in presence of UPy-peptides (which were also functionalized with a urea-linker).

Arguably, the performance of similar experiments using a UPy-polymer with completely amorphous backbone such as PEB, instead of semi-crystalline PCL, might have allowed even better identification of UPy-based self-assembly in electrospun microfibers. However, WAXS profiles of UPy-PEB polymers are also dominated by a broad halo due to the amorphous PEB structure.[12] Furthermore, UPy-PEB cannot be dissolved in HFIP and electrospinning from a different solvent might influence the self-assembled structures of interest. Altogether, both the currently presented AFM and WAXS data support the previously assumed presence of self-assembled structures within the electrospun UPy-PCL polymer. Electrospinning of UPy-polymer biomaterials thus not only provides the opportunity to create porous, freestanding membranes. This processing technique also complements the self-assembled nanofibrous structure with a microfibrous super-structure. Hence, UPy-polymers allow for the recreation of hierarchical fibrous morphologies as found in natural cellfeijsupporting structures. Since the polymer was electrospun from hydrogen-bond breaking solvent, the self-assembled structures should either form in a fraction of a second during spinning, after spinning, or both. For drop-cast films of UPy-PEB (of which the UPy-moieties are functionalized with a chiral carbon-tail at the 6-position of the pyrimidinone-ring and in which the UPy-moieties are linked to the polymer via a urea functionality) it has been observed that self-assembled nanofibers grow over time and are enhanced by annealing.[13] This indicates that both the age of electrospun meshes and their history (e.g. irradiation by UV as studied in chapter 4) might influence their nanoscale morphology, which in turn is of influence of the mechanical properties of the material. Both nanoscale morphology and mechanical properties are of influence to the behavior of cells.

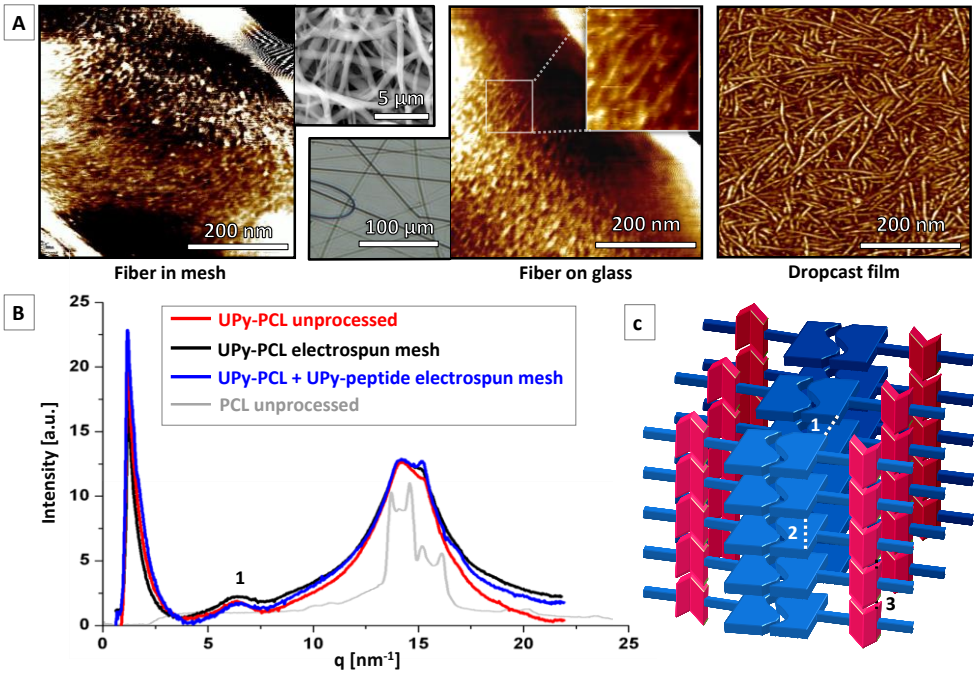

Figure 3. Structural organization at the nanoscale within UPy-PCL electrospun microfibers. A) AFM phase images of surfaces prepared from HFIP consisting of UPy-PCL (with urea linker); an electrospun microfiber in a mesh (left, SEM micrograph attached) and on a flat glass surface (middle, bright field micrograph attached), and a drop-cast film (right). Nanofibers, attributed to the phase separated UPy-urea stacks (C) are best observed in the drop-cast film. B) WAXS diffraction patterns of three different UPy-PCL samples and non-functionalized, unprocessed PCL (as received from the supplier). The intensity of the diffraction pattern of PCL was scaled to allow better comparison with the diffraction patterns of UPy-PCL samples and does not correspond to the indicated intensity in the graph (max. signal PCL was ~100). The peak in the diffraction signal indicated with 1 is related with the stack-to-stack distance as indicated in C. C) A schematic representation of an ordered assembly of three clustered stacks of UPy-dimers. UPy-dimer stacking is aided by the urea-linkers depicted in red. Distance 2 and 3 between stacked UPy-dimers and hydrogen bonded urea, respectively, are superimposed on the alkyl halo in the WAXS diffraction pattern in B.

2.3 Renal epithelial cell adhesion on electrospun UPy-PCL meshes

In contrast to CE-UPy-PEG (see chapter 7), UPy-PCL does allow cells to adhere even in absence of specific bioactive cues. As such, membranes spun from THF/water have been applied as BM mimic in past studies towards the formation of a bioartificial renal membrane.[6] Nonetheless, the introduction of bioactive ECM-peptides in the membrane has been demonstrated to enhance the performance of primary human renal epithelial cells.[9] Here, the ability of renal epithelial cells to form a tight confluent, polarized cell layer on UPy-PCL membranes electrospun from HFIP was assessed. For the formation of a bioartificial renal membrane model for studies in this thesis, the supramolecular biomaterial membranes are combined with human kidney-2 (HK-2) cells. This is an immortalized human renal proximal tubule epithelial cell line.[14]

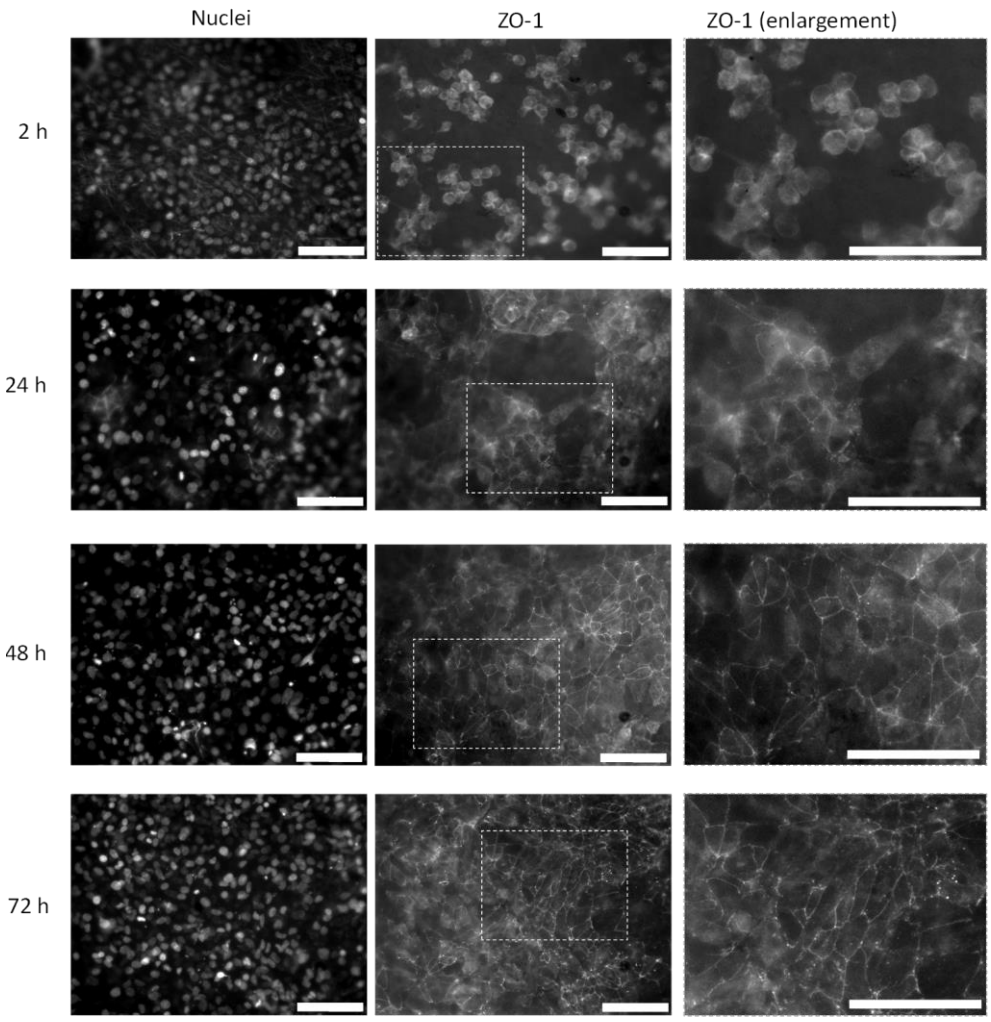

Figure 4. Formation of a bioartificial renal membrane model. Fluorescence micrographs of HK-2 cells seeded on electrospun UPy-PCL from HFIP. Cell nuclei are stained with DAPI and zona occludens 1 protein (ZO-1) is labelled via immunohistochemistry. All scale bars represent 100 µm.

A high cell density was seeded and the formation of tight junctions between cells, indicative for formation of a tight confluent layer and cell polarization, was monitored in time. Cultures were fixed, stained and imaged using fluorescence microscopy at 2, 24, 48, and 72 hours after cell seeding (Figure 4). The staining of zona occludens-1 protein (ZO-1) allowed visualisation of tight junction formation between cells, whereas the staining of cell nuclei more clearly indicated the position of individual cells. Fluorescent micrographs revealed attached, but primarily round cells 2 hours after seeding. ZO-1 protein is expressed, but not yet specifically allocated in tight-junctions. These round cells spread

somewhere during the next 22 hours. At that time, some initial concentration of ZO-1 in tight-junctions was observed as fine-lines at cell-cell contacts. This was more distinctly visible 48 hours after cell seeding. Although the cell nuclei indicated a homogeneously distributed confluent cell density, still gaps were observed in the fine-lined ZO-1 pattern. This indicated that at this point in time the tight-junction formation was not yet complete. A tighter cell layer was observed after an additional 24 hours of maturation of the culture, showing the characteristic fine-lined ZO-1 pattern. These results indicate that HK-2 cells, when seeded in a high density, can form a tight confluent, polarized cell layer on UPy-PCL membranes electrospun from HFIP in approximately three days.

These cell-biomaterial constructs will be applied in subsequent experiments described in chapter 8 that require a bioartificial renal tubule membrane model. The applied HK-2 cells might not be the most appropriate cells to use when focusing on future clinical applications. However, the cell-based tests performed within the scope of this thesis, merely focus on the function of new biomaterial membranes or organotypical culture environments. For this purpose, these cells provide sufficient typical renal epithelial features for relevant read-out.

3. Conclusion

UPy-PCL without and with bioactive UPy-functionalized ECM-peptides was successfully electrospun from a single solvent; HFIP. The ability of this solvent to dissolve a wide variety of compounds, allows for the electrospinning of many potential UPy-biomaterial combination using this solvent. For the first time empirical evidence confirmed the assumed presence of self-assembled nanostructures within electrospun microfibers. Hence, UPy-functionalized supramolecular polymers truly enclose the potential to form hierarchical fibrous structures for structural mimicry of natural ECM, such as renal BM. Renal epithelial HK-2 cells showed to form a tight confluent, polarized cell layer within three days after seeding on top of UPy-PCL membranes electrospun from HFIP. This assembly of renal epithelial cells on a synthetic BM mimic will form a basic bioartificial renal membrane model for subsequent studies described in this thesis.

4. Acknowledgements

Serge Söntjens is acknowledged for providing the UPy-PCL polymer and Eva Wisse for the UPy-ECM peptides. Wilco Appel is acknowledged for AFM imaging, Giuseppe Portale for help with WAXS measurements and data analysis and Jan Kolijn for initial optimization of electrospinning conditions from HFIP.

5. Experimental section

Materials

UPy-PCL and UPy-PEG were synthesized as described in chapter 2 and UPy-peptides similarly as previously described. [9,15]

Electrospinning

Electrospinning was performed on an in-house built electrospun setup. Polymer solutions, which were stirred overnight at room temperature before electrospinning, were fed by a syringe pump (KR analytical) at the outside of the electrospinning cabinet to the flat-tip stainless-steel 23 g needle (Intertronics, United Kingdom) inside the cabinet, via a 35 cm long 1 mm I.D. PTFE tube. Inside the cabinet, the solution was spun by the application of a high voltage (kV) between a tip-to-target distance (cm). Fibers were collected on a 12 x 12 cm grounded collector plate. To enable facile removal of the non-woven electrospun membrane, the collector was covered with a thin sheet of polyethylene film. If needed the fiber deposition was interrupted several times to move the static collector plate over a 3x3 grid to enlarge the area of fiber deposition and to achieve a more homogeneous layer thickness. The electrospun scaffold was gently removed from the collector and placed *in vacuo* at 40° C overnight to remove any residual solvent.

Electrospinning solution of UPy-PCL was prepared in 1,1,1,3,3,3-hexafluoro-2-propanol (HFIP, 147545000, Acros) in a glass vail. The applied polymer concentration depended on the batch used. UPy-PCL **2-I** (synthesized via the former synthesis method) was dissolved at a concentration of 15 wt/wt% in HFIP, UPy-PCL **2-II** (synthesized via the new route described in chapter **2**) was dissolved at a concentration of 17.5 wt/wt%. For the bioactive UPy-PCL, first the UPy-ECM-peptides **11-14** were dissolved in HFIP, at a concentration of 1 mol% each, compared to the UPy-PCL that was added (The solution containing peptides was prepared with UPy-PCL **2-I**). Approximately 1 - 1.5 mL of the solution was fed at 0.02 mL min^{-1} and spun by application of 17.5 kV over a 12 cm distance to the collector plate.

Scanning Electron Microscopy

Environmental scanning electron microscopy (ESEM) imaging was performed by using FEI Quanta 600 and Xt Microscope Control software. Samples were prepared by placing small pieces of each scaffold, facing top side up on double-sided sticky carbon tape on a metal stub. The uncoated samples were directly visualized in a low vacuum (~0.5 mbar) with an accelerating voltage of 18 kV and a working distance of 8 mm. Images were recorded up to 10,000 times magnification. Both backscattering electrons (BSE) and secondary electrons (SE) were detected. Microfiber diameters were determined from multiple high magnification images using ImageJ software and expressed as average ± standard deviation.

Atomic force microscopy (AFM) on UPy-PCL drop cast and electrospun surface

Atomic Force Microscopy (AFM) measurements were performed on a Digital Instrument Multimode Nanoscope IV using PPP-NCHR-50 silicon tips (Nanosensors) in the soft tapping mode (280-290 kHz) at room temperature. The nanoscale surface morphology of both electrospun microfibers and a film of UPy-PCL was visualized. The UPy-PCL **2-I** polymer film was made by casting a few drops of a 1 mg/mL solution in chloroform on glass cover slips cleaned with DCM and acetone and subsequent evaporation to air for at least 1 hour, followed by annealing *in vacuo* at 40 °C overnight. The electrospun UPy-PCL (**2-I**) fibers were prepared as described above. Both fibers in a self-supporting mesh and separate fibers collected on a glass cover slip were imaged (Appel, 2011).

Wide-Angle X-ray Scattering (WAXS) on UPy-PCL

Wide-angle X-ray scattering measurements were performed at the European Synchrotron Radiation Facility (ESRF) in Grenoble (France) at the DUBBLE beamline (BM26b) using a VHR detector (2657 × 3955 pixels) from Photonic Science. Measurable dimensions are 1-15 Å. Samples were prepared by filling DSC pans with polymer material; either the white solid as obtained from precipitation in heptane in the last step of UPy-PCL **2-I** synthesis, or this polymer processed into a microfibrous mesh by electrospinning from HFIP. For comparison, non-UPy functionalized PCL (2000 g/mole) as received from the manufacturer was added to the sample group. Measurements were performed at room temperature.

Human Kidney-2 cell culture

Human Kidney-2 (HK-2) cells, an immortalized proximal tubule epithelial cell line,[14] were routinely cultured and expanded for experimentation in tissue culture treated polystyrene flaks (BD Falcon)in complete medium consisting of Dulbecco's Modified Eagle Medium (DMEM, Gibco) supplemented with 10 v% heat inactivated fetal bovine serum (26140-079, Gibco, Invitrogen) and 1 v% penicillin-streptomycin solution (Gibco, Invitrogen), at 37 °C and 5% CO_2 in a humidified atmosphere. Cells cultured up to 80-90% confluence were washed with phosphate buffered saline (PBS, Sigma Aldrich) twice and detached from the culture flask using 0.05 % trypsin-EDTA (25300-054, Gibco, Invitrogen). Trypsin was inactivated by addition of complete medium. The cell suspension was transferred to a 50 mL falcon tube and centrifuged at 300 g for 5 minutes. The supernatant was aspirated and the cell pellet was resuspended in a known volume of complete medium. Cell concentration was determined via cell counting in a hemocytometer and adjusted to the desired concentration for seeding on UPy-biomaterial samples.

UPy-biomaterial sample preparation and cell seeding

Round-shaped 12 mm Ø samples were cut from the electrospun mesh. Samples were sterilized by UV-irradiation for 1 hour on each side. Samples were fixed in Minusheet tissue carriers with 13 mm O.D. (Minucells and Minutissue vertriebs gmbh). The carriers with samples were placed in a 24-well tissue culture plate (BD Biosciences). Each mesh was wet in an ample volume of complete medium, which was removed right before cell seeding until the fluid level reached the upper surface of the carrier, followed by removal of residual medium on top of the scaffold sample. Cells were seeded in 50 µL within the opening of the carrier ring. To assess the ability and speed of HK-2 cells to form a tight cell layer when seeded in a confluent density, a very high cell number of ~3 x 10^5 HK-2 cells was seeded per sample. The cells were left to adhere for 2 hours at 37° C, 5 % CO_2 and 90 % humidity. Then the first samples were fixed, while the rest was washed to remove non-adhered cells and cultured further in 1 mL of complete medium at 37° C, 5 % CO_2 and 90 % humidity.

Cell fixation, staining and visualization

After 24, 48 and 72 hours after cell seeding other samples were fixed. The samples were washed with PBS twice. Then adhered cells were fixed by incubation with 4 v% formaldehyde (Fluka) in PBS solution for 10 minutes at room temperature. Samples were again washed with PBS twice and subsequently incubated for 1 hour in blocking buffer of 5 wt/v% BSA (Sigma Aldrich) in PBS. First samples were incubated for 1 hour with mouse-anti-human ZO-1 (1 : 100, BD Biosciences) in 2 wt/v% BSA in PBS, followed by three times washing with PBS. Then samples were incubated for 45 minutes with goat anti-mouse Alexa 555 conjugated antibody (1:400, Molecular probes, invitrogen) in 2 wt/v% BSA in PBS, directly followed by incubation for 10 minutes with 4',6-diamidino-2-phenylindole (DAPI, 1:1000, Invitrogen) in 2 wt/v% BSA in PBS. The samples were washed three times with PBS, taken out of the supporting rings and embedded between a microscopy slide and

cover glass. The samples were visualized by fluorescence microscopy using a Zeiss Axio observer D1 equipped with an AxioCam Mrm camera and Zeiss Axiovision software (Carl Zeiss).

6. References

(1) Schindler, M.; Ahmed, I.; Kamal, J.; Nur-E-Kamal, A.; Grafe, T. H.; Young Chung, H.; Meiners, S. A Synthetic Nanofibrillar Matrix Promotes in Vivo-like Organization and Morphogenesis for Cells in Culture. *Biomaterials* **2005**, *26*, 5624–5631.

(2) Taylor, G. Electrically Driven Jets. *Proc. Roy. Soc. London* **1969**, *A313*, 453–475.

(3) Casper, C. L.; Stephens, J. S.; Tassi, N. G.; Chase, D. B.; Rabolt, J. F. Controlling Surface Morphology of Electrospun Polystyrene Fibers: Effect of Humidity and Molecular Weight in the Electrospinning Process. *Macromolecules* **2004**, *37*, 573–578.

(4) Uyar, T.; Besenbacher, F. Electrospinning of Uniform Polystyrene Fibers: The Effect of Solvent Conductivity. *Polymer* **2008**, *49*, 5336–5343.

(5) Deitzel, J. M.; Kleinmeyer, J.; Harris, D.; Beck Tan, N. C. The Effect of Processing Variables on the Morphology of Electrospun Nanofibers and Textiles. *Polymer* **2001**, *42*, 261–272.

(6) Dankers, P. Y. W.; Boomker, J. M.; Huizinga-van der Vlag, A.; Smedts, F. M. M.; Harmsen, M. C.; van Luyn, M. J. A. The Use of Fibrous, Supramolecular Membranes and Human Tubular Cells for Renal Epithelial Tissue Engineering: Towards a Suitable Membrane for a Bioartificial Kidney. *Macromol. Biosci.* **2010**, *10*, 1345–1354.

(7) Kautz, H.; van Beek, D. J. M.; Sijbesma, R. P.; Meijer, E. W. Cooperative End-to-End and Lateral Hydrogen-Bonding Motifs in Supramolecular Thermoplastic Elastomers. *Macromolecules* **2006**, *39*, 4265–4267.

(8) Botterhuis, N. E.; van Beek, D. J. M.; van Gemert, G. M. L.; Bosman, A. W.; Sijbesma, R. P. Self-Assembly and Morphology of Polydimethylsiloxane Supramolecular Thermoplastic Elastomers. *J. Polym. Sci. Part Polym. Chem.* **2008**, *46*, 3877–3885.

(9) Dankers, P. Y. W.; Boomker, J. M.; Huizinga-van der Vlag, A.; Wisse, E.; Appel, W. P. J.; Smedts, F. M. M.; Harmsen, M. C.; Bosman, A. W.; Meijer, E. W.; van Luyn, M. J. A. Bioengineering of Living Renal Membranes Consisting of Hierarchical, Bioactive Supramolecular Meshes and Human Tubular Cells. *Biomaterials* **2011**, *32*, 723–733.

(10) Lim, C. T.; Tan, E. P. S.; Ng, S. Y. Effects of Crystalline Morphology on the Tensile Properties of Electrospun Polymer Nanofibers. *Appl. Phys. Lett.* **2008**, *92*, 141908.

(11) Wietor, J.-L.; van Beek, D. J. M.; Peters, G. W.; Mendes, E.; Sijbesma, R. P. Effects of Branching and Crystallization on Rheology of Polycaprolactone Supramolecular Polymers with Ureidopyrimidinone End Groups. *Macromolecules* **2011**, *44*, 1211–1219.

(12) Appel, W. P. J.; Portale, G.; Wisse, E.; Dankers, P. Y. W.; Meijer, E. W. Aggregation of Ureido-Pyrimidinone Supramolecular Thermoplastic Elastomers into Nanofibers: A Kinetic Analysis. *Macromolecules* **2011**, *44*, 6776–6784.

(13) Hutin, M.; Burakowska-Meise, E.; Appel, W. P. J.; Dankers, P. Y. W.; Meijer, E. W. From Molecular Structure to Macromolecular Organization: Keys to Design Supramolecular Biomaterials. *Macromolecules* **2013**, *46*, 8528–8537.

(14) Ryan, M. J.; Johnson, G.; Kirk, J.; Fuerstenberg, S. M.; Zager, R. A.; Torok-Storb, B. HK-2: An Immortalized Proximal Tubule Epithelial Cell Line from Normal Adult Human Kidney. *Kidney Int* **1994**, *45*, 48–57.

(15) Dankers, P. Y. W.; Adams, P. J. H. M.; Löwik, D. W. P. M.; van Hest, J. C. M.; Meijer, E. W. Convenient Solid-Phase Synthesis of Ureido-Pyrimidinone Modified Peptides. *Eur. J. Org. Chem.* **2007**, *22*, 3622–3632.

Chapter 4

The effect of UV irradiation on UPy-based biomaterials

Abstract: *Supramolecular polymers based on ureido-pyrimidinone (UPy) are considered to be very useful as biomaterial. Here, the effect of UV irradiation of these polymers, which is used to sterilize the materials, is studied. Besides anticipated crosslinking effects, UV irradiation induces a fluorescent property in telechelic UPy-polymers. UPy-model compounds confirm a relation between the UV-induced changes and the UPy-moiety. UV-induced fluorescence and IR-spectral changes are (partially) reversible by heat and/or application of solvent. The results indicate the presence of at least two distinct UV-induced molecular species. UPy-model compounds with specific tautomeric forms directly relate fluorescence to UPy-enol tautomers. Photo-enolization is hypothesized to occur via an excited state intermolecular double proton transfer. For successful application as biomaterial in tissue engineering applications, it is important to identify and understand factors that can influence the dynamics of UPy-based materials, such as changes in UPy-tautomeric equilibrium and crosslinking. In broader perspective, these results underline the awareness required upon handling dynamic supramolecular biomaterials.*

This work has been submitted for publication. B.B. Mollet, Y. Nakano, P.C.M.M. Magusin, A.J.H. Spiering, J.A.J.M. Vekemans, P.Y.W. Dankers, E.W. Meijer; *The effect of ultra violet light irradiation on ureido-pyrimidinone based biomaterials.*

1. Introduction

Sterility of biomaterials used in cell-culture studies or regenerative medicine applications is essential to prevent contamination with microbial organisms. Sterilization methods that are applied for solid biomaterials can be subdivided in three categories; heat sterilization, chemical sterilization and sterilization by radiation. Each sterilization method induces modifications to some extend to the chemical, physical and/or thermo-mechanical properties of biomedical materials, which can influence material functionality.[1] Hence, choice of the correct sterilization treatment is a crucial step in the development and application of new biomaterials.

To sterilize the ureido-pyrimidinone (UPy) based biomaterials in our studies, we have chosen to use UV irradiation, which is a relative mild, low energy sterilization method. The principle of sterilization by UV irradiation is based on the introduction of defects in the DNA of microorganisms, making them unable to reproduce and effectively kill them. UV photons of different energies have various effects on DNA, but the overall most abundant UV induced DNA damage is the formation of various pyrimidine dimers. A 2+2 cycloaddition reaction occurs between two adjacent pyrimidine bases, cytosine (C) and/or thymine (T).[2,3] UV irradiation is routinely used at lab scale for the sterilization of biomaterials because of its easy, safe and on lab available application via a germicidal UV lamp. It proved to be sufficient for sterilization of our UPy-biomaterials when applied on hydrogelator powders,[4] hydrogels,[5] drop-cast films[6,7] and electrospun[8-10] solid UPy-biomaterial surfaces. Cells were successfully cultured routinely on and in these sterilized materials, even in absence of antibiotics in the culture media[11] and for prolonged culture times (up to 25 days).[10] Furthermore, *in-vivo* studies did not show any unexpected inflammatory and foreign body responses at several implantation sites, i.e. subcutaneously,[12] as vascular graft,[13] in the kidney [4] and in the myocardium.[5]

Although the intensity and duration of UV irradiation applied in biomaterial sterilization are generally considered as non-harmful to the materials used, we surprisingly observed the formation of highly fluorescent species as a result of UV irradiation of our UPy-biomaterials. In general, UV-induced crosslinking or backbone scissions in polymers can occur, while more specifically even 2+2 cycloaddition reactions between UPy-moieties can be foreseen, given their structural similarity with DNA's pyrimidine bases. Hence, this prompted us to investigate the effect of UV irradiation on UPy-based materials in more detail and elucidate a possible molecular mechanism from which the UV-induced changes originate. Herein we describe the study of several UPy-compounds before and after irradiation with UV. The applied analysis methods comprise fluorescence microscopy, photoluminescence spectroscopy, attenuated total reflectance Fourier transform infrared spectroscopy (ATR-FTIR), magic angle spinning nuclear magnetic resonance (MAS NMR), and gel permeation chromatography (GPC). Based on all these empirical data a mechanism for the UV-induced changes in UPy-biomaterials is proposed.

2. Results and discussion

In the following paragraphs, we use the UPy-polymers and UPy-model compounds shown in scheme 1 and discuss the following: Firstly, the initial observations of UV-induced effects in UPy-polymers **1**-**4** and UPy-model compound **5** were investigated by photoluminescence spectroscopy and ATR-FTIR. Secondly, studies were performed on UPy-polymer and UPy-model compounds to elucidate any form of UV-induced material degradation and dependency of UV-induced effects on UPy-dimer stacking. Thirdly, studies were performed to gain insight into a hypothesized relation between UV-induced changes and tautomerization of UPy-moieties using UPy-model compounds **9** and **10.** Finally, a mechanism for UV induced changes, based on the presented empirical data, is proposed.

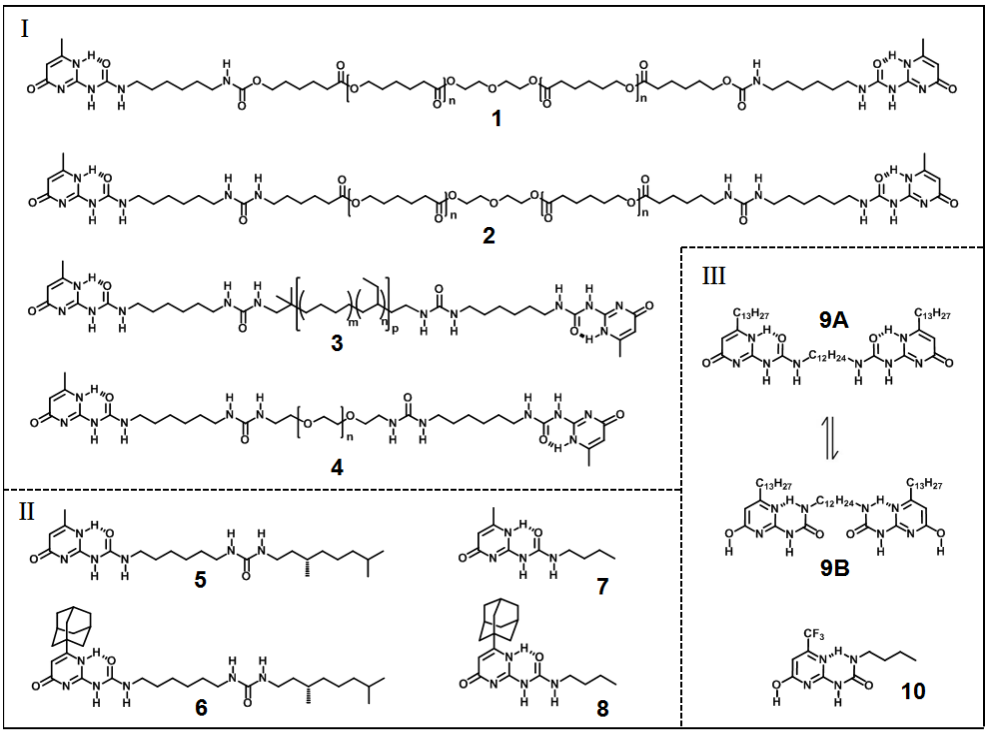

Scheme 1: *Chemical structures of telechelic UPy-functionalized polymers **1**-**4** and UPy-model compounds **5**-**10**.*

2.1 Initial observations of UV-induced changes in UPy-based materials

Fluorescence and changes in infrared spectra in UPy-polymers

In studies towards the application of UPy-functionalized polymer UPy-PCL (**2**, scheme 1-I) as cell-culture substrate,[8-10] the material was drop cast on a glass substrate to obtain

a thin film or electrospun to form a membrane consisting of microfibers. The films and membranes were exposed to light of a germicidal UV lamp for one hour, before application as cell-culture substrate. Surprisingly, substrates of **2** appeared to gain bright blue fluorescent properties after UV irradiation, as observed with fluorescence microscopy (Figure 1a). To elucidate whether this observation was a general phenomenon for UPy-functionalized polymers, **2** and three additional UPy-end functionalized polymers (**1**, **3** and **4**, Scheme 1-I) were studied by photoluminescence spectroscopy. UV-induced fluorescence intensity increase was observed in drop-cast samples of all four UPy-functionalized polymers (Figure 1b), which indicated that the fluorescence originated from a UV-induced change in the UPy-moiety. This was furthermore underlined by the absence of UV-induced fluorescence in polymers with similar structure as **3**, a poly(ethylene butylene) backbone, but which were non-functionalized (enol-terminated) or end-functionalized with a phenol-group instead of the UPy-urea functionality (data not shown).

Photoluminescence excitation and emission (PL/PLE) maxima for UPy-polymers **1**-**4** after UV-irradiation were observed around 345 and 400 nm, respectively. Nevertheless, the observed intensity of these maxima varied for the different UPy-polymers. Minor differences in sample thickness and UPy-content could potentially have caused variations in the observed fluorescence intensity. On the other hand, there seemed to be a consistent relation between UPy-polymer crystallinity and fluorescence intensity. For UPy-polymer **3**, with an amorphous poly(ethylene butylene) (PEB) backbone, the most intense fluorescence was observed, whereas the crystalline poly(ethylene glycol) (PEG)-based UPy-polymer **4** showed the lowest fluorescence intensity. UPy-polymer **2**, comprising of semi-crystalline polycaprolactone, UPy-functionalized via the same double hydrogen-bond forming urea-linker as **3** and **4**, showed average fluorescence intensity. However, when the linker was replaced by a urethane-linker increased fluorescence intensity was measured, as observed for polymer **1**. This urethane-linker only forms one hydrogen-bond and thus promotes UPy-dimer stack formation to a lesser extent compared to the urea-linker,[14]

The relation between UV-induced changes and the UPy-moiety in polymers **1**-**4**, was further underlined by ATR-FTIR spectra (Figure 2). After irradiation by UV the four UPy-polymers showed severe changes in the spectral parts that are specifically attributed to bonds in the UPy-moiety, in the form of disappearance, shifts and broadening of absorption bands. Furthermore, these spectral changes were found to become more pronounced after longer exposure of the UPy-polymers to UV light. The UV-induced IR spectral changes observed for **3** were very similar to the changes that were previously described for this polymer at elevated temperature.[15,16] However, those changes were found to be reversible upon cooling down, whereas here the changes continue to exist as they were observed after UV irradiation.

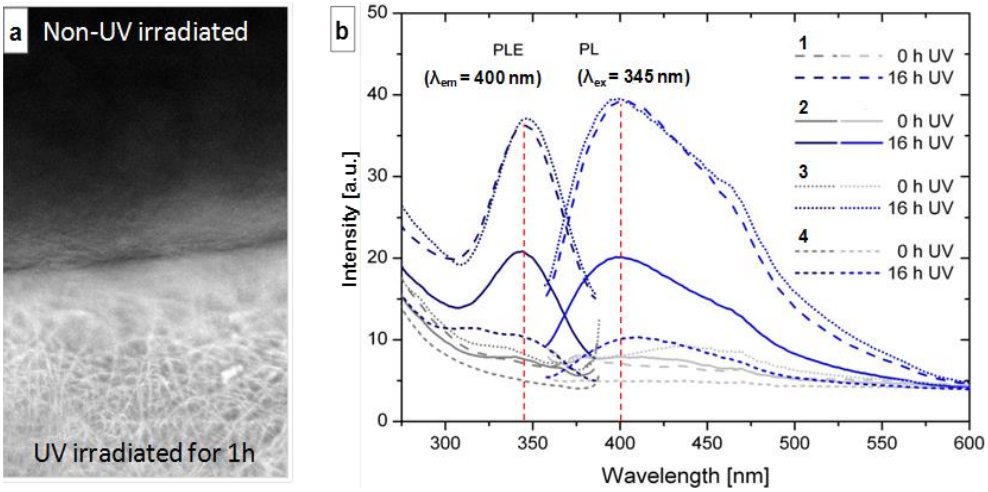

Figure 1. UV-induced fluorescence in UPy-polymers. *a) UV-induced fluorescence in a UPy-polymer was first identified by fluorescence microscopy. Here a microfibrous membrane of* ***2,*** *electrospun from HFIP, was cut in half. The lower half was irradiated with UV for 1 hour and subsequently imaged simultaneously with the non-irradiated half. b) PL/PLE spectra of UPy-polymers* ***1****-****4****. Drop-cast films were prepared from chloroform. Spectra were recorded of non-irradiated films and films irradiated with UV for 16 hours.*

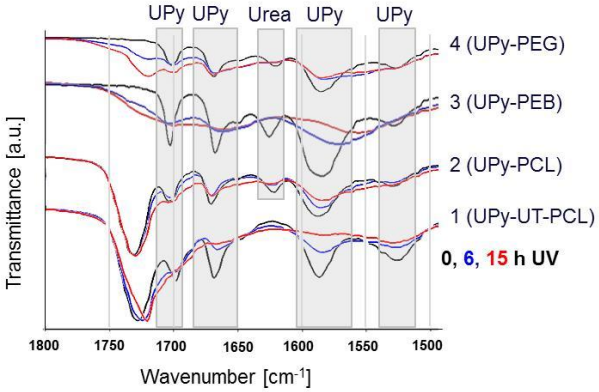

Figure 2. UV-induced IR-spectral changes in UPy-polymers. *Partial ATR-FTIR spectra of non-UV irradiated, 6 and 15 hours UV irradiated drop-cast films of UPy-polymer* ***1****-****4****. The spectral part shows the bands that are related with the UPy.*

UV-induced changes in UPy-model compound ***5***

UPy-model compound **5**, which consisted of a single UPy-moiety linked via a urea to a short aliphatic tail (Scheme 1-II), was studied to exclude interfering or shielding effects of the polymer backbones. These studies were performed on **5** in the solid state, as a thin layer of drop-cast crystalline deposit on glass coverslips.

Photoluminescence spectroscopy revealed a very pronounced UV-induced increase in fluorescence intensity of **5** (Figure 3b). After one hour of exposure to UV, clear fluorescence spectra were observed with excitation and emission maxima at 335 and 380 nm, respectively. The intensity of the spectra further increased and the maxima displayed slight red-shifts after longer UV-irradiation times. After 16 hours of UV irradiation, excitation and emission maxima were observed at similar wavelengths as for the UPy-polymers, at 345 and 400 nm, respectively. Furthermore, a shoulder at 465 nm appeared in the emission spectrum, which was also present in the spectra of the UV-irradiated UPy-polymers.

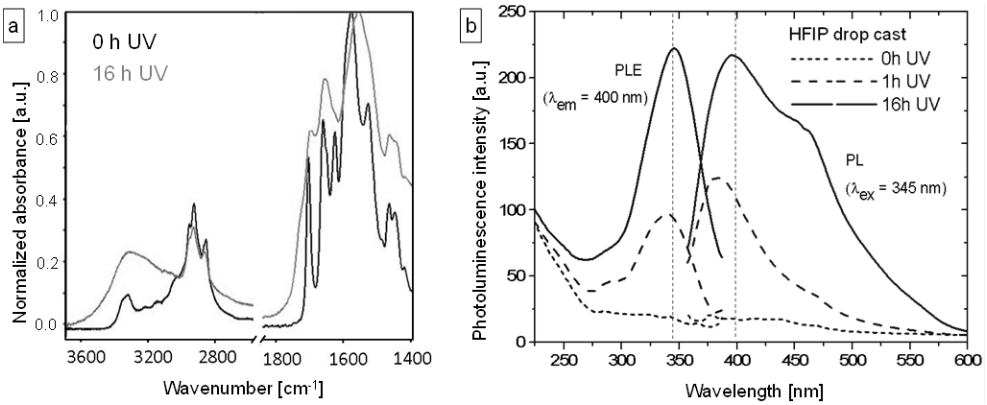

Figure 3. UV-induced spectral changes in 5. *ATR-FTIR spectra (a) and photoluminescence excitation and emission (PL/PLE) spectra (b) of UV-irradiated and non-irradiated drop cast samples of UPy-model compound **5**.*

ATR-FTIR showed clear spectral changes for drop-cast compound **5** after UV irradiation for 16 hours (Figure 3a). Signals between 1500 and 1700 cm^{-1}, which are related to the UPy-moiety, became less well-defined due to broadening and fusion. A distinct change was the band-shift from 1579 to 1552 cm^{-1}. This shift was also distinguished in the ATR-FTIR spectra of UPy-polymer **3**. Furthermore, the absorption band at 1622 cm^{-1}, attributed to strongly hydrogen-bonded urea-carbonyl,[17] disappeared. This was also seen for the three UPy-polymers with a urea-linker (**2**,**3**,**4**). Between 3000 and 3500 cm^{-1} a very broad signal appeared after UV irradiation of **5**. This effect was seen in all four UPy-polymers (1-4) as well (data not shown).

*Reversibility of UV-induced effects in UPy-model compound **5***

Drop-cast samples of compound **5** were treated in various sequences with UV irradiation, heat and solvent and monitored with fluorescence microscopy (Figure 4) and ATR-FTIR spectroscopy (Figure 5). Drop casting of **5** from HFIP on a glass substrate resulted in an opaque white, crystalline powdery deposit, which was non-fluorescent (1). This white, opaque drop cast transformed to a transparent film by heating up to the melt and

immediate cooling to room temperature (5). The effect of subsequent UV irradiation differed for the drop-cast crystalline and the transparent film as observed by fluorescence microscopy, but not according to ATR-FTIR. Although ATR-FTIR spectra showed similar UV-induced changes in both the transparent film (6) and the opaque crystalline form (2) of **5** (Figure 5c), it was observed that **5** only acquired a fluorescent property when irradiated with UV in the opaque crystalline form (Figure 4 (2)). This fluorescence could be reduced via the conversion to a transparent film by heat (3) as observed by fluorescence microscopy, but ATR- FTIR spectra showed limited reversed changes by this sample treatment (Figure 5a). Re-crystallization from HFIP, however, almost completely restored the material to its original, non-UV irradiated state, according to ATR-FTIR spectra (Figure 5b). Interestingly, the fluorescent property, reduced in the transparent film, appeared to be 'stored' in the material and was regained via this re-crystallization from HFIP (Figure 4 (4)). The non-fluorescent transparent film (5), did not acquire a fluorescent property after UV irradiation (6) although typical UV-induced IR spectral changes were observed (Figure 5c (6)). Also, after subsequent recrystallization from HFIP, the material appeared non-fluorescent (7). However, when UV-irradiated from this crystalline state, fluorescence was acquired (8).

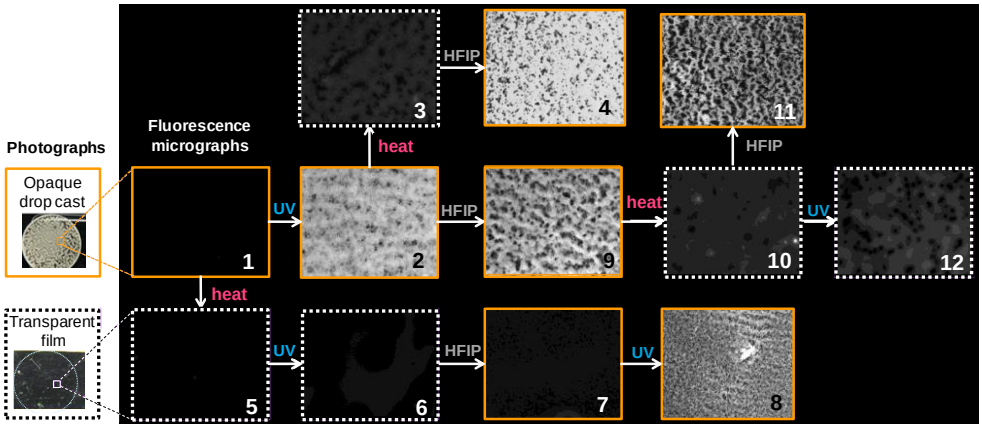

Figure 4. Switching of fluorescence and physical appearance of 5. *Photographs and fluorescence micrographs show the physical appearance (solid orange line indicates opaque crystalline deposit, dotted line indicates transparent film. A dark image indicates no fluorescence, whereas shades of gray up to white indicate increasing fluorescence intensities) and fluorescence intensity of drop-cast samples of **5** on glass coverslips. The samples were monitored throughout different sequential series of treatments with UV irradiation (16 h), heat (melt at 170 °C and immediate cooling down to room temperature) and solvent (application of a drop of HFIP followed by evaporation to air).*

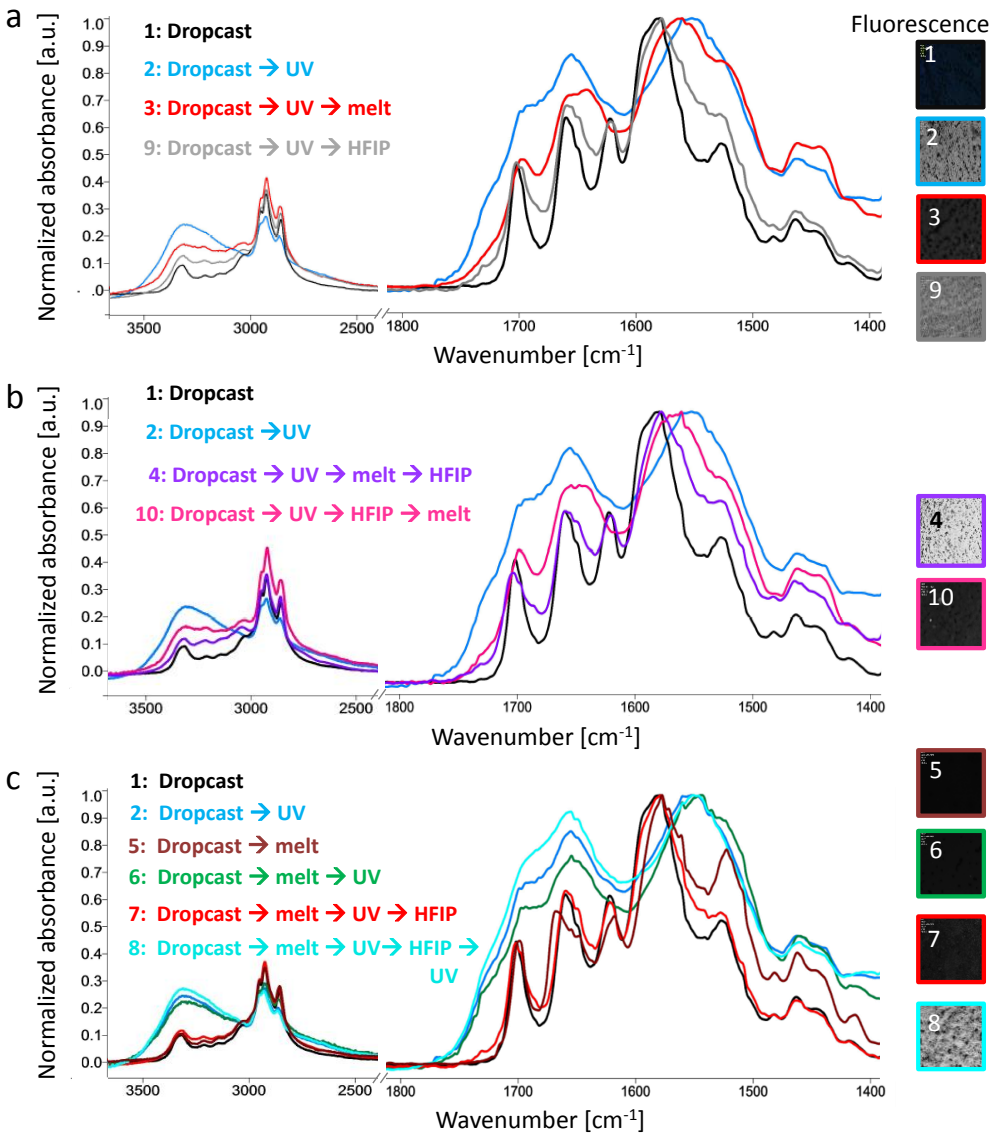

Figure 5. Switching of IR spectral changes in 5. *ATR-FTIR spectra and corresponding fluorescence micrographs of drop-cast samples of compound **5** treated with UV (irradiation for 16 hours), heat (melt at 170 °C and immediate cooling down to room temperature) and HFIP (a drop of HFIP is applied on the material and left to evaporate) in varying sequence. The numbers indicated correspond to the numbers in figure 4.*

The mismatch in reversibility of UV-induced changes in 5 observed by fluorescence microscopy and ATR-FTIR, suggest that we are looking at more than one (partially) reversible or switchable UV-induced effect. The observed UV-induced fluorescence could originate from a very small percentage of highly fluorescent compound. The fluorescence appears to be related to the crystalline state of UPy-moieties. The different spectral changes observed in ATR-FTIR are most probable the result of another, or possibly even multiple, UV-induced products.

2.2 Studies on UV-induced degradation and crosslinking in UPy-materials

Material degradation, such as crosslinking and backbone scission, are common effects in polymers when exposed to UV. In the following paragraphs, we discuss studies on UPy-polymers and UPy-model compounds to elucidate whether UV-induced degradation reactions occur in UPy-based materials.

Evidence of UV-induced crosslinking in UPy-polymer

UPy-polymer **3**, a PEB-UPy, showed relative bright fluorescence and severe IR spectral changes upon UV irradiation. This polymer was studied by GPC to elucidate changes in mass that could indicate UV-induced material degradation. The solubility of this UPy-polymer in chloroform was reduced after longer exposure to UV. Furthermore, slightly larger molecular weights were observed by GPC in the soluble fraction (Figure 6). These observations indicate some UV-induced crosslinking reaction in **3**, by which the solubility deviates as well.

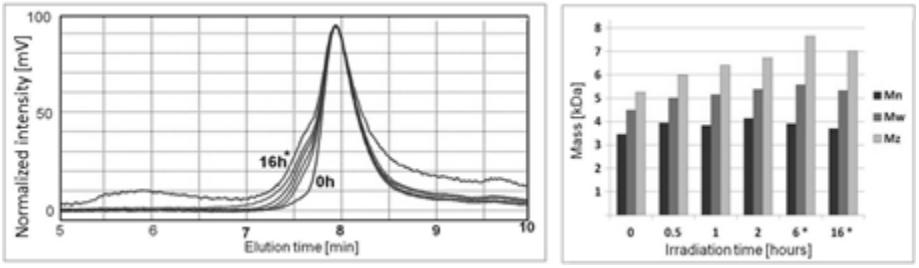

Figure 6. GPC indicates UV-induced mass increase in 3. *Drop-cast samples of **3** prepared from chloroform were UV irradiated for 0, 0.5, 1, 2, 6 or 16 and measured by GPC. Not all samples dissolved completely in the eluens (chloroform) during sample preparation for GPC. Especially the samples that were UV irradiated longer, dissolved poorly, (indicated with *). All samples were filtered before GPC measurement. The values measured by GPC only reflect the soluble fraction of each sample. GPC traces were normalized to maximum intensity to allow direct comparison of peak shape. With increasing UV-irradiation time a shoulder of faster eluting polymer species was observed. Calculated molecular weights (calibration via polystyrene standard) showed an overall increase for the soluble fraction of each sample, after longer UV irradiation.*

No evidence of UV-induced degradation of the UPy-moiety

A very broad absorption band appeared between 3000 and 3500 cm^{-1}.In ATR-FTIR spectra of both UV-irradiated UPy-polymers **1**-**4** (Figure 2) and UPy-compound **5** (Figure 3). This broad signal is usually attributed to free O-H and N-H. A UV-induced degradation reaction of the UPy-moiety, resulting in urea and 6-methylisocytosine was considered as possible mechanism for the formation of new free O-H and N-H. However, reference spectra of these compounds did not match the ATR-FTIR spectra of UV-irradiated UPy-compound **5** (Figure 7). Although both urea and 6-methylisocytosine showed signals in the region between 3000 and 3500 cm^{-1}, they are unlikely to result in the broad band observed for UV-irradiated **5** when superimposed. Furthermore, the shifted band at 1552 cm^{-1} present in UV-irradiated **5** is not represented in either of these suggested degradation products.

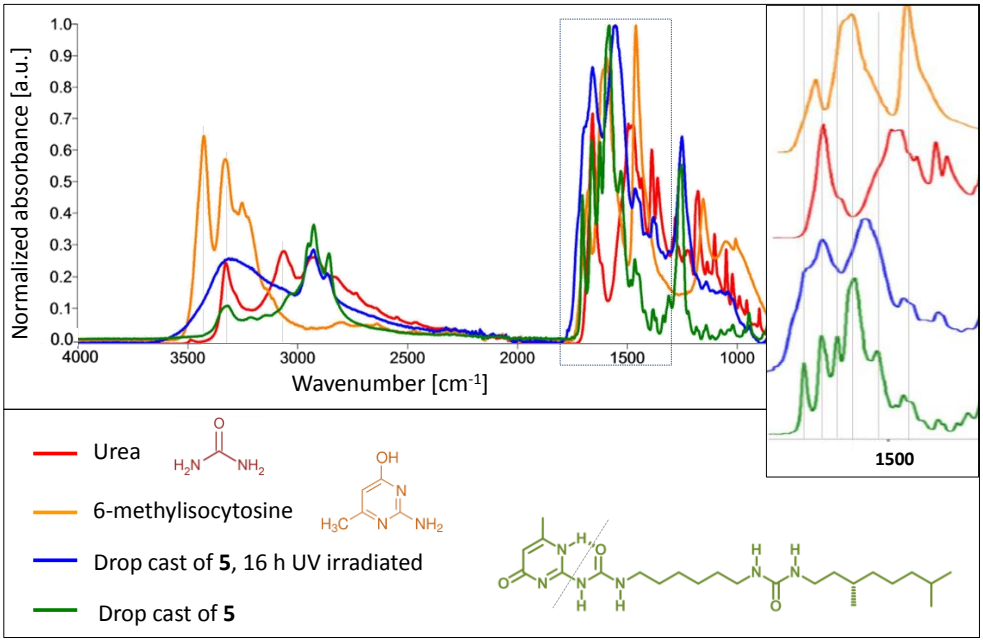

Figure 7. UPy-degradation studied by ATR-FTIR. *IR spectra of compound **5**, before and after UV-irradiation, compared to the spectra of possible degradation products; urea and isocytosine. The enlargement on the right displays a stacked representation of the spectra in the region between 1300 and 1800 cm^{-1}.*

*Evidence of UV-induced crosslinking in UPy-model compound **5***

Solid state MAS ^{1}H NMR was performed at samples of **5**, comparing non-irradiated white, crystalline powder with material exposed to UV for 16 hours. The latter colored slightly yellowish. Despite this visually observed change, no UV-induced shifts were observed for the small UPy-related signals between 5 ppm and 14 ppm (Figure 8b).

Interestingly, a shift of these signals was observed after heating non-irradiated compound **5** at 110 °C for one hour. Spectra recorded at an elevated temperature (60 °C) induced sharpening of the broad and intense signal between 0 and 2 ppm. This signal is attributed to the aliphatic parts of **5**. In UV-irradiated material this peak appeared slightly broader compared to non-irradiated material (Figure 8c). This effect is comparable to observations by MAS NMR for peroxide-crosslinking of EPDM rubber,[18] in which the peak broadening indicated impaired mobility of the aliphatic chains. This hence hints towards some form of UV-induced chemical reaction in UPy-compound **5**. This is in line with the observation of reduced solubility after exposure of **5** to UV for 16 hours.

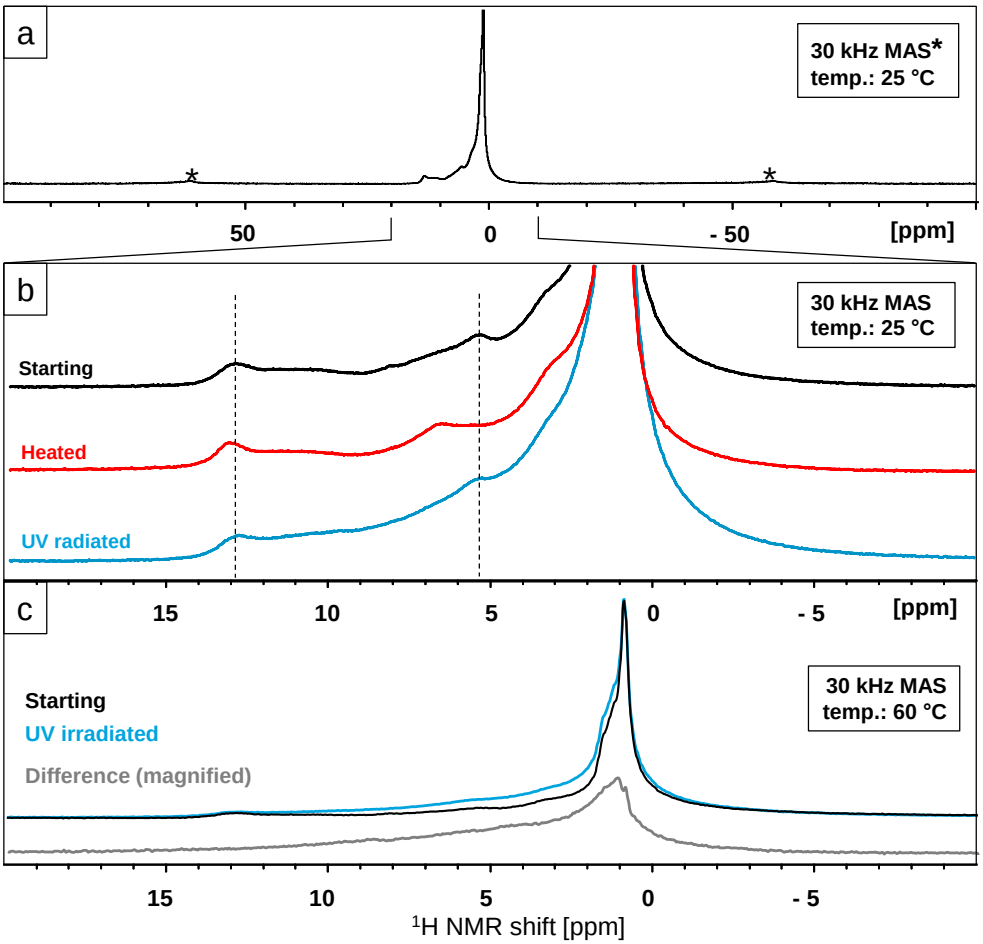

Figure 8. Solid state ^{1}H NMR spectra of 5. *Spectra of **5** were recorded at magic angle spinning (MAS) frequencyof 30 kHz. The material was untreated, UV-irradiated for 16 hours or heated up to 110 °C for 1 hour and quickly cooled to room temperature. a) The total spectrum of the starting material. Spinning side bands are marked by *. b) Samples measured at 25 °C. c) Samples measured at elevated temperature (60 °C) to increase aliphatic chain mobility and to narrow the related peak.*

Studies on the relation between UV-induced effects and UPy-dimer stacking

A molecular mechanism for crosslinking of UPy-moieties was proposed, based on the structural similarity of the UPy-moiety and DNA pyrimidine-based building blocks. As mentioned in the introduction, UV irradiation is known to cause a 2+2 cycloaddition between two adjacent thymines, or a thymine and cytosine, in a single DNA-strand of the double alpha helix. For a similar process to occur in the UPy-based materials, a close proximity of UPy-moieties in the UPy-dimer stack was proposed to be required.

To study the dependence of UV-induced effects on UPy-stacking, a panel of four UPy-model compounds was studied; model compound **5** and three additional compounds (**6**-**8**) with varying impaired capacity of UPy-dimer stack formation compared to **5** (Scheme 1-II). The design of these compounds was based on two principles. Firstly, the exclusion of the adjacent urea-linker omits additional hydrogen bonding that favor stack formation in compound **5.** Secondly, the addition of a bulky adamantyl-substituent at the 6-position on the pyrimidinone ring prevents UPy-dimer stack formation via steric hindrance.[19]

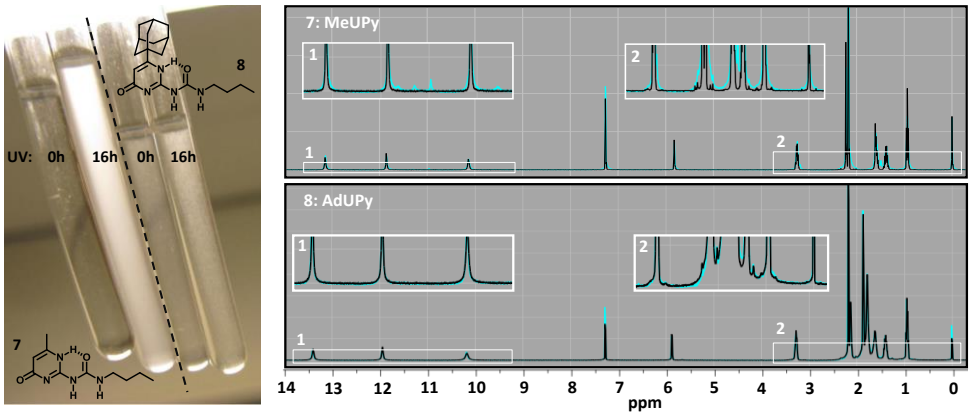

Figure 9. NMR study on 7 and 8. *A photograph of solutions of non-UV irradiated and UV-irradiated compound **7** and **8** in $CDCl_3$. The scattering of light, observed in the tubes containing the UV-irradiated samples, reveals the presence of solid particles in solution and hence indicate that solubility is affected by UV-irradiation. This points towards some form of UV-induced crosslinking in the UPy-moiety. ^{1}H NMR spectra of the samples however show no or only minor changes, which do not indicate the formation of newly formed covalent bonds.*

Evidence of UV-induced crosslinking was observed for chloroform soluble compound **7** and **8**, which both became partially insoluble after irradiation with UV (Figure 9a). This effect was more severe for compound **7**, MeUPy. ^{1}H NMR spectra (which only represent the soluble fraction) of the non-irradiated and UV-irradiated AdUPy **8** did not reveal any changes. The spectrum of UV-irradiated compound **7** was of lower quality due to the minimal amount of soluble material. Nevertheless, it did reveal minor changes between 9 and 12 ppm, where the signals of hydrogen bonded protons are located. This might indicate the presence of a small amount of different UPy-tautomer species. Nevertheless, these spectra did not show signs of newly formed covalent bonds. Hence, these results

neither allowed the identification of the UV-induced crosslinked product (Figure 9), nor supported the presumably UPy-dimer stack dependent 2+2 cycloaddition as hypothesis for UV-induced crosslinking of the UPy-moieties.

The fluorescence observed might still be related to the UV-induced chemical crosslinking products. However, UPy-tautomerization is another molecular mechanism that is possibly involved. To allow comparison with compound **5** (Figure 3) and to gain insight into the effect of UPy-dimer stacking on UV-induced fluorescence and IR spectral changes, the three additional model compounds **6**-**8** were subjected to further studies (Figure 10). Model compound **6**, with similar structure as **5**, except for the adamantly-substituent at the 6-position on the pyrimidinone ring, was drop cast from HFIP. Photoluminescence spectra showed clear fluorescence intensity increase after longer UV-irradiation time (Figure 10b). Compared to the spectra of compound **5**, the observed intensities for **6** after UV irradiation were lower and a smaller Stokes shift was measured. The emission maximum was, comparable as for **5**, observed around 400 nm. However, the excitation maximum was found at 375 nm instead of 345 nm. ATR-FTIR spectra of **6** (Figure 10a) showed very similar UV-induced changes compared to **5**; a clear shift of the signal at ~1580 cm^{-1} to a lower wavenumber, and the appearance of a very broad signal between 3000 and 3500 cm^{-1}. Interestingly, the strongly hydrogen-bonded urea carbonyl-related signal that was observed in the non-irradiated compound **5** at ~1622 cm^{-1} (and which disappeared after UV irradiation) was not observed in the non-UV irradiated compound **6**. Probably, the anticipated effect of the adamantly-substituent (prevention of UPy-dimer stack formation), also prevents hydrogen-bonding of the urea. Logically, this absorption band at ~ 1622 cm^{-1} was absent in the spectra of compound **7** and **8** (Figure 10c and e), which lack the urea-linker. The signal at ~1580 cm^{-1} did not shift for both adamantly-substituted compound **7** and methyl-substituted compound **8**. Remarkably, the broad signal between 3000 and 3500 cm^{-1} was measured for UV-irradiated compound **7**, but not for **8**.

PL/PLE spectra of compound **7** and **8** (Figure 10d, f) revealed opposite drop cast solvent-dependent UV-induced fluorescence intensity. For compound **7**, the intensity after 16 hours exposure to UV was comparable to that of compound **6** when both drop cast from HFIP. However, when **7** was drop cast from chloroform and exposed to UV for 16 hours, a 3-4 fold increase in UV-induced fluorescence intensity was observed compared to samples drop casts from HFIP. This was opposite for **8**, which showed an overall increased signal after UV irradiation when drop cast from HFIP, compared to drop casts from chloroform. The shape of excitation and emission spectra for compound **8** (spectra recorded at the excitation and emission maxima as determined for compound **5**) deviated strongly from the observed spectra of compound **5**-**7**. In the excitation spectrum of compound **8** prior to UV exposure, a clear peak was observed around 290 nm. In the emission spectrum a maximum was observed at ~ 475 nm. This is the same wavelength as the shoulder in the emission spectra of UV-irradiated compound **5** and UPy-polymers **1**-**4**.

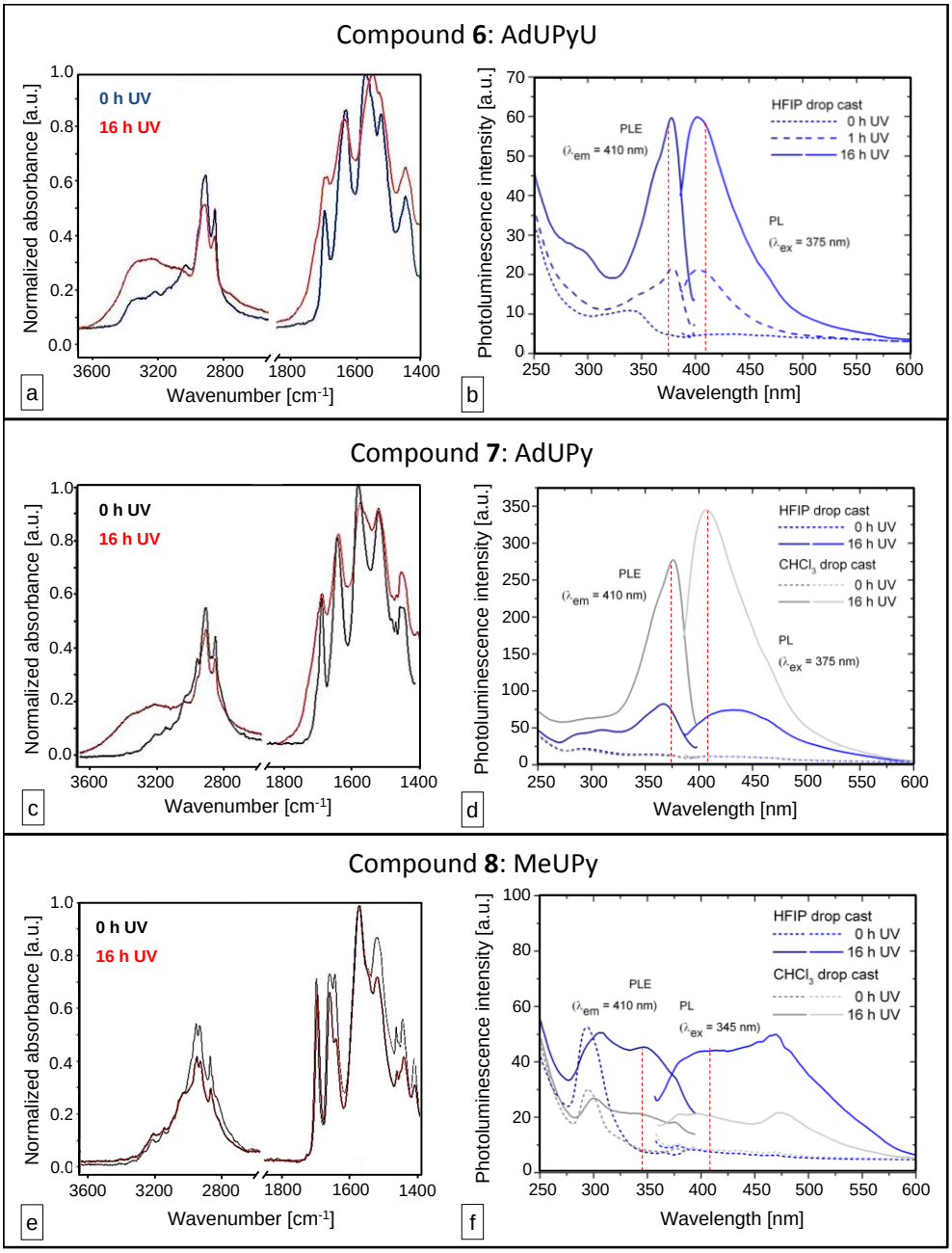

Figure 10. UV-induced spectral changes in 6-8. *FT-IR spectra (a, c, e) and photoluminescence excitation and emission (PL/PLE) spectra (b, d, f) of UV-irradiated and non-irradiated drop-cast samples of UPy-model compounds **6-8**.*

2.3 Studies on UPy-tautomer related fluorescence

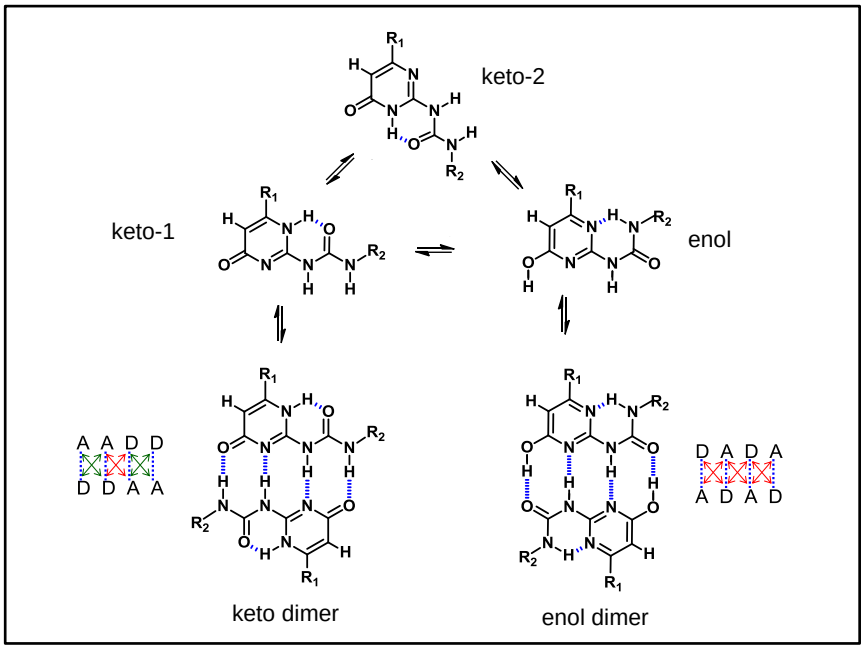

Scheme 2. UPy-tautomers and dimerization. *Equilibria between monomers and dimers of the three known tautomeric forms of ureido-pyrimidinone (UPy). Secondary electrostatic repulsive interactions between two hydrogen bond donors (D) or two hydrogen bond acceptors (A) in a dimer are indicated by the red arrows. (based on Beijer et al. 1998)*[20]

The UV-induced changes observed in the UPy-related FTIR spectral region of UPy-polymers and UPy-model compounds, were hypothesized to relate with a shift in tautomeric ratio. In the solid state, UPy-moieties normally exist as dimers, either as enol or keto-1 tautomeric homodimer (Scheme 2). Both these tautomers have a distinct ATR-FTIR spectrum.[20,21] Keto-1 dimerizes via a DDAA (D, H-bond donor; A, H-bond acceptor) hydrogen-bond array, whereas the enol-tautomer dimerizes via an ADAD array. In general, the DDAA array forms the more stable dimer, as the alternating hydrogen-bond donors and acceptors in the ADAD array lead to a higher number of secondary electrostatic repulsive interactions, which weaken the hydrogen bonds.[20,22] Hence, in the dimerized form, the keto-1 tautomer is generally the predominant tautomer as it is stabilized by the favorable dimerization. The third UPy-tautomeric form (keto-2) is thermodynamically the most stable tautomer. Keto-2 cannot dimerize and is only favored when no intermolecular and intramolecular hydrogen bonds can exist, such as in presence of a strongly hydrogen bond breaking solvent like DMSO,[20] or when heated. However, UPy-tautomeric equilibria not only depend on self-association, temperature and solvent polarity. The predominant tautomeric form depends on a complicated interplay of many different parameters, which

also includes substituent effects, both at the 6-position on the pyrimidinone ring and at the ureido group,[20] and stacking interactions.[23] Since tautomeric ratios can be affected by external factors such as solvent and temperature, and are dependent on subtle molecular changes, it is likely that UV-irradiation can have an effect on these equilibria as well. Furthermore, the effect of heat and solvent on UV-induced fluorescence and ATR-FTIR spectral changes supports a relation to UPy-tautomer.

UPy-tautomer related fluorescence in the solid state

To gain insight into a possible relation between UV irradiation, UPy-tautomeric form in the solid state and fluorescence, compound **9** was studied. Compound **9** can be switched from keto-1 to enol by the application of heat (Figure 11a).[24] Upon cooling, the compound is trapped in the enol-tautomeric form. This allowed for controllable and direct comparison of both tautomers. The heat-induced tautomer transition was monitored by ATR-FTIR (Figure 11d). The keto-1 tautomer (**9A**) showed four distinct signals in the spectral region between 1500 and 1720 cm^{-1}. After short heating up to melt and cooling down to room temperature, three distinct signals in the same spectral region indicated the transition towards UPy-enol tautomer (**9B**).[24] Photographs were taken of both **9A** and **9B** in daylight and UV light (254 nm, Figure 11b). **9A**, a white powder in daylight, appeared completely dark when visualized under UV light. UPy-enol compound **9B** on the other hand showed clear fluorescence under UV light, as observed by eye. PL/PLE spectra of **9** confirmed this fluorescence increase after melting the material (Figure 11c). This observation directly linked UPy-fluorescence to the UPy-enol tautomer, although no UV irradiation is needed to generate this fluorescent species. To connect this to the observations of UV-induced fluorescence in the UPy-materials drop-cast compound **9A** was irradiated with UV light for 16 hours and subsequently measured by ATR-FTIR (Figure 11d). The spectrum showed a mixture of the keto-1 and UPy-enol specific signals in the region between 1500 and 1720 cm^{-1} confirming that UV irradiation can induce a UPy-keto to enol tautomer shift. One distinction when comparing the IR spectrum of UV-irradiated compound **9A** with non-irradiated **9A** and heated **9B**, was the appearance of the broad signal between 3000 and 3500 cm^{-1}. This observation forms a striking similarity with spectra of UV-irradiated UPy-polymers **1**-**4** (Figure 2) and UPy-keto model compounds **5**-**7** (Figure 3, 10). It suggests that this broad band is the result of additional UV-induced products, other than fluorescent UPy-enol.

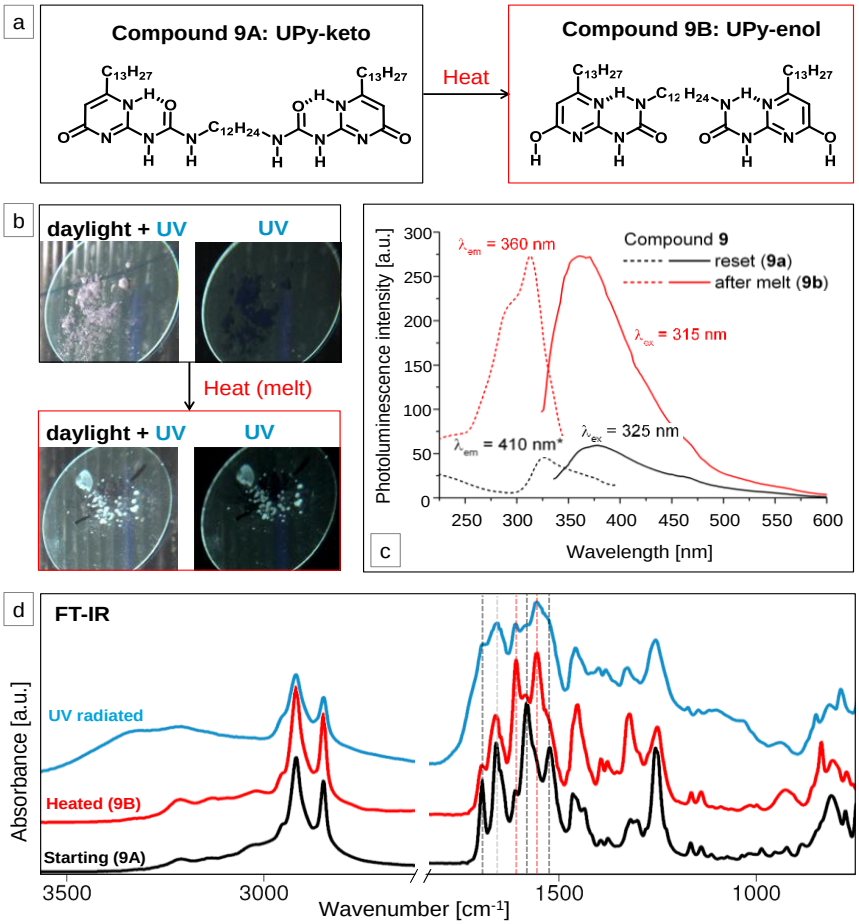

Figure 11. Tautomer switching of 9. *a) Model compound **9** converts from keto-1 (**9A**) to enol tautomer (**9B**) when heated. Upon cooling the compound remains trapped in the UPy-enol tautomeric form **9B**.[23] b) Photographs of **9A** and **9B**, taken in daylight and UV-light. c) PL-PLE spectra of **9A** and **9B**. d) ATR-FTIR spectra of compound **9A** and **9B** show distinct absorption bands (indicated by the dotted lines). UV-irradiated compound **9** shows a mixture of these bands.*

UPy-tautomer related fluorescence in solution

The results with compound **9** provided compelling evidence of UPy-enol related fluorescence in the solid state. We were eager to see whether this relation would also be observed in solution. Fluorinated UPy-model compound **10** exists for > 99% as UPy-enol dimer when dissolved in chloroform, whereas the methyl-substituted compound **8** forms > 99% UPy-keto dimer (determined by ^{1}H NMR in $CDCl_3$).[20] Indeed, fluorescence intensity was observed to be much higher for UPy-enol compound **10** compared to UPy-keto **8**; maximum emission was ~16.5 times higher when both compounds were dissolved in chloroform at a concentration of 5 mM (Figure 12).

Additional studies showed effects of solvent polarity on the fluorescence excitation and emission maxima of **10** in solution. A clear bimodal emission spectrum in presence of methanol, with maxima at 330 and 400 nm, indicated the coexistence of two fluorescent species. Only the emission around 330 nm was measured for **10** in the solid state after heat treatment (data not shown).

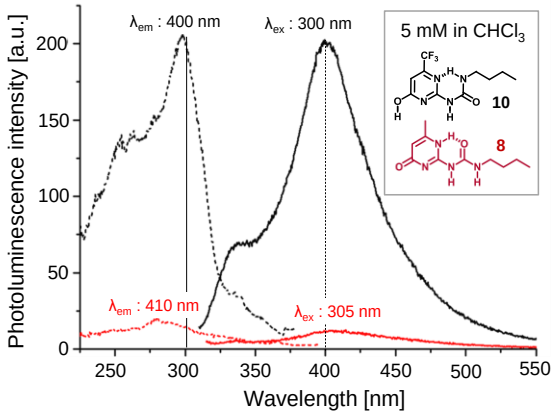

Figure 12. UPy-enol fluorescence in solution. *PL/PLE spectra of UPy-compound **8** (keto) and **10** (enol) in solution, 5 mM in chloroform.*

2.4 Hypothesis for photo-enolization of UPy-moieties

How exactly UV irradiation can cause a tautomer shift or can facilitate a more stable environment for fluorescent UPy-enol to prevail, is still unclear. At this point we can only speculate on the molecular picture from which the described observations originate. Nonetheless, we endeavor to coin a hypothesis based on similarities with known molecular systems. Without going into detail on all separate observations described in the present work, we see possible analogies with compounds capable of hydrogen bonding that are known to undergo excited state proton transfer (ESPT). As a result of the proton transfer, a tautomer transition takes place. ESPT is a fast transition from the excited normal state (n*) to the excited tautomer state (t*), which occurs in the order of pico-seconds.[25] ESPT can occur intramolecular or intermolecular and depending on the starting tautomer results either in enolization or ketonization. This mechanism of photo-tautomerization is well-known in fluorescent or phosphorescent dyes with typical large Stokes shifts and in photostabilizing compounds.[26]

For our UPy-dimers we propose an *inter*molecular double proton transfer. Ten electron movements result in the exchange of two protons, which converts the DDAA-4(1H)keto-dimer, without a true topological change, into the ADAD-enol-dimer with enolized urea (Scheme 3, route I). The current study on UPy-materials only focused on identification of changes that are observed after UV irradiation, hence stable or possibly permanent changes induced by UV. Time resolved studies are outside the scope of the current work, but would allow for better insight into fast occurring molecular changes, such as the identification of ESPT.

The presented results indicate that photo-enolization of UPy-moieties occurs and that at least part of the enol tautomers that are formed are stable. If ESPT is indeed involved in this mechanism, this means that the reverse proton transfer (in the ground state) does not spontaneously occur for these stable enolized molecules (Scheme 3, route II). This implicates that the UPy-moiety is not suitable as endurable photostabilizing agent in polymers. The exceptional stability of the UV-induced fluorescent species was underlined by reversibility studies on compound **5** (Figure 4). Although UV-induced fluorescence in the crystalline state of the material vastly decreased when converted to a transparent film by application of heat (3), fluorescence was regained upon recrystallization from HFIP (4). This was clearly evidenced by live fluorescence microscopy monitoring during HFIP evaporation (Figure 13). In contradiction, UV-induced changes as observed by ATR-FTIR did show reversibility by the application of solvent, whereas the effect of heat was minimal (Figure 5a). Co-existence of highly fluorescent UPy-enol dimer species together with more common UPy-keto-1 dimers could be envisioned. Previous studies have shown that mixed stacks of both tautomer-dimers occur.[23]

Besides stability of the fluorescent UPy-species, the results with compound **5** furthermore imply that fluorescence is enhanced in the crystalline state, or reduced in the amorphous state. Typically fluorescence is enhanced by molecular rigidity,[27] as this decreases non-radiative decay. Both intramolecular and intermolecular hydrogen bonding in UPy-moieties enhance structural rigidity. Furthermore, UPy-dimers can stack and form highly ordered rigid structures. Although molecular aggregation is known to induce static quenching in many cases, highly ordered, rigid stack formation can also result in an increase in fluorescence intensity. This is for example seen for bipyridine systems, such as 3,3'-bis(acylamino)-2,2'-bipyridine and 2,2'-bipyridine-3,3-diol, in which a double proton transfer leads to fluorescence, which is enhanced by the formation of rigid aggregates.[28] Such aggregate dependent fluorescence intensity could explain why certain factors showed to have an effect on the observed UV-induced fluorescence. Examples of such factors are the polymer backbone in UPy-polymer 1-4 and the UPy-substituent and drop-cast solvent for model compound **7** and **8**.

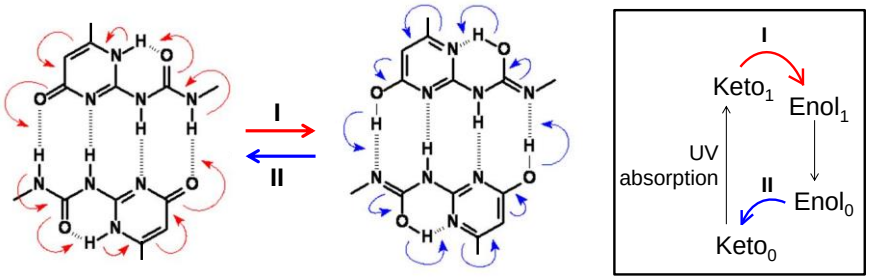

Scheme 3. Hypothesized photo-enolization of UPy-moieties. *The hypothesized tautomeric switch between the AADD-4(1H)keto-dimer and the ADAD-enol-dimer with enolized urea function. Enolization (I) is hypothesizd to occur via an excites state intermolecular double proton transfer, while II would represent the reverse proton transfer in the ground state.*

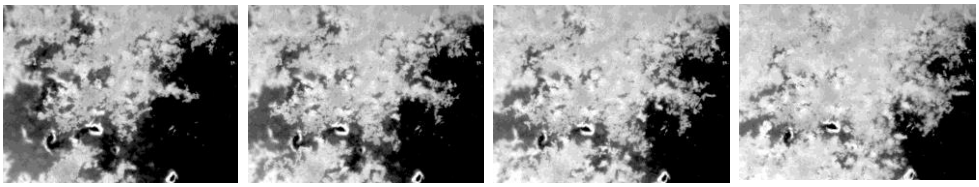

Figure 13. Crystallinity related fluorescence in 5. *Sequential fluorescence micrographs (from left to right) of drop cast compound **5** during recrystallization from HFIP. The sample was originally drop cast from HFIP on a glass cover slip to yield a non-fluorescent crystalline deposit, then irradiated by UV for 16 hours by which the material acquired a fluorescent property, followed by heating up to melt which changed the fluorescent crystalline material to a low or non-fluorescent transparent film. After that, a drop of HFIP was applied on top of the film. Upon evaporation of HFIP, the material recrystallized.*

Next to UV-induced enolization and fluorescence, evidence for UV-induced crosslinking was found, both for UPy-polymers and UPy-model compounds. From the presented results we cannot conclude a relation between the two effects. Probably both UV-induced processes, enolization and crosslinking, coincide without being related. The observations for model compound **4**, plea for such separation of UV-induced processes in UPy-moieties. This compound showed deviating UV-induced fluorescence and IR spectra compared to model compounds **1**-**3**, whereas severely reduced solubility after UV irradiation did indicate crosslinking.

3. Conclusions and discussion

UPy-based supramolecular materials form a promising class of new biomaterials. Sterilization by irradiation with UV light was observed to induce changes in UPy-based biomaterials. The results presented here revealed: I) UV-induced changes specifically related to the UPy-moiety. These were manifested in the form of fluorescence, changes in ATR-FTIR spectra, and II) reduced solubility. The latter indicated photocrosslinking upon exposure to UV, which is a general effect on organic compounds and hence not surprising for the UPy-moiety. No evidence for a 2+2 cycloaddition reaction, which was hypothesized in analogy with UV-induced DNA defects, could be confirmed based on the empirical data presented herein. III) Fluorescence in UPy-moieties revealed to be related to the UPy-enol tautomer. IV) UV-induced enolization of the UPy-moieties was hypothesized to occur via an excited state intermolecular double proton transfer. The presented data support this hypothesis, but additional time-resolved experiments would be needed for absolute confirmation.

Photo-tautomerization has to our knowledge not been described before for the UPy-moiety. Hence, the results presented and discussed here lead to deeper understanding of the already extensively studied UPy-moieties. This knowledge is important for the

successful application of UPy-based systems and materials. UPy-tautomerism influences the association constant and the lifetime of UPy-dimers and hence affects the 'supramolecular synthesis' and dynamics of systems based on this interaction. In UPy-biomaterials, both the supramolecular polymerization and biofunctionalization rely on UPy-dimerization. In general, materials based on dynamic, supramolecular interactions such as the UPy-moiety, are considered more responsive towards their environment compared to covalent materials. In biomaterials, this implies opportunities towards mimicry of dynamic natural ECM, but also induces a higher level of complexity in controlling the material properties. The presented findings demonstrate that in principle every handling or small change in the materials history might induce a change at the molecular level, relevant to the final application. This underlines the awareness required when working with supramolecular biomaterials to enable controllable and successful application in the field of tissue engineering and regenerative medicine.

4. Acknowledgements

We thank Jef Vekemans for useful discussions and the proposed mechanism for UV-induced UPy- tautomerization. Pieter Magusin is acknowledged for his help with solid state NMR measurements, Jolanda Spiering, Serge Söntjens and Felix Beijer for providing compounds.

5. Experimental section

Materials. The synthesis of all compounds used is described in Chapter 2.

Drop cast preparation and UV irradiation. Materials were drop cast from ~ 30 uL HFIP or chloroform on glass 12 or 13 mm Ø coverslips to yield homogeneously dispersed films or crystalline deposits. UPy-polymers **1**-**4** were drop cast from chloroform 10 mg/mL and all yielded transparent films. UPy-model compound **5** and **6** were only drop cast from HFIP (did not dissolve well in $CHCl_3$), compound **7** and **8** were drop cast from both HFIP and chloroform. Model compound drop casts were prepared from 0.15 M solutions. For UV irradiation samples were placed for the indicated time under a germicidal UV lamp (Osram, HNS 30W G13, 13.4 W radiated power UVC 200-280 nm, with 90% of relative spectral radial power at 254 nm) at a distance of 10-20 cm, inside a lamellar airflow cabinet (constant air flow of ~0.2 m/s).

Infrared spectroscopy. Infrared spectra were recorded on a Fourier transformed infrared spectrometer (Perkin Elmer Spectrum Two, with a Universal ATR sampling Accessory and diamond crystal, Perkin Elmer Instruments, The Netherlands). Transmission spectra were recorded at room temperature in the range from 4000–450 cm^{-1} at a resolution of 4 cm^{-1} and with an accumulation of 4 scans. A sample, consisting of a drop cast film of material on a glass coverslip was placed on the crystal and covered with a glass slide. To achieve good contact between the sample and the crystal, force was applied on top of the glass slide. To allow for better comparison of spectra with varying

intensity, absorption spectra were normalized to the maximum intensity peak (in the region of interest).

Photoluminesce spectroscopy (solid materials). Photoluminescence excitation and emission (PL/PLE) spectra of solid materials were measured on a JASCO fluorescence spectrometer FP-6500, equipped with a solid sample attachment (FDA-430, JASCO) to hold the cover slip samples. Spectra were recorded at room temperature.

Photoluminesce spectroscopy in solution. Solutions of 5 mM 8 and 10 were prepared in chloroform. Solutions were transferred to a quartz cuvette with 10 mm pathway (Hellma). Fluorescence excitation and emission spectra were recorded on a Carry Eclips spectrophotometer (Varian) at room temperature. Excitation and emission slit were both set at 5 nm, data acquisition settings at 30 nm/min scan rate, 0.5 nm data interval and 1 sec averaging time.

Fluorescence microscopy. To get an initial idea of fluorescence intensity and excitation and emission wavelengths, the samples were visualized with fluorescence microscopy. Fluorescence micrographs were recorded on a Zeiss Axio Observer D1 microscope equipped with a Zeiss AxioCam Mrm camera and automated reflector shutter, controlled by Axiovision software (Zeiss). A mercury short ARC lamp HXP (Osram) was used in combination with fluorescence filtersets (Zeiss). Samples of **5** on glass coverslips were imaged using 1000 ms exposure time for each of the following filters: 49 DAPI (λ_{ex}: 335-383 nm, beamsplit: 395 nm, λ_{em} 420-470); 47 HE CFP (λ_{ex}: 424-448 nm, beamsplit:455 nm, λ_{em}: 460-500), 48 CFP/YFP (λ_{ex}: 426-446 nm, beamsplit: 455 nm, λ_{em}: 520-550), 38 HE GFP (λ_{ex}: 450-490 nm, 495 nm, λ_{em}: 500-550 nm); 46 HE YFP (λ_{ex}: 488-512 nm, beamsplit: 512 nm, λ_{em}: 512-550 nm); 43 HE Ds Red (λ_{ex}: 538-562nm, beamsplit: 570nm, λ_{em}: 570-640 nm). The images obtained with each separate filterset were overlayed to give a representative idea of total fluorescence intensity over the whole measured spectra.

Gel permeation chromatography. GPC was performed on a Shimadzu 10AD VP liquid chromatograph equipped with a PLgel 5 µm Mixed-C and PLgel 5Mm Mixed-D column, a Shimadzu SPD M10A VP Diode Array Detector and a Shimadzu RID 10A Refractive Index Detector. Samples were prepared by dissolving ~10 mg in 1 mL THF $CDCl_3$. For UV irradiated samples, the material was first drop cast on a glass surface, irradiated and then dissolved.

Solid state magic angle spinning (MAS) NMR. Solid state NMR spectra were recorded on a Bruker DMX500 spectrometer. Samples were prepared as follows. Material was dissolved in HFIP, drop cast in two big glass petridishes and dried to air at room temperature to yield homogeneously dispersed crystalline deposits. Residual solvent was removed *in vacuo* at 40 °C for 4 hours. The resulting thin and even layer of white crystalline powder in one petridish was exposed to UV light, by placement under a germicidal lamp at a distance of ~8 cm of the bulb, for 16h. The non-irradiated powder and irradiated powder were scraped from the dishes. (The UV-irradiated powder colored slightly yellowish compared to non-irradiated powder. IR spectra of the powders corresponded with spectra recorded of previous samples of 5 prepared on coverslips.) 2.5 mm rotors of commercial Bruker ultra-fast MAS probe were filled with powder, 4.1 mg of non-irradiated powder and 6.7 mg of UV-irradiated powder. Solid state NMR spectra were recorded at ^{1}H Larmor frequency of 500.1 MHz. MAS frequency was set at 30 kHz at 25 °C or 20 kHz for spectra recorded at 60 °C. The 90° pulse length was 2 ms, 128 scans (t1-increments) were acquired per spectra. TMS and/or adamantane were used as standard to determine peak positions. Additional spectra of the non-irradiated sample were taken, after heating the sample (inside the rotor) at 110 °C in a hot air oven for 1 hour.

Proton nuclear magnetic resonance (1H NMR). Spectra were recorded on a 400 Varian MR 400 MHz spectrometer. Proton chemical shifts are expressed in ppm relative to tetramethylsilane (TMS).

Samples were prepared in $CDCl_3$. Splitting patterns were assigned as a singles (s), doublet (d), triplet (t), or a multiplet (m).NMR

Heat to melt. Samples were heated up to melt by sliding the coverslip with UPy-material on top, over a Kofler bank (Reichert Jung). Opaque white drop cast samples of compound **5** were melted at 180-190°C, kept at this temperature position for ~10 seconds and allowed to cool to room temperature, to yield a transparent film. The powder of compound **9A** was heated at 130 °C to allow transition to **9B**.

Reversibility study of UV-induced effects. Compound 5 was drop cast from HFIP on glass 12 mm Ø cover slips, leaving a thin layer of crystalline white material (0.3-0.4 mg on each glass). From there different samples were treated in a different sequence of three different handlings; UV irradiation, heat up to melt and solvent application. UV irradiation and heat to melt were performed as described before. Solvent application was done by dripping 20 uL HFIP on top of the material. The HFIP, which immediately spread out over the entire surface of the sample, was left to evaporate at room temperature.

6. References

(1) Francesco Tessarolo; Giandomenico Nollo. Sterilization of Biomedical Materials. In *Encyclopedia of Biomaterials and Biomedical Engineering*; Informa Healthcare, 2008; pp. 2501–2510.

(2) Cadet, J.; Sage, E.; Douki, T. Ultraviolet Radiation-Mediated Damage to Cellular DNA. *Mutat. Res. Mol. Mech. Mutagen.* **2005**, *571*, 3–17.

(3) Cadet, J.; Mouret, S.; Ravanat, J.-L.; Douki, T. Photoinduced Damage to Cellular DNA: Direct and Photosensitized Reactions†. *Photochem. Photobiol.* **2012**, *88*, 1048–1065.

(4) Dankers, P. Y. W.; van Luyn, M. J. A.; Huizinga-van der Vlag, A.; van Gemert, G. M. L.; Petersen, A. H.; Meijer, E. W.; Janssen, H. M.; Bosman, A. W.; Popa, E. R. Development and in-Vivo Characterization of Supramolecular Hydrogels for Intrarenal Drug Delivery. *Biomaterials* **2012**, *33*, 5144–5155.

(5) Bastings, M. M. C.; Koudstaal, S.; Kieltyka, R. E.; Nakano, Y.; Pape, A. C. H.; Feyen, D. A. M.; van Slochteren, F. J.; Doevendans, P. A.; Sluijter, J. P. G.; Meijer, E. W.; Chamuleau, S. A. J.; Dankers, P. Y. W. A Fast pH-Switchable and Self-Healing Supramolecular Hydrogel Carrier for Guided, Local Catheter Injection in the Infarcted Myocardium. *Adv. Healthc. Mater.* **2014**, *3*, 70–78.

(6) Dankers, P. Y. W.; Harmsen, M. C.; Brouwer, L. A.; Van Luyn, M. J. A.; Meijer, E. W. A Modular and Supramolecular Approach to Bioactive Scaffolds for Tissue Engineering. *Nat. Mater.* **2005**, *4*, 568–574.

(7) Kieltyka, R. E.; Bastings, M. M. C.; Almen, G. C. van; Besenius, P.; Kemps, E. W. L.; Dankers, P. Y. W. Modular Synthesis of Supramolecular Ureidopyrimidinone–peptide Conjugates Using an Oxime Ligation Strategy. *Chem. Commun.* **2012**, *48*, 1452–1454.

(8) Dankers, P. Y. W.; Boomker, J. M.; Huizinga-van der Vlag, A.; Smedts, F. M. M.; Harmsen, M. C.; van Luyn, M. J. A. The Use of Fibrous, Supramolecular Membranes and Human Tubular Cells for Renal Epithelial Tissue Engineering: Towards a Suitable Membrane for a Bioartificial Kidney. *Macromol. Biosci.* **2010**, *10*, 1345–1354.

(9) Dankers, P. Y. W.; Boomker, J. M.; Huizinga-van der Vlag, A.; Wisse, E.; Appel, W. P. J.; Smedts, F. M. M.; Harmsen, M. C.; Bosman, A. W.; Meijer, E. W.; Luyn, M. J. A. Bioengineering of Living Renal Membranes Consisting of Hierarchical, Bioactive Supramolecular Meshes and Human Tubular Cells. *Biomaterials* **2011**, *32*, 723–733.

(10) Mollet, B. B.; Comellas-Aragonès, M.; Spiering, A. J. H.; Söntjens, S. H. M.; Meijer, E. W.; Dankers, P. Y. W. A Modular Approach to Easily Processable Supramolecular Bilayered Scaffolds with Tailorable Properties. *J. Mater. Chem. B* **2014**.

(11) Unpublished data.

(12) Dankers, P. Y. W.; van Leeuwen, E. N. M.; van Gemert, G. M. L.; Spiering, A. J. H.; Harmsen, M. C.; Brouwer, L. A.; Janssen, H. M.; Bosman, A. W.; Van Luyn, M. J. A.; Meijer, E. W. Chemical and Biological

Properties of Supramolecular Polymer Systems Based on Oligocaprolactones. *Biomaterials* **2006**, *27*, 5490–5501.

(13) Almen, G. C.; Talacua, H.; Ramaekers, M.; Mollet, B. B.; Simonet, M.; Smits, A. I. P. M.; Kluin, J.; Dankers, P. Y. W. Development of Non-Cell Adhesive Vascular Grafts: From Supramolecular Building Blocks towards in Situ Vascular Tissue Engineering. *(submitted)*

(14) Kautz, H.; van Beek, D. J. M.; Sijbesma, R. P.; Meijer, E. W. Cooperative End-to-End and Lateral Hydrogen-Bonding Motifs in Supramolecular Thermoplastic Elastomers. *Macromolecules* **2006**, *39*, 4265–4267.

(15) Appel, W. P. J.; Portale, G.; Wisse, E.; Dankers, P. Y. W.; Meijer, E. W. Aggregation of Ureido-Pyrimidinone Supramolecular Thermoplastic Elastomers into Nanofibers: A Kinetic Analysis. *Macromolecules* **2011**, *44*, 6776–6784.

(16) Appel, W. P. J. Synthesis, Characterization and Applications of Quadrupole Hydrogen Bonded Polymers. Thesis, Technical University of Eindhoven: Eindhoven, The Netherlands, 2011.

(17) Lortie, F.; Boileau, S.; Bouteiller, L. N,N'-Disubstituted Ureas: Influence of Substituents on the Formation of Supramolecular Polymers. *Chem. – Eur. J.* **2003**, *9*, 3008–3014.

(18) Orza, R. A.; Magusin, P. C. M. M.; Litvinov, V. M.; van Duin, M.; Michels, M. A. J. Mechanism for Peroxide Cross-Linking of EPDM Rubber from MAS ^{13} C NMR Spectroscopy. *Macromolecules* **2009**, *42*, 8914–8924.

(19) Van Beek, D. J. M.; Spiering, A. J. H.; Peters, G. W. M.; te Nijenhuis, K.; Sijbesma, R. P. Unidirectional Dimerization and Stacking of Ureidopyrimidinone End Groups in Polycaprolactone Supramolecular Polymers. *Macromolecules* **2007**, *40*, 8464–8475.

(20) Beijer, F. H.; Sijbesma, R. P.; Kooijman, H.; Spek, A. L.; Meijer, E. W. Strong Dimerization of Ureidopyrimidones via Quadruple Hydrogen Bonding. *J. Am. Chem. Soc.* **1998**, *120*, 6761–6769.

(21) Beijer, F. H. Cooperative Multiple Hydrogen Bonding in Supramolecular Chemistry. Thesis, Eindhoven University of Technology: Eindhoven, The Netherlands, 1998.

(22) Jorgensen, W. L.; Pranata, J. Importance of Secondary Interactions in Triply Hydrogen Bonded Complexes: Guanine-Cytosine vs Uracil-2, 6-Diaminopyridine. *J. Am. Chem. Soc.* **1990**, *112*, 2008–2010.

(23) Folmer, B. J. B.; Sijbesma, R. P.; Kooijman, H.; Spek, A. L.; Meijer, E. W. Cooperative Dynamics in Duplexes of Stacked Hydrogen-Bonded Moieties. *J. Am. Chem. Soc.* **1999**, *121*, 9001–9007.

(24) Söntjens, S. H. M. Dynamics of quadruply hydrogen-bonded systems. Thesis, Eindhoven University of Technology: Eindhoven, The Netherlands, 2002.

(25) Kosower, E. M.; Huppert, D. Excited State Electron and Proton Transfers. *Annu. Rev. Phys. Chem.* **1986**, *37*, 127–156.

(26) Heller, A.; Williams, D. L. Intramolecular Proton Transfer Reactions in Excited Fluorescent Compounds. *J. Phys. Chem.* **1970**, *74*, 4473–4480.

(27) Nijegorodov, N. I.; Downey, W. S. The Influence of Planarity and Rigidity on the Absorption and Fluorescence Parameters and Intersystem Crossing Rate Constant in Aromatic Molecules. *J. Phys. Chem.* **1994**, *98*, 5639–5643.

(28) Toele, P.; van Gorp, J. J.; Glasbeek, M. Femtosecond Fluorescence Studies of Self-Assembled Helical Aggregates in Solution. *J. Phys. Chem. A* **2005**, *109*, 10479–10487.

Chapter 5

UPy-biomaterial screening: towards a materiomics approach

Abstract: *UPy-biomaterials are eminently suitable for biomaterial diversification. To match UPy-biomaterial properties with specific needs, screening is required. In this chapter a cell-adhesion screening on a small UPy-biomaterial library is discussed. The library is based on telechelic UPy-modified polycaprolactone (UPy-PCL), a cell-adhesive polymer, mixed with telechelic UPy-modified poly(ethylene glycol) (UPy-PEG), or with UPy-modified RGD-peptide (UPy-RGD). A scrambled peptide variant is included in the library as negative control (UPy-scrRGD). Two distinct techniques assess the ability of 3T3 fibroblast cells to adhere to the different biomaterials in absence of serum. Fluorescence microscopy monitors the number of cells and morphology of cells that adhere to electrospun meshes of the materials. The optical tweezers technique determines the adhesion probability of single electrosprayed microbeads to the cells and the force required to disrupt the bead/cell interaction. Expected trends of reduced cell adhesion in presence of UPy-PEG and increased cell-adhesion in presence of UPy-RGD are observed. Nevertheless, no clear black-and-white differences result from either technique, as is often the case in cell-based experiments. A high-throughput biomaterial screening, or materiomics approach, will provide opportunities to more quickly identify biomaterials with the desired properties and effects on cells. It will also provide a platform to obtain statistically relevant amounts of data and powerful tools to extract information from non-black-and-white results. Naturally, methods need to be developed, optimized and standardized first before materiomics can enable us to optimally benefit from the possibilities of the supramolecular biomaterials and their building blocks.*

Part of this chapter will be submitted for publication: Y. Nakano, K. Berghoff, A.C.H. Pape, B.B. Mollet, H. Kress, E.W. Meijer, P.Y.W. Dankers. *Determination of the cell supramolecular material interaction using optical tweezers.* (manuscript in preparation)

Part of this chapter was modified from: B.B. Mollet, A.C.H. Pape, R.P. Félix Lanao, S.C.G. Leeuwenburgh, P.Y.W. Dankers, *Materiomics using synthetic materials: metals, cements, covalent polymers and supramolecular systems*, p. 31-50 in Materiomics: *High-Throughput Screening of Biomaterial Properties*, Edited by J. de Boer and C.A. van Blitterswijk, Cambridge University Press, 2013.

1. Introduction

1.1 The need for high-throughput biomaterial screening

The biomaterial system based on ureido-pyrimidinone (UPy) entails broad possibilities towards biomaterial scaffold diversification. Possible methods are by molecular design of UPy-biomaterial building blocks, by mixing-and-matching of components,[1,2] and by modular formation of the scaffold (discussed in chapter 6). The optimal window of polymer and/or peptide combination/concentration to mimic a specific cell niche might be very narrow. Ideally continuous gradients should be screened to enclose all possible combinations. However, on a 2D surface, a maximum of only three components, or two variables, can be displayed in a continuous gradient. In practice, usually 1D gradients are applied, limited to variations of two components, or 1 variable. Discrete screening could be used to identify 'hits' within a library of biomaterials, that might be further optimized using a gradient screen in later experiments. The size of a discrete biomaterial array will rise very fast with the number of material components (n) or number of discrete steps (m) between varying concentrations of components (Table 1). Suppose one has a biomaterial system with 8 components that can be mixed to form new biomaterials. A screening of all discrete combinations with variations of 10 wt% will comprise 19,448 unique combinations, whereas the same array with steps of 5 wt% counts 888,030 unique combinations!

Table 1. Number of unique material combinations for a material system with n possible components, mixed in m steps to a total of 100 wt% (Bose-Einstein statistics, equation 1).

		Material components (n)							
step %	m	1	2	3	4	5	6	7	8
100	1	1	2	3	4	5	6	7	8
50	2	1	3	6	10	15	21	28	36
33.33	3	1	4	10	20	35	56	84	120
25	4	1	5	15	35	70	126	210	330
20	5	1	6	21	56	126	252	462	792
12.5	8	1	9	45	165	495	1,287	3,003	6,435
10	10	1	11	66	286	1,001	3,003	8,008	19,448
8.33	12	1	13	91	455	1,820	6,188	18,564	50,388
6.25	16	1	17	153	969	4,845	20,349	74,613	245,157
5	20	1	21	231	1,771	10,626	53,130	230,230	888,030
4	25	1	26	351	3,276	23,751	142,506	736,281	3,365,856
3.33	30	1	31	496	5,456	46,376	324,632	1,947,792	10,295,472
2.5	40	1	41	861	12,341	135,751	1,221,759	9,366,819	62,891,499
2	50	1	51	1,326	23,426	316,251	3,478,761	32,468,436	264,385,836
1.25	80	1	81	3,321	91,881	1,929,501	32,801,517	470,155,077	5,843,355,957
1	100	1	101	5,151	176,851	4,598,126	96,560,646	1,705,904,746	26,075,972,546

Equation 1:

$$W(m,n) = \frac{(\mathrm{m}+\mathrm{n}-1)!}{\mathrm{m}!\,(\mathrm{n}-1)!} \qquad (1)$$

Identification of the best biomaterial will be faster using high-throughput screening, or a 'materiomics approach'. Materiomics – the combination of 'material' with '-omics' – is most simply defined as the holistic study of materials systems.[3] The multidisciplinary field focusses on the rapid screening and the careful investigation of parameter spaces of the many parameters influencing the success of a new biomaterial.[3] This requires next to material sciences and cell biology, also computational technology. At the apex of these fields, materiomics attempts to reconcile biological function with material interactions and properties, based on an overwhelming stream of information. In this chapter we will discuss this emerging field in relation to UPy-based biomaterials.

1.2 Synthetic biomaterials in materiomics approaches

Different synthetic biomaterials are used for biomedical applications, varying from metals and ceramic cements, to polymers and supramolecular systems. To screen biomaterials in a materiomics approach libraries of materials are produced. The properties that are varied and methods that are used to create variation within these libraries depend on the type of biomaterial. For the hard metal and ceramic based biomaterials, primarily the surface interaction with tissue is the property of interest. Therefore properties such as surface roughness and topography are varied. An advanced example which has embraced the materiomics approach is the TopoChip.[4] Mathematical algorithms were applied to design non-biased, random surface features. Arrays with 2,176 different topographies were imprinted in chips of poly(lactic acid) and high-content imaging was applied to read-out the performance of human mesenchymal stromal cells (MSC) on top of each unique topography array. This enabled the identification of formerly unknown surface topographies that induce MSC proliferation or osteogenic differentiation. The parameters of the mathematical algorithms were correlated to these cellular responses. This allowed unraveling of the interplay between MSC behavior and surface topographies, facilitating control over cell parameters by topological design in future bone tissue engineering applications.

Covalent polymers are diversified using combinatorial chemistry. The polymer can be chemically varied by choosing monomers and monomer ratios before polymerization. Other options to change material properties are blending different polymers. Also the processing of the materials can have a profound influence on the material properties. A large polymer-based biomaterial screen was described by Hook *at al.*[5] They used 25 commercially available acrylate-monomers to prepare 576 different polymers in a microarray format. All monomers were dissolved in DMF and monomer combinations were premixed in 384-well plates. Sequentially, the mixtures were deposited on a poly(hydroxyethyl methyl)acrylate (pHEMA) coated glass microscopy slide. pHEMA inhibits cell adhesion, providing a 'blank' background, while providing a layer on which the monomer mixtures could be polymerized. To prevent spreading of the deposited monomer droplets, the mixtures were exposed to UV light to polymerize after each

deposition round. In total 1,728 spots of monomer mixtures, i.e. the array in triplicate, were printed on a single microscope slide. A drawback of the array preparation method was that due to washing and differences in monomer reactivity the exact composition of the polymer in each spot was unknown. Stem cells were seeded on top of the array and studied with fluorescence microscopy to gain insight into polymer effects on stem cell attachment and differentiation. In this study, the quantitative analysis was done by hand. However, high-content image analysis could be adapted for the analysis of these microarrays in the future to further exploit the materiomics approach.

1.3 Perspective on supramolecular chemistry in materiomics

Supramolecular chemistry holds both opportunities and challenges in relation to materiomics. The dynamic nature of supramolecular chemistry introduces a new perspective on material diversification and the generation of libraries via combinatorial approaches, without the need of covalent synthesis. Once the building blocks are available, a supramolecular biomaterial system allows for a mix-and-match principle as long as the requirements for self-assembly are met. Nevertheless, to this date no examples of supramolecular biomaterial library screening are found in literature. Perhaps this is due to the challenges that are related with the dynamic nature of supramolecular biomaterials. These materials are hypothesized to be more responsive towards cells compared with covalent biomaterials. However, that means that these materials are more susceptible for changes by any external factor. Such unforeseen changes at the molecular level could cause alterations at scales relevant for the application. This makes the control of properties of supramolecular biomaterials more complex compared to their covalent counterparts. On the other hand, dynamics of supramolecular interactions can also be used to an advantage in high-throughput screening applications. A non-biomaterial related example is the identification of ligands using the non-covalent, dynamic nature of the interactions between biological molecules. In phage display and systematic evolution of ligands by exponential enrichment (SELEX),[6] the selection of the best ligand candidates from large protein libraries is based on the strongest non-covalent interactions.

We foresee that a materiomics approach will aid to benefit from the potential within UPy-based biomaterials in the future. The screening of libraries of UPy-biomaterials can also be employed to gain insight into fundamental properties of these materials. Here we discuss an example study applied on a small library of UPy-based biomaterials, using two distinct techniques.

2. Screening cell-biomaterial interactions: a UPy-based biomaterial library

2.1 Experimental setup

To gain insight into the relation between cell and biomaterial interactions across time and length scales, we studied a small library of UPy-PCL based biomaterials using two distinct experimental techniques. With fluorescence microscopy the interaction of cells with a microfibrous mesh morphology was studied over a period of 4 hours. Both the number of adhered cells and the morphology of these cells was monitored. In the other approach, the binding interaction between a single cell and a UPy-biomaterial bead was measured using optical tweezers (performed by Yoko Nakano, with the help of Konrad Berghoff). The optical tweezers technique applies a focussed laser beam to manipulate a small (order of few µm) bead. In our experiments a single cell adhered to a flat surface, was brought in contact with the bead for 60 seconds. Upon retraction of the cell, the displacement of the bead was recorded (Figure 1). The displacement from the trap center could be converted to a force applied on the bead via a linear relationship. By this method, the strength of single binding events between ligands on a biomaterial surface and cell-surface receptors have been measured.[7-9]

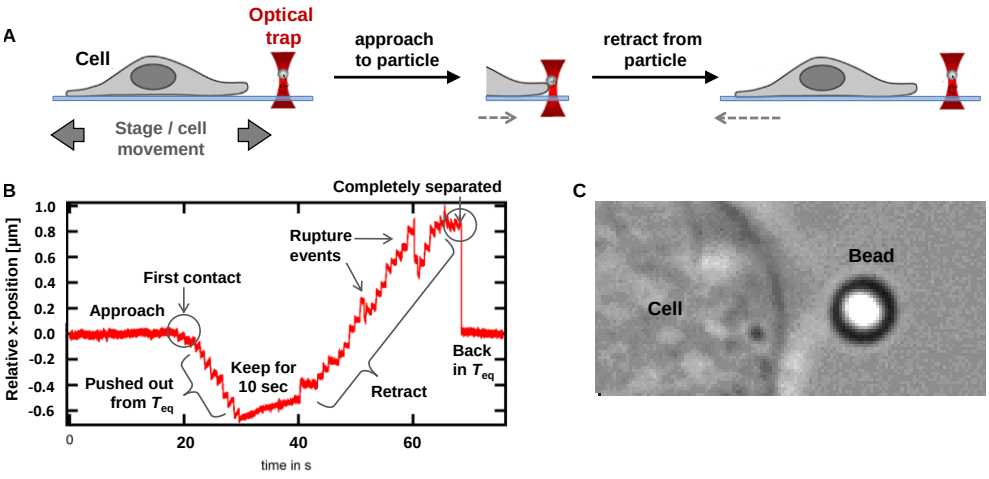

Figure 1: Optical tweezers to study cell-biomaterial bead interaction. A) Schematic representation of a single measurement: the cell is brought in contact with a trapped bead, and retracted after a certain contact time. B) A typical graph resulting from such measurement, representing the relative x-position of the bead in reference to the equilibrium trapped position (T_{eq}) in time. When the cell is brought in contact with the bead, the bead is pushed slightly out of T_{eq}. Upon retraction of the cell, the bead is pulled along when bound to the cell during contact time. Rupture events indicate disruption of single receptor-ligand interactions between cell and bead. When the last interaction is disrupted, the bead is pulled back in its T_{eq}. The displacement of the bead is linearly related to force. C) A micrograph of a biomaterial bead and part of a cell. The high contrast of the bead indicates a high refractive index, which enables the optical entrapment of the bead by a focused laser beam.

The applied UPy-biomaterial library was made from UPy-PCL, UPy-PEG and UPy-RGD , all compounds which were introduced in chapter 2. The library comprised pure UPy-PCL (1), and UPy-PCL mixed with: 10 mol% UPy-PEG (2), 30 mol% UPy-PEG (3), 4 mol% UPy-RGD (4), and 4 mol% UPy-scrRGD (5). The latter was a similar peptide as UPy-RGD, but the amino acid sequence was scrambled from GGRGDS to GSGDRG. This induced loss of the integrin receptor binding capacity and hence loss of cell binding capacity. This peptide was included in the study as a negative control for bioactivation with UPy-RGD. Hydrophilic UPy-PEG was introduced to induce a non-cell adhesive character to the hydrophobic, cell-adhesive UPy-PCL as described and applied in chapter 5. The UPy-biomaterials were processed into microbeads and microfibrous meshes by electrospraying (performed by Bram Pape) and electrospinning (see chapter 3), respectively. These materials were applied to study cell-biomaterial interactions using 3T3 mouse fibroblast cells. The studies were performed in cell-culture media without serum. The composition of serum is not well-defined and the mechanisms of influence on cells are not well-understood. Nevertheless, serum is commonly added to cell-culture media because of its positive influence on cell performance. In absence of serum in the culture media even the robust 3T3 fibroblasts have shown to experience difficulties to grow on UPy-PCL films over a two day period.[1] From earlier experiences we have reasons to assume that serum in the culture media interferes with the direct cell-biomaterial interactions which we want to investigate here. The heterogeneous pool of proteins present in serum influence or shield the interaction between cells and biomaterial surfaces (Figure 2).

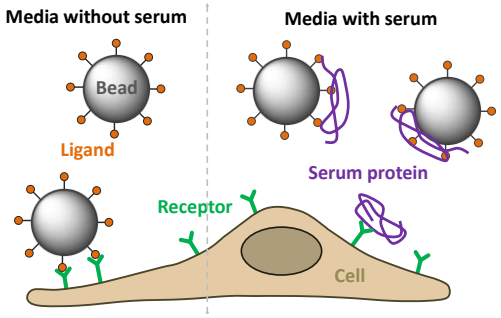

Figure 2. Interference of serum proteins in cell-biomaterial interactions. Biomaterials, here depicted as beads, are functionalized with specific bioactive ligands, e.g. RGD-peptides which can interact with integrin receptors at the cell membrane. When studying this interaction, serum proteins present in the culture medium can interfere by binding to the cell receptors, to the ligands at the biomaterial surface, or by adsorption to the biomaterial surface.

In biomaterial applications in contact with blood, such effects of protein adsorption are known to severely influence the effective surface of a biomaterial. For example hydrophobic surfaces have been observed to gain hydrophilicity by the adsorbed protein layer. Furthermore, the layer changes in composition over time. Abundant mobile proteins adsorb first, which are sequentially replaced for other proteins with lower mobility but higher affinity for the biomaterial surface. This is called the 'Vroman effect'.[10] In certain applications it is highly relevant to include the effect of protein adsorption when studying cell-biomaterial interactions. For example in *in-situ* tissue engineering of heart valves.[11] There, a bare biomaterial scaffold is placed as functional valve in the heart, intended to

capture relevant cells from the blood. These are then stimulated to deposit their own matrix and in time replace the biomaterial for neo-tissue. However, for an *in-vitro* application such as the culture of a bioartificial renal tubular membrane, the direct interaction of the epithelial cells with the biomaterial are of interest. The need for serum should ideally be circumvented by optimal stimulation of the cells by the biomaterial. Furthermore, the pre-urine with which renal epithelial cells are normally in contact, is free of most serum proteins as these cannot pass the glomerular filter (see chapter 1).

2.2 Results

UPy-biomaterial electrospun meshes and electrosprayed beads

The electrospun UPy-biomaterial meshes all displayed randomly oriented fibers in the 2D plane with diameters smaller than 1 µm (Figure 1). This gave rise to porous surfaces with apparent pore sizes smaller than 5 µm. Based on these morphologies, all meshes were appropriate as 2D scaffold for 3T3 fibroblast cell culture. For the optical tweezers experiments, beads with a size of ~3 µm were selected from the heterogeneous pool of bead sizes that resulted from the electrospraying process.

Microfibrous meshes: Cell adhesion number and morphology

3T3 fibroblast cells were seeded on UPy-PCL based microfibrous meshes in a density of $5{\cdot}10^4$ per mesh. The cells that adhered during an incubation time of 4 hours were fixed and stained. To enable unbiased sample visualization by microscopy, the study was performed 'blind'. A fluorescent micrograph was taken from the middle of each sample using a low magnifying (4x) objective. This enabled the capturing of the main region of interest in one image. From these images the average number of cells that adhered to each material was determined. A large variation was observed between the samples in a single biomaterial group, which resulted in non-significant differences (Figure 4). A weak trend could be seen, which followed lower cell adhesion in presence of more UPy-PEG, and elevated cell adhesion in presence of UPy-RGD. However, the negative control with the scrambled RGD did not indicate this latter effect to be the result of specific bioactivation. In comparison to the high numbers of cells that adhered to all the meshes, even in absence of serum, we were surprised to see extremely low cell adhesion to meshes that contained the scrambled peptide in presence of serum in the culture medium (data not shown). To these meshes an average of <70 cells adhered. This observation was verified, but remains elusive.

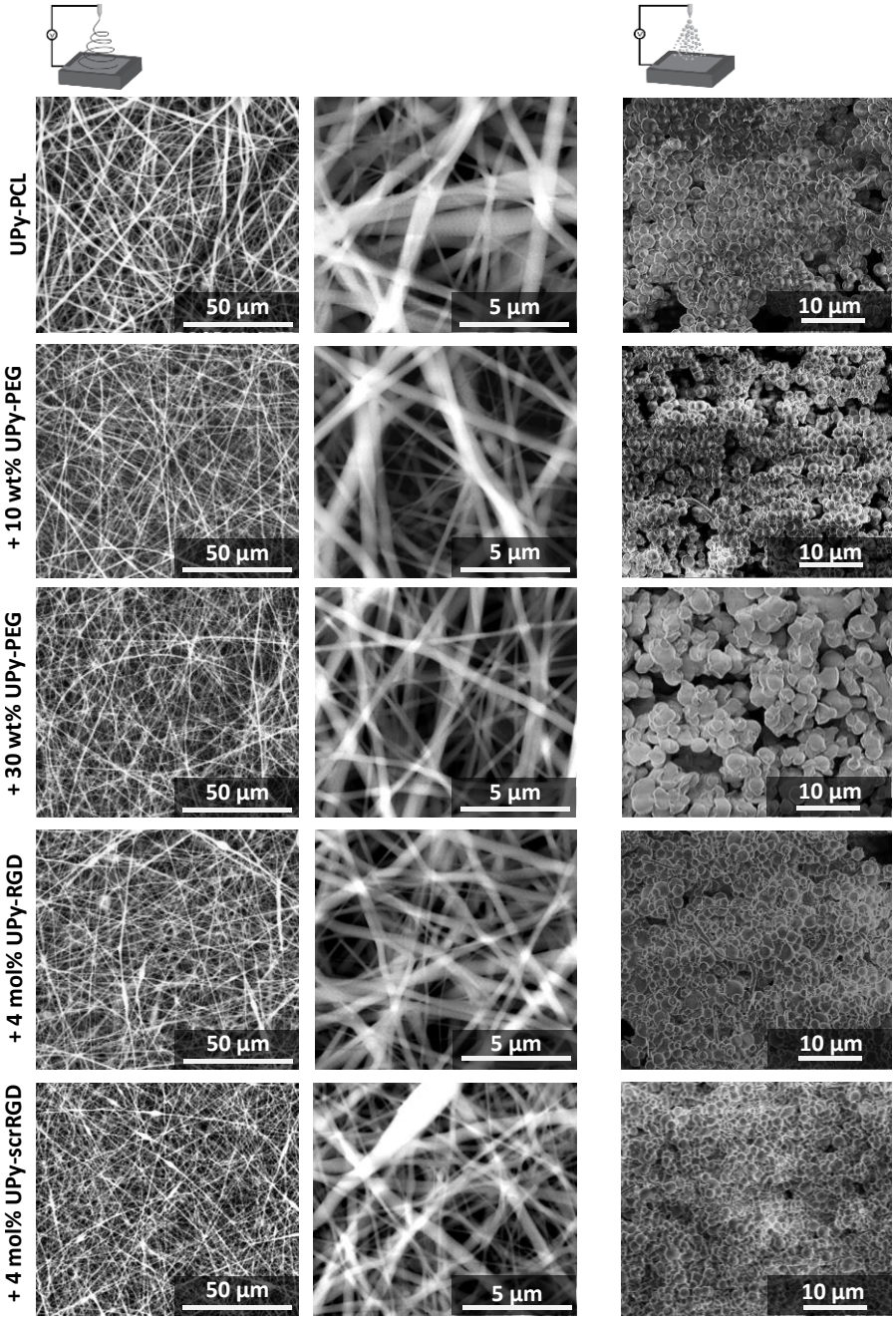

Figure 3. The morphology of electrospun microfibrous meshes and electrosprayed microbeads. Scanning electron micrographs of UPy-PCL based biomaterial meshes and beads. Five different biomaterial compositions, all containing UPy-PCL, were processed. Concentrated, viscous solutions by resulted in fibrous meshes by electrospinning. More dilute, less viscous solutions yielded electrosprayed beads.

Figure 4. The average number of adhered cells. Fibroblasts were incubated for 4 hours in absence of serum, on electrospun meshes of UPy-PCL based biomaterials. Non-adhered cells were washed away, the nuclei of adhered cells were stained. Cells were counted from fluorescence micrographs of 3 or 4 samples per biomaterial. Error bars represent standard deviations.

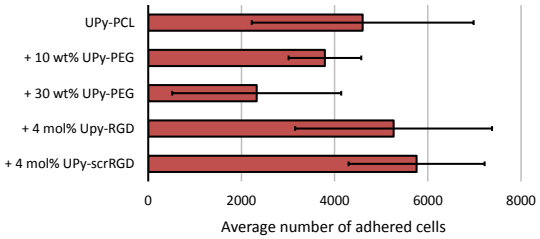

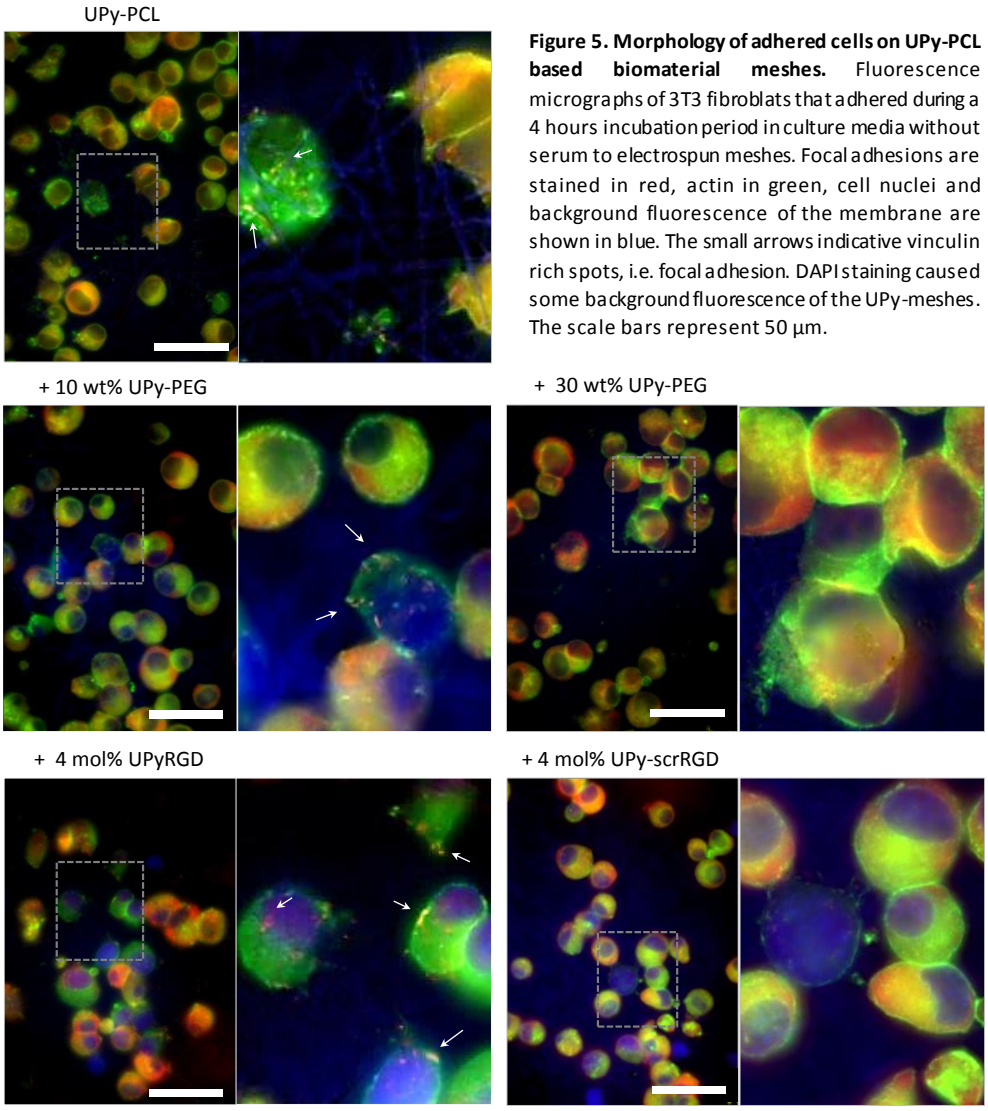

Figure 5. Morphology of adhered cells on UPy-PCL based biomaterial meshes. Fluorescence micrographs of 3T3 fibroblats that adhered during a 4 hours incubation period in culture media without serum to electrospun meshes. Focal adhesions are stained in red, actin in green, cell nuclei and background fluorescence of the membrane are shown in blue. The small arrows indicative vinculin rich spots, i.e. focal adhesion. DAPI staining caused some background fluorescence of the UPy-meshes. The scale bars represent 50 µm.

Immunofluorescent staining of vinculin and fluorescent staining of actin filaments and cell nuclei enabled the study of adhered cell morphology by fluorescence microscopy. In adherent cells actin typically organizes into well-defined filaments, forming the cells cytoskeleton. Such structures were observed in control cultures of 3T3 fibroblast cells grown on glass in the presence of serum (data not shown). For these cells also the typical organization of vinculin in focal adhesion spots at the ends of these actin filaments was observed. Such well-defined structures were not visible for the cells that adhered to any of the UPy-biomaterial meshes in absence of serum within 4 hours. At first glance, the adhered cells showed similar round morphologies on all meshes (Figure 5). However, upon better inspection, small differences were observed. Some fibroblasts that adhered to pure UPy-PCL seemed to span between separate electrospun fibers via stretched filopodia. Occasionally, this was accompanied by a vinculin rich focal adhesions along the fiber. However, clear organization of actin filaments appeared to be absent. In presence of increasing ratios of UPy-PEG, these filopodia and focal adhesions became less prevalent and cells generally remained in a completely round morphology. Upon availability of UPy-RGD, more cells displayed filopodia stretching to the biomaterial microfibers and more cells were observed to localize vinculin in focal adhesions. This effect of specific bioactivation by UPy-RGD was confirmed by the absence of such effects for meshes containing the scrambled-RGD equivalent. Although these observations seem to meet the expected results in this 'blind' microscopy study, it should be noted that the number of analyzed samples was limited as well as the number of recorded micrographs, which were analyzed by hand. To draw solid conclusions from morphological studies witch entail such subtle differences, higher number of samples, micrographs and ideally automated image analysis should be applied, i.e. a materiomics type of approach.

Interaction of single cells and beads: binding probability and strength

Microscopy studies are widely applied in the field of tissue engineering to assess biomaterial and cell interactions. In our case, the results hinted towards the expected trends of reduced cell adhesion by presence of UPy-PEG and increased cell adhesion by UPy-RGD. Nevertheless, the morphology studies only provided very minor qualitative differences, whereas the cell counting resulted in non-statistical differences. Optical tweezers were expected to provide more black-and-white quantitative data by analysis of adhesion probability and the forces required to rupture the interaction between a cell and biomaterial bead. In initial studies short (10 sec) contact times between a cell and biomaterial bead in presence of serum were employed. The observed differences between UPy-biomaterials were small, if present. Contact time was increased to 60 seconds and serum-free medium was applied. Against all expectations, the introduction of UPy-PEG was not observed to lower cell adhesion probability. When comparing UPy-PCL without and with 30 wt% UPy-PEG, these probabilities were 0.79 ± 0.11 and 0.75 ± 0.09, respectively. Furthermore, the force required to separate attached cells and beads was observed to increase in presence of UPy-PEG. More interactions were classified as non-

rupturable (within the applied settings using 200 mW trap power), i.e. the bead was pulled out the trap (Figure 6). For the UPy-RGD enriched beads an adhesion probability of 0.89 ± 0.07 was determined. In comparison to both bare UPy-PCL and UPy-scrRGD containing beads, much more interactions were classified as non-rupturable. These results confirm the presentation of the peptide at the beads surface, available to interact with integrins at the membranes of cells. Furthermore, the distribution of rupture forces for bare UPy-PCL and UPy-PCL with scrambled UPy-RGD peptide were comparable. This indicates that the effect of UPy-RGD is truly the result of specific bioactivity, rather than the result of an alteration in the material by mixing in a UPy-peptide.

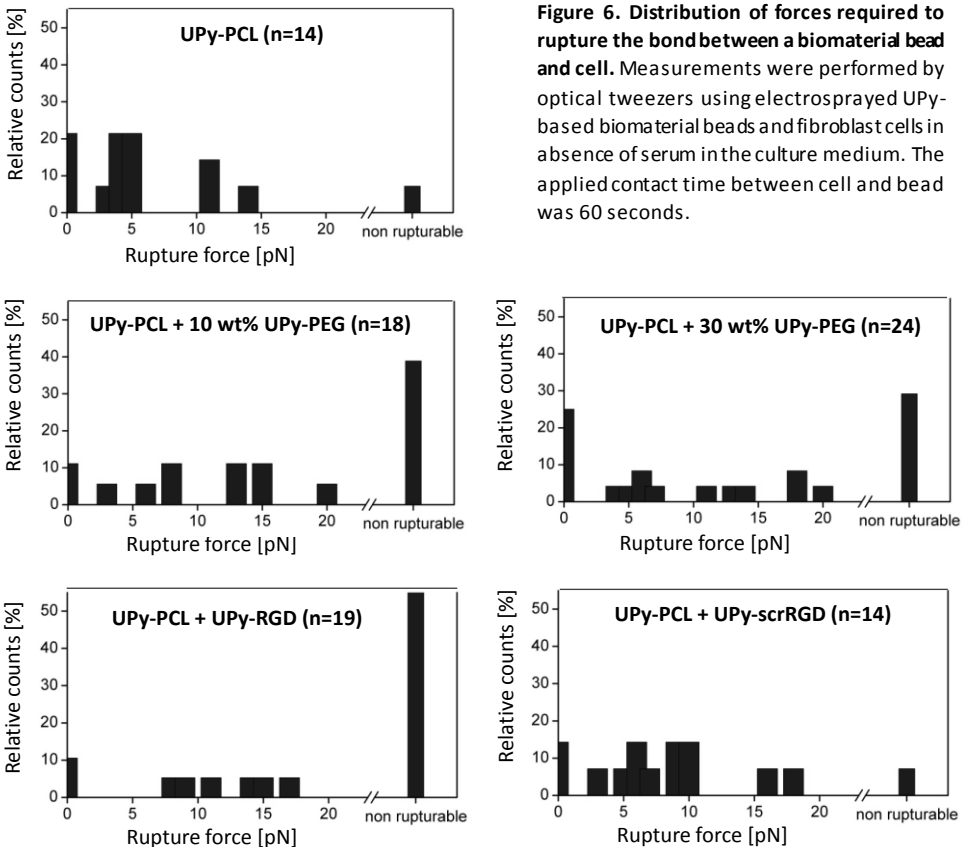

Figure 6. Distribution of forces required to rupture the bond between a biomaterial bead and cell. Measurements were performed by optical tweezers using electrosprayed UPy-based biomaterial beads and fibroblast cells in absence of serum in the culture medium. The applied contact time between cell and bead was 60 seconds.

3. Discussion

UPy-PCL has been successfully applied as cell-adhesive material in the past. However, in absence of serum in the culture media 3T3 fibroblasts have demonstrated to have difficulties to grow on films of this material over a two day period.[1] Under these serum

depleted conditions, here a positive effect resulting from the addition of cell-adhesive UPy-RGD could be distinguished. The results for UPy-PEG containing biomaterials remain difficult to interpret. Here two concentrations, 10 wt% and 30 wt% compared to UPy-PCL, were applied. Neither showed convincing anti-cell adhesive effects under the applied experimental conditions. Cell morphologies studied by fluorescence microscopy showed less signs of cell spreading. However, the results obtained by optical tweezers measurements indicated that cells that adhered in presence of UPy-PEG, adhere more strongly compared to cells that adhere to pure UPy-PCL. Nevertheless, this does not necessarily mean we should revise our hypothesis of PEG induced reduction of cell adhesion by deflection of protein interactions with the material surface. Plausibly, more PEG is needed to prevent 3T3 fibroblast adhesion. Also, for the fibers and beads applied in these experiments the distribution of UPy-PEG and presentation at the biomaterial surface was unknown. The long term effect of each biomaterial surface on cell development was outside the scope of the current study. Although these studies spanned time scales from a single minute to 4 hours, the applied adhesion/culture times are still short in comparison to times relevant for applications. For translation towards applications, longer culture periods are required. It will be interesting to see how the observed cell-biomaterial interactions at initial time points develop and relate to observations over longer time periods.

As mentioned before, the UPy-based biomaterial tool box could in principle be expanded with virtually any UPy-functionalized building block. The possibilities to diversify biomaterials are not the limiting factor in forming optimal candidates for specific applications. The methods that we apply to identify them are. The biomaterial library studied and discussed here only comprised five UPy-biomaterials, but effectively tested only two variations; the addition of UPy-PEG at two concentrations, and the addition of UPy-RGD (with UPy-scrRGD as negative control condition). Despite this small biomaterial library size, the experiments were very labor-intensive. In addition, the quantitative analysis of both adhered cell counting on meshes and determination of binding probability and strength at single-cell/bead level revealed difficulty to obtain statistically relevant results. The results obtained in cell-biomaterial studies are often not black-and-white. However, the combination with intrinsically dynamic biomaterials makes it even more challenging to gain control over reproducible results and statistically relevant data. A high-throughput materiomics approach will not only provide opportunities to test the many different biomaterial combinations. It will also provide a platform to obtain statistically relevant amounts of data and powerful tools to extract information from such non-black-and-white results.

The characterization of materials with a dynamic and responsive nature -whether it is analysis of material properties or their performance in cell based experiments- is not straightforward. This demands for deeper and more deliberate analysis, taking thermodynamic versus kinetic aspects of the materials into account. For these biomaterials it is even more important than for covalent materials to perform the analysis

under conditions that are relevant for the final application. For example body temperature when compared to room temperature can have a profound effect on the outcome of the material properties that are measured. One should even consider a possible effect of the characterization method itself on the material. For example in the analysis of hydrophilicity by water contact angle measurements on a material that is built up from molecules that are connected through hydrogen bonds. The applied water may cause reorganization of molecules at the surface, resulting is enhanced surface exposure of hydrophilic components. Hence, the characterization method itself might influence the material property that is measured. Both characterization and standardization methods will have to be revised first before a materiomics approach can unleash the full potential of this new generation of supramolecular biomaterials.

The fact that materials can change, either in time or as a reaction on changes in the environment, is often neglected in biomaterials research using covalent synthetic and/or natural materials. For natural materials, such as protein based ECM components, the higher order protein structures play a key role in the specific material properties. These structures highly rely on non-covalent interactions. It is foreseeable, although often forgotten, that the same caution should be taken as with synthetic supramolecular biomaterials when analyzing these materials. It might not be so obvious for covalent material systems, but also these materials can be susceptible to change. Certain synthetic polymeric materials have monomeric components that are linked through reversible covalent bonds.[12,13] Other processes to think of might be slow crystallization in time or effects of water uptake.

4. Concluding remarks

Supramolecular biomaterials are eminently suitable for biomaterial diversification and library formation. Via a modular mix-and-match approach building blocks can be combined to form new biomaterials with combined properties. Such diversity and flexibility in material formation would allow to tailor properties towards requirements for specific applications. This aspect will be further examined in the next chapter. Nevertheless, identification of the best match depends on proper analysis tools. To allow high-throughput screening of dynamic supramolecular biomaterials in a materiomics approach we will need: 1) better understanding and control over spatio-temporal variations of the material, and 2) robust screening methods that respect the thermodynamic and kinetic aspects of these materials.

5. Acknowledgements

We thank Bram Pape for the preparation of the UPy-biomaterial beads and Yoko Nakano, Konrad Berghoff and Holger Kress for the elaborate optical tweezers measurements. We thank Marta Comellas-Aragonès for UPy-scrRGD synthesis.

6. Materials and Methods

Materials

UPy-PCL (batch 2-II), UPy-PEG (both with a polymer backbone with M_n = 2 kg · mol^{-1}) and UPy-RGD were synthesized as described in chapter 2. The scrambled UPy-RGD (UPy-scrRGD) was synthesized similar as UPy-RGD, but the peptide was synthesized with an altered amino acid sequence: GSGDRG instead of GGRGDS. 1,1,1,3,3,3-hexafluoro-2-propanol (HFIP) (Acros) was used without further purification. Sterile phosphate buffered saline (PBS) was prepared by dissolution of PBS tablets (P4417, Sigma Aldrich) in distilled water, followed by steam autoclavation.

Electrospinning of fibrous UPy-PCL based meshes on glass

A home-built electrospinning setup equipped with a syringe pump (KD Scientific) was used. The electrospin solutions were prepared according to table 2 by dissolution of the different compounds in HFIP, starting with the peptide or UPy-PEG when present. For the UPy-based meshes a constant of 17.5 wt% of UPy-PCL (**2**) was used.

Table 2: composition of electrospinning solutions.

Material nr Mole ratio in final product	UPy-PCL [wt%]	UPy-PEG [wt%]	UPy-RGD [wt%]	UPy-scrRGD [wt%]	HFIP [wt%]
1: 100% UPy-PCL	17.5	-	-	-	82.5
2: 90/10 UPy-PCL/UPy-PEG	17.5	1.9	-	-	80.6
3: 70/30 UPy-PCL/UPy-PEG	17.5	7.5	-	-	75
4: UPy-PCL+ 4% UPy-RGD	17.5	-	0.26	-	82.5
5: UPy-PCL+ 4% UPy-scrRGD	17.5		-	0.26	82.5

Each polymer solution was loaded in a 2.5 mL glass syringe (Hamilton) and fed through teflon tubing to a blunt end 23 G needle at a rate of 0.02 mL min^{-1} under the control of a Chemyx Nexus 3000 syringe pump. The solution was electrospun by application of 18.5 kV between a tip-to-target distance of 12 cm. Electrospun fibers were collected on round glass coverslips (12mm ∅, Marienfeld GmbH) that were placed on a thin PE film that covered the metal collector plate, until a dense fibrous mesh covered all coverslips. Each electrospun membrane was, as a whole on the PE film, placed *in vacuo* at 40 °C overnight to remove any residual solvent. The morphology of the fibrous meshes was analyzed with scanning electron microscopy (SEM) on a FEI Quanta 600F ESEM. Samples were imaged in low vacuum mode (~0.5 mbar) with a high voltage of 18 kV.

Electrospraying of UPy-PCL based microbeads

Beads were produced using the same equipment as for electrospinning. The UPy-PCL based solutions were prepared in HFIP as well, using the same compositional ratio's as for the electrospun meshes. However, UPy-PCL was dissolved in HFIP at a concentration of 7 wt/wt%. Solutions were stirred for 2h before they were electrosprayed. The solutions were fed at a flow speed of 1 ml h^{-1}

and sprayed under application of 18.5 kV. The distance between the needle and the collector was 12 cm. Samples were collected on PE cling film. After half an hour, the film with deposited material was removed from the collector and dried *in vacuo* overnight at 40°C. The particles were removed from the film and analyzed by SEM in high vacuum mode, applying a low voltage of 2kV.

3T3 cell culture

Mouse fibroblast 3T3 cells were routinely cultured in tissue culture treated polystyrene culture flasks at 37 °C and 5% CO_2 in a humidified atmosphere with refreshment of complete medium every 2-3 days. Complete culture medium consisted of Dulbecco's Modified Eagle Medium (DMEM) supplemented with 10 v/v% fetal bovine serum (26140, Gibco, Invitrogen). For the actual experiments, this FBS was not added to the medium. In addition, for studies with fluorescence microscopy, DMEM media without phenol red (21063, Gibco, Invitrogen) was applied.

Cell seeding and adhesion to electrospun meshes

The coverglasses, covered with a mesh of fibers were cut from the electrospun polymer membranes. These samples were sterilized by irradiation with UV for 1h on both the glass and polymer side. For each of the six electrospun materials, four samples were clamped in separate MINUSHEET 13 mm cell supports (Minucells & Minutissue) and placed in a 24-well plate. The electrospun polymer samples were pre-wetted by application of 100 µL DMEM medium in the inside of the Minusheet ring. This pre-wet medium was removed prior to seeding of and $5{\cdot}10^4$ 3T3 cells in 75 µL per sample. Cells were left to adhere for 4 h at 37 °C and 5% CO_2 in a humidified atmosphere. Then, each sample was gently washed with DMEM and fixed by incubation at room temperature for 20 min with 2% formaldehyde in DMEM. The samples were washed with PBS twice and stored under PBS at 4°C until stained for analysis with fluorescence microscopy.

Cell staining and analysis with fluorescence microscopy

Quantitative analysis: Cell nuclei counting

The cell nuclei of the fixed 3T3 cells were stained by incubation with 4',6-diamidino-2-phenylindole (DAPI, 1:1000, invitrogen) in PBS for 15 minutes at room temperature. The samples were washed twice with PBS and visualized using a 4x magnifying objective (Zeiss Achroplan) on a fluorescence microscope (Zeiss Axiovert 200M) equipped with a camera (AxioCam HRm, Zeiss). An image of the center of each sample was taken. The obtained gray value images were step-wise converted, via a simple convolution filter, brightness/contrast adjustment, threshold and watershed, to optimized black and white images appropriate for automated counting (analyze particles, ImageJ software). The average number of cells was calculated for each sample group. Error bars represent standard deviation.

Qualitative analysis: Cell morphology, actin skeleton and vinculin organization

The fixed 3T3 cells on the electrospun meshes were stored in 5 wt/v% BSA in PBS until stained. The cells were incubated overnight at 4 °C with mouse anti-vinculin antibody (Sigma Aldrich) diluted 1:400 in PBS with 2 wt/v% BSA and 0.1 v/v% triton X-100. The cells were then washed with 0.3% triton X-100 in PBS once and twice with PBS. Subsequently, each sample was incubated for 30 min with goat anti-mouse antibody with alexa 555 label (1:400; invitrogen), phalloidin atto-488 (1:500, Sigma Aldrich) and 4,6-diamidino-2-phenylindole (DAPI; 1:1000; Sigma Aldrich) in PBS with 2wt/v% BSA and 0.1% triton X-100. The samples were washed three times with PBS, taken out of the Minusheet tissue culture rings and embedded between a microscopy slide and coverglass in Vectashield hard-set mounting media (Vector labs). The samples were visualized with fluorescence microscopy using a 40x oil emersion objective on a Zeiss Axio observer D1 equipped with an AxioCam Mrm camera and Zeiss Axiovision software (Carl Zeiss).

Optical tweezers

Sample preparation

3T3 Fibroblasts suspended in medium were seeded on a microscope slide (5,000 cells/200 µL) and adhered for 18-23 hours in a culture area of 0.8 cm^2, then washed with phosphate-buffered saline (Sigma) (3×). Just prior to optical trapping, 100 µL of beads suspension (3.3 µg/mL) was plated. All procedure was performed on a microscope slide (24 mm × 36 mm, 0.13-0.16 mm thickness) in a 0.8 cm^2 silicon square frame (Lab-Tek) and covered with a coverslip (18 mm × 18 mm, 0.13-0.16 mm thickness), then mounted into the Nikon Eclipse Ti microscope equipped with optical tweezers.

Experimental setup

A sketch of the experimental setup is shown in Figure 1. Life cell imaging and DIC imaging of the custom-made samples were applied using an inverted microscope (Nikon, Nikon Eclipse Ti) with a long working distance water-immersion objective (Nikon, APL LWD 40x, N.A. = 1.15). For the generation of the optical trap, a 1064 nm fiber laser (IPG Photonics, IPG YLM-5-LP-SC, max. output 5 Watts) was coupled into the observation path of the system and was broadened to slightly overfill the back-opening of the microscope objective. The laser power was set to 200 mW at the entrance of the microscope with a power management device and the trap center was adjusted to match the center of the observation plane in the imaging path of the microscope. With these settings the optical trap was calibrated to a trap stiffness of 25 pN μm^{-1} by applying the equipartition theorem of classical statistical mechanics to the thermal fluctuations of the trapped bead.[14] Image acquisition at a fixed frame rate of 1000 fps and 50 µs shutter speed was done by a high speed camera (Photron, FastCam SA3). DIC images were obtained using an EMCCD camera (Andor, Andor Ixon+). Both cameras were connected to the microscope via a dual camera port (Andor, Andor TuCam) to monitor the same observation plane simultaneously. For rough alignment of the sample in-between the measurements the translation stage of the microscope was used. During the measurement a motorized 3D piezo stage (Mad City Labs, Nano-Drive NANO-LP100) with custom-made LabView®-control provided the sample movement. A stepwise ramp motion with 1 µm s^{-1} was applied, enabling the monitoring of the trap stiffness during approaching and removing.

Image analysis

Particle tracking was applied by using a MATLAB® crosscorrelation tracking algorithm (written by Kress et al, with courtesy of Dufresne Lab, Yale University) providing sub-pixel precision of the center of the target bead. By simulations the accuracy of the algorithm was determined to be ± 6 nm. Further data analysis, including the calculation of force extension curves, was done with IGOR Pro data analysis software (Wavemetrics, IGOR Pro 6).

7. References

(1) Dankers, P. Y. W.; Harmsen, M. C.; Brouwer, L. A.; Van Luyn, M. J. A.; Meijer, E. W. A Modular and Supramolecular Approach to Bioactive Scaffolds for Tissue Engineering. *Nat. Mater.* **2005**, *4*, 568–574.

(2) Dankers, P. Y. W.; Meijer, E. W. Supramolecular Biomaterials. A Modular Approach towards Tissue Engineering. *Bull. Chem. Soc. Jpn.* **2007**, *80*, 2047–2073.

(3) *Materiomics: High-Throughput Screening of Biomaterial Properties*; de Boer, J.; van Blitterswijk, C. A., Eds.; Cambridge University Press: Cambridge, 2013.

(4) Unadkat, H. V.; Hulsman, M.; Cornelissen, K.; Papenburg, B. J.; Truckenmüller, R. K.; Carpenter, A. E.; Wessling, M.; Post, G. F.; Uetz, M.; Reinders, M. J. T.; Stamatialis, D.; Blitterswijk, C. A. van; Boer, J. de. An Algorithm-Based Topographical Biomaterials Library to Instruct Cell Fate. *Proc. Natl. Acad. Sci.* **2011**, *108*, 16565–16570.

(5) Hook, A. L.; Anderson, D. G.; Langer, R.; Williams, P.; Davies, M. C.; Alexander, M. R. High Throughput Methods Applied in Biomaterial Development and Discovery. *Biomaterials* **2010**, *31*, 187–198.
(6) Ellington, A. D.; Szostak, J. W. In Vitro Selection of RNA Molecules That Bind Specific Ligands. *Nature* **1990**, *346*, 818–822.
(7) Shergill, B.; Meloty-Kapella, L.; Musse, A. A.; Weinmaster, G.; Botvinick, E. Optical Tweezers Studies on Notch: Single-Molecule Interaction Strength Is Independent of Ligand Endocytosis. *Dev. Cell* **2012**, *22*, 1313–1320.
(8) Litvinov, R. I.; Shuman, H.; Bennett, J. S.; Weisel, J. W. Binding Strength and Activation State of Single Fibrinogen-Integrin Pairs on Living Cells. *Proc. Natl. Acad. Sci.* **2002**, *99*, 7426–7431.
(9) Thoumine, O.; Kocian, P.; Kottelat, A.; Meister, J.-J. Short-Term Binding of Fibroblasts to Fibronectin: Optical Tweezers Experiments and Probabilistic Analysis. *Eur. Biophys. J.* **2000**, *29*, 398–408.
(10) Vroman, L.; Adams, A. L.; Fischer, G. C.; Munoz, P. C. Interaction of High Molecular Weight Kininogen, Factor XII, and Fibrinogen in Plasma at Interfaces. *Blood* **1980**, *55*, 156–159.
(11) Bouten, C. V. C.; Driessen-Mol, A.; Baaijens, F. P. T. In Situ Heart Valve Tissue Engineering: Simple Devices, Smart Materials, Complex Knowledge. *Expert Rev. Med. Devices* **2012**, *9*, 453–455.
(12) Lehn, J.-M. Dynamers: Dynamic Molecular and Supramolecular Polymers. *Prog. Polym. Sci.* **2005**, *30*, 814–831.
(13) Corbett, P. T.; Leclaire, J.; Vial, L.; West, K. R.; Wietor, J.-L.; Sanders, J. K. M.; Otto, S. Dynamic Combinatorial Chemistry. *Chem. Rev.* **2006**, *106*, 3652–3711.
(14) Neuman, K. C.; Block, S. M. Optical Trapping. *Rev. Sci. Instrum.* **2004**, *75*, 2787–2809.

Chapter 6

Modular supramolecular bilayered scaffolds

Abstract: *Engineering of structurally and/or functionally anisotropic tissues demands extracellular matrix (ECM) mimicking scaffolds with an asymmetric distribution of functionalities. In the case of a bioartificial renal membrane, a thin bilayered scaffold with both a non-fouling, hemocompatible and a renal epithelial cell-adhesive layer would be required. A convenient, modular approach to form porous bilayered scaffolds with tailorable properties is described in this chapter. Hydrogen-bonding ureido-pyrimidinone (UPy) functionalized biomaterial building blocks, both polymers and peptides, are easily mixed-and-matched. This enables exploration of new material combinations with optimal properties. Mixing of 70 wt% hydrophobic, mechanically stable UPy-functionalized polycaprolactone (UPy-PCL) with 30 wt% hydrophilic and mechanically weak poly(ethylene glycol) (UPy-PEG) results in a stable non-cell adhesive material. Incorporation of 4 mol% of UPy-modified Arg-Gly-Asp peptide (UPy-RGD) yields a bioactive material that is adhesive for kidney epithelial cells. Processing of these combinatorial supramolecular biomaterials by electrospinning enables the formation of modular fibrous scaffolds. Spinning of layers with varying composition forms bilayered scaffolds with both a non-cell adhesive and cell-adhesive layer. These findings show that the UPy-based supramolecular biomaterial system offers a versatile toolbox to form modular multilayered scaffolds for tissue engineering and regenerative medicine applications such as the formation of membranes for a living bioartificial kidney.*

The work described in this chapter has been published: B.B. Mollet, M. Comellas-Aragonès, A.J.H. Spiering, S.H.M. Söntjens, E.W. Meijer, P.Y.W. Dankers, *A modular approach to easily processable supramolecular bilayered scaffolds with tailorable properties*, J. Mater. Chem. B., **2014**, 2, 2483-2493.

1. Introduction

Both the development of new materials[1,2] and processing techniques[3,4] have successfully captured parts of the structural characteristics and functions of the natural extracellular matrix (ECM) in synthetic materials. However, the complex, multifunctional character of the ECM makes true mimicry an extremely intricate task. In addition, there is a strong tissue related structural and functional variability.[5] Furthermore these non-static natural scaffolds display ongoing changes upon interaction with cells and overall remodelling plays an important role in for example tissue development and pathological events.[6,7] Therefore, a dynamic, supramolecular biomaterial system that allows a modular or combinatorial approach will best suffice in finding both optimal and versatile solutions to mimic natural biomaterials.[8,9] The ureido-pyrimidinone (UPy) functionality in our supramolecular biomaterials proved useful as 'molecular Velcro' in previous studies. It allowed us to unify a UPy-polymer and UPy-peptides to form a bioactive biomaterial assembly.[10] Here the modularity of the UPy-based biomaterial system is further explored in the formation of anisotropic scaffolds for tissue engineering.

Most tissues have anisotropic properties, both at structural and functional levels. As a result, tissue engineering often demands anisotropic scaffold materials. This anisotropy can be the result of difference in chemical composition or of physical structure. The simplest form of anisotropy is achieved via the formation of a bilayered structure, which results in uniaxial asymmetry. Many examples of bilayered scaffolds are found in the literature in which chemical and/or structural properties vary uniaxially. An example of a single component bilayer is a vascular graft scaffold that is formed from a synthetic, biodegradable elastomer, using two different processing techniques.[11] The inner layer is first produced via thermally induced phase separation (TIPS) to form a highly porous sponge structure. Next a microfibrous outer layer is formed directly on top of the inner layer via electrospinning. Structural bilayers can also be formed with a single processing technique. For example gelatin and chitosan bilayered scaffolds are formed, with variable pore sizes in each layer via a modified freeze-drying procedure.[12] For interface tissue engineering as for osteochondral defects, bilayered scaffolds are needed with tailored space-specific properties, both at biological and mechanical levels.[13] Two separate scaffolds are first produced from different materials with different fabrication techniques, and then joined to form one bilayered scaffold. A bilayer based on anisotropic material composition can easily be formed by the use of one processing technique, as long as a layer-by-layer deposition is possible. This has for example been applied in non-woven textile technologies such as electrospinning.[14]

Telechelic UPy-functionalized polycaprolactone UPy-PCL (Figure 1) allows processing by electrospinning to form a microfibrous porous scaffold. These scaffolds were successfully applied as supports for the culture of renal epithelial cells.[10,15] A bifunctional organization has been proposed to be an inherent property of the natural sopport for renal epithelial cells, the basement membrane (BM).[16] Furthermore, a functional

asymmetry is a fundamental requirement of synthetic membranes for the bioengineering of a bioartificial kidney membrane; one hemocompatible and one cytocompatible surface are needed.[17] Hence, previous work is expanded here towards the formation of bilayered scaffolds for bioartificial renal membrane tissue engineering. Simultaneously, we explore the UPy-based supramolecular biomaterial system's potential to function as a modular synthetic biomaterial platform. We aimed to form a bilayered scaffold with one non-cell adhesive and one cell adhesive side, in which sufficient structural stability is combined with hydrophilic and bioactive properties. Three different UPy-biomaterial building blocks, two polymers and one peptide, are applied in a 'mix-and-match' approach. Similar as described in chapter 5, UPy-PCL is applied as base component. UPy-modified poly(ethylene glycol) (UPy-PEG) is added to establish improved wettability and a cell-adhesion resistant character in the scaffold.[18] As bioactive component the UPy-modified cell-adhesive Arg-Gly-Asp[19,20] peptide (UPy-RGD) is introduced. This UPy-peptide is adapted from previously reported designs (see also chapter 2).[21,22] A short oligo(ethylene glycol) (OEG) linker is inserted between the UPy-moiety and the peptide. This should allow presentation of the peptide at the material surface even in the presence of a hydrated PEG-layer and thereby increase availability for interaction with cells.

Two microfibrous bilayered scaffolds are formed via layered electrospinning of varying compositions of these three UPy-building blocks (Figure 1). In the first bilayer, UPy-PCL and UPy-PEG are applied in a 'mix-and-match' approach with the intention to generate a cell-adhesive layer and a more hydrophilic, non-cell adhesive layer. The second bilayer is entirely based on the hydrophilic, non-cell adhesive material mixture, but one side is supplemented with a small quantity of UPy-RGD to stimulate cell adhesion. Both scaffolds are investigated for chemical composition, morphology and hydrophilicity at their surfaces. Finally their effect on the adhesion ability and morphology of human kidney epithelial cells is assessed. In addition to this, more detailed cell-studies are performed on thin electrospun meshes and drop-cast films of the three UPy-biomaterials mixtures.

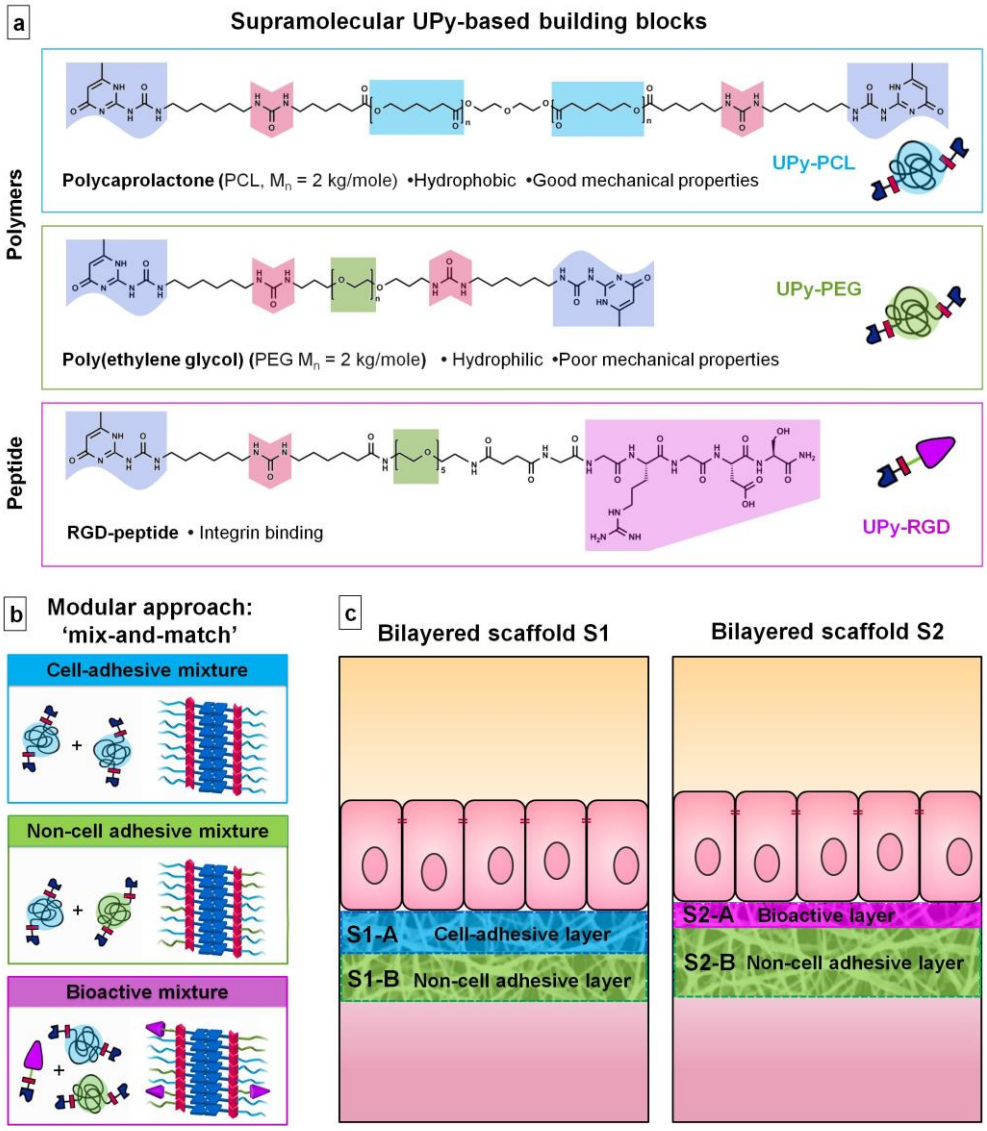

Figure 1. Supramolecular UPy-based building blocks and bilayered scaffolds. (a) Chemical structures and schematic representations of the supramolecular polymers UPy-PCL and UPy-PEG and the supramolecular bioactive component, UPy-RGD. (b) Schematic representations that show the proposed formation of new supramolecular materials via incorporation of the different UPy-building blocks into the stacks of UPy-dimers when mixed, and (c) bilayered scaffolds S1 and S2 that are electrospun using these combined supramolecular building blocks. These bilayered scaffolds are designed to facilitate cell adhesion on their top layer A and to prevent cell adhesion to the bottom layer B, as envisioned to be required for a bioartificial living renal membrane.

2. Results and discussion

2.1 Preparation and morphology of bilayered electrospun scaffolds

Two different bilayered scaffolds, S1 and S2, with distinct layer properties were prepared via layered electrospinning. The first bilayered scaffold (S1) aimed to include a layer adhesive for cells via aspecific interactions (S1-A), and one non-cell adhesive layer (S1-B). The relatively hydrophobic UPy-PCL was applied to form the cell-adhesion compatible layer S1-A. In layer S1-B 30 wt% of the hydrophilic UPy-PEG was added in the electrospinning process, with the aim to form a more hydrophilic, non-cell adhesive layer. This change in electrospin composition was achieved by simply exchanging the feeding syringe attached to the PTFE tubing that guided the solution to the spinning needle, for another feeding syringe that had been pre-filled with the new solution of UPy-polymers. In this layer UPy-PCL and UPy-PEG were mixed. UPy-PEG alone could not be processed into a fibrous polymer mesh using electrospinning, but resulted in electrosprayed droplets (see chapter 3). However, the addition of 30 wt% UPy-PEG to UPy-PCL did not negatively influence the electrospinning process at the chosen processing settings.

SEM imaging was performed in low vacuum mode without the application of a conducting layer, such as sputtered gold, on the specimen. This allowed recording of both backscattering electron (BSE) and secondary electron (SE) signals directly from the sample. This allowed us to distinguish both layers based on a small difference in chemical composition (Figure 2). The layers are tightly adhered as shown by the absence of a sharp transition at their interface. It was found that the layers formed one continuous membrane when the electrospinning solution was fed continuously. The fiber density throughout bilayer S1 was evenly distributed, as observed in the cross-section of the scaffold. The top and bottom-views of bilayer S1 showed similar morphologies (Figure 2). The deposition of randomly oriented fibers with diameters typically in the submicron range resulted in apparent pore sizes smaller than 5 μm for both layers S1-A and S1-B (top and bottom views), which should allow adherent renal epithelial cells to grow on top of the scaffold surface, rather than inside the scaffold.

In bilayered scaffold S2, both layers S2-A and S2-B were formed using the supramolecular polymer combination of UPy-PCL + 30 wt% UPy-PEG, with 4 mol% of cell-adhesive UPy-RGD added to layer S2-A. Hence, the difference in atomic composition between the layers of scaffold S2 was very small and was not observed in SEM imaging (Figure 2). For scaffold S2, the transition between both layers in the cross-section was marked by a slightly more densely packed fiber structure in layer S2-B. This correlated with the overall smaller fiber diameter (283 ± 139 nm) in this layer as observed in the bottom-view of the scaffold, compared to layer S2-A in the top-view of the scaffold (428 ± 226 nm).

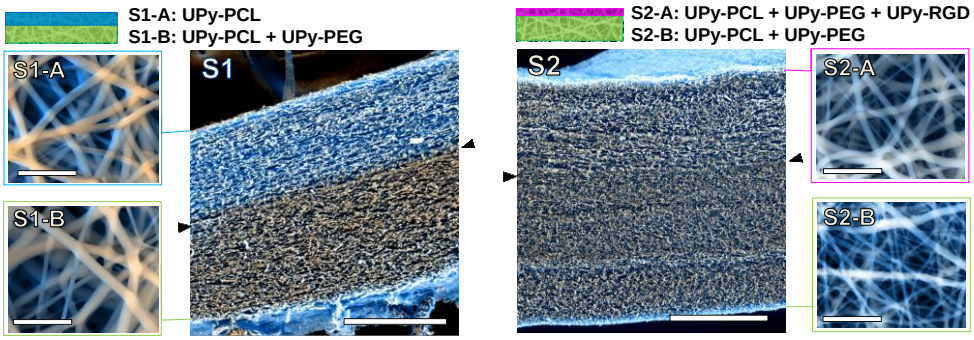

Figure 2. SEM micrographs of electrospun bilayered scaffold S1 and S2. In the cross-section of the scaffolds the layer transition is indicated by the black arrows (scale bars represent 200 µm). Top (A) and bottom (B) views show the fiber diameters and apparent pore sizes of each scaffold layer (scale bars represent 5 µm). Average fiber diameters ± standard deviation were determined from these and other micrographs: S1-A: 576 ± 215 nm, S1-B: 636 ± 359 nm, S2-A: 428 ± 226 nm, S2-B: 283 ± 139 nm. In these overlay images the BSE signal is indicated in yellow, SE signal in bleu. The SE signal is strongly influenced by the angle of the sample, giving rise to higher intensities to the edges of the cross-sectioned samples. At the cross-section, differences in chemical composition cause the difference in detected intensity.

Successful electrospinning of the bilayered scaffolds demonstrates that the UPy-based biomaterial approach allows the facile combination of different UPy-polymers and UPy-peptide to construct layered scaffolds with this processing technique. Furthermore, successful electrospinning of layers S1-B and S2-B demonstrates that a convenient combination of different UPy-polymers into new supramolecular copolymers is possible via a mix-and-match approach. This allows us to make use of distinct polymer properties in a joint supramolecular biomaterial assembly, and thereby allows tailoring of scaffolds towards desired material requirements.

2.2 Chemical composition and wettability of bilayered scaffold surfaces

Attenuated total reflectance Fourier transform infrared spectroscopy (ATR-FTIR) was performed on both the top and bottom layers of scaffolds S1 and S2. The recorded spectra were compared to reference spectra of pure UPy-PCL and UPy-PEG to monitor the chemical composition of each layer surface (Figure 3). As expected the spectrum of layer S1-A corresponded to pure UPy-PCL. For layer S1-B, a mixed spectrum of UPy-PCL and UPy-PEG was observed. This was especially seen in the changed ratio of C-O vibrations at 1160 cm^{-1} (ester) and 1094 cm^{-1} (ether). This indicated that both UPy-PEG and UPy-PCL were present at the surface of the electrospun fibers. For bilayered scaffold S2 the spectra of both layers S2-A and S2-B corresponded, as expected, to this mixed polymer composition. The presence of UPy-RGD in layer S2-A was not observed by this technique. This does not mean that the RGD peptide was not present at the surface of scaffold layer S2-A. The UPy-RGD largely resembles the UPy-PEG and UPy-PCL in terms of chemical bond

composition. Only the peptide part would generate distinct signals in ATR-FTIR. However, this technique was not sensitive enough to detect the small quantity of UPy-RGD that was added.

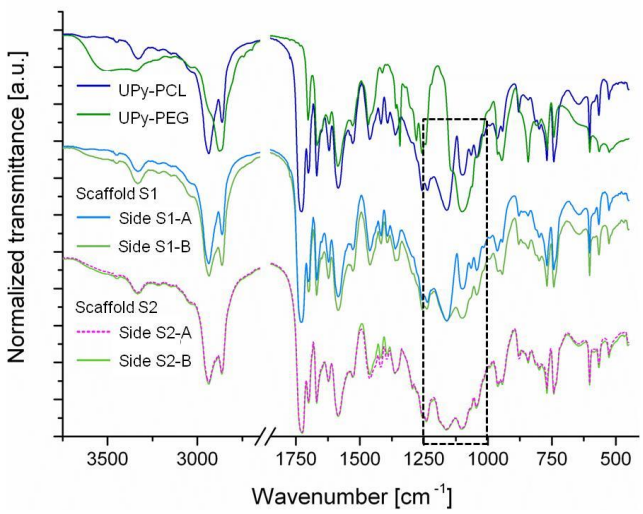

Figure 3. ATR-FTIR spectra of electrospun bilayer surfaces and reference compounds. Spectra of both sides A and B of the electrospun bilayered scaffolds S1 and S2 containing: (S1-A) UPy-PCL, (S1-B, S2-B) UPy-PCL + 30 wt% UPy-PEG and (S2-A) UPy-PCL + 30 wt% UPy-PEG + 4 mol% UPy-RGD, are compared to spectra of pure UPy-PCL and UPy-PEG. The marked spectral region indicates the most pronounced change in the FTIR spectra when mixing UPy-PCL and UPy-PEG.

Water contact angle (WCA) measurements were performed to study the influence of UPy-PEG on the wettability of the electrospun layers (Table 1). Images were recorded at a rate of 25 frames per second, up to 60 seconds after the initial contact of the water drop with the scaffold surface. Layer S1-A, composed of 100% UPy-PCL, showed high contact angles (120.5 ± 2.5°). This was as expected for the hydrophobic PCL backbone in this supramolecular polymer and the additional reducing effect on the wettability by the roughness of the electrospun fibrous morphology.[23] Furthermore, no significant decrease of contact angle was observed during the measuring period of 60 seconds. Also, the drop did not change in size, indicating that the water was not able to enter the pores of the scaffold within the timeframe measured. A completely different behaviour was seen for scaffold layer S1-B in which hydrophilic UPy-PEG was present. Upon initial contact with the scaffold the water contact angle was 50.0 ± 2.9°, which was significantly lower compared to S1-A. This indicated that the surface of S1-B was more hydrophilic than the surface of S1-A, and that this was caused by the addition of 30 wt% UPy-PEG during the electrospinning of layer S1-B. After initial contact, the angle quickly reduced further. This was attributed to the absorbance of water into the porous material. As the volume of the drop on top of the scaffold reduced, the height of the drop reduced and hence the contact

angle became smaller until it could no longer be measured. This state was reached within 2 seconds. For bilayer S2, the observed initial contact angles for sides S2-A and S2-B were 55.5 ± 4.4° and 60.1 ± 4.0°, respectively. For both sides similar quick drop absorption times (< 2 sec) were observed. From these results no conclusion on difference in chemical make-up at the mesh surfaces as result from the presence of 4 mol% UPy-RGD in layer S2-A can be drawn. Even if all RGD would be presented at the fibers surfaces, the effect on hydrophilicity would be small. Furthermore, the accuracy for determining water contact angles on these absorbing materials is limited. Although the chemical compositions of layers S1-B and S2-B were equal, a difference in the average initial contact angle of ~10° was observed. This could be attributed to the minor morphological difference; water had more difficulty to penetrate the slightly smaller apparent pores of S2-B. However, the limited speed at which the images were recorded (25 frames per second), combined with the fast absorption of water, caused an offset in what was observed as the initial contact; for some samples a decrease of > 10° was observed between two consecutive frames directly after initial contact.

The ATR-FTIR results show the presence of UPy-PEG at the surface of layers S1-B, S2-B and S2-A. According to WCA measurements, this leads to an increase of hydrophilicity and extreme enhancement of scaffold wettability. Bilayered scaffold S1 demonstrates a uniform structure while anisotropic chemical composition results in distinct wettability of each scaffold side. This uniaxial asymmetry is a result of the layered processing technique. There are no indications of demixing of the building blocks within each layer. The small confinement of the different components during the formation of electrospun fibers and the fast evaporation of the single solvent may contribute to a homogeneously mixed distribution of components, but the shared UPy-functionality is assumed to further enhance the establishment of a molecularly mixed composition via the formation of a joint supramolecular biomaterial assembly.

Table 1. Water contact angles (°) on electrospun bilayer surfaces. Measurements were performed in time. The average of n=3 samples is expressed ± standard deviation.

Time (s)	S1-A UPy-PCL	S1-B UPy-PCL +UPy-PEG	S2-B UPy-PCL +UPy-PEG	S2-A UPy-PCL +UPy-PEG +UPy-RGD
0.0	120.5 ± 2.5	50.0 ± 2.9	60.1 ± 4.0	55.5 ± 4.4
0.2	-	40.1 ± 6.0	47.0 ± 5.2	35.0 ± 9.1
0.4	-	31.7 ± 5.1	39.6 ± 6.2	21.2 ± 15.2
1.0	-	17.7 ± 8.8	18.0 ± 1.4	15.7 ± 7.3
2.0	-	N.A.	N.A.	N.A.
10.0	120.0 ± 2.4	-	-	-
60.0	119.4 ± 2.7	-	-	-

2.3 Cell adhesion and cell morphology on bilayered scaffolds

Human kidney epithelial cells (HK-2) were seeded in a high density (~180 x 10^3 cells per sample) on the bilayered scaffolds to investigate the effect of increased hydrophilicity and introduced bioactivity in the separate scaffold layers. Cell adhesion and morphology was studied using fluorescence microscopy imaging of the actin cytoskeleton which was stained with fluorescently labelled phalloidin 14 hours after cell seeding. For bilayered scaffold S1, cell adhesion and spreading on layer S1-A confirmed the cell-adhesive character of electrospun UPy-PCL as observed in previous studies.[10,15] The addition of 30 wt% UPy-PEG to layer S1-B, which showed increased hydrophilicity and scaffold wettability, was hypothesized to reduce cell adhesion. Indeed fewer cells were observed on layer S1-B. In addition these cells remained in a rounded morphology, indicating that no cell spreading or proper cell adhesion occurred. Similar lowered cell density and round morphology was observed for scaffold S2 on layer S2-B. In contrast, different cell behavior was observed for the HK-2 cells that were seeded on scaffold layer S2-A. Here HK-2 cells adhered, spread and formed a near confluent cell layer within 14 hours. The chemical difference of layer S2-A compared to both layers B of scaffolds S1 and S2 was only 4 mol% UPy-RGD. This demonstrated that at least part of the RGD-peptide that was added to the electrospinning solution was presented at the surface of the polymer fibers, available for specific interaction with cells. This had not been demonstrated for a two-component UPy-polymer mix before. Here the presence of the hydrophilic UPy-PEG component might interfere with the surface presentation of the peptide, in particular when the material is hydrated in the aqueous cell-culture environment. To anticipate this effect, a short oligo(ethylene glycol) linker was incorporated between the UPy-moiety and the peptide to allow bridging of the expected hydrated PEG-layer at the material surface. The difference in cell behavior on layer S2-A and both layers B not only confirms RGD-peptide presentation at the surface of the electrospun fibers, but also shows that the amount of peptide present at the surface provided enough anchoring points to allow the HK-2 cells to adhere and spread on an otherwise cell-adhesion repulsive material. Nonetheless, the applied quantity of UPy-RGD might still be optimized. Possibly smaller amounts of bioactive compounds provide equal or even better effects with respect to cell adhesion. For HK-2 cells cultured on electrospun fibrous supports consisting of polymethylmethacrylate (PMMA) with different collagen I coatings, it has been reported that the largest amount of proteins adsorbed on fibers does not lead to the best performance in terms of cell attachment and proliferation in vitro.[24]

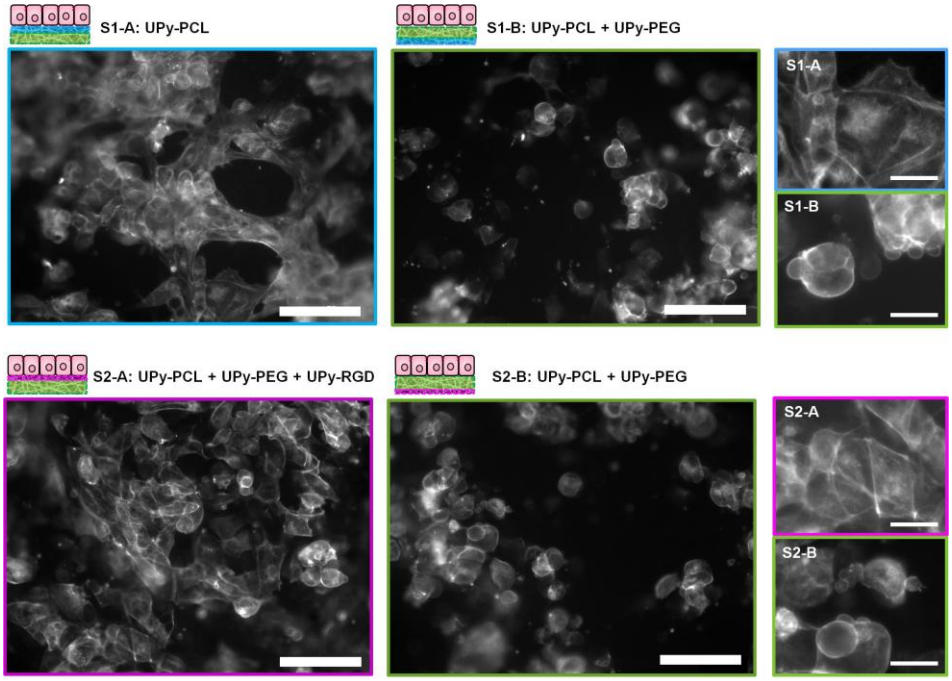

Figure 4. HK-2 cell adhesion and morphology on bilayered scaffolds. Fluorescence micrographs of the actin cytoskeleton of HK-2 cells on the different bilayered scaffold sides 14 hours after seeding. Scale bars represent 100 µm. In the enlarged views (right, scale bars represent 25 µm) the morphological differences between the HK-2 cells on the different scaffold sides is clearly seen. In absence of UPy-PEG (S1-A) cells adhere and spread, in presence of UPy-PEG (S1-B, S2-B) cells remain in a round morphology due to lack of cell attachment. The presence of blebs in these cells indicates decoupling of the cytoskeleton from the plasma membrane and advancing apoptosis. Addition of UPy-RGD (S2-A) allows cells to adhere and spread, even in presence of UPy-PEG.

2.4 Detailed investigation and discussion of the interaction between HK-2 cells and UPy-biomaterials

The interaction between cells and biomaterials is very complex and influenced by many factors that have a direct or indirect effect. This complexity makes that cell-biomaterial interaction studies are rarely straightforward and often gives rise to non-black-and-white results. As shown, cells do adhere to some extent to the 'non-adhesive' scaffold sides S1-B and S2-B, albeit cell morphology was observed to be less spread compared to the cell-adhesive scaffold sides S1-A and S2-A. To investigate the cell-biomaterial interaction for our supramolecular UPy-based biomaterials in more detail, we seeded HK-2 cells on both drop-cast films and electrospun meshes on glass. Both sample groups represented all the three different UPy-biomaterial combinations that were used in the bilayered scaffolds. Scanning electron micrographs of the electrospun meshes on glass supports revealed differences in average fiber diameter for the three different UPy-biomaterial combinations; 827 ± 364 nm for UPy-PCL, 534 ± 146 nm for UPy-PCL + 30 wt%

UPy-PEG and 437 ± 90 nm for UPy-PCL + 30 wt% UPy-PEG + 4 mol% UPy-RGD. Although average fiber diameter directly influences apparent pore size, all meshes showed to be dense enough to prevent adhesion of cells to the glass support instead of to the UPy-electrospun fibers. The meshes furthermore all possess a homogeneous, flat surface (Figure 5). These flat meshes and flat drop-cast films allow for more detailed studies between biomaterial surface and cells, via fluorescence microscopy imaging at the single cell level.

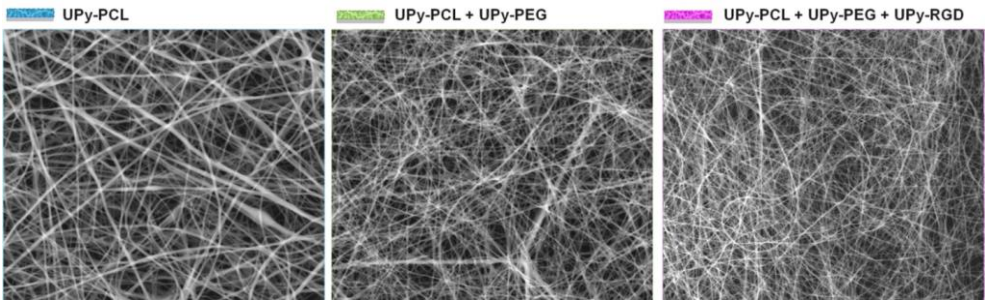

Figure 5. Scanning electron micrographs of electrospun meshes on glass. UPy-biomaterial meshes were prepared as thin layers of randomly oriented microfibers on glass coverslips. These micrographs give an impression of the overall mesh morphology (scale bars represent 50 µm). From micrographs recorded at higher magnification (not shown here), average fiber diameters were determined: UPy-PCL: 827 ± 364 nm, UPy-PCL+UPy-PEG: 534 ± 146 nm, UPy-PCL+UPy-PEG+UPy-RGD: 437 ± 90 nm.

First HK-2 cells were seeded at a high density of approximately 180 x 10^3 cells per sample and imaged 14 hours after seeding as was done for the bilayered scaffolds (Figure 6). For the drop-cast films differences were observed in the amount of cell adhesion that followed the expectations; almost confluent cell densities adhered to the pure UPy-PCL and UPy-RGD containing films, whereas noticeably less cells adhered on the UPy-PCL + UPy-PEG film, although to the latter also small patches with high cell densities were identified (Figure 6 top). Apparently the cells were able to adhere at selective places and probably cluster together there, in absence of more places to adhere. For the electrospun meshes on the other hand, cells adhered on the presumed non-cell adhesive UPy-PCL + UPy-PEG in similar high, near confluent density (Figure 6, bottom). Besides comparable cell numbers, the cell morphology appears to be similar for the different meshes at low magnification. For the UPy-PCL + UPy-PEG mixture these results seem inconsistent with the distinctly rounded HK-2 cell morphology that was observed for bilayered scaffold sides S1-B and S2-B, which are of the same chemical composition. The ability of epithelial cells to form epithelial bridges to span non-adhesive surfaces[25] was considered as possible mechanism for these deviating results. Hence cell seeding density was lowered in an attempt to circumvent cell-cell interactions to overshadow initial cell-biomaterial interactions. Furthermore, reduction of cell-cell interactions was assumed to benefit the visualisation of cell-biomaterial interaction via fluorescent labelling of vinculin, since vinculin is both present at focal adhesions and adherent junctions.[26]

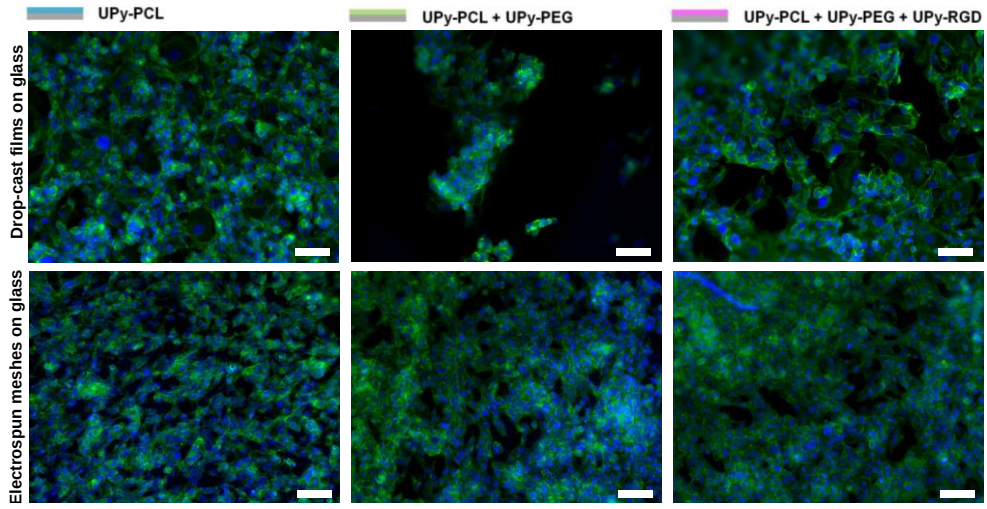

Figure 6. Fluorescence micrographs of HK-2 cells on drop-cast films and electrospun meshes. Cells were imaged 14 hours after seeding a high density (~180 x 10^3 cells per sample) on different UPy-biomaterial drop-cast films (top row) and electrospun meshes (bottom row). Cell nuclei (blue) and actin cytoskeleton (green) show the cell density and spreading of the cells. The cell-adhesion repulsive effect of UPy-PEG and cell adhesion inducing effect of UPy-RGD is clearly seen for the drop-cast films, whereas no clear differences are observed for the electrospun meshes. Scale bars represent 100 µm.

For the different drop-cast films a clear variation in the number of adhered cells was observed when HK-2 cells were seeded at a low cell density of approximately 36 x 10^3 cells per sample (Figure 7a). Corresponding to what was observed for the bilayered scaffolds, fewer cells adhered and spread on the non-cell adhesive combination (UPy-PCL + 30 wt% UPy-PEG), while the presence of UPy-RGD restored cell adhesion and spreading in this supramolecular co-polymer.

Micrographs taken at higher magnification allowed visualisation of focal adhesion points and showed clear differences at single cell morphology level. Lack of cell adhesion and spreading on the UPy-PCL + UPy-PEG drop-cast films coincided with the lack of both a well-defined actin skeleton and vinculin-rich focal adhesion points, which were formed by HK-2 cells cultured on the pure UPy-PCL and UPy-RGD supplemented films.

When HK-2 cells were seeded at a low density on the electrospun meshes, again a more equivalent number of cells seemed to adhere to all three different UPy-biomaterial compositions (Figure 7b), as was observed at high cell seeding density (Figure 6). When cell-mesh interactions were studied in more detail at single-cell level differences between the different meshes were clearly visible. Higher magnification micrographs revealed vinculin-rich focal adhesions which clearly collocate with the fibers of the pure UPy-PCL mesh. This was also visible for cells on the UPy-RGD containing mesh, although less pronounced due to the smaller fiber diameters in this mesh. Such focal adhesion formation was not observed 14 hours after cell seeding on the UPy-PCL + UPy-PEG mesh, confirming the cell adhesion repulsive character of this UPy-polymer combination.

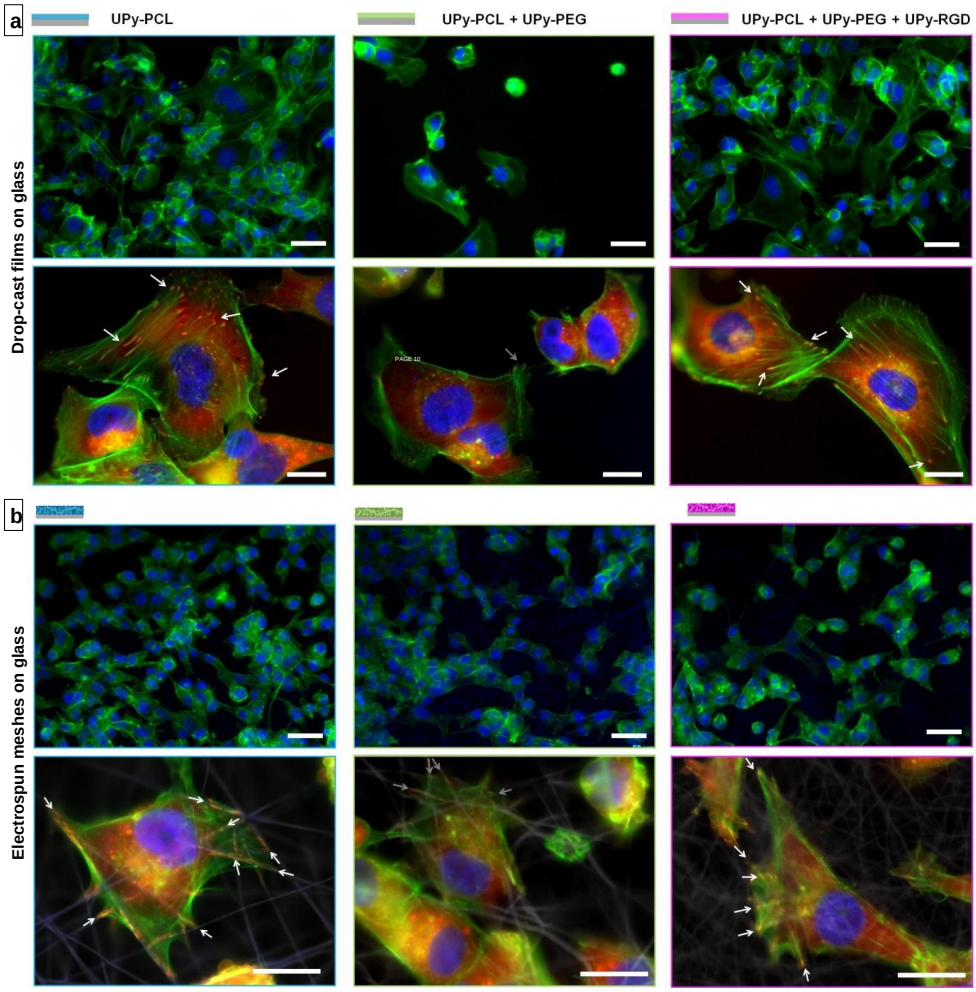

Figure 7. Fluorescence micrographs of HK-2 cells seeded at low density on films and meshes. Cells were stained 14 hours after seeding ~36 x 10^3 cells per sample for actin (green), vinculin (red, for clarity not shown in the small magnification images) and cell nuclei (blue), and imaged at small and high magnification (scale bars represent 50 µm and 20 µm, respectively). **a)** Drop-cast films: Small magnification micrographs indicate the difference in adhered cell number and cell spreading; In presence of UPy-PEG and absence of UPy-RGD, fewer cells adhere and relative more cells remain in a round morphology. In the enlarged views the single cell morphological differences are clearly visible. On UPy-PCL + UPy-PEG the cells display an ill-defined actin skeleton and vinculin is not concentrated in focal adhesion points. In presence of UPy-RGD, vinculin-rich focal adhesion points are observed at the ends of well-defined stress-fibers of the cytoskeleton, which is also seen for HK-2 cells seeded on pure UPy-PCL drop-cast films (indicated by the white arrows). **b)** Electrospun meshes: The adverse effect of UPy-PEG on cell adhesion is not clearly observed at low magnifications. Hence, also no clear positive effect of UPy-RGD is distinguished. Higher magnification images show vinculin concentrated at focal adhesion points, which collocate with the electrospun fibers (indicated by white arrows, arrow direction corresponds to fiber direction. These focal adhesions are most pronounced on the pure UPy-PCL mesh. In presence of UPy-PEG focal adhesions are absent or not observed at places where they would be expected (indicated with gray arrows). In presence of UPy-RGD the characteristic focal adhesion points are present (appear in yellow, due to overlap of red and green).

To investigate the development of these cultures in time, evaluation of the low density cell cultures on the electrospun meshes was performed 3 days after cell seeding. The adhered cells proliferated and formed a near-confluent cell layer with tight junction formation between the cells on all three different UPy-biomaterial compositions (Figure 8). Remarkably, when looking at a 3-day cell culture on bilayered scaffold S1, the cells that initially adhered to the UPy-PCL + UPy-PEG side after seeding a high cell density were not capable of such a development. Instead of increasing cell numbers, fewer cells remained over time (Figure 9).

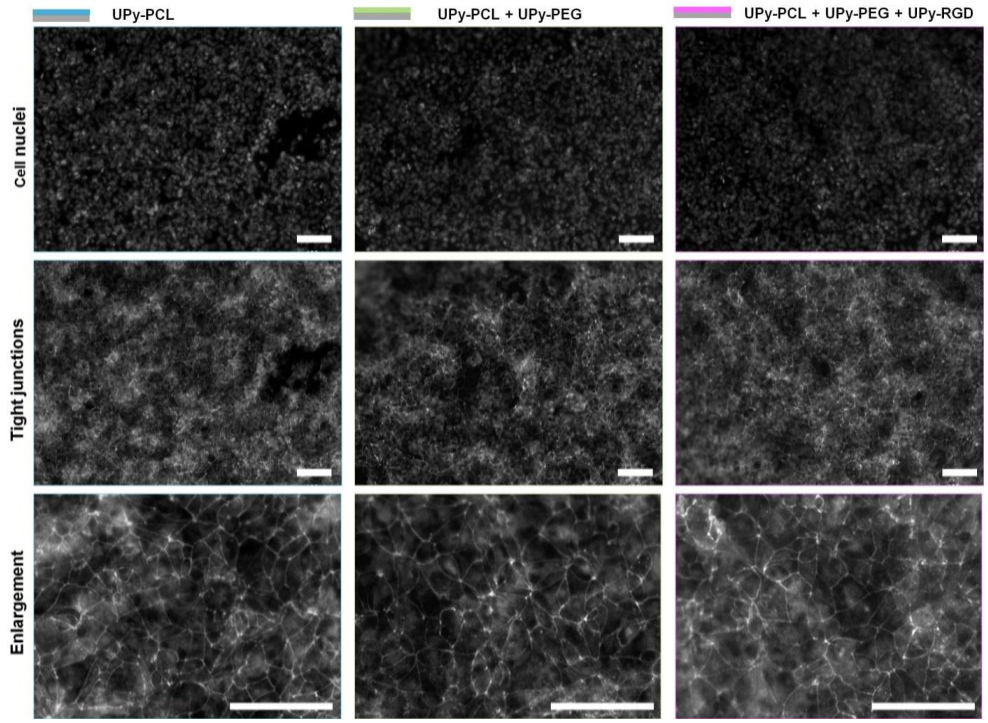

Figure 8. Fluorescence micrographs of HK-2 cells on electrospun meshes after 3 days. HK-2 cells were seeded at low density (~36 x 10^3 cells per sample). Large patches of confluent cells are observed for all three mesh compositions. Staining of cell nuclei (top row) indicates a high cell density, and staining of zona occludens-1 (ZO-1) protein shows the presence of tight junctions (middle and bottom row) throughout the confluent cell layer. The magnified micrographs of ZO-1 staining (bottom) show the characteristic fine-lined pattern indicating tight cell-cell contact in the confluent epithelial cell layer. All scale bars represent 100 µm.

A resazurin assay performed on the low and high density cultures on the electrospun meshes provided more quantitative information on the viability and activity of the cells on the different supports (Figure 10). This assay, based on the mitochondrial conversion of resazurin into fluorescent resorufin, allows monitoring of total mitochondrial activity and hence gives an indirect indication of the number of viable cells present on the meshes.

Indeed on average an equal signal for the different UPy-biomaterial meshes in the resazurin assay was observed after seeding the HK-2 cells. For the high cell seeding density, which provided enough cells to form an instant confluent cell layer upon cell adhesion, no increase in cell number was observed when comparing the cultures after 1 day and after 3 days. When a lower, sub-confluent cell density was seeded, increase in signal over time was observed, which indicated cell proliferation.

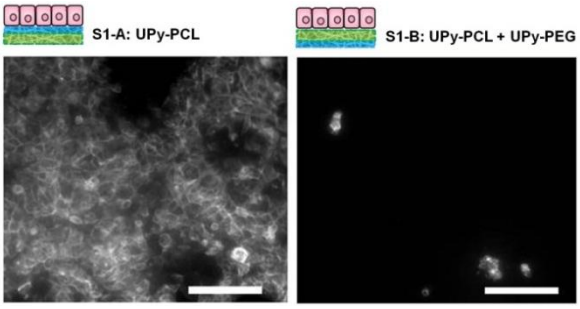

Figure 9. HK-2 cells on bilayered scaffold 1 after 3 days. The actin cytoskeleton of the cells was stained and visualized 3 days after seeding ~180 x 10^3 cells. The HK-2 cells appear to proliferate on the pure UPy-PCL S1-A scaffold side to form larger confluent patches. On the contrary, for the UPy-PEG containing scaffold side S1-B, the number of cells present on that scaffold side decreased over time (Scale bars represent 200 µm).

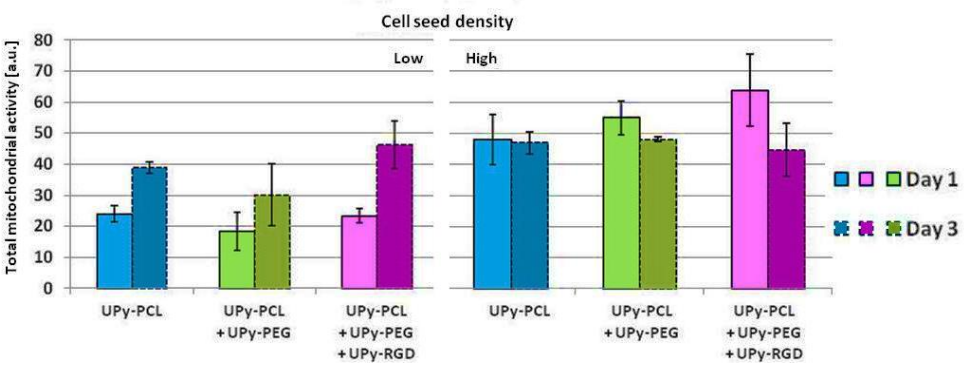

Figure 10. Resazurin mitochondrial activity assay on HK-2 cells cultured on electrospun meshes. The assay was performed at day 1 and day 3 on the same samples (n=3), after seeding HK-2 cells at high (180 x 10^3 cells per sample) or low (36 x 10^3 cells per sample) density. More cells adhered when seeded in a higher density, independent of chemical composition of the mesh. Assuming that an increase of total mitochondrial activity relates to an increase of viable cells, these results indicate that HK-2 cells that attached to the meshes remain viable and are able to proliferate when seeded in a sub-confluent density.

Altogether, these results show differences in cellular development on supramolecular biomaterial supports with equal overall chemical composition. Differences in cellular behaviour between drop-cast films and electrospun microfibrous surfaces might be the result of differences in surface morphology. However, also a strongly variable behaviour was observed when comparing the electrospun bilayers and the electrospun meshes on glass. This might be explained by deviations in surface distribution of the different

supramolecular building blocks. These results thus underline not only the complexity of cell-biomaterial interaction in general, in which already many direct or indirect factors may play a role, but more specifically the difficulty when working with intrinsically dynamic supramolecular biomaterials. In comparison with covalently built-up biomaterials, supramolecular systems can adjust and change their properties in time and are more responsive towards their environment. This can be considered advantageous in combination with cells when the goal is to mimic natural ECM. However, extra care has to be taken while interpreting experimental results when working with such materials. Very small, uncontrolled parameters during biomaterial production might have a unforeseen influence on the biomaterial assembly, such as for example the temperature and humidity during the electrospinning process. Furthermore, also small variations in the history of the material could potentially cause deviating experimental results. Overall, the results demonstrated that it is possible to use supramolecular UPy-biomaterial building blocks in a modular approach. However, more work is needed to better understand which factors influence the 'supramolecular synthesis' of these materials, to gain in-depth insight into material dynamics, and to ultimately control the material and its dynamics, before total control over cell behaviour can be established.

3. Conclusion

In this chapter we have demonstrated the use of a supramolecular approach to form anisotropic electrospun scaffolds, based on UPy-modified polymers and peptide building blocks. Two different UPy-polymers, UPy-PCL and UPy-PEG, were successfully combined. Unmodified PCL and PEG are difficult to mix and tend to crystalize[27] and phase-separate[28] at room temperature. This demonstrates that UPy-modification enhances miscibility as a result of the unifying UPy-moiety. The resulting supramolecular co-polymer biomaterial carries specific properties of both components; suitable mechanical properties to allow the formation of a microfibrous, porous scaffold by electrospinning and the desired hydrophilic and furthermore anti-adhesive property for cells, respectively. Furthermore, reactivation of cell-adhesion in this UPy-polymer mix, was established by addition of UPy-modified cell-adhesive RGD-peptides. To our knowledge, this is the first example where PCL, PEG, and RGD are employed in a supramolecular material system that can be used in a modular approach to form microfibrous electrospun bilayered scaffolds.

The advantage of this modular biomaterial approach is that no covalent synthesis is needed to generate new biomaterials. Once the UPy-building blocks are available they can be mixed-and-matched to combine desired biomaterial properties. The choice of both polymer backbones and bioactive peptides that can be applied is endless. Therefore this UPy-based biomaterial system provides a convenient and versatile platform for the formation of new biomaterials. Combined with high throughput screening, i.e. a materiomics approach, this supramolecular biomaterial system is proposed to benefit the

exploration and identification of biomaterials with ECM or BM-mimicking properties. However, additional care is needed when screening these supramolecular, dynamic biomaterials. Small changes, not only during the 'supramolecular synthesis' of the materials, but also during read-out can cause unforeseen changes in the experimental outcome. Hence in-depth research is needed to gain more insight into and control over supramolecular biomaterial dynamics, before total control over cellular behaviour can be achieved via these materials.

4. Acknowledgements

We thank Bas Meusen for initial experiments, and Geert van Almen and Ewelina Burakowska-Meise for useful discussions. The research leading to these results has received funding from the Ministry of Education, Culture and Science (Gravity program 024.001.035), the Netherlands Organisation for Scientific Research (NWO) and the European Research Council (FP7/2007-2013) ERC Grant Agreement 308045 and 246829. This research forms part of the Project P3.01 BioKid of the research program of the BioMedical Materials institute, co-funded by the Dutch Ministry of Economic Affairs. The financial contribution of the Dutch Kidney Foundation is gratefully acknowledged.

5. Experimental section

Synthesis of UPy-polymers and UPy-peptide

The syntheses of the compounds UPy-PCL (batch 2-II),[10,29] UPy-PEG and UPy-RGD peptide[22, 21] was adopted from previously reported descriptions and is described in chapter 2.

Preparation of electrospun bilayered scaffolds, thin meshes and drop-cast films

Bilayered scaffold S1

Two electrospinning solutions were prepared in glass vials. For the bottom layer (S1-B) 17.5 wt/wt% UPy-PCL was dissolved in 82.5 wt/wt% 1,1,1,3,3,3-hexafluoro-2-propanol (HFIP, 147545000, Acros) (B). For the top layer (S1-A), 7.5 wt/wt% UPy-PEG was first dissolved in 75 wt/wt% HFIP, then 17.5 wt/wt% UPy-PCL was added (A). The solutions were stirred overnight at room temperature and then transferred to separate 2.5 mL glass syringes (Hamilton). Approximately 1 mL of the first solution (B) was fed at 0.02 mL min^{-1} using a syringe pump (KR analytical) at the outside of the electrospinning cabinet to the flat-tip stainless-steel 23 g needle (Intertronics, United Kingdom) inside the cabinet, via a 35 cm long 1 mm I.D. PTFE tube. Inside the cabinet, the solution was spun with an in-house built electrospun setup by the application of 18.5 kV between a tip-to-target distance of 12 cm. Fibers were collected on a 12 x 12 cm grounded collector plate. To enable facile removal of the non-woven electrospun membrane, the collector was covered with a thin sheet of polyethylene film. The fiber deposition was interrupted several times to move the static collector plate over a 3x3 grid to enlarge the area of fiber deposition and to achieve a more homogeneous layer thickness. Then the feeding syringe was replaced with the syringe containing mixed polymer solution A and the flow rate was set at 0.015 mL min^{-1}. Small indentations were created along the thin edges of electrospun layer

S1-B to enable visual control of an evenly distributed fiber deposition during spinning of the second layer S1-A. Fibers, again formed from approximately 1 mL polymer solution, were collected on top of the previously deposited fiber layer S1-B. The polyethylene film was gently removed from the electrospun scaffold. The scaffold was placed *in vacuo* at 40° C overnight to remove any residual solvent.

Bilayered scaffold S2

The electrospinning solution for bottom layer S2-B was prepared as for bilayered scaffold S1; by first dissolving 7.5 wt/wt% UPy-PEG in 75 wt/wt% HFIP, after which 17.5 wt/wt% UPy-PCL was added. For the top layer (S2-A) first 4 mol% UPy-RGD (compared to total mol polymer) was dissolved in the appropriate amount of HFIP (75 wt/wt%), then 7.5 wt/wt% UPy-PEG was added to dissolve and last 17.5 wt/wt% UPy-PCL. Electrospinning was performed as described for bilayer S1.

Thin meshes on glass coverslips

For meshes on glass, three polymer solutions, UPy-PCL, UPy-PCL+ 30 wt% UPy-PEG and UPy-PCL+ 30 wt% UPy-PEG + 4 mol% UPy-RGD, were prepared as for the bilayered scaffolds. Also equal electrospinning settings were applied. On top of the collector plate, which was covered with a thin sheet of polyethylene (PE) film, round glass coverslips of 12 mm Ø were placed. Electrospun fibers were collected until an opaque, thin sheet was formed. The glasses with meshes were removed from the collector together with the PE film and placed as a whole *in vacuo* at 40° C overnight to remove any residual solvent.

Drop-cast films on glass coverslips

The UPy-biomaterial solutions as used for the preparation of electrospun meshes on glass were diluted five times with HFIP. Thin drop-cast films were prepared by distributing 25 µL of such a solution on a 12 mm Ø glass coverslip. The HFIP was evaporated. To remove any residual solvent, the drop-cast films on glasses were placed *in vacuo* at 40° C overnight.

Scaffold and mesh morphology: Scanning electron microscopy

Environmental scanning electron microscopy (ESEM) imaging was performed by using FEI Quanta 600 and Xt Microscope Control software. Samples were prepared by placing small pieces of each scaffold, facing top and bottom side up, and a sample of each batch of meshes on glass, on double-sided sticky carbon tape on a metal stub. A cross-section of the scaffolds was gently cut with a razor blade and placed sideways on the tape. The uncoated samples were directly visualized in a low vacuum (~0.5 mbar) with an accelerating voltage of 18 kV and a working distance of 8 mm. Images were recorded up to 10,000 times magnification. Both backscattering electrons (BSE) and secondary electrons (SE) were detected. Artificially colored images were constructed by overlaying the resulting images from both detectors. Microfiber diameters were determined from multiple high magnification images using ImageJ software and expressed as average ± standard deviation.

Chemical composition of bilayered scaffold surfaces: Infrared spectroscopy

Infrared spectra were recorded on a Fourier transform infrared spectrometer (Perkin Elmer Spectrum Two, with a Universal ATR sampling accessory and diamond crystal, Perkin Elmer Instruments, The Netherlands). Transmission spectra were recorded at room temperature in the range of 4000–450 cm^{-1} at a resolution of 4 cm^{-1} and with an accumulation of 4 scans. Both sides of the bilayered scaffolds were measured separately. A sample was placed on the crystal and covered with a glass slide. Then gentle force was applied on top of the glass slide using a flat shoe to achieve good contact between the sample and the crystal. As control, spectra of both pure UPy-PCL and UPy-PEG were recorded. Transmission spectra were normalized to the maximum intensity peak

(1728 cm^{-1}, C=O stretch vibrations of the ester carbonyl group for UPy-PCL containing samples and 1094 cm^{-1}, ether C–O–C stretch in pure UPy-PEG).

Hydrophilicity of bilayered scaffolds: Water contact angle measurements

Water contact angle measurements were performed on a contact angle system OCA 30 from Dataphysics using SCA20 software. Round-shaped 0.5 cm Ø samples were cut from the bilayered scaffolds and fixed on a glass microscopy slide using double sided sticky-tape. For each scaffold side, three samples were prepared and measured. A 50 µL drop of deionized water was placed in the middle of each sample and images were captured at a rate of 25 frames per second, up to 60 seconds after placement of the water drop. Water contact angles were determined from the recorded images. The mean of three samples ± standard deviation was expressed.

UPy-biomaterial sample preparation and cell seeding

Round 12 mm Ø samples were cut from the bilayered scaffolds. For the meshes, individual 12 mm Ø glasses covered with a UPy-biomaterial mesh, were separated from the PE sheet. Samples were sterilized via UV-irradiation for 1 hour on each side. Samples were fixed in Minusheet tissue carriers with 13 mm O.D. (Minucells and Minutissue vertriebs gmbh). For each bilayered scaffold different samples had either side A or side B facing up. The carriers with samples were placed in a 24-well tissue culture plate (BD Biosciences). Each bilayered scaffold sample was wet in an ample volume of complete medium, which was removed right before cell seeding until the fluid level reached the upper surface of the carrier, followed by removal of residual medium on top of the scaffold sample. HK-2 cells were cultured and harvested as described in chapter 3. After cell trypsinisation, the concentration of the cell suspension was adjusted. On each scaffold sample 180 x 10^3 HK-2 cells were seeded in 50 µL within the opening of the carrier ring. For the meshes and films on glass, two densities were seeded, ~36 × 10^3 (low) or ~180 x 10^3 (high) in 75 µL within the opening of the carrier ring on the dry samples. In all cases the cells were initially left to adhere for 2 hours at 37° C, 5 % CO_2 and 90 % humidity, then 700 uL of complete medium was added per well and cells were further cultured for 12 hours or 3 days.

Cell fixation, staining and visualization

Bilayered scaffold samples

After the culture period, the scaffold samples were washed with PBS twice. Then adhered cells were fixed by incubation with 4 v% formaldehyde (Fluka) in PBS solution for 10 minutes at room temperature. Samples were again washed with PBS twice and subsequently incubated for 1 hour in blocking buffer of 5 wt/v% BSA (Sigma Aldrich) in PBS. The cell's actin skeleton was stained with atto-488-conjugated phalloidin (1 : 1000, Sigma Aldrich) in 2 wt/v% BSA in PBS by incubation at room temperature for 60 minutes, then cell nuclei were stained with Hoechst (1 : 1000, Sigma Aldrich) for 15 minutes. The samples were washed three times with PBS, taken out of the supporting rings and embedded between a microscopy slide and cover glass in Vectashield (Brunschwig Chemie). The samples were visualized by fluorescence microscopy using a 20x magnifying objective on a Zeiss Axio observer D1 equipped with an AxioCam Mrm camera and Zeiss Axiovision software (Carl Zeiss).

Meshes and films on glasses

After the culture period, the samples were washed wih PBS twice. Then adhered cells were fixed by incubation with 4 v% formaldehyde (Fluka) in PBS solution for 10 minutes at room temperature. Samples were again washed in PBS twice and subsequently cells were permeabilized by incubation with 0.5 v/v% Triton X-100 (Sigma Aldrich) in PBS for 10 minutes at room temperature. The samples

were washed with PBS twice before incubation for 1 hour with blocking buffer of 5 wt/v% BSA (Sigma Aldrich) in PBS.

Samples fixed at 14h after cell seeding were stained for actin, vinculin and nuclei. First samples were incubated for 1 hour with mouse anti-human vinculin (1 : 400, Sigma Aldrich) in 2 wt/v% BSA in PBS, followed by washing with 0.1 v/v% polysorbate 20 (Merck) in PBS twice and PBS once. Then samples were incubated for 45 minutes with goat anti-mouse Alexa 555 conjugated antibody (1:400, Molecular probes, invitrogen) and atto-488-conjugated phalloidin (1:500, Sigma Aldrich) together in 2 wt/v% BSA in PBS, directly followed by incubation for 10 minutes with 4',6-diamidino-2-phenylindole (DAPI, 1:1000, Invitrogen) in 2 wt/v% BSA in PBS. The samples were washed with 0.1 v/v% polysorbate 20 in PBS twice and once in PBS.

Samples fixed 3 days after cell seeding were stained for zona occludens-1 (ZO-1), vinculin and nuclei. The staining protocol is as described for the samples fixed at 14 h after cell seeding, except for the first antibody incubation step, mouse-anti-human ZO-1 (1 : 100, BD Biosciences) was used.

After staining, samples were taken out of the supporting rings, if possible the supporting glass coverslip was removed, and the mesh or film was embedded between a microscopy slide and cover glass with glycerol–PBS solution (Citifluor, Agar scientific). The samples were visualized by fluorescence microscopy using a 10x and 20x, and 40x oil magnifying objective on a Zeiss Axio observer D1 equipped with an AxioCam Mrm camera and Zeiss Axiovision software (Carl Zeiss).

Resazurin mitochondrial activity assay

To assess cell viability a mitochondrial activity assay was used based on the mitochondrial conversion of non-fluorescent resazurin to fluorescent resorufin. Resazurin salt (Sigma Aldrich) dissolved in PBS in a 88 10^{-5} M stock solution, was diluted 20 x in complete media to yield a 4.4 × 10^{-5} M concentration. The HK-2 cells cultured on meshes on glass were incubated for 3 h at 37 °C and 5% CO_2 in a humidified atmosphere with 800 µL of the resazurin solution. Per mesh, three samples of 200 µL resazurin solution were transferred to a black 96-well plate (Thermo Scientific) and fluorescence was measured (λ_{ex} = 550, λ_{em} = 584) with a Fluoroscan plate reader (Thermo Fisher Scientific). The non- invasive assay was performed at day 1 and day 3 after cell seeding. The average total mitochondrial activity of n=3 for each UPy-biomaterial mix was calculated at both time points and expressed ± standard deviation.

6. References

(1) Lutolf, M. P.; Hubbell, J. A. Synthetic Biomaterials as Instructive Extracellular Microenvironments for Morphogenesis in Tissue Engineering. *Nat. Biotechnol.* **2005**, *23*, 47–55.

(2) Kim, B.-S.; Mooney, D. J. Development of Biocompatible Synthetic Extracellular Matrices for Tissue Engineering. *Trends Biotechnol.* **1998**, *16*, 224–230.

(3) Ma, P. X.; Zhang, R. Synthetic Nano-Scale Fibrous Extracellular Matrix. *J. Biomed. Mater. Res.* **1999**, *46*, 60–72.

(4) Wang, X.; Ding, B.; Li, B. Biomimetic Electrospun Nanofibrous Structures for Tissue Engineering. *Mater. Today* **2013**, *16*, 229–241.

(5) Adams, J. C.; Watt, F. M. Regulation of Development and Differentiation by the Extracellular Matrix. *Dev.-Camb.*- **1993**, *117*, 1183–1183.

(6) Timpl, R.; Brown, J. C. Supramolecular Assembly of Basement Membranes. *BioEssays* **1996**, *18*, 123–132.

(7) Zamir, E.; Geiger, B. Molecular Complexity and Dynamics of Cell-Matrix Adhesions. *J. Cell Sci.* **2001**, *114*, 3583–3590.

(8) Boer, J. de; Blitterswijk, C. A. van. *Materiomics: High-Throughput Screening of Biomaterial Properties*; Cambridge University Press, 2013.

(9) Hook, A. L.; Anderson, D. G.; Langer, R.; Williams, P.; Davies, M. C.; Alexander, M. R. High Throughput Methods Applied in Biomaterial Development and Discovery. *Biomaterials* **2010**, *31*, 187–198.

(10) Dankers, P. Y. W.; Boomker, J. M.; Huizinga-van der Vlag, A.; Wisse, E.; Appel, W. P. J.; Smedts, F. M. M.; Harmsen, M. C.; Bosman, A. W.; Meijer, E. W.; van Luyn, M. J. A. Bioengineering of Living Renal Membranes Consisting of Hierarchical, Bioactive Supramolecular Meshes and Human Tubular Cells. *Biomaterials* **2011**, *32*, 723–733.

(11) Soletti, L.; Hong, Y.; Guan, J.; Stankus, J. J.; El-Kurdi, M. S.; Wagner, W. R.; Vorp, D. A. A Bilayered Elastomeric Scaffold for Tissue Engineering of Small Diameter Vascular Grafts. *Acta Biomater.* **2010**, *6*, 110–122.

(12) Mao, J. S.; Zhao, L. G.; Yin, Y. J.; Yao, K. D. Structure and Properties of Bilayer Chitosan–gelatin Scaffolds. *Biomaterials* **2003**, *24*, 1067–1074.

(13) Nooeaid, P.; Roether, J. A.; Weber, E.; Schubert, D. W.; Boccaccini, A. R. Technologies for Multilayered Scaffolds Suitable for Interface Tissue Engineering. *Adv. Eng. Mater.* **2013**, *15*, n/a – n/a.

(14) Kidoaki, S.; Kwon, I. K.; Matsuda, T. Mesoscopic Spatial Designs of Nano- and Microfiber Meshes for Tissue-Engineering Matrix and Scaffold Based on Newly Devised Multilayering and Mixing Electrospinning Techniques. *Biomaterials* **2005**, *26*, 37–46.

(15) Dankers, P. Y. W.; Boomker, J. M.; Huizinga-van der Vlag, A.; Smedts, F. M. M.; Harmsen, M. C.; van Luyn, M. J. A. The Use of Fibrous, Supramolecular Membranes and Human Tubular Cells for Renal Epithelial Tissue Engineering: Towards a Suitable Membrane for a Bioartificial Kidney. *Macromol. Biosci.* **2010**, *10*, 1345–1354.

(16) Halfter, W.; Monnier, C.; Müller, D.; Oertle, P.; Uechi, G.; Balasubramani, M.; Safi, F.; Lim, R.; Loparic, M.; Henrich, P. B. The Bi-Functional Organization of Human Basement Membranes. *PLoS ONE* **2013**, *8*.

(17) Ueda, H.; Watanabe, J.; Konno, T.; Takai, M.; Saito, A.; Ishihara, K. Asymmetrically Functional Surface Properties on Biocompatible Phospholipid Polymer Membrane for Bioartificial Kidney. *J. Biomed. Mater. Res. A* **2006**, *77A*, 19–27.

(18) Lensen, M. C.; Schulte, V. A.; Diez, M. Cell Adhesion and Spreading on an Intrinsically Anti-Adhesive PEG Biomaterial. In *Biomaterials - Physics and Chemistry*; Pignatello, R., Ed.; InTech, 2011.

(19) Pierschbacher, M. D.; Ruoslahti, E. Cell Attachment Activity of Fibronectin Can Be Duplicated by Small Synthetic Fragments of the Molecule. *Nature* **1984**, *309*, 30–33.

(20) Hersel, U.; Dahmen, C.; Kessler, H. RGD Modified Polymers: Biomaterials for Stimulated Cell Adhesion and beyond. *Biomaterials* **2003**, *24*, 4385–4415.

(21) Kieltyka, R. E.; Bastings, M. M. C.; van Almen, G. C.; Besenius, P.; Kemps, E. W. L.; Dankers, P. Y. W. Modular Synthesis of Supramolecular Ureidopyrimidinone–peptide Conjugates Using an Oxime Ligation Strategy. *Chem. Commun.* **2012**, *48*, 1452.

(22) Dankers, P. Y. W.; Adams, P. J. H. M.; Löwik, D. W. P. M.; van Hest, J. C. M.; Meijer, E. W. Convenient Solid-Phase Synthesis of Ureido-Pyrimidinone Modified Peptides. *Eur. J. Org. Chem.* **2007**, *22*, 3622–3632.

(23) Ahmed, F.; Choudhury, N. R.; Dutta, N. K.; Zannettino, A.; Knott, R. Near Superhydrophobic Fibrous Scaffold for Endothelialization: Fabrication, Characterization and Cellular Activities. *Biomacromolecules* **2013**, *14*, 3850–3860.

(24) Polini, A.; Pagliara, S.; Stabile, R.; Netti, G. S.; Roca, L.; Prattichizzo, C.; Gesualdo, L.; Cingolani, R.; Pisignano, D. Collagen-Functionalised Electrospun Polymer Fibers for Bioengineering Applications. *Soft Matter* **2010**, *6*, 1668.

(25) Vedula, S. R. K.; Hirata, H.; Nai, M. H.; Brugués, A.; Toyama, Y.; Trepat, X.; Lim, C. T.; Ladoux, B. Epithelial Bridges Maintain Tissue Integrity during Collective Cell Migration. *Nat. Mater.* **2014**, *13*, 87–96.

(26) Palovuori, R.; Eskelinen, S. Role of Vinculin in the Maintenance of Cell-Cell Contacts in Kidney Epithelial MDBK Cells. *Eur. J. Cell Biol.* **2000**, *79*, 961–974.

(27) Chuang, W.-T.; Jeng, U.-S.; Sheu, H.-S.; Hong, P.-D. Competition between Phase Separation and Crystallization in a PCL/PEG Polymer Blend Captured by Synchronized SAXS, WAXS, and DSC. *Macromol. Res.* **2006**, *14*, 45–51.

(28) Chuang, W.-T.; Shih, K.-S.; Hong, P.-D. Kinetics of Phase Separation in Poly(ε-caprolactone)/Poly(ethylene Glycol) Blends. *J. Polym. Res.* **2005**, *12*, 197–204.

(29) Dankers, P. Y. W. Supramolecular Biomaterials - Introducing a Modular Approach. Thesis, Eindhoven University of Technology: Eindhoven, The Netherlands, 2006.

Chapter 7

Elastic microfibrous 2D and 3D hybrid hydrogel scaffolds composed of chain-extended UPy-modified PEG and gelatin

Abstract: *Multiblock PEG-based copolymers with ureido-pyrimidinone (UPy) moieties in the backbone were recently discovered to form hydrogels with remarkable mechanical properties. This is the result of multiple UPy-dimerizations between chains, which form a physically cross-linked supramolecular polymer network. In this chapter we explore the use of this chain-extended UPy-PEG (CE-UPy-PEG) hydrogel as scaffold material to mimic the basement membrane (BM) and interstitial extracellular matrix (ECM). Such scaffolds are here applied and tested for 2D renal membrane and 3D cardiac patch tissue engineering, respectively. No cells adhere to the inert CE-UPy-PEG hydrogel material. The addition of gelatin induces some cell adhesion to drop-cast films, although the effect is limited as a result of phase separation of both hydrogel components. Electrospinning of CE-UPy-PEG with up to 30 wt% gelatin results in homogeneous microfibrous scaffolds. Without the need of chemical cross-linking, the microfibrous morphology is preserved in the hydrated state. The microfibrous hydrogels display elastic properties with moduli between 0.60 and 0.66 MPa. In a fatigue experiment exposure to ~5000 cycles of 20% strain is endured by a hybrid hydrogel scaffold. Scaffolds with submicron fiber diameters (in the dry state) and fine pore structure function as BM mimics. Renal epithelial cells adhere and form the desired tight, confluent morphology on top of BM mimics with 20 wt% gelatin. Scaffolds of this hybrid hydrogel with a more open pore structure function as 3D interstitial ECM mimics. Undifferentiated cardiomyocyte progenitor cells (CMPCs) seeded inside these 3D scaffolds deposit their own matrix proteins already after one day and remain viable for at least 9 days. These results provide proof-of-concept for the applicability of CE-UPy-PEG as bio-inert basis for scaffolds for 2D, 3D, and mechanically loaded tissue engineering applications. Furthermore, the combination with gelatin demonstrates the possibility to make hybrid scaffolds with natural bioactive proteins. Synthetic UPy-peptide based approaches towards more specific and controlled bioactivation might be explored in the future.*

Part of this work will be submitted for publication: B.B. Mollet, S. Spaans, P. Goodarzy Fard, N.A.M. Bax, C.V.C. Bouten, P.Y.W. Dankers, *Elastic microfibrous 2D and 3D hybrid hydrogel scaffolds composed of chain-extended ureido-pyrimidinone modified PEG and gelatin*. (manuscript in preparation)

1. Introduction

1.1 Properties of natural ECM

In the field of regenerative medicine, the formation of biomaterials that can mimic the natural 3D interstitial extracellular matrix (ECM) or 2D specialized ECM, the basement membrane (BM), is still a major challenge. This is due to the multifunctional, complex and dynamic nature of these natural structures. Characteristic properties of ECM are the hydrogel-like physical appearance and remarkable mechanical properties, which are the result of multiple components. The fibrous proteins collagen and elastin are the major structural contributors to ECM, providing tensile strength and elastic properties, respectively. This enables tissues to bear repetitive mechanical stress, without plastic deformation or rupture. These fibrous protein networks lie in a viscous interstitial environment rich of glycoproteins, proteoglycans (PGs) and glycosaminoglycans (GAGs).[1] PGs and GAGs sequester water, giving rise to the hydrogel-like physical appearance of ECM. In this chapter we focus on the formation of freestanding microfibrous hydrogel scaffolds with good mechanical properties, intended for application as 2D BM or 3D ECM mimics in tissue engineering.

1.2 Biomaterial hydrogels and hydrogel scaffolds

A diversity of biomaterial hydrogels, ranging from natural to synthetic, have been extensively studied and described in literature. Each hydrogel system was found to possess its own advantages and limitations. Hydrogels of natural origin, such as collagen and its denatured form gelatin, the GAG hyaluronic acid, and Matrigel, a widely applied commercial BM simulant, all provide endogenous signals that promote cellular interaction and tissue formation. On the other hand, the possibility to tune the mechanical or physical properties of these molecularly pre-defined materials is limited. In addition, the variable composition of these materials, and their complex and not-well understood interactions with cells challenge controlled application. On top of that, origin related safety concerns puts constraints on their use in the medical field. Inert synthetic hydrogels on the other hand, allow controllable and adjustable composition and hence predictable and tunable properties. However, synthetic materials lack functional sites that act as bioactive cues for engagement of specific interaction with cells. To bridge the gap between natural and synthetic hydrogels, researchers have simply mixed hydrogel components of natural and synthetic origin. The complementary properties of these components are ought to result in hybrid hydrogels with synergistic effects.[2]

To enable the formation of structurally defined, freestanding scaffolds, the hydrogel system must allow processing and requires certain mechanical strength. Electrospinning forms an attractive processing technique for the formation of fibrous 2D and 3D scaffolds. By controlling fiber diameter, the pore sizes can be tuned. This allows the formation of

scaffolds either distinctly suitable to function as 2D support, or 3D scaffolds that allow cell infiltration. Electrospinning of natural,[3,4] synthetic[5,6,7,8] and hybrid[9] hydrogelators has been described in literature. However, all these biomaterials required chemical cross-linking post-electrospinning to prevent complete dissolution or fast degradation of the nano-to-micro fibrous structures in aqueous environment and/or to improve poor mechanical properties. A hydrogel material that forms strong physical cross-links could provide both the opportunity for processing and circumvent the need of chemical cross-linking, i.e. a thermoplastic elastomer hydrogel is desired.

1.3 Supramolecular UPy-PEG based hydrogels

End-functionalization of covalent oligomers or polymers with supramolecular self-complementary, quadruple hydrogen-bonding ureido-pyrimidinone (UPy) moieties has resulted in the formation of thermoplastic elastomers, as described in Chapter 1. Examples are UPy-functionalized polycaprolactone (UPy-PCL) or polyethylene butylene (UPy-PEB). Here we focus on poly(ethylene glycol) (PEG) as hydrogel basis. PEG is a highly hydrophilic, anti-fouling, non-toxic and biocompatible synthetic polymer. Based on these properties PEG has been successfully and extensively used in the biomedical field.[10] The high hydration yields favorable nutrient and oxygen transport, which benefit applications as 3D tissue engineering scaffold. PEG hydrogels were shown to maintain the viability of encapsulated cells and allow ECM deposition as they degrade.[11] In earlier work, our research group developed supramolecular polymer hydrogels based on UPy-end-functionalization of high molecular weight PEG. The formation of the supramolecular hydrogel relies on the hydrogen-bonding interactions between UPy-moieties, which need to be shielded from the water.[12,13] A hydrophobic pocket, formed by short-chain oligo-methylene spacers between the PEG and UPy-functionalities, provided this shield. These telechelic UPy-PEG hydrogelators form highly dynamic hydrogel networks, which are responsive to concentration, temperature and pH.[14-17] The use of these hydrogelators as drug delivery vehicle has been demonstrated. However, their weak and brittle material properties limited their applicability as freestanding scaffolding material in tissue engineering. Mechanical properties of UPy-PEG based biomaterials could be improved via mixing with another UPy-polymer, such as UPy-PCL. However, this does not result in a hydrogel.[18]

1.4 Chain-extended UPy-PEG: a new hydrogel with remarkable properties

An adapted supramolecular UPy-hydrogelator design vastly improved mechanical properties (scheme 1). The hydrogelator consists of a multiblock PEG-based copolymer with multiple UPy-moieties contained within the backbone.[19] By this design, each supramolecular monomer can form multiple physical cross-links with other monomers via UPy-dimerization. Although this chain-extended UPy-PEG (CE-UPy-PEG) has a nearly

identical chemical composition compared to its telechelic analogues, it exhibits completely different, exceptional mechanical properties. In the dry state, this supramolecular polymer forms a tough material with shape memory properties, whereas in the hydrated state a strong and highly elastic hydrogel is formed. The solid-to-hydrogel transition was studied by differential scanning calorimetry (DSC), cryo-transmission electron microscopy (cryo-TEM) and small angle x-ray scattering (SAXS). In the dry state a lamellar microphase separated structure is formed by crystalline PEG and the hydrophobic domains. The latter consists of oligo-methylene segments and UPy-dimers. In presence of water, the hydrophilic PEG-segments quickly absorb water, causing swelling and dissociation of the crystalline lamellae. When fully hydrated the hydrophobic segments concentrate into small spherical domains surrounded by amorphous PEG.[19] In the equilibrium hydrated state, the bulk hydrogel (with 10 kg · mol^{-1} PEG-block) contains ~85 wt% water. This hydrogel material showed nearly perfect strength recovery even at large deformation (> 300%).[19] Hence, the increased chain length realized through chain-extension and the ability to form physical cross-links substantially enhanced the strength, ductility, and stability of this material in water. It should be explicitly noted that no chemical cross-linking is needed to achieve these remarkable material properties. Furthermore, the physical cross-links formed by hydrogen-bonding between UPy-dimers are reversible by nature. They can be completely dissociated and reformed as desired in a controlled fashion. This offers attractive processing opportunities.

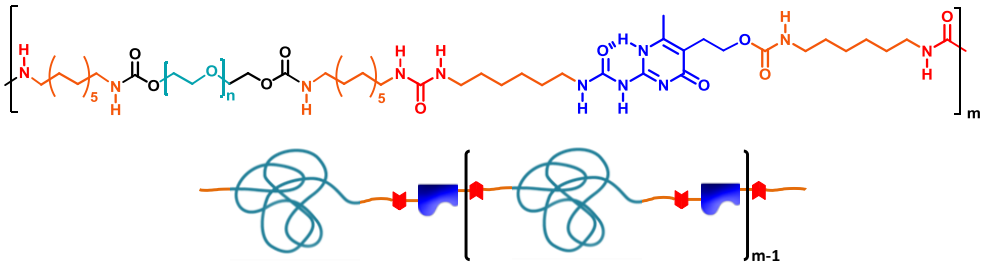

Scheme 1. Chain-extended UPy-PEG. Structural formula and schematic representation. In the applied CE-UPy-PEG in this chapter, n=~227 (M_w PEG = 10,000), m is not well defined (estimated at ~ 50, PDI > 3).

1.5 Chain-extended UPy-PEG as new hydrogel scaffold material

Based on its properties, CE-UPy-PEG was hypothesized to be well suited as hydrogel scaffold material for tissue engineering applications. To induce a cell adhesive character to the undoubtedly bio-inert CE-UPy-PEG, hybridization with a bioactive natural hydrogel component will be required. For this purpose gelatin, the denatured form of natural BM and ECM major component collagen, was chosen. Gelatin is produced by partial hydrolysis of collagen. As such, it contains the same bioactive peptide sequences, such as RGD, that facilitates cell adhesion through recognition by integrins at the cell membrane. These RGD

sequences were found to be more exposed to interaction with cells in denatured collagen versus native collagen.[20] With an eye on desired processing by electrospinning and collagens tendency to denature when electrospun from fluoroalcohols,[21] gelatin is a better choice for economic reasons. Furthermore, gelatin is commercially available in different gel strengths and can be processed by electrospinning.[22,23]

In this chapter initial studies towards application of CE-UPy-PEG as hydrogel scaffold are described. These studies comprise assessment of the electrospinability of both the pure synthetic CE-UPy-PEG and hybridized variants with gelatin, and the mechanical performance of resultant fibrous hydrogel scaffolds. In pursue of forming both 2D BM and 3D ECM mimics, scaffolds with distinct fiber diameters and pore sizes are formed. These are tested in a specific 2D (with P. Goodarzy Fard) and 3D (by S. Spaans) tissue engineering application for the formation of a bioartificial renal membrane and cardiac niche, respectively (Figure 1).

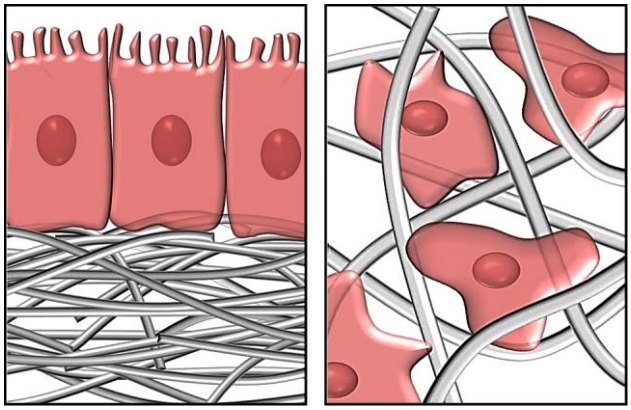

Figure 1. Two scaffold types: a 2D BM mimic and 3D ECM mimic. Left: A schematic representation of a zoomed view of a bioartificial renal membrane formed by renal epithelial cells on top of a dense submicron fibrous mesh. Right: A cardiac patch consisting of cardiac progenitor cells growing inside an open pore interstitial ECM mimicking scaffold. Scaffold porosity is altered by tuning fiber diameter size. Thin (<1 µm) fibers result in dense meshes used as 2D BM mimics. Thicker fibers automatically yield more void space, allowing cells to infiltrate in this 3D ECM mimic.

2. Results

2.1 CE-UPy-PEG hybridization with gelatin induces cell adhesion on films

Cells were expected to be unable to adhere to CE-UPy-PEG. This assumption was based on the well-known anti-fouling and bio-inert character of PEG and high fraction of PEG-content in CE-UPy-PEG (0.93 for CE-UPy-PEG with 10 kg · mol^{-1} PEG-block).[19] To facilitate cell adhesion, CE-UPy-PEG was mixed with a cell adhesive biopolymer, gelatin.

The mixing of both CE-UPy-PEG and gelatin and the effect on cell adhesion was first tested for drop-cast films with varying ratios of both components. Homogeneous mixing of both components was achieved when they were both dissolved in hexafluoroisopropanol (HFIP). Dilute solutions (1 wt/v%) of CE-UPy-PEG and gelatin, mixed in different ratios, were drop cast on glass substrates. When water was applied on the dried thin films, gelation and swelling occurred. Visual observations revealed lower swelling ratios with increased percentage of gelatin in the film (Figure 2). This was attributed to the relatively more hydrophobic gelatin, compared to CE-UPy-PEG, which lead to reduced hydrophilicity of the hybrid material.

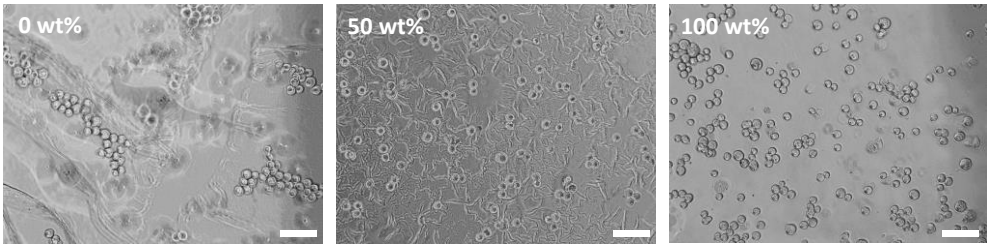

Figure 2. Hydrated CE-UPy-PEG/gelatin film morphology and cell distribution. Phase contrast transmitted light micrographs of human kidney (HK-2) cells on hydrated films. The films contain varying ratios of CE-UPy-PEG/gelatin (wt% gelatin is indicated). Micrographs were taken 10 minutes after cell seeding. The pure CE-UPy-PEG film swelled largely in x-y plane upon hydration, which causes folds in the surface. Cells accumulate in the valleys of the hydrogel film resulting in inhomogeneous cell distributions. The swelling and wrinkling of the hydrated film become less with increasing gelatin content. The 100% gelatin film remains completely flat. The scale bars indicate 100 μm.

The gelatin present in the hybrid hydrogel films did induce the desired effect of cell adhesion (Figure 3). However, more gelatin did not necessarily result in more adhered cells. HK-2 cells grew in a patchy manner. They did not form a confluent monolayer on any of the tested hybrid hydrogel films although enough cells were seeded to form a near confluent monolayer. This could be seen on the 100% gelatin film (Figure 3). A twofold explanation could be given for the patchy cell growth on hydrated gels with low gelatin content. Firstly, the non-flat surface resulted in accumulation of cells and inhomogeneous seeding (Figure 2). Secondly, the limited amount of gelatin does not provide sufficient adherence sites for cells. However, neither effects explain the disappointingly low degree of cell adhesion to the flat hybrid films with high gelatin content. The distribution of gelatin in the films was examined since phase separation is known to occur for gelatin/PEG/water systems.[24] In our material system, gelatin was found to concentrate in globular domains which increased in size with increasing gelatin content (Figure 4). This accumulation of the bioactive component restricts availability at the hydrogel surface for interaction with cells, and hence provides an explanation for the limited and inhomogeneous cell adhesion.

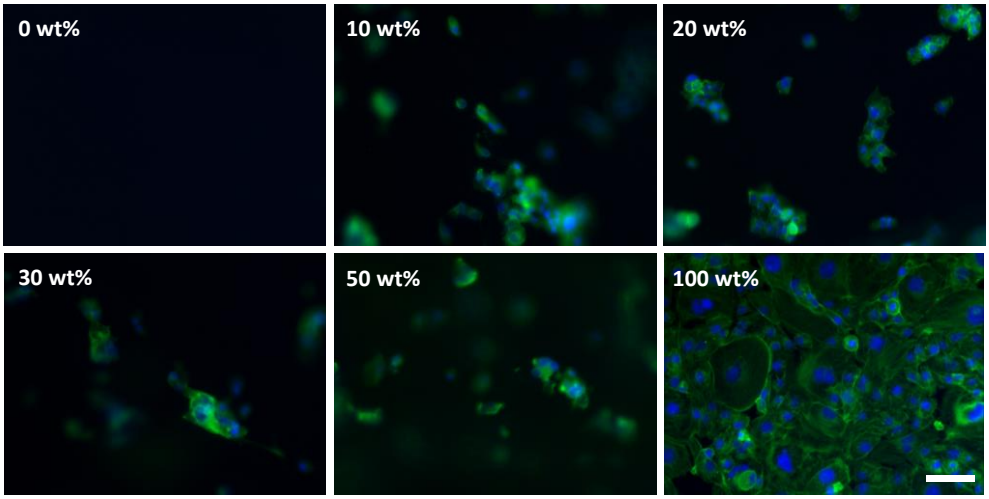

Figure 3. Cell adhesion to hybrid hydrogel films of CE-UPy-PEG and gelatin. Fluorescence micrographs of HK-2 cells 22 hours after seeding on hydrogel films of varying CE-UPy-PEG and gelatin ratio. The wt% of gelatin per sample is indicated. Non-adhered cells were washed away, the cell nuclei of adhered cells are indicated in blue and the actin cytoskeleton in green. All micrographs were recorded at the same magnification. The scale bar indicates 100 µm.

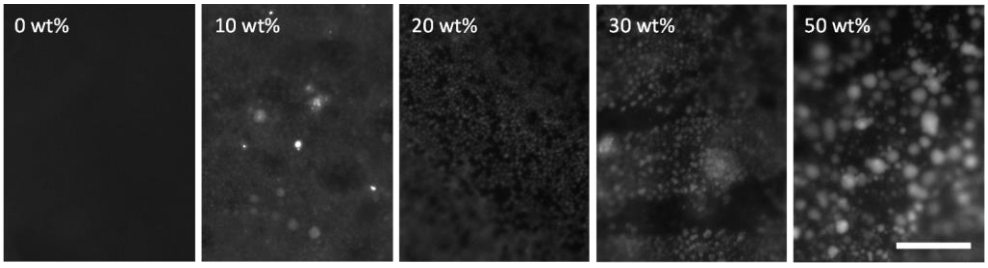

Figure 4. CE-UPy-PEG and gelatin phase separation in hybrid drop-cast films. Fluorescence micrographs show the location of fluorescently stained gelatin in hydrogel films with varying CE-UPy-PEG/gelatin ratio (wt% gelatin is indicated). The film containing 75 wt% gelatin fell completely apart during the staining procedure of gelatin, which was performed overnight at 37 °C in a buffered aqueous solution. All micrographs were taken at the same magnification. The scale bar indicates 100 µm.

2.2 Electrospinning of CE-UPy-PEG to form microfibrous hydrogel scaffolds

Processing of hybridized CE-UPy-PEG by electrospinning was desired to form microfibrous BM and ECM mimicking structures. In addition, electrospinning was hypothesized to reduce the undesired phase separation of components by the fast evaporation of solvent and confined space in the microfibers. CE-UPy-PEG had not been processed by this method before. Therefore, the feasibility to produce microfibrous

scaffolds, the effect of hydration and the stability of these scaffolds in cell-culture conditions was initially tested for the pure, non-hybridized material.

A homogeneous, viscous solution is required for electrospinning. The dissolution of the polymer requires disruption of the physical cross-links in the material. This was achieved in a strong hydrogen bond breaking organic solvents, methanol (MeOH) and hexafluoroisopropanol (HFIP). Both solvents were successfully applied for electrospinning of CE-UPy-PEG, yielding opaque white meshes. Electron microscopy (SEM) showed randomly oriented fibers with diameters typically smaller than 1 µm for meshes spun from either solvent (Figure 5 shows the morphologies of a mesh spun from HFIP. This solvent was applied in further experiments as it allows dissolution of both CE-UPy-PEG and gelatin). Upon contact with water, the meshes hydrated and formed semi-transparent hydrogel scaffolds (Figure 5d, II). The meshes could take up over 12 times their dry weight in water (~93 wt%). This was much more compared to the bulk CE-UPy-PEG material which was determined to take up ~ 5.7 times its dry weight in water (85 wt% water) in equilibrated hydrated state.[20] This difference is attributed to the porous structure of the scaffold. Upon hydration the fibers swell, but also the empty spaces between them become completely filled with water as a result of capillary force. In contrast to bulk material, which swells proportionally equal in all directions, the meshes appeared to swell primarily in their smallest dimension, i.e. their height, whereas the x and y dimensions remained roughly the same. For individual fibers collected on a glass substrate it was clearly observed how contact with water increased both diameter and length upon hydration. Due to the high ratio between both dimensions, the proportional swelling resulted in buckling of the fibers between contact points. Upon drying, the fibers preserved this shape (Figure 5d). After exposure of a hydrated scaffold to cell-culture conditions (37 °C, buffered aqueous solution at ~ pH 7), contours of individual fibers could still be observed by phase contrast microscopy (Figure 5b). Hydrated samples of the mesh were dried and imaged by SEM to gain a rough idea of the effect of hydration on the mesh morphology at microscale (Figure 5b, II). Overall, the remaining fibrous structure was less well defined compared to the original dry mesh as-spun. Nevertheless, contours of individual fibers could still be distinguished at most places in the mesh. Fibers appeared partially fused, fiber diameters increased, and apparent pore sizes decreased.

The demonstrated combination of processability by electrospinning and maintained microfibrous morphology in the hydrated gel-state is not trivial. Hydrogelators described in literature that are processed by electrospinning, typically require chemical cross-linking post-processing to secure the microfibrous morphology. This unique combination of properties for CE-UPy-PEG is attributed to the strong physical cross-links in this material, which are reversible in nature. These UPy-based cross-links are temporarily broken in strong hydrogen-bond breaking organic solvents allowing processing by electrospinning. During solidification of the fibers, UPy-moieties dimerize and the physical cross-links are formed. In the hydrated state the cross-links are protected from water by the hydrophobic

pockets in which they reside. These results confirm that CE-UPy-PEG does not dissolve in water, not even when the surface to volume ratio is greatly increased.

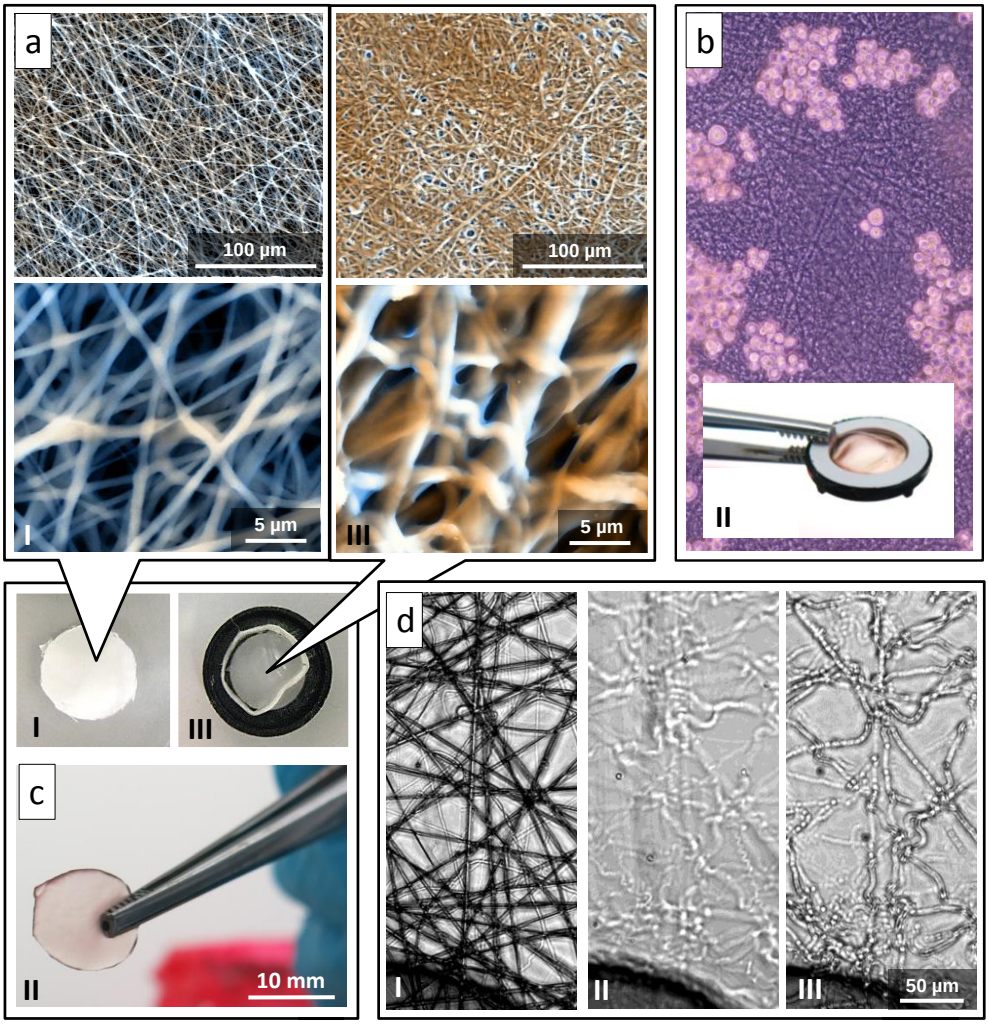

Figure 5. Electrospun CE-UPy-PEG and the effect of hydration. a) Scanning electron micrographs show the microfibrous morphology of electrospun CE-UPy-PEG meshes as-spun from a solution in HFIP, with average fiber diameters of 0.68±0.23 µm (I) and after hydration and subsequent drying (III). b) A phase contrast micrograph of HK-2 cells one day after seeding on a hydrated CE-UPy-PEG electrospun mesh. The round morphology of these normally adherent cells indicates the lack of cell adhesion. Instead, the cells form clusters which freely move in the culture media when agitated. The freestanding hydrogel mesh is fixed in a carrier ring during cell-culture experiments to facilitate easy handling. The rose-coloured appearance of the mesh is the result of hydration in cell-culture media containing phenol red. c) Phase contrast transmitted light Photographs of samples of the electrospun meshes as-spun (I), in hydrated (II), and dehydrated state (III). d) Phase contrast micrographs of a thin layer of electrospun microfibers on a glass substrate as-spun (I), in the swollen hydrated state (II) and dehydrated state (III).

2.3 Electrospinning of hybrid hydrogel scaffolds

The drop-cast hybrid hydrogel films showed that gelatin could induce cell adhesion. However, the effect was limited due to inhomogeneous surface morphology and phase separation of components. CE-UPy-PEG and gelatin were assumed to be molecularly dissolved in HFIP. Hence the observed phase separation should occur during drying of the film. It was therefore hypothesized that electrospinning could enhance the homogeneous distribution of both components. Both the fast evaporation of solvent and confined space in the microfibers could help to reduce demixing of both components. Viscous mixtures of CE-UPy-PEG+gelatin in HFIP (5 wt/v%), were successfully electrospun. In literature, increase in gelatin content has been described to reduce fiber diameters upon electrospinning by the same conditions for mixtures with various synthetic polymers. Examples comprise polycaprolactone (PCL),[11,25] poly(L-lactide-co-e-caprolactone) (PLCL),[26] poly(lactic-co-glycolic acid) (PLGA)[27] and polyglycolic acid (PGA).[28] However, the addition of gelatin to CE-UPy-PEG did not induce a noticeable effect to the electrospinning process. Up to 30 wt% gelatin could be added whilst meshes with similar morphology compared to pure CE-UPy-PEG were formed without changing the electrospinning parameters (Figure 6).

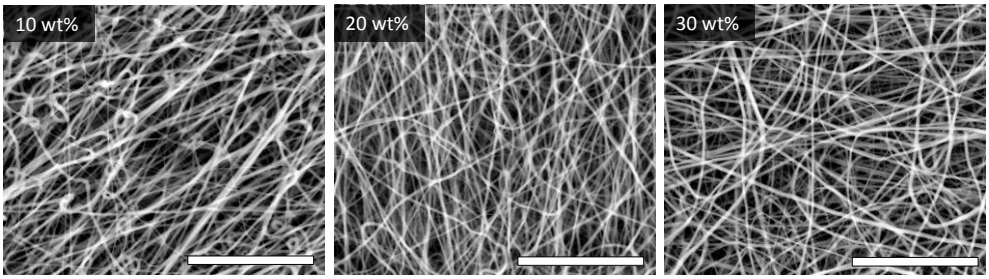

Figure 6. Electrospun CE-UPy-PEG with gelatin. Scanning electron micrographs of electrospun meshes of CE-UPy-PEG with 10, 20, and 30 wt% gelatin. All meshes were generated using the same electrospinning parameters; 5 wt/v% polymer solutions in HFIP, 0.05 mL min^{-1} flow rate, spun at 18.5 kV and 12 cm tip-to-target distance. The scale bars indicate 50 µm. Average fiber diameters, determined from higher magnification micrographs, are 0.72±0.35 µm (10 wt% gelatin), 0.63±0.36 µm (20 wt% gelatin), and 0.65±0.39 µm (30 wt% gelatin)

The hybrid electrospun meshes were evaluated for their gelatin distribution via fluorescent labelling of gelatin. Gelatin was demonstrated to be homogeneously distributed throughout each mesh at a scale relevant to cells (Figure 7). This promises improved cell adhesion compared to the drop-cast films. The fluorescence micrographs did however not provide enough detail to explicitly determine the gelatin distribution at the level of single electrospun fibers. The distribution of both components at that level is expected to influence the mesh stability and mechanical properties, since a chain is only as strong as its weakest link. Discontinuous CE-UPy-PEG segments, or in other words continuous gelatin segments, would be prone to dissolution in an aqueous environment

and hence diminish the mesh integrity under physiological conditions. Hydration of the hybridized meshes and incubation in water at 37 °C did not provide reasons for such concern. A possible effect of gelatin on the mechanical properties of the hydrogel meshes was assessed in biaxial tensile tests.

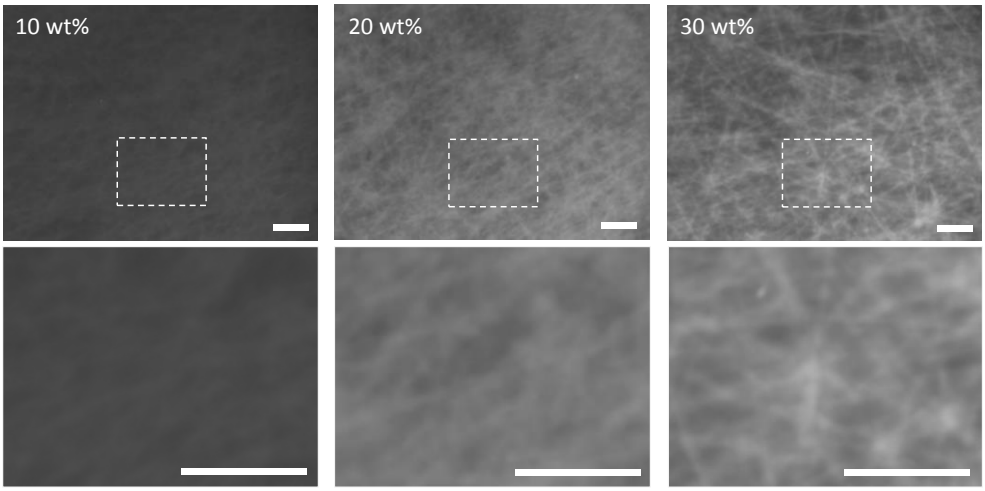

Figure 7.Gelatin distribution in electrospun hybrid hydrogel meshes. Fluorescence micrographs show the location of fluorescently stained gelatin in hydrated electrospun meshes of CE-UPy-PEG with 10, 20, and 30 wt% gelatin. The mesh with 0% gelatin (not shown) appeared dark. All scale bars indicates 50 µm.

2.4 Elastic properties of microfibrous hydrogel meshes

The extraordinary mechanical behaviour of the CE-UPy-PEG bulk hydrogel was one of the reasons to explore this material for tissue engineering scaffolding purposes. Elasticity of the scaffold is of high importance in for example cardiovascular, lung and muscle tissue engineering applications, which involve reoccurring or cyclic strain. CE-UPy-PEG bulk hydrogel showed elastic behaviour with nearly perfect strength recovery even at large deformation (> 300%).[20] The mechanical properties of electrospun scaffolds are highly dependent on the processing parameters. Next to polymeric composition, also fiber diameter and orientation are major factors that determine the elastic modulus of electrospun meshes. [11] To gain an idea on the mechanical properties of electrospun CE-UPy-PEG, hydrated meshes were subjected to biaxial tensile tests (Figure 8). The effect of gelatin was determined by comparison of meshes of CE-UPy-PEG with 0, 20 and 30 wt% gelatin. These experiments were performed on meshes with sub-micron fiber diameters in dry state.

It was anticipated that low stresses would be needed to stretch the electrospun hydrogel meshes as a result of the buckling of microfibers upon hydration (Figure 5b). Fibers are initially straightened between contact points, without being stretched. Only when completely straightened between contact points, fibers will be mechanically loaded

and exert stress. However such behaviour was not evidenced from the acquired force/displacement curves. From the measured forces, the stresses were calculated taking the thicknesses of the wet samples into account. The elastic moduli were determined from the slope of the linear region in the global stress-strain curves. As expected the random orientation of the fibers in these meshes, resulted in isotropic elastic behavior in X and Y direction. Elastic moduli were determined for pure CE-UPy-PEG meshes, and hybridized meshes with 20 and 30 % gelatin (Table 1). Initial measurements did not reveal a negative influence of the addition of gelatin on the mechanical properties of the meshes. Elastic moduli varied between 0.60 ± 0.15 and 0.66 ± 0.01 MPa. Compared to the elastic moduli of natural tissues, these scaffolds are in the appropriate range for the engineering of 'soft' tissues, such as for example cardiac muscle, skin and arterial walls.[11]

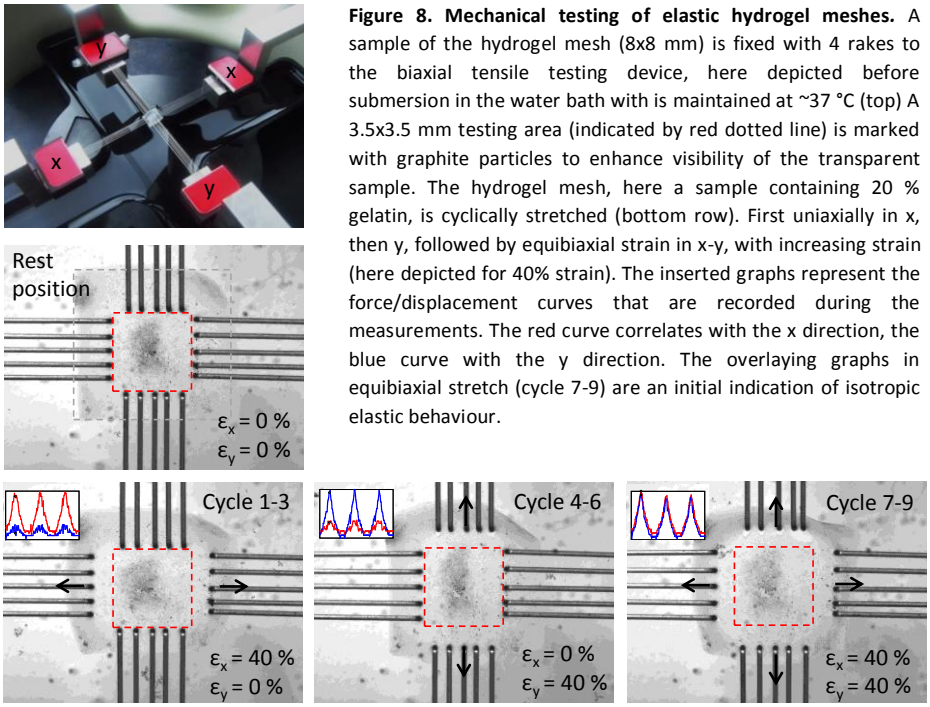

Figure 8. Mechanical testing of elastic hydrogel meshes. A sample of the hydrogel mesh (8x8 mm) is fixed with 4 rakes to the biaxial tensile testing device, here depicted before submersion in the water bath with is maintained at ~37 °C (top) A 3.5x3.5 mm testing area (indicated by red dotted line) is marked with graphite particles to enhance visibility of the transparent sample. The hydrogel mesh, here a sample containing 20 % gelatin, is cyclically stretched (bottom row). First uniaxially in x, then y, followed by equibiaxial strain in x-y, with increasing strain (here depicted for 40% strain). The inserted graphs represent the force/displacement curves that are recorded during the measurements. The red curve correlates with the x direction, the blue curve with the y direction. The overlaying graphs in equibiaxial stretch (cycle 7-9) are an initial indication of isotropic elastic behaviour.

Table 1: Elastic moduli of electrospun CE-UPy-PEG hydrogel meshes, without and with gelatin

CE-UPy-PEG /gelatin ratio	Number of samples	Average fiber diameter [µm]	Average thickness [a] [µm]	Average E modulus [b] [MPa]
100/0	N=3	0.68 ± 0.23	459 ± 36	0.64 ± 0.06
80/20	N=3	0.63 ± 0.36	374 ± 51	0.60 ± 0.15
70/30	N=2	0.65 ± 0.39	519 ± 141	0.66 ± 0.01

[a] Thickness of hydrated samples. [b] Elastic moduli were determined as the slope of the linear range of stress-strain curves.

In an initial test to assess the durability of the hybrid hydrogel scaffold, a mesh composed of 80/20 wt/wt% CE-UPy-PEG/gelatin was subjected to biaxial cyclic strain of 20% for ~5000 cycles. The material submerged in water of approximately 37 °C survived this repeated mechanical load. However, the sample displayed some evidence of plastic deformation; it appeared slightly bigger in x-y direction leading to forces measured below zero in unloaded state. Comparison of uniaxial stress-strain curves at 30% stretch before and after cyclic straining showed a ~20 % decrease in modulus. This indicates that the material suffers from some fatigue when exposed to moderate strains which do not structurally damage the material.

The hydrogel meshes exhibited substantial strain-to-failure. The meshes could, depending on their thickness, withstand stretches of at least 40%. At higher deformations, the material started to tear at the points where the mesh was punctured with thin metal pins for attachment to the biaxial tensile testing device. When strains were further increased, eventually total rupture would always occur along a row of these pins. At these points in the material, locally higher stresses occur. Hence the determined strain-to-failure and stress-to-failure, which are based on the global values, will be lower than what the meshes can actually bear. This also means that the currently derived elastic moduli are probably underestimates as these were derived from global stress-strain curves. However the strain-to failure could be considered representative for applications that require for example suturing of the hydrogel meshes.

Altogether, these preliminary mechanical data indicate that CE-UPy-PEG based electrospun scaffolds could potentially be applied in tissue engineering applications that involve stretching of the construct. However, more samples should be tested, ideally on samples of the same age and all with similar homogeneous thickness. Also, sample loading over a longer period of time under physiological conditions would provide insight into the loss of material integrity over time. Ultimately, the mechanical properties and their profile in time should match the specific application. In some applications the scaffold might be solely required to provide physical support to the cells, under either static or dynamic loading, whereas for other applications the scaffold is required to provide resistance to certain mechanical loading for at least a certain period of time. Gradual decrease of material stiffness should then be matched with the ability of the newly formed tissue, consisting of cells and their deposited ECM, to bear the mechanical loads. Both static and cyclic straining of cell-populated scaffolds has been shown to influence ECM deposition. For example an increase of ECM deposition by human dermal fibroblasts in a knitted poly(ethylene terephthalate) mesh was demonstrated when cyclically strained.[29] Direction of collagen remodeling by myofibroblasts in a fibrin based scaffold was shown to differ between static or cyclic straining.[30] The chemistry of CE-UPy-PEG provides opportunities to modulate the mechanical properties, for example by varying the PEG-block length and number of UPy-moieties per chain.

2.5 Hybrid hydrogel meshes as 2D BM mimic in a bioartificial kidney membrane

The microfibrous morphology, proven stability in water and homogeneous distribution of gelatin pave the way for the application of CE-UPy-PEG/gelatin scaffolds in tissue engineering studies. The series of established electrospun scaffolds with gelatin contents up to 30 wt%, showed randomly oriented fibers with average submicron fiber diameters and apparent pore sizes smaller than 10 µm. These dry state mesh morphologies were expected to provide an appropriate support in hydrated state for adherent cells to grow on, rather than inside. These meshes were tested for their functionality as BM mimics in bioartificial kidney membrane tissue engineering.

In an initial test, the ability of human kidney-2 (HK-2) renal epithelial cells to interact with the hybridized meshes was assessed. The cells were seeded in sub-confluent density to enable focus on cell-biomaterial interactions rather than cell-cell interactions. As expected, cells could not adhere to the pure CE-UPy-PEG hydrogel mesh. In contrast, cells did adhere to the hybrid meshes. Formation of focal adhesions by attached HK-2 cells was identified as vinculin rich spots one day after cell seeding. The chance of confusion with vinculin complexes within adherens junctions at cell-cell contacts[31,32] was eliminated by visualization of a single HK-2 cell (Figure 9).

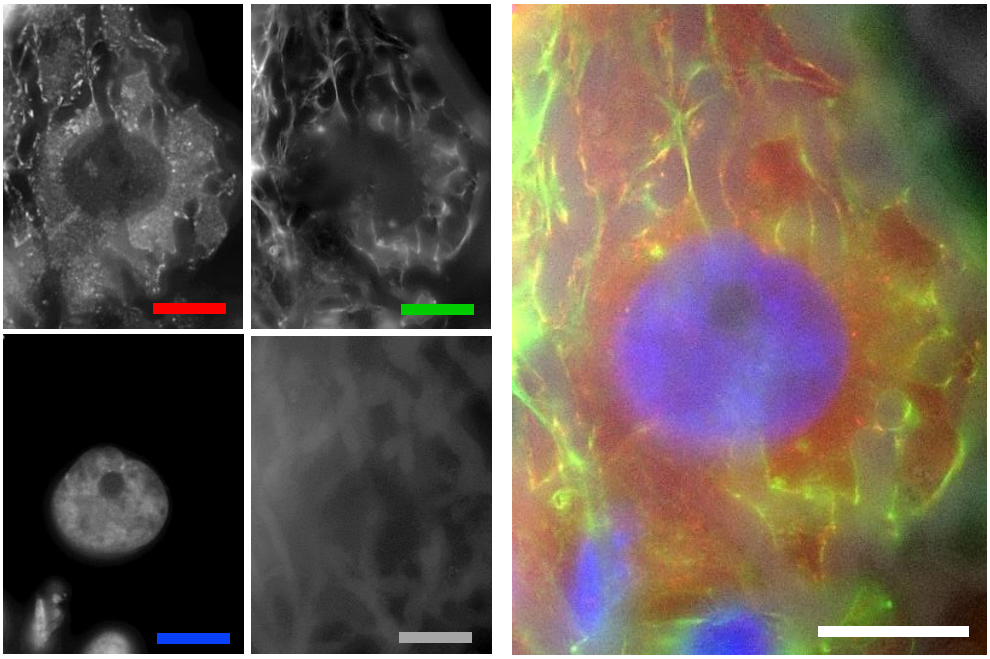

Figure 9. HK-2 cells adhere to a hybrid CE-UPy-PEG hydrogel mesh. Fluorescence micrographs, focussed on a single HK-2 cell 1 day after seeding on an electrospun mesh of CE-UPy-PEG with 30 wt% gelatin. Separate micrographs with vinculin (red), actin (green), cell nucleus (blue), the mesh (grey), and the merged image are shown. All scale bars represent 20 µm.

The formation of focal adhesions provide evidence for the interaction between HK-2 cells and the hybrid mesh. This thus confirmed the presence of the gelatin at the fibers surface, available for interaction with cells. In the focal plane of the shown image (Figure 9), one large single cell formed multiple focal adhesion sites per fiber in a mesh containing 30 wt% gelatin. This indicates a homogeneous distribution of gelatin at the scale relevant for cells.

Next, a high density of HK-2 cells, enough to form an instant monolayer, was seeded on the hybridized meshes. The adhered cells were allowed to mature for 3 days prior to evaluation of their morphology by fluorescence microscopy (Figure 10). Again, no cells adhered to the pure CE-UPy-PEG hydrogel mesh (data not shown). The presence of 10 wt% gelatin in the CE-UPy-PEG mesh allowed some HK-2 cells to adhere and grow in a patchy conformation, comparable as was observed for the drop-cast films with varying ratios of gelatin. Interestingly, in presence of 20 wt% gelatin the HK-2 cells formed a near confluent layer. Staining of zona occludens-1 (ZO-1) protein and visualization by fluorescence microscopy revealed the presence of tight junctions between the cells. This indicated the formation of a truly tight renal epithelial cell layer on this hybrid hydrogel mesh.

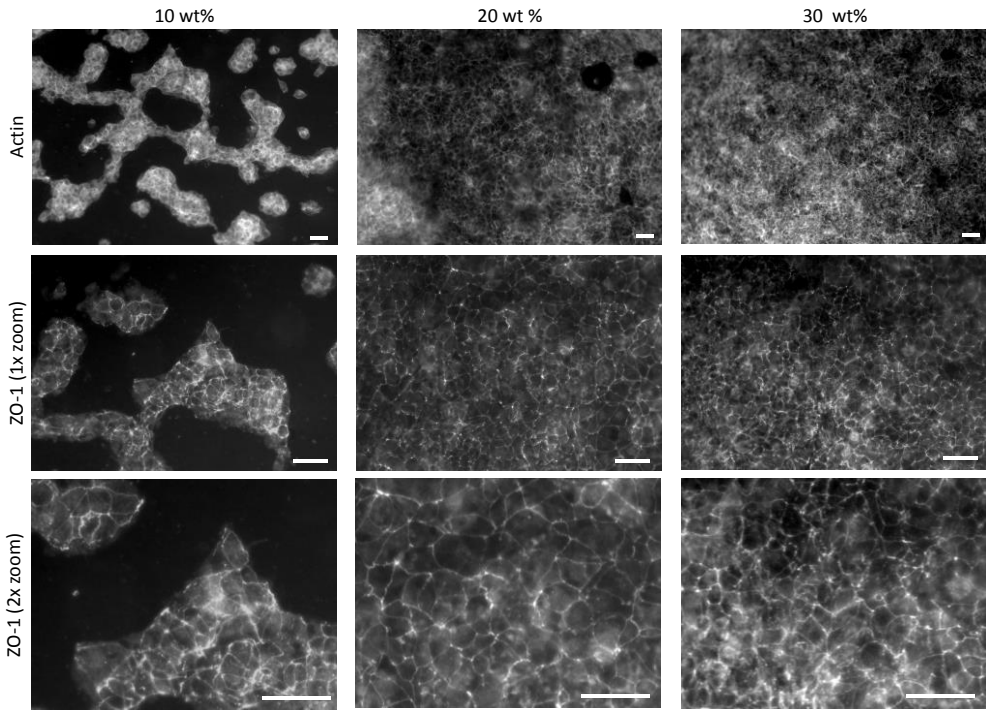

Figure 10. HK-2 cells adhere to hybrid hydrogel BM mimics. Fluorescence micrographs of HK-2 cells 3 days after seeding on electrospun meshes of CE-UPy-PEG with 10, 20, and 30 wt% gelatin. Staining of the actin skeleton shows the extent of cell adhesion and spreading on the meshes, ZO-1indicates the formation of tight-junctions between these cells. All scale bars represent 50 µm.

These results indicate suitability of the hybridized microfibrous hydrogels to function as cell support for formation of a bioartificial kidney membrane. This provides a proof-of-concept for application of such scaffolds as BM mimic.

2.6 Hybrid hydrogel scaffolds as 3D interstitial ECM mimic in a cardiac patch

The successful application of the hybrid hydrogel scaffold as BM mimic, encouraged exploration towards the applicability of this hybrid material in 3D cell culture. Scaffolds of hybrid hydrogel with a more open pore structure were hypothesized to function as 3D ECM mimic. This was tested by application of such scaffold in the formation of a cardiac patch in conjunction with an immortalized variant of human cardiomyocyte progenitor cells (CMPCs). The function of the hydrogel in such a patch is to contain the cells, support their growth and differentiation, and facilitate their coupling to the native myocardium. It should hence act as a temporarily 3D microenvironment which resembles the native extracellular microenvironment until the cells have formed their own ECM. In the initial tests described here, CE-UPy-PEG/gelatin was evaluated for scaffold formation with an open pore structure, seeding of CMPCs inside this scaffold, cell viability and the ability of the cells to deposit their own matrix.

Scaffolds with a more open pore structure were successfully prepared by electrospinning fibers with bigger diameters. This was achieved by increasing the concentration and hence viscosity of the electrospinning solution. Spinning of a concentrated (10 wt/v%) solution of 80/20 wt/wt% CE-UPy-PEG/gelatin in HFIP resulted in a scaffold with average fiber diameters of 2.14 ± 0.63 μm and apparent pore sizes bigger than 10 μm (Figure 11).

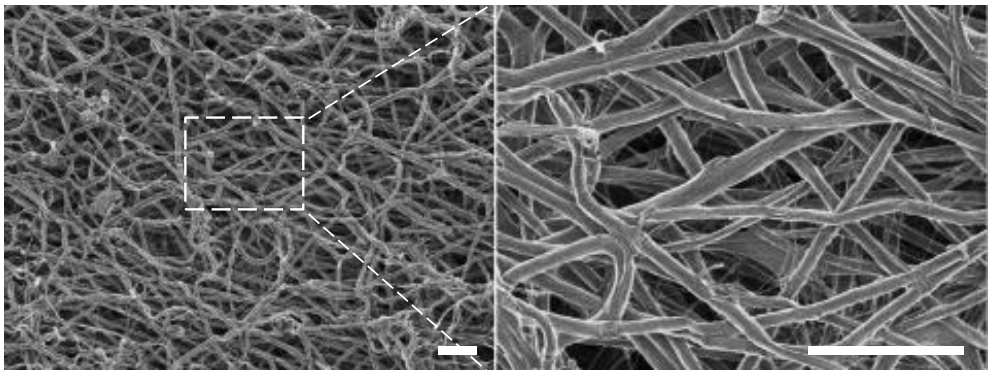

Figure 11. Electrospun hybridized CE-UPy-PEG open-pore 3D scaffolds. Scanning electron micrographs of an electrospun scaffold prepared from a concentrated solution of CE-UPy-PEG with 20 wt% gelatin. The scale bars represent 20 μm.

To allow facile infiltration of CMPCs into the scaffolds, the fiber diameters and pore sizes would ideally be bigger. Hence, cell infiltration in these meshes was considered to be challenging. To actively aid cell infiltration, cells were spin seeded. Cell infiltration depth in the hybrid CE-UPy-PEG/gelatin scaffold was enhanced from an approximate 20 µm by static seeding to 69 µm by the application of centrifugal force (Figure 12).

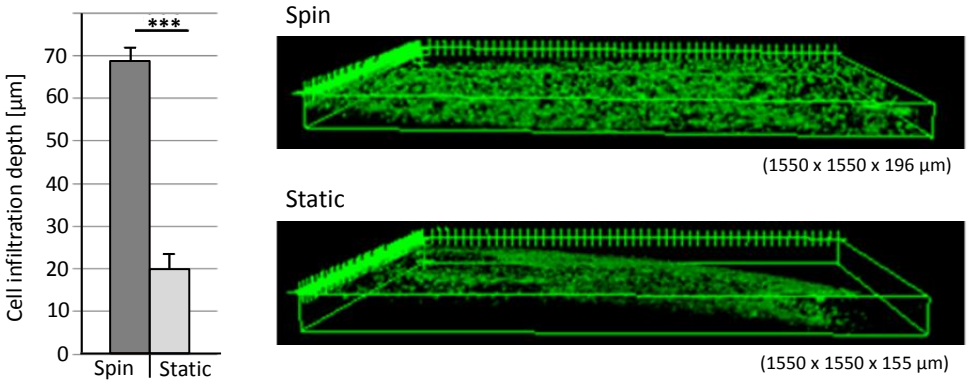

Figure 12. CMPC infiltration depth in hydrogel scaffolds is dependent on seeding method. CMPCs were seeded under static conditions or by spin seeding employing a centrifuge, in 80/20 wt/wt% CE-UPy-PEG/gelatin meshes. Z-stacks of confocal laser scanning micrographs visualized the infiltration depth of the cells. A Gaussian distribution was fit through the z-stack intensities to derive the average cell infiltration depth and standard deviations, depicted in the graph on the left.

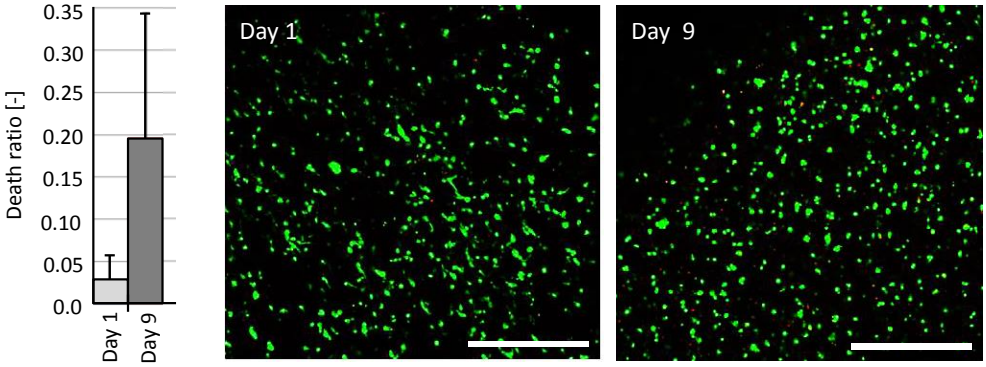

Figure 13. CMPC viability is high inside 3D hybrid hydrogel mesh. Confocal laser scanning micrographs of CMPCs, 1 and 9 days after spin seeding. The cytoplasm of live cells is stained with calcein (green), the nuclei of dead cells with propidium iodide (red). Scale bars indicate 500 µm) Live and dead cells from such images were counted and the average death ratio (dead/dead+live) and standard deviations are depicted in the graph on the left.

The viability of CMPCs was high one day after seeding (Figure 13). After 9 days of pre-differentiation inside the hydrogel scaffold, cell viability slightly decreased. In general cell survival is lower in 3D cultures due to the more restricted oxygen and nutrient supply compared to 2D cultures. Furthermore, the CMPCs were exposed to the cytotoxic 5-

azacytidine during a differentiation treatment at day 1, 2 and 3. Nonetheless, the vast majority of the cells survived inside the hybrid hydrogel scaffold. Next to cell viability, CMPC proliferation inside the hydrogel scaffold was confirmed by Ki-67 staining at day 1 (data not shown).

Deposition of ECM proteins by CMPCs was determined (Figure 14), by immunofluorescent staining and imaging of collagen I, III, IV and fibronectin. After one day of culture inside the hybrid scaffold, CMPCs were observed to contain a limited amount of cytoplasmic collagen I, whereas a limited amount of BM component collagen IV was already deposited. Co-staining of collagen III and membrane marker integrin β1 revealed the presence of collagen III between cells. Furthermore, fibronectin was deposited after one day, which formed a fibrous structure at the attachment points with the scaffold. One of the hurdles of hybrid hydrogels composed of a synthetic and natural component is that the biological ECM component often degrades more rapid than their replacement. The fast deposition of ECM proteins by the CMPCs thus provides a promising start for successful long-term outcome.

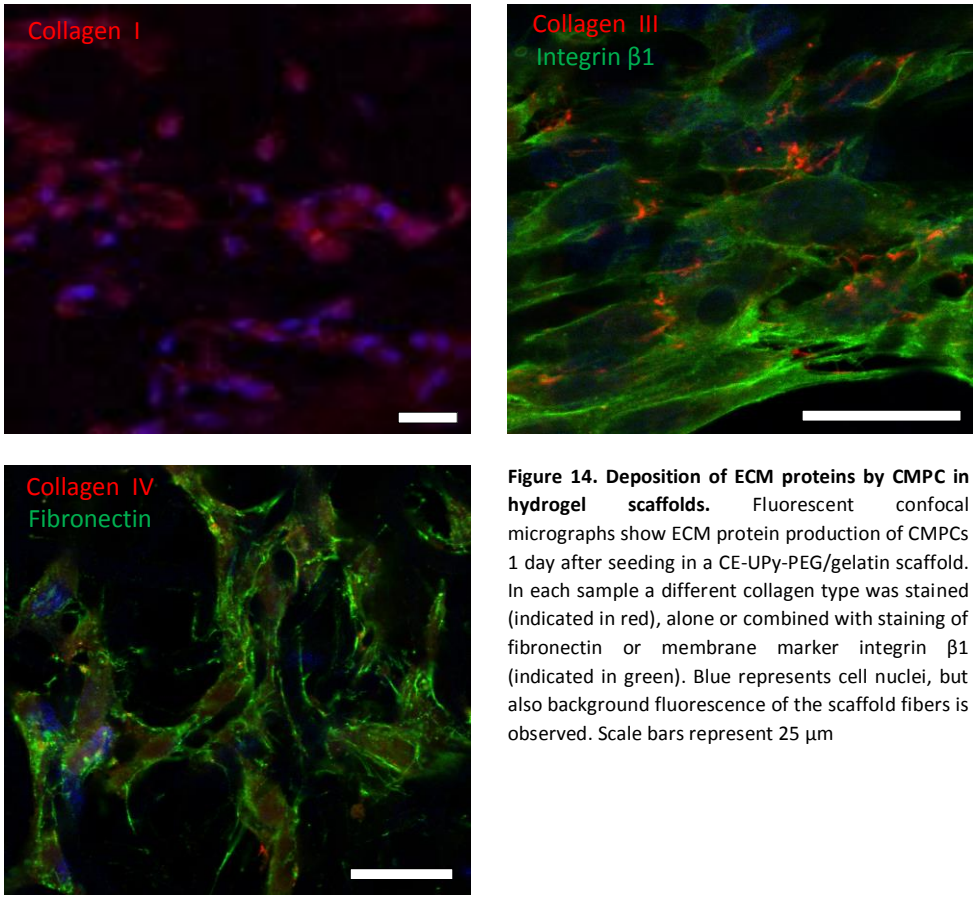

Figure 14. Deposition of ECM proteins by CMPC in hydrogel scaffolds. Fluorescent confocal micrographs show ECM protein production of CMPCs 1 day after seeding in a CE-UPy-PEG/gelatin scaffold. In each sample a different collagen type was stained (indicated in red), alone or combined with staining of fibronectin or membrane marker integrin β1 (indicated in green). Blue represents cell nuclei, but also background fluorescence of the scaffold fibers is observed. Scale bars represent 25 µm

3. Discussion and outlook

The presented results provide proof-of-concept for application of CE-UPy-PEG as basis for 2D BM and 3D interstitial ECM mimicking hydrogel scaffolds. The physical cross-links, formed by UPy-moieties distributed over the macromolecular monomer backbone, contribute to the formation of a stable hydrogel scaffold structure. This by-passes the need of chemical cross-linking post-processing. The long-term stability and biodegradability of the electrospun CE-UPy-PEG under physiological relevant conditions were outside the scope of the reported initial studies. These should be assessed in future experiments.

Bioactivation of CE-UPy-PEG via simple mixing with a natural polymer, gelatin, was proven successful. Electrospinning of the hybrid biomaterial improved distribution of both components compared to drop-cast films of the same composition. This aided the bioactive effect exerted by the incorporated gelatin and improved the induced cell adhesion. The stability of the gelatin, which is assumed to be simply entangled in the CE-UPy-PEG physically cross-linked network, was not assessed. Cross-linking of both synthetic and natural components in other examples of hybrid hydrogels has shown to improve mechanical properties (increases elastic modulus) and long-term biofunctionality.[33,34] Functionalization of the bioactive, natural hydrogel component with UPy-moieties, could be a possibility to allow incorporation in the physically cross-linked network. Although porcine derived gelatin proved effective for cell adhesion in the presented initial in-vitro studies, future applications will benefit from different bioactive sources. An interesting alternative could be recombinant human gelatin. Recombinant gelatin provides improved safety, traceability, reproducibility, and quality compared with animal derived equivalents.[35] Furthermore, it allows for incorporation of tailorable bioactive properties by redesign of the amino acid sequence. Another appealing approach towards the formation of a completely synthetic UPy-based bioactive hydrogel system, involves UPy-modified peptides.[36] This approach was successfully applied in solid bifunctional[18,37] and chain-extended (unpublished data) UPy-polymer biomaterials, and can possibly be applied in telechelic and monofunctional UPy-PEG based hydrogel systems. However, the design of the UPy-peptide should be optimized to facilitate incorporation within the CE-UPy-PEG hydrogel network and representation of the biofunctionality at the hydrogel surface.

Elastic behavior of both pure CE-UPy-PEG and hybridized electrospun meshes was demonstrated as well as durability of the latter under cyclic loading. Preliminary results demonstrated an elastic modulus of ~0.63 MPa, which could be appropriate for the tissue engineering of a diversity of soft tissues. Furthermore, this synthetic material might provide a similar function as that of glycosaminoglycans (GAG) in the ECM, i.e. providence of hydration and swelling pressure to the tissue and thereby generating resistance to compressive forces. It will therefore also be interesting to investigate the compressive strength of CE-UPy-PEG meshes.

The modular synthetic approach of CE-UPy-PEG allows facile tailoring of physical and mechanical properties.[19] The UPy-polymer platform furthermore provides opportunities to tailor and fine-tune physical and mechanical properties post chemical synthesis, via supramolecular synthesis. Simple mixing of CE-UPy-PEG with other chain-extended, telechelic or monofunctional UPy-modified building blocks offers a resourceful opportunity to tune dynamics, stability, mechanical properties and physical properties.

4. Conclusions

The results shown in this chapter indicate that CE-UPy-PEG can function as basis for self-supporting hydrogel scaffolds that mimic 2D BM and 3D interstitial ECM in tissue engineering applications. CE-UPy-PEG was successfully processed by electrospinning into relevant fibrous morphologies, which are stable under physiological conditions without the need of chemical cross-linking. The combination with gelatin demonstrates the possibility to make hybrid scaffolds with natural bioactive proteins, while synthetic UPy-peptide based approaches towards more specific and controlled bioactivation might be explored in the future. The elastic behaviour of the hydrogel scaffolds and durability under cyclic loading widens the scope of possible tissue engineering applications. Furthermore, CE-UPy-PEG-based scaffolds allow tunability of their mechanical properties at many levels, including the chemistry of the supramolecular macromolecule building block, by supramolecular mix-and-matching with other UPy-building blocks, and processing parameters (i.e. fiber diameter, alignment etc.). Taken together, the unification of all these properties and therefore possibilities make CE-UPy-PEG a unique and attractive biomaterial. It will be worthwhile to explore further its function as new platform for tissue engineering applications by formation of BM and interstitial ECM mimicking scaffolds. Besides scaffolding material, CE-UPy-PEG provides enticing opportunities for exploration in other medical applications, such as in drug delivery or as wound closure material.

5. Acknowledgements

R.A.H van der Velden is thanked for his initial electrospun work. P. Goodarzy Fard is acknowledged for her experiments on hybridization of CE-UPy-PEG, electrospinning of these materials and initial experiments on HK-2 cell adhesion. S. Spaans is acknowledges for his experiments and providence of the data on CE-UPy-PEG as 3D scaffold in the cardiac patch.

6. Experimental section

Materials

CE-UPy-PEG with 10 kg mol^{-1} number-average molar mass (Mn) per PEG segment was synthesized as described in literature.[20] As a consequence of the high polydispersity index (PDI >3) the number of repeats, or UPy-functionalities, per macromolecular monomer is poorly defined but was estimated to be around 50 repeats on average based on average molecular weight determined by GPC. Gelatin type A, derived from porcine skin with ~300 g Bloom (275-325 g Bloom) gel strength, and 1,1,1,3,3,3-hexafluoro-2-propanol (HFIP) 99.5+% pure were purchased from Sigma Aldrich.

Drop-cast films

Film preparation

Stock solutions of both CE-UPy-PEG and gelatin were prepared in HFIP at a concentration of 1 wt%. Mixtures at volumetric ratios of 100/0, 90/10, 80/20, 70/30, 50/50, 25/75 and 0/100 of CE-UPy-PEG/gelatin solution were prepared and drop cast on glass cover slips to yield films with alike wt/wt% CE-UPy-PEG/gelatin, respectively. After drying to air, residual solvent was removed at 40 °C *in vacuo* during 2 hours.

Cell seeding and staining

Films were sterilized by exposure to light of a germicidal UV lamp for 1 hour. The glasses with films were placed in the static culture system comprising of Transwell inserts (Corning) and custom-made clamping caps (described in Chapter 8). Samples were pre-wet with complete media (DMEM with 1 v% penicillin/streptomycin and 10 v% FBS, see chapter 3), before seeding 55 x 10^3 HK-2 cells per sample with a surface area of 1.12 cm^2. Cells were left to adhere for 22 hours. After this culture period, the samples were washed with PBS twice by adding PBS in the insert and decanting. The adhered cells on the films were fixed by incubation with 4 v% formaldehyde (Fluka) in PBS at room temperature for 10 minutes. Samples were again washed with PBS twice and subsequently permeabilized by incubation with 0.5 v% Triton X-100 in PBS. Samples were again washed with PBS twice before incubation for 1 hour in blocking buffer of 5 wt/v% BSA (Sigma Aldrich) in PBS. The cell's actin skeleton was stained with atto-488-conjugated phalloidin (1 : 1000, Sigma Aldrich) in 2 wt/v% BSA in PBS by incubation at room temperature for 60 minutes. Then the cell nuclei were stained with 4',6-diamidino-2-phenylindole (DAPI, 1 : 1000, Sigma Aldrich) in 2 wt/v% BSA in PBS for 15 minutes. The samples were washed three times with PBS, taken out of the supporting culture inserts and embedded between a microscopy slide and cover glass in citifluor AF1 glycerol/PBS solution (Agar scientific). The samples were visualized by fluorescence microscopy using a Zeiss Axio observer D1 equipped with an AxioCam Mrm camera and Zeiss Axiovision software (Carl Zeiss).

Electrospun scaffolds

CE-UPy-PEG and hybrid thin fiber 2D meshes

Electrospinning solutions of 5 wt/v% were prepared in glass vials, i.e. 200 mg solid material dissolved in 4 mL solvent. Weight ratios of 100/0, 90/10, 80/20, 70/30 of CE-UPy-PEG /gelatin were applied. First the CE-UPy-PEG fraction was dissolved in HFIP, then gelatin was added. The solutions were stirred overnight at room temperature and transferred to 2.5 mL glass syringes (Hamilton). The electrospun solution was fed at 0.05 mL min^{-1} using a syringe pump (KR analytical) at the outside of the electrospinning cabinet to the flat-tip stainless-steel 23 g needle (Intertronics, United Kingdom) inside the cabinet, via a ~35 cm long 1 mm I.D. PTFE tube. Inside the cabinet, each solution was spun with an in-house built electrospun setup by the application of 18.5 kV between a tip-to-target distance of 12 cm. To enable facile removal of the non-woven electrospun membrane, the collector

was covered with a thin sheet of polyethylene film. To provide a flat surface and extra support to thin samples of the electrospun mesh, fibers were collected on 12 mm round glass coverslips. The fiber deposition was interrupted several times to move the static collector plate over a 3x3 grid to enlarge the area of fiber deposition and to achieve a more homogeneous mesh thickness. The electrospun mesh (on coverslips) was gently removed from the collector plate together with the polyethylene film and placed *in vacuo* at 40° C overnight to remove any residual solvent. The meshes were stored protected from light and contact to open air to prevent uptake of moisture, to prolong the stability of the PEG-based material. Mesh degradation, both structurally (cavities in mesh structure were observed by SEM), mechanically (brittle in both dry and hydrated state) and molecularly (degradation of PEG) has been observed to occur otherwise.

Environmental scanning electron microscopy (ESEM) imaging was performed by using FEI Quanta 600 and Xt Microscope Control software. Samples were prepared by placing small pieces of each scaffold on double-sided sticky carbon tape on a metal stub. The uncoated samples were directly visualized in a low vacuum (~0.5 mbar) with an accelerating voltage of 15-18 kV and a working distance of 6.9-8.2 mm. Images were recorded up to 10,000 times magnification. In low vacuum, both backscattering electrons (BSE) and secondary electrons (SE) were detected. Microfiber diameters were determined from multiple high magnification images using ImageJ software and expressed as average ± standard deviation.

Thick fiber 3D hybrid scaffolds

A highly viscous solution of 80/20 CE-UPy-PEG/gelatin in HFIP was prepared by dissolving 400 mg CE-UPyPEG and 100 mg gelatin in 5 mL HFIP (10 wt/v% solution) and stirred at 40˚C overnight. The clear viscous solution was transferred to a syringe and connected via PTFE 1 mm I.D. tube and needle to the climate controlled electrospinning apparatus (IME technologies, Eindhoven) set at 22-23°C and 25% humidity. Solution was fed at 75 µL min^{-1}, spun by 12 kV and collected during an hour at an aluminium foil covered rotating drum with 28 mm diameter, rotating at 100 rpm. The dry thickness of the collected CE-UPyPEG/gelatin scaffold was 300 µm, respectively, which was measured with an automatic ruler. Scanning electron micrographs were obtained using the FEI Quanta 600F ESEM at high vacuum, with a voltage of 1 kV, working distance of 10mm and spot size of 3.0 mm.

Gelatin staining with CNA35

Prewet CE-UPy-PEG hydrogel samples on glass, both drop-cast film and electrospun meshes with varying gelatin content were incubated overnight at 37 °C with a solution of CNA35mTurquase2 in PBS at a concentration of 1 µmol L^{-1}.[38] Samples were washed once with PBS before imaging with fluorescence microscopy (Zeiss).

Mechanical testing of electrospun meshes

The mechanical performances of CE-UPy-PEG electrospun meshes with fiber diameters of typically 1 µm or smaller, both with and without gelatin, were measured. Square samples of approximately 8 x 8 mm were cut from the meshes. The samples were weighed before and after hydration to gain insight into swelling behavior and the thickness of the samples was determined using a digital microscope (Keyence, VHX-500F). The samples were marked with graphite particles to allow the determination of local strains using particle tracking image analysis of images recorded during the straining protocol. The hydrated sample was mounted in a biaxial tensile testing device equipped with 1.5 N load cells (CellScale, Waterloo, ON, Canada), as illustrated in Figure 8. Four rakes (BioRake Delicate, 0.7 mm, 30 mm, CellScale) each consisting of five metal hooks of 250 µm Ø, were attached to the sample, leading to a square testing area 3500 x 3500 µm. The sample was emerged in a water bath, which was maintained at 37°C, during the straining protocol.

For determination of elastic moduli and confirmation of isotropic behavior of the meshes with randomly oriented fibers, the meshes were cyclically loaded with three repeats of uniaxial stretch in both x and y direction, and three repeats of equibiaxial stretch. Stretch was applied at a rate of 2% s^{-1} and each final stretch was applied for 2 s. Between cycles, the sample was not loaded for 5 s to allow the fibers to relax and return to their initial configuration. The applied stretch was increased after each set of cycles starting at 10% up to 50% with increments of 10%. Then the mesh was further loaded with double cycles of increasing equibiaxial stretch with steps of 10% until the yielding point was reached (total rupture of the mesh). During the whole protocol images were taken with a digital camera at a frequency of 1 Hz, while numerical data, i.e global stretch, or displacement in µm and force in mN, was generated at a frequency of 30 Hz. The images were used as reference for visual control of sample integrity. Data was converted with Matlab to calculate stresses (force/area) and matched with the applied global strains. As the signal to noise ratio for the measured forces was low, the average stress was determined per second from the redundant data acquisition frequency. The elastic moduli in both x- and y-direction were determined from uniaxial tensile cycles up to 30% stretch from the linear elastic region of the derived stress-strain curves. To determine the durability of the hybrid hydrogel mesh consisting of 80/20 wt/wt% CE-UPy-PEG/gelatin, a sample was measured with the previously described protocol before and after subjection to ~5000 cycles of 20% equibiaxial stretch, applied at a speed of 20% s^{-1} with 0 s rest at maximum stretch and 0.5 s recovery time at 0% stretch.

Renal epithelial cell seeding on 2D BM mimicking meshes

Round-shaped 12 mm Ø samples, supported by a glass coverslip, were cut from the electrospun meshes. Samples were sterilized via UV-irradiation for 1 hour on each side and fixed in MINUSHEET tissue carriers with 13 mm O.D. (Minucells and Minutissue vertriebs gmbh) or Transwell static culture system with cap (chapter 8). The carriers with samples were placed in a 24-well tissue culture plate (BD Biosciences). Each mesh sample was submerged in an ample volume of complete medium, which was removed right before cell seeding. For low cell density 55 x 10^3 cells were seeded on samples fixed in Transwell inserts, for high cell density 100 x 10^3 cells were seeded on samples fixed in Minusheet carriers and cultured at 37° C, 5 % CO2 and 90 % humidity. The low density cells were fixed after 1 day and stained with actin, vincullin and DAPI. High cell density samples were cultured for 3 days and then fixed and stained with ZO-1 and DAPI.

Cell fixation and staining of actin and vinculin

Before fixation, the samples were washed with PBS twice. Then adhered cells were fixed by incubation with 4 v% formaldehyde (Fluka) in PBS solution for 10 minutes at room temperature. Samples were again washed with PBS twice and subsequently incubated for 1 hour in blocking buffer of 5 wt/v% BSA (Sigma Aldrich) in PBS. For vinculin staining, first samples were incubated for 1 hour with mouse anti-human vinculin (1 : 400, Sigma Aldrich) in 2 wt/v% BSA in PBS, followed by washing with 0.1 v/v% polysorbate 20 (Merck) in PBS twice, and PBS once. Then samples were incubated for 45 minutes with goat anti-mouse Alexa 555 conjugated antibody (1:400, Molecular probes, invitrogen) and atto-488-conjugated phalloidin (1:500, Sigma Aldrich) together in 2 wt/v% BSA in PBS, directly followed by incubation for 10 minutes with 4',6-diamidino-2-phenylindole (DAPI, 1:1000, Invitrogen) in 2 wt/v% BSA in PBS. The samples were washed with 0.1 v/v% polysorbate 20 in PBS twice and once in PBS.

Immunofluorescent staining of ZO-1

For ZO-1 staining, first samples were incubated for 1 hour with mouse-anti-human ZO-1 (1 : 100, BD Biosciences) in 2 wt/v% BSA in PBS, followed by washing with 0.1 v/v% polysorbate 20 (Merck) in

PBS twice, and PBS once. Then samples were incubated for 45 minutes with goat anti-mouse Alexa 555 conjugated antibody (1:400, Molecular probes, invitrogen) in 2 wt/v% BSA in PBS, directly followed by incubation for 10 minutes with 4',6-diamidino-2-phenylindole (DAPI, 1:1000, Invitrogen) in 2 wt/v% BSA in PBS. The samples were washed with 0.1 v/v% polysorbate 20 (Merck) in PBS twice, and PBS once and taken out of the supporting rings and embedded between a microscopy slide and cover glass. The samples were visualized by fluorescence microscopy using a Zeiss Axio observer D1 equipped with an AxioCam Mrm camera and Zeiss Axiovision software (Carl Zeiss).

CMPC culture and seeding inside 3D hybrid scaffolds

L9TB CMPCs, immortalized human cardiomiocyte progenitor cells (kind gift from group Prof. Goumans, Leiden) were routinely cultured in polystyrene culture flasks pre-coated with 0.1wt/v% gelatin (Sigma) in PBS. Undifferentiated CMPCs were cultured in SP++ growth medium (GM) that consisted of M199 (Gibco)/EGM2 (3:1) supplemented with 10 v% fetal bovine serum (FBS), 1 v% penicillin/streptomycin (Lonza DE17-602E) and 1 v% non-essential amino acids (Gibco). CMPCs were passaged when they were 80-90% confluent and differentiation was ideally started when they are 90% confluent. Differentiation of CMPCs was performed as described earlier.[39] Briefly, CMPCs are treated with 5 µM azacytidine (Sigma A2385) for 72 hours in differentiation medium (DM) that consists of 94,8 v% IMDM (Iscove's Modified Dulbecco's Medium, Lonza BE12-722F)/Ham-F12 (Lonza BE12-625F) (1:1) supplemented with 2 v% horse serum (HS, Invitrogen 16050-122), 1 v% non-essential amino acids (Lonza), 0.2 v% insulin-transferrin-selenium (Lonza), 1% penicillin/streptomycin and 1 v% glutamax (Gibco, VX35050087). After 72 hours of 5-azacytidine treatment medium was changed and supplemented with 10^{-4} M vitamin C. Differentiation was continued by changing the medium that was supplemented with 1 ng/mL TGFβ1 (Prepotech, 100-21) and 10^{-4} M vitamin C twice a week. Round samples with 12 mm diameter were cut from electrospun scaffolds and constrained in Minusheet tissue carriers in the dry state. Undifferentiated CMPCs were seeded into the scaffold (250 x 10^3 or 1000 x 10^3 cells per scaffold) by centrifugal force according to previously described method for skin tissue engineering.[40] Differentiation was started 1 day after seeding. Cultures were analyzed at day 1 (undifferentiated) and day 9 (differentiated) with Live/Dead staining and sacrificed for immunofluorescent staining.

Live/Dead staining of CMPC's and quantification

Live/Dead staining was performed using Calcein-AM (Fluka 17783) and propidium iodide (PI; Invitrogen P3566). Gels were washed two times with PBS, followed by incubation in warmed-up serum free GM/DM with 10 µM Calcein-AM and PI for 60 min at 37 °C. Again the gels were washed two times with PBS and incubated in warmed-up serum-free GM/DM for 30min at 37 °C. Lastly, washed two times with PBS and incubated in GM/DM at 37 °C until imaging. The live (green) and dead (red) cells were counted using Mathematica. Dead ratio was expressed as dead/total number of cells. Infiltration depth was approximated by fitting a gaussian distribution through the amount of intensity in the z-direction using Matlab.

Immunofluorescent staining of CMPC's

Immunofluorescent staining started by washing the hydrogels two times with PBS, fixing with 3.7% formaldehyde in PBS for 20 min on the shaking table at room temperature, followed by two times washing with PBS. Cell permeabilization was performed by incubation with 0.5 v% Triton X-100 in PBS for 10 minutes at room temperature. Blocking was performed with 10% HS in PBS for 20 minutes. Incubation with the first antibody in NET-gel (50 mM pH 7.4 Tris; 150 mM NaCl; 5mM EDTA; 0,25 wt/v% gelatin from porcine skin in MilliQ) + 1% HS was performed at 4 ˚C overnight. The next day the hydrogels were washed six times with NET-gel for 5 minutes, incubated with the

second antibody for 1 hour in NET-gel, washed two times with NET-gel for 5 minutes, incubated with DAPI in PBS for 10 minutes, washed again five times with PBS for 5 minutes and finally mounted on cover glasses with Mowiol (Sigma, 81381). All primary and secondary antibodies and matching dilutions are listed in table 2.

Table 2: Antibodies used in immunohistology of CMPCs

Antigen	Source	Cat No	Isotype	Label	Species	Dilution
Ki-67	-	RB1510P0	IgG		Rabbit	1/50
Collagen I	SA	C2456	IgG1		Mouse	1/50
Collagen III	Abcam	Ab7778	IgG		Rabbit	1/100
Collagen IV	Abcam	Ab86042	IgG1		Mouse	1/100
Fibronectin	SA	F3648	IgG		Rabbit	1/200
Integrin-β1	SC	Sc53711	IgG1		Mouse	1/50
Mouse IgG1	IG	A21121	IgG1	AlexaFluor 488	Goat	1/200
Rabbit IgG	IG	A21428	IgG(H+L)	AlexaFluor 555	Goat	1/200
Mouse IgG1	MP	A21127	IgG1	AlexaFluor 555	Goat	1/200
Rabbit IgG	MP	A11008	IgG(H+L)	AlexaFluor 488	Goat	1/200

7. References

(1) Muiznieks, L. D.; Keeley, F. W. Molecular Assembly and Mechanical Properties of the Extracellular Matrix: A Fibrous Protein Perspective. *Biochim. Biophys. Acta BBA - Mol. Basis Dis.* **2013**, *1832*, 866–875.

(2) Jia, X.; Kiick, K. L. Hybrid Multicomponent Hydrogels for Tissue Engineering. *Macromol. Biosci.* **2009**, *9*, 140–156.

(3) Matthews, J. A.; Wnek, G. E.; Simpson, D. G.; Bowlin, G. L. Electrospinning of Collagen Nanofibers. *Biomacromolecules* **2002**, *3*, 232–238.

(4) Liu, L.; Yoshioka, M.; Nakajima, M.; Ogasawara, A.; Liu, J.; Hasegawa, K.; Li, S.; Zou, J.; Nakatsuji, N.; Kamei, K.; Chen, Y. Nanofibrous Gelatin Substrates for Long-Term Expansion of Human Pluripotent Stem Cells. *Biomaterials* **2014**, *35*, 6259–6267.

(5) Im, J. S.; Yun, J.; Lim, Y.-M.; Kim, H.-I.; Lee, Y.-S. Fluorination of Electrospun Hydrogel Fibers for a Controlled Release Drug Delivery System. *Acta Biomater.* **2010**, *6*, 102–109.

(6) Stephens-Altus, J. S.; Sundelacruz, P.; Rowland, M. L.; West, J. L. Development of Bioactive Photocrosslinkable Fibrous Hydrogels. *J. Biomed. Mater. Res. A* **2011**, *98A*, 167–176.

(7) Gestos, A.; Whitten, P. G.; Wallace, G. G.; Spinks, G. M. Actuating Individual Electrospun Hydrogel Nanofibres. *Soft Matter* **2012**, *8*, 8082.

(8) Çay, A.; Mohsen Miraftab. Properties of Electrospun Poly(vinyl Alcohol) Hydrogel Nanofibers Crosslinked with 1,2,3,4-Butanetetracarboxylic Acid. *J. Appl. Polym. Sci.* **2013**, *129*, 3140–3149.

(9) Kim, K.-O. Cells Attachment Property of PVA Hydrogel Nanofibers Incorporating Hyaluronic Acid for Tissue Engineering. *J. Biomater. Nanobiotechnology* **2011**, *02*, 353–360.

(10) Zalipsky Samuel; Harris J. Milton. Introduction to Chemistry and Biological Applications of Poly(ethylene Glycol). In *Poly(ethylene glycol)*; ACS Symposium Series; American Chemical Society, 1997; Vol. 680, pp. 1–13.

(11) Vatankhah, E.; Semnani, D.; Prabhakaran, M. P.; Tadayon, M.; Razavi, S.; Ramakrishna, S. Artificial Neural Network for Modeling the Elastic Modulus of Electrospun Polycaprolactone/gelatin Scaffolds. *Acta Biomater.* **2014**, *10*, 709–721.

(12) Greef, T. F. A. de; Nieuwenhuizen, M. M. L.; Stals, P. J. M.; Fitié, C. F. C.; Palmans, A. R. A.; Sijbesma, R. P.; Meijer, E. W. The Influence of Ethylene Glycol Chains on the Thermodynamics of Hydrogen-Bonded Supramolecular Assemblies in Apolar Solvents. *Chem. Commun.* **2008**, 4306–4308.

(13) Stals, P. J. M.; Haveman, J. F.; Martín-Rapún, R.; Fitié, C. F. C.; Palmans, A. R. A.; Meijer, E. W. The Influence of Oligo(ethylene Glycol) Side Chains on the Self-Assembly of Benzene-1,3,5-Tricarboxamides in the Solid State and in Solution. *J. Mater. Chem.* **2009**, *19*, 124.

(14) Dankers, P. Y. W.; Hermans, T. M.; Baughman, T. W.; Kamikawa, Y.; Kieltyka, R. E.; Bastings, M. M. C.; Janssen, H. M.; Sommerdijk, N. A. J. M.; Larsen, A.; van Luyn, M. J. A.; Bosman, A. W.; Popa, E. R.; Fytas, G.; Meijer, E. W. Hierarchical Formation of Supramolecular Transient Networks in Water: A Modular Injectable Delivery System. *Adv. Mater.* **2012**, *24*, 2703–2709.

(15) Bastings, M. M. C.; Koudstaal, S.; Kieltyka, R. E.; Nakano, Y.; Pape, A. C. H.; Feyen, D. A. M.; van Slochteren, F. J.; Doevendans, P. A.; Sluijter, J. P. G.; Meijer, E. W.; Chamuleau, S. A. J.; Dankers, P. Y. W. A Fast pH-Switchable and Self-Healing Supramolecular Hydrogel Carrier for Guided, Local Catheter Injection in the Infarcted Myocardium. *Adv. Healthc. Mater.* **2014**, *3*, 70–78.

(16) Kieltyka, R. E.; Pape, A. C. H.; Albertazzi, L.; Nakano, Y.; Bastings, M. M. C.; Voets, I. K.; Dankers, P. Y. W.; Meijer, E. W. Mesoscale Modulation of Supramolecular Ureidopyrimidinone-Based Poly(ethylene Glycol) Transient Networks in Water. *J. Am. Chem. Soc.* **2013**, *135*, 11159–11164.

(17) Pape, A. C. H.; Bastings, M. M. C.; Kieltyka, R. E.; Wyss, H. M.; Voets, I. K.; Meijer, E. W.; Dankers, P. Y. W. Mesoscale Characterization of Supramolecular Transient Networks Using SAXS and Rheology. *Int. J. Mol. Sci.* **2014**, *15*, 1096–1111.

(18) Mollet, B. B.; Comellas-Aragonès, M.; Spiering, A. J. H.; Söntjens, S. H. M.; Meijer, E. W.; Dankers, P. Y. W. A Modular Approach to Easily Processable Supramolecular Bilayered Scaffolds with Tailorable Properties. *J. Mater. Chem. B* **2014**.

(19) Guo, M.; Pitet, L. M.; Wyss, H. M.; Vos, M.; Dankers, P. Y. W.; Meijer, E. W. Tough Stimuli-Responsive Supramolecular Hydrogels with Hydrogen-Bonding Network Junctions. *J. Am. Chem. Soc.* **2014**, *136*, 6969–6977.

(20) Davis, G. E. Affinity of Integrins for Damaged Extracellular Matrix: A< Sub> V</sub> B< Sub> 3</sub> Binds to Denatured Collagen Type I through RGD Sites. *Biochem. Biophys. Res. Commun.* **1992**, *182*, 1025–1031.

(21) Zeugolis, D. I.; Khew, S. T.; Yew, E. S. Y.; Ekaputra, A. K.; Tong, Y. W.; Yung, L.-Y. L.; Hutmacher, D. W.; Sheppard, C.; Raghunath, M. Electro-Spinning of Pure Collagen Nano-Fibres – Just an Expensive Way to Make Gelatin? *Biomaterials* **2008**, *29*, 2293–2305.

(22) Huang, Z.-M.; Zhang, Y. Z.; Ramakrishna, S.; Lim, C. T. Electrospinning and Mechanical Characterization of Gelatin Nanofibers. *Polymer* **2004**, *45*, 5361–5368.

(23) Zhang, S.; Huang, Y.; Yang, X.; Mei, F.; Ma, Q.; Chen, G.; Ryu, S.; Deng, X. Gelatin Nanofibrous Membrane Fabricated by Electrospinning of Aqueous Gelatin Solution for Guided Tissue Regeneration. *J. Biomed. Mater. Res. A* **2009**, *90A*, 671–679.

(24) Yanagisawa, M.; Yamashita, Y.; Mukai, S.; Annaka, M.; Tokita, M. Phase Separation in Binary Polymer Solution: Gelatin/Poly(ethylene Glycol) System. *J. Mol. Liq.*

(25) Ghasemi-Mobarakeh, L.; Prabhakaran, M. P.; Morshed, M.; Nasr-Esfahani, M.-H.; Ramakrishna, S. Electrospun Poly(ε-Caprolactone)/gelatin Nanofibrous Scaffolds for Nerve Tissue Engineering. *Biomaterials* **2008**, *29*, 4532–4539.

(26) Lee, J.; Tae, G.; Kim, Y. H.; Park, I. S.; Kim, S.-H.; Kim, S. H. The Effect of Gelatin Incorporation into Electrospun Poly(l-Lactide-Co-Ɛ-Caprolactone) Fibers on Mechanical Properties and Cytocompatibility. *Biomaterials* **2008**, *29*, 1872–1879.

(27) Meng, Z. X.; Wang, Y. S.; Ma, C.; Zheng, W.; Li, L.; Zheng, Y. F. Electrospinning of PLGA/gelatin Randomly-Oriented and Aligned Nanofibers as Potential Scaffold in Tissue Engineering. *Mater. Sci. Eng. C* **2010**, *30*, 1204–1210.

(28) Hajiali, H.; Shahgasempour; Naimi-Jamal, M. R.; Peirovi. Electrospun PGA/gelatin Nanofibrous Scaffolds and Their Potential Application in Vascular Tissue Engineering. *Int. J. Nanomedicine* **2011**, 2133.

(29) Aulin, C.; Foroughi, F.; Brown, R.; Hilborn, J. Extracellular Matrix–polymer Hybrid Materials Produced in a Pulsed-Flow Bioreactor System. *J. Tissue Eng. Regen. Med.* **2009**, *3*, 188–195.

(30) De Jonge, N.; Kanters, F. M. W.; Baaijens, F. P. T.; Bouten, C. V. C. Strain-Induced Collagen Organization at the Micro-Level in Fibrin-Based Engineered Tissue Constructs. *Ann. Biomed. Eng.* **2013**, *41*, 763–774.

(31) Geiger, B.; Ayalon, O.; Ginsberg, D.; Volberg, T.; Fernández, J. L. R.; Yarden, Y.; Ben-Ze'ev, A. Cytoplasmic Control of Cell Adhesion. *Cold Spring Harb. Symp. Quant. Biol.* **1992**, *57*, 631–642.

(32) Hazan, R. B.; Kang, L.; Roe, S.; Borgen, P. I.; Rimm, D. L. Vinculin Is Associated with the E-Cadherin Adhesion Complex. *J. Biol. Chem.* **1997**, *272*, 32448–32453.

(33) Fu, Y.; Xu, K.; Zheng, X.; Giacomin, A. J.; Mix, A. W.; Kao, W. J. 3D Cell Entrapment in Crosslinked Thiolated Gelatin-Poly(ethylene Glycol) Diacrylate Hydrogels. *Biomaterials* **2012**, *33*, 48–58.

(34) Daniele, M. A.; Adams, A. A.; Naciri, J.; North, S. H.; Ligler, F. S. Interpenetrating Networks Based on Gelatin Methacrylamide and PEG Formed Using Concurrent Thiol Click Chemistries for Hydrogel Tissue Engineering Scaffolds. *Biomaterials* **2014**, *35*, 1845–1856.

(35) Báez, J.; Olsen, D.; Polarek, J. W. Recombinant Microbial Systems for the Production of Human Collagen and Gelatin. *Appl. Microbiol. Biotechnol.* **2005**, *69*, 245–252.

(36) Dankers, P. Y. W.; Harmsen, M. C.; Brouwer, L. A.; Van Luyn, M. J. A.; Meijer, E. W. A Modular and Supramolecular Approach to Bioactive Scaffolds for Tissue Engineering. *Nat. Mater.* **2005**, *4*, 568–574.

(37) Dankers, P. Y. W.; Boomker, J. M.; Huizinga-van der Vlag, A.; Wisse, E.; Appel, W. P. J.; Smedts, F. M. M.; Harmsen, M. C.; Bosman, A. W.; Meijer, E. W.; van Luyn, M. J. A. Bioengineering of Living Renal Membranes Consisting of Hierarchical, Bioactive Supramolecular Meshes and Human Tubular Cells. *Biomaterials* **2011**, *32*, 723–733.

(38) Aper, S. J. A.; van Spreeuwel, A. C. C.; van Turnhout, M. C.; van der Linden, A. J.; Pieters, P. A.; van der Zon, N. L. L.; de la Rambelje, S. L.; Bouten, C. V. C.; Merkx, M. Colorful Protein-Based Fluorescent Probes for Collagen Imaging. PLoS ONE 2014, 9, e114983.

(39) Smits, A. M.; van Vliet, P.; Metz, C. H.; Korfage, T.; Sluijter, J. P.; Doevendans, P. A.; Goumans, M.-J. Human Cardiomyocyte Progenitor Cells Differentiate into Functional Mature Cardiomyocytes: An in Vitro Model for Studying Human Cardiac Physiology and Pathophysiology. *Nat. Protoc.* **2009**, *4*, 232–243.

(40) El Ghalbzouri, A.; Lamme, E.; Ponec, M. Crucial Role of Fibroblasts in Regulating Epidermal Morphogenesis. *Cell Tissue Res.* **2002**, *310*, 189–199.

Chapter 8
Renal organotypical culture environments

Abstract

Abstract: *Relevant cell-screening tests on new ureido-pyrimidinone (UPy) based basement membrane (BM) mimics require an organotypical culture environment. For this purpose, culture environments are designed with a focus on renal membrane tissue engineering. To separate a urine-like and blood-like volume, compartmentalization of media at each side of the tissue engineered construct forms the main design requirement. Both a static culture system and two flow culture bioreactors are developed. The static culture system is based on commercial Transwell inserts. A custom-made cap allows the placement of any flat support instead of the commercially attached membrane. This enables the performance of compartmentalized cell culture, cell migration, leakage and transport studies. The two bioreactors also allow free choice of culture support and media compartmentalization. In addition, a flow of media can be applied through each compartment. The bioreactors furthermore enable monitoring of the culture by eye and via in-situ visualization by microscopy. The first bioreactor contains a single membrane. This bioreactor successfully cultures human kidney-2 (HK-2) cells on UPy-based BM mimics under flow conditions for longer periods of time. Cell viability, morphology, and renal epithelial phenotype are maintained after 21 days of culture. The second bioreactor 2 is designed for the culture of three parallel triplicates, thus nine membranes in total, with the aim to function as a screening type of culture device. This multi-membrane bioreactor requires further optimization before application in routine cell-biomaterial screenings is possible. The static culture system and single-membrane bioreactor allow assessment of new BM mimics in cell-based experiments under organotypical conditions; either in a facile static test or under long term flow conditions, respectively.*

Parts of this work are submitted for publication. B.B. Mollet, I.L.J. Bogaerts, G.C. van Almen, P.Y.W. Dankers; *The development of a bioartificial environment for kidney epithelial cells through a supramolecular polymer basement membrane mimic and an organotypical culture system.*

1. Introduction

In-vitro applications, such as hemodialysis treatments and nephrotoxicity tests could potentially be improved by the implementation of renal tubular epithelial cells. This requires these cells to remain viable, highly differentiated, functional outside of the human body. However, tubular epithelial cells are prone to lose their characteristic confluent monolayer morphology and specific functions, such as active transport of uremic toxins, when cultured *in vitro*.[1,2] It is expected that optimal cell function will be retained when these cells are cultured in a bioartificial *in-vitro* environment that is ideally indistinguishable from the cells' natural environment, as perceived by the cell. Hence, to form a functional living bioartificial kidney tubular membrane, there is need for better *in-vitro* mimicry of the natural environment of renal epithelial cells. In this natural environment the basement membrane (BM) plays a key role. Ureido-pyrimidinone (UPy) based biomaterials are being explored as synthetic BM mimics to provide the cells with a suitable foundation to grow on *in vitro*. Furthermore organotypical surrounding factors are of influence to cells. Prime organotypical surrounding factors for renal epithelial cells are a (pre)urine flow at the apical epithelial cell side and a nearby blood-flow. Together, these form a compositional gradient. In this chapter the development of three organotypical culture devices is described, intended for both the culture of bioartificial renal membranes and for assessment of their functionality (Figure 1); one static culture system and flow two bioreactors.

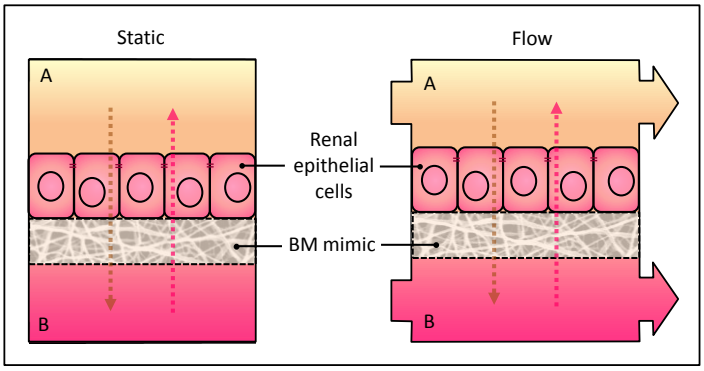

Figure 1. Organotypical renal epithelial cell environments. A schematic representation of a compartmentalized static and flow environment for renal epithelial cells. These environments allow the culture and assessment of bioartificial renal tubule membranes. The latter consist of renal epithelial cells cultured on BM mimicking synthetic culture support. The side of the membrane at which the cells and pre-urine volume are situated, is referred to as the 'apical side' (A). The other side of the membrane, at which the blood-volume would be, is referred to as the 'basal side' (B). The static culture system allows easy assessment of the functionality of a bioartificial renal tubule membrane, e.g. via read-out of leakage and active transport over the membrane when between both compartments are filled with media of a different composition. The flow system furthermore allows culture of bioartificial renal tubule membranes under continuous flow of media, mimicking natural kidney and *in-vitro* hemodialysis applications.

The static culture system is designed to facilitate media compartmentalization at each side of a BM mimic of choice. By application of different media in both compartments a compositional gradient is formed over the membrane, as between blood and pre-urine in the natural environment. As such, the *in-vitro* environment is hypothesized to enable stimulation of renal epithelial cell function through culture under such organotypical circumstances. The function of the bioartificial kidney membrane, composed of the renal epithelial cells and BM mimic, can be tested. For example leakage and active transport assays are possible by the presence of the compositional gradient over the tissue engineered construct. Hence the organotypical culture environments allow for the assessment of the performance of new UPy-based membranes as BM mimics.

Next to static culture systems we are interested in an organotypical flow culture bioreactor. This allows in addition to free choice of culture support and compartmentalization of media, also the application of continuous flow of these culture media at each side of the support. A diversity of flow culture bioreactors suitable to culture epithelial cells have been described in literature. Different tissue engineering applications that involve epithelial cells use bioreactors to achieve their goal. For example a bioreactor for the development of human bronchiole[5] or intestine[6] have been described in literature. Also devices dedicated to mimicry of a small part of the kidney tubular structure have been reported.[7–9] Although these so-called 'organs-on-chip' facilitate the culture of renal epithelial cells under flow conditions, they do not allow culture on different supports or are limited in the kind of supports that can be applied. A bioreactor design that allows easy application of different culture supports was described by Sun *et al*.[10] s, However, this device was limited to the application of culture media at one side of the membrane. An interesting microfluidic bioreactor presented by Ferrel *et al.* established renal epithelial cell culture on thin membranes under application of flow via microfluidic channels at the apical side. This was furthermore combined with integrated transepithelial electrical resistance electrodes to evaluate the integrity of the epithelial cell layer formed.[11] Commercially, only a limited number of bioreactors that provide a culture environment relevant to renal epithelial cells, are available. The ones that allow a free choice of support material and application of flow at each membrane side is to our knowledge limited to the culture systems of Minucells and Minutissue GmbH.[12] However, none of these systems meet the exact requirements which are desired for the cell-studies on our UPy-based BM mimics. Those requirements comprise not only the application of a separate flow of media to each side of a BM mimic of choice. Also *in-situ* visualization by microscopy is desired to allow visual monitoring of the culture in time. Furthermore, sufficient volume of the compartment at each side of the membrane provides the freedom to perform different assays on the media (in case of static incubation of media inside the bioreactor). Naturally, the bioreactor should allow thorough cleaning and sterilization. In addition, the bioreactor needs to be leak-free both externally and internally (i.e. no connection between the media at each side of the membrane, other

than through the membrane. Lastly, the design should be optimized to prevent adverse effects of air bubbles that tend to form and accumulate in such flow culture systems.

According to these requirements we developed a custom-made bioreactor system that allows for both flow culture and assessment of single bioartificial renal tubule membranes *in vitro*. In this chapter, the design and initial validation tests of this newly developed bioreactor system are described. The performance of the bioreactor at basic functionalities is tested, such as sterility, leak-free assembly and prevention of air-bubble accumulation. The bioreactor is furthermore tested via a series of cell-based experiments. In these tests human kidney-2 cells (HK-2), immortalized renal proximal tubule epithelial cells, are applied. Bioartificial renal tubule test membranes were formed (as described in chapter 3) by seeding HK-2 cells on our established UPy-based supramolecular biomaterial BM mimics.[13,14] *In-situ* visualization of the culture by microscopy is tested. Furthermore long-term flow cultures are performed after which cell viability, morphology and phenotype are assessed.

We furthermore describe an initial endeavor for the development of a multi-membrane (3x3) bioreactor. This bioreactor is intended for the simultaneous screening of multiple membranes and/or culture conditions.

2. Results and discussion

Three organotypical culture and assessment systems for bioartificial renal membranes were designed and manufactured (Figure 2). In the following paragraphs we will discuss: I) The design of the static culture system based on commercial Transwell® Permeable Supports (hereafter referred to as Transwell). For this system we describe initial non-cell based tests. II) The design of a flow culture bioreactor system, suitable for a single membrane. Cell-based experiments that were done to validate the performance of this organotypical culture system are described. III) The design of a 3x3 flow culture bioreactor system. Of this bioreactor initial basal functionality tests are described.

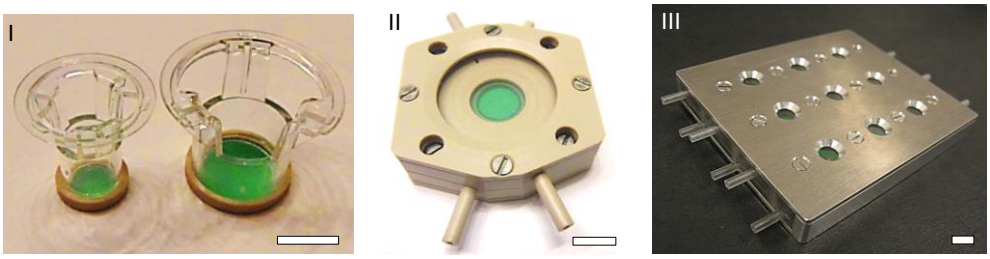

Figure 2. Organotypical renal epithelial cell-culture systems. Photographs of our three compartmentalized organotypical culture and assessment systems for bioartificial renal membranes. I) A static culture system based on commercial Transwells. II) A flow culture bioreactor systems suitable for a single membrane. III) A 3x3 flow culture bioreactor system suitable for nine membranes. The sale bars roughly indicate 1 cm.

I. The static culture system

Ia Identification of shortcomings of available systems

Commercial systems that allow compartmentalization of media are available as disposable inserts for standard tissue culture well plates. Transwell® Permeable Supports (Corning, BD biosciences, referred to as 'Transwell inserts' hereafter) and Millicell® Cell Culture Inserts (Millipore) divide a culture well in two compartments, separated by a porous synthetic membrane. These inserts have been applied in the assessment of *in vitro* renal epithelial cells function for over 25 years.[3,4] In these systems cells are cultured on the fixed porous membrane. These are available in a limited number of polymers, such as polycarbonate, polyester and PTFE. Unfortunately these culture systems do not allow the free application of other membranes. CellCrown™ (Scaffdex) is a disposable well plate insert which can be loaded with researcher´s own membrane. However, the clamping mechanism is comparable to a drum in which the drumhead is stretched over the shell and fixed. This mechanism requires both certain compliance and mechanical strength of the culture support and is hence not suitable for either very stiff flat supports or mechanically weak materials. We sought to develop a compartmentalized static culture system that would allow the application of any flat material, without putting constraints on mechanical properties or support thickness.

Ib Design of the static culture system based on Transwell inserts

The static culture system was designed based on commercial Transwell inserts. By supplementation with a custom-made cap any flat culture support could be attached to the Transwell insert instead of the commercially attached membrane (Figure 3 and 4). This idea was implemented for two of the available Transwell insert sizes; the ones that fit standard 24-wells plates, referred to as 'small', and those that fit 12-wells plates, referred to as 'big'. The caps were successfully machined from poly(ether ether ketone) (PEEK) via milling. The resultant rings with an L-shaped cross-section (Figure 3), form the clamping-bed in which the flat support is placed. The size of this bed equaled the inner and outer diameter of the shaft of the related Transwell insert. The upper rim of the cap, of 1 mm thick and 1.7 mm high, was made tight-fit to the outer diameter of the Transwell insert shaft. The bottom-end of this shaft has a small rim at the inner diameter to which the commercial membrane is attached. After easy removal of this prefixed membrane, this small rim helped the flat fixation of the new culture support in the cap. Due to this rim there was a small space left toward the outer diameter of the shaft of the Transwell insert (Figure 3), allowing some play at the edge of the clamped material. Without this rim clamping a non-rigid support was experienced to result in wrinkling towards the support's center and thus a non-flat culture surface. The rim was hence supposed to reduce stresses in the support which are caused by clamping between the cap and Transwell insert.

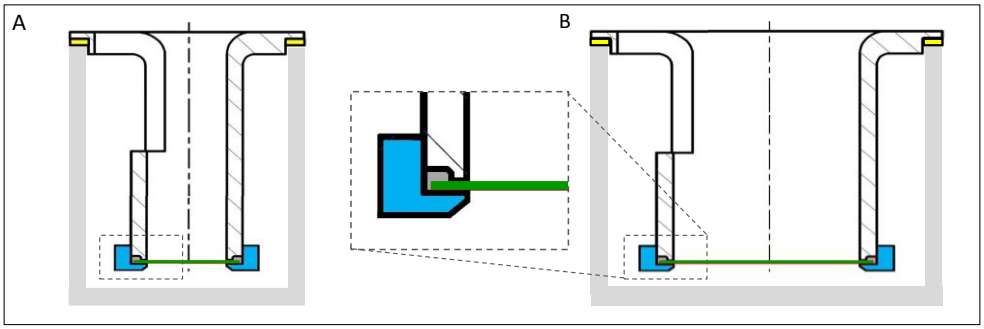

Figure 3. The design of the static culture system. Schematic representation of the longitudinal cross-section of the Transwell-based compartmentalized static culture system. Both sizes compatible with 24-wells plates (A, 0.33 cm^2 culture surface) and a 12-wells plates (B, 1.12 cm^2 culture surface) are depicted. The caps (bleu) clamp a culture support (green), e.g. a membrane to the stripped Transwell insert, while the spacer-ring (yellow) places the whole system a little higher in the well (grey) to provide extra space in the bottom compartment.

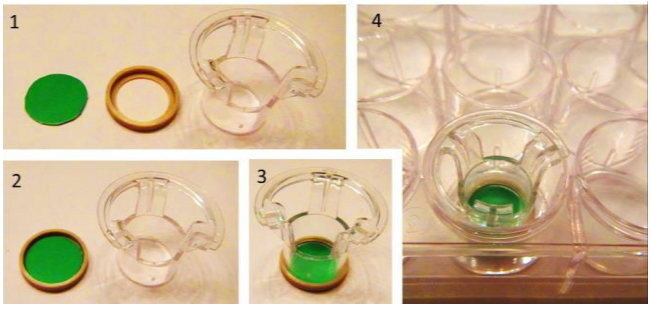

Figure 4. The static culture system and its assembly. The separate parts of the static culture system; a flat support, a cap and a Transwell insert (1) are sterilized separately. The culture support, here replaced for a green piece of paper, is placed in the cap (2). The Transwell insert is pressed on top of the cap (3) and the assembly is placed in a culture well plate (4). Here the system compatible with 12-wells plates is shown.

The system was for both sizes tested for leak-free assembly using thin non-permeable sheets of material. Materials with different stiffness and thickness, such as parafilm, polyethylene film and cover glasses, all resulted in leak-tight assembly. The caps preserved their tight fit to the Transwell inserts after repeated sterilization treatments by either ethanol or autoclaving for 20 minutes at 121 °C. The cap was, besides clamping a support, furthermore designed to minimize the chance of air getting trapped by the cap underneath the support when the system is placed in a well which is prefilled with media. The lower rim of the cap was minimized to a 0.5 mm thickness and the bottom inner side of this rim was tapered at an angle of 45° (Figure 3). Both adjustments were tested to contribute to the desired effect. To adjust for the space lost underneath the support by the presence of the cap, spacer-rings were manufactured with equal thickness as the cap's lower rim (Figure 3). These rings were successfully punched from 0.5 mm polypropylene

sheets using tailor-made metal stamps. Multiple spacer-rings could be stacked to further increase the space underneath the support in a well, for example to adjust for additional height-loss when thicker supports are applied. The height of supports that can be successfully clamped with the currently designed cap was however limited due to the limited height of the upper rim of the cap. When desired this height could be increased in future designs. The static culture system was successfully applied in cell-culture studies described in chapter 7.

II. The single membrane bioreactor

To create an organotypical flow culture environment for a single bioartificial renal membrane a bioreactor was designed and successfully manufactured. Photographs and a schematic cross-section of the bioreactor are shown in Figure 5.

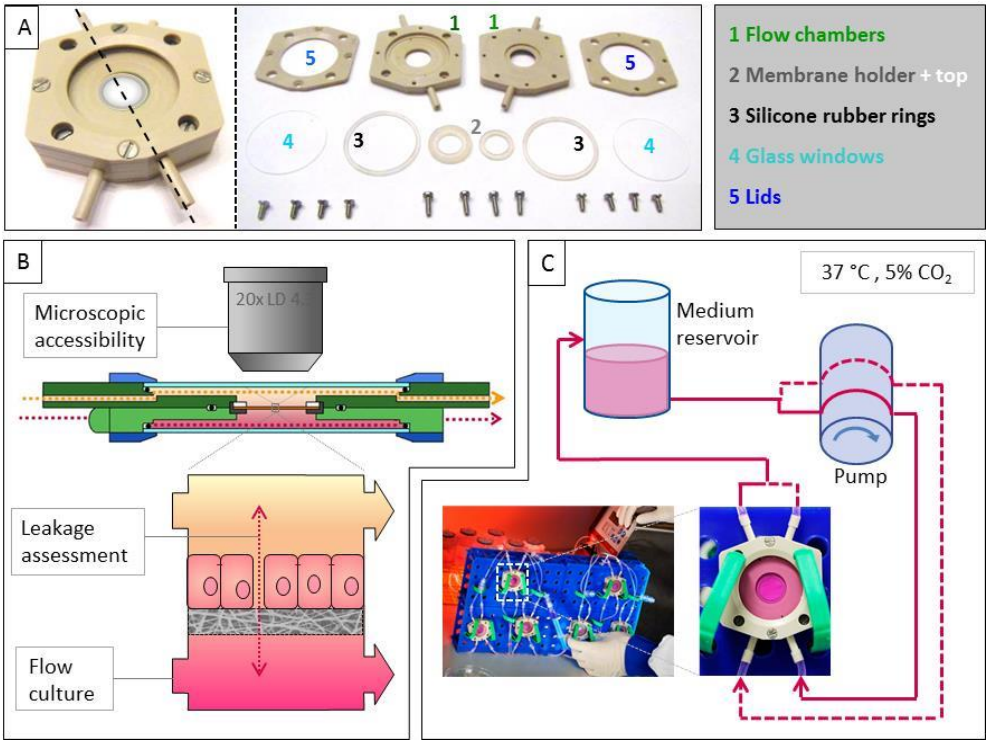

Figure 5. The custom-made bioreactor. A: Photographs of the bioreactor in assembled and disassembled state. B: A schematic, cross-section (indicated in A by the dotted line) of the bioreactor. The different parts are color-coded, in correspondence with the legend. Different applications that were tested and described in the present work are indicated. C: A schematic representation of a total continuous flow culture setup, depicted here for one bioreactor that is provided with the same media at both chambers. The bioreactor is placed vertically, connected to a reservoir with culture medium via silicone rubber tubing. A tubing pump can generate flow for multiple bioreactors at the same time. The complete assembly of multiple bioreactors, media reservoirs and the pump, as shown in the photograph, is placed inside an incubator at 37 °C and 5% CO_2.

Primary design criteria were the possibility to apply any flat culture support and to culture under continuous flow conditions. Furthermore, visual and microscopic accessibility to the membrane and sufficient volume of the culture compartments was desired. The culture support should thus be clamped between two compartments that each have a flow inle, outlet and a window. The materials used to construct the bioreactor should be re-useable, endurable, and sterilizable. The main parts of the bioreactor were constructed from PEEK supplemented with glass windows, silicone rubber sealing rings and stainless-steel screws. In disassembled state, the bioreactor could be thoroughly cleaned and sterilized by autoclaving. By attaching the assembled bioreactor to a continuous flow of water, leak-free assembly was demonstrated. This was amongst other measures established by integrating the function of culture support holder with the function of sealing ring. In earlier prototypes the function of support holder was fulfilled by a Minusheet carrier which is made of a relative stiff plastic that does not provide a leak-free sealing when placed inside the bioreactor. For this purpose, support holders were manufactured from silicone rubber rings. These holders allowed successful fixation of supports with varying thickness and stiffness inside the bioreactor, whilst taking over the function of an O-ring in the previous design. Improving the leak-free assembly of the earlier prototype furthermore resulted in replacement of round-profile O-rings between the glass windows and the PEEK main-parts by silicone rubber sealing rings with a square cross-sectional profile. The latter were noticed to be placed more easily in position and allowed faster leak-free assembly. The bioreactors could be assembled in a modular fashion. This allowed the use of the bioreactor during cell seeding. With the upper lid still open, cells could be seeded exclusively on top of the fixed membrane. After closing this lid, the bioreactor could be connected via the inlet and outlet of both chambers to a medium reservoir and pump by silicone rubber tubing. This allowing culture under constant flow of media at a later stadium of a cell culture experiment. Air-bubbles tend to form in such flow systems as a result of the gas permeable silicone tubing. The wide area inside the chambers at both sides of the membrane functioned as a buffer for any air that entered the flow-chamber via the lower inlet. The air could freely move upward to exit via the upper outlet (when placing the bioreactor in a vertical position), without interfering the membrane. The bioreactor was subjected to a series of experiments involving bioartificial kidney membranes which consist of renal epithelial cells cultured on UPy-based biomaterial BM mimics.

IIa In-situ monitoring of cultures inside the bioreactor using microscopy

The bioreactor was designed with wide cross-section windows that allow visual access to the membrane and the surrounding chamber. Chamber height (distance between the membrane and the glass window) was minimized to furthermore facilitate accessibility to the membrane by microscopy. The resulting distance that had to be bridged by the microscope objective was formed by a 3.2 mm thick aqueous medium layer and 0.7 mm

thick glass window. The possibility of *in-situ* monitoring of cultures inside the bioreactor by microscopy was validated. A test culture with HK-2 cells on non-bioactive UPy-PCL membranes (see chapter 3) was placed inside the bioreactor. Since these membranes are opaque, fluorescent staining of the cells was required to enable visualization. Here we applied a fluorescent live/dead staining. Prior to visualization, the bioreactor was filled with culture medium. The bioreactor with stained cells inside, was placed in an incubator in-between imaging sessions to maintain cell viability. Fluorescence microscopy imaging proved to be successful using low numerical aperture objectives (Figure 6a). Of the tested objectives a maximum of 20x magnification with minimum 4.3 mm working distance (based on standard 0.13 mm glass cover slip and air as barrier between the objective and the sample) still resulted in clear micrographs of the fluorescently stained cells. This magnification was appropriate for monitoring of general features of the culture such as cell density and viability. The cells on the opaque UPy-PCL membranes inside the bioreactors remained well visible by fluorescence microscopy up to at least two days after the live/dead staining was performed (Figure 6b).

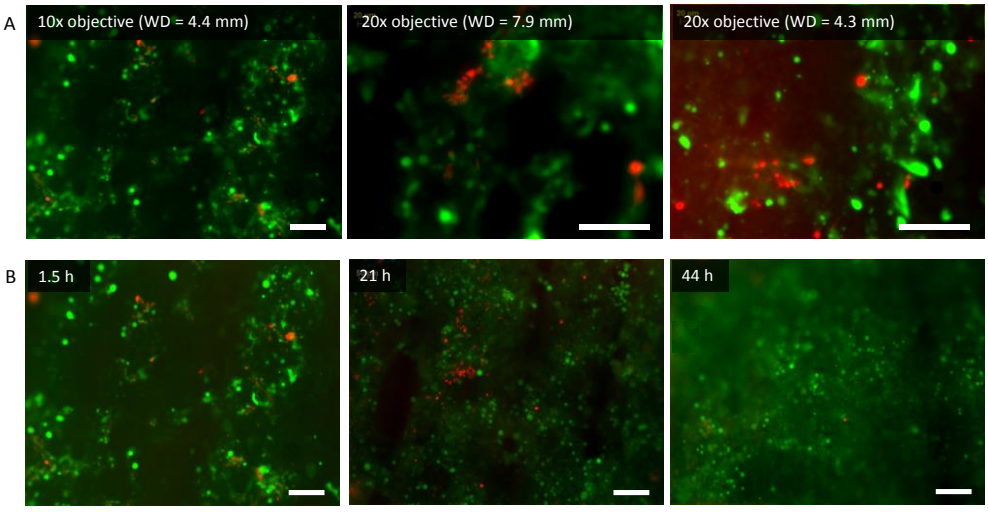

Figure 6. *In-situ* microscopy imaging. Fluorescence micrographs of live (green) / dead (red) stained HK-2 cells on an electrospun UPy-PCL membrane inside the bioreactor. A) Micrographs recorded with low aperture objectives with varying magnification and working distance (WD). B) Micrographs of the cells recorded with the 10x magnifying objective 1.5, 21 and 44 hours after live/dead staining. All scale bars represent 100 µm.

When using transparent culture supports inside the bioreactor *in-situ* visualization by simple bright field microscopy will in particular provide a beneficial tool for monitoring the culture. However, when applying opaque supports fluorescent labelling of cells is required to provide visual information by *in-situ* microscopy of cultures inside the bioreactor. Non-invasive fluorescent staining, such as the staining of live cells with calcein can provide visual access to the cells up to few cell passages. An alternative approach that could

provide stable fluorescence and enable monitoring of specific cell features during experiments inside the bioreactor is genetically encoded labelling through transfection.

IIb Membrane leakage: diffusion test inside the bioreactor

The bioreactor was designed with a separate chamber at each side of the culture support. Hence, a membrane placed inside the bioreactor, divides the system into two separate compartments that are connected through the porous membrane. Both chambers were provided with their own flow inlet and outlet. This allowed separate flow of media at both the apical and basal membrane side, mimicking organotypical compartmentalization. Beside the aim of stimulated polarization of renal epithelial cells,[8] the compartmentalization was intended to facilitate readout of cell functionality, similar as described for the static system. Via the application of media with a different composition in each compartment, a compositional gradient can be applied. Thereby, Diffusion or active transport of a particular substrate by the renal epithelial cells over the porous membrane can be studied. To demonstrate this possibility in the bioreactor, the difference in diffusion of fluorescein isothiocyanate labeled inulin (FITC-inulin) over bare membranes was compared to membranes seeded with HK-2 cells. Inulin has long been used as the standard to determine the kidneys glomerular filtration rate (GFR). This compound is not bound to plasma proteins, is freely filtered in glomeruli, and is neither reabsorbed nor secreted in the kidneys tubular track.[15] Leakage of this compound through an epithelial cell monolayer was found to be a measure for the integrity of the tight-junction barrier[16] and thus offers an opportunity to assess the formation of tight epithelial monolayers *in vitro*.

For this experiment bare UPy-PCL membranes were applied. These were pre-wet and placed in a bioreactor. Culture media containing inulin-FITC was flown into the bioreactor chamber at the presumably basal side of membrane and bare culture media at the apical side. After an incubation period of 4 hours, the media from each chamber was separately collected and fluorescence intensity was measured. The experiment was repeated with an incubation time of 24 hours. Then HK-2 cells were seeded on the apical side of the same membranes. After maturation of the cultures for 3 days, the inulin diffusion experiment was repeated. After both 4 and 24 hours of incubation at 37 °C, a significant decrease in FITC-inulin diffusion was observed over the electrospun UPy-PCL membranes when covered with epithelial cells (Figure 7). This indicated the formation of a (near) tight monolayer at the apical side of the membrane.

In a similar way active transport studies could in the future be performed. For example by applying a uremic toxin at the basal volume and monitoring of its transport towards the apical volume by the renal epithelial cells. To discriminate between active transport and diffusion, the test should be performed in absence and presence of a transport inhibitor.[17] When using fluorescently labeled compounds in the bioreactor, diffusion or transport might potentially also be monitored in real time using fluorescence microscopy through the glass windows of both chambers. Furthermore, here the test was

performed under static incubation conditions, whereas the bioreactor provides the opportunity to perform similar studies under flow conditions. This provides advantages over the performance of such assays in a static setup. Such flow better resembles the renal epithelial niche and will influence diffusion kinetics as under natural conditions. There is however one difficulty when studying pure diffusive or active transport processes by the cell while applying continuous flow. A zero pressure gradient over the membrane should be maintained, despite the applied flow at each membrane side, to rule out convection. On the other hand, application of convection over the membrane could be interesting for the study of a different renal structure than the tubular tract. In the glomerulus leaky cell-contacts allow passive filtration of blood to result in the formation of pre-urine. This process is based on convection.

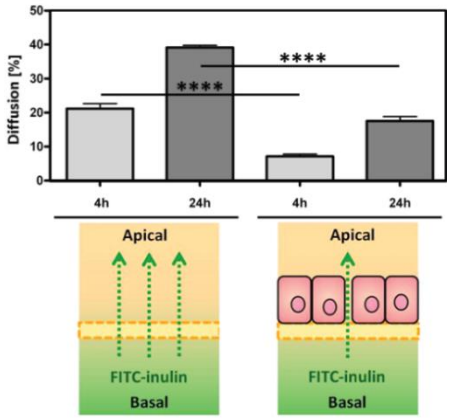

Figure 7. Epithelial cell layer integrity assessed by leakage. Transmembranal FITC-inulin diffusion is determined as a measure for leakage (50% diffusion = maximum). Results are given for both 4 and 24 hours diffusion time at 37 °C through UPy-PCL membranes without and with HK-2 cells. Significant differences of $p<0.0001$ between membranes in absence and presence of cells are indicated by ****.

IIc Long term cell culture under flow conditions inside the bioreactor

The possibility to provide a continuous flow of sterile media and culture a bioartificial kidney membrane under flow conditions was tested. The bioreactor was connected via a closed system of tubing to a media reservoir. A peristaltic tubing-pump provided a continuous circulating, lightly pulsating flow. The performance of the bioreactor culture setup was assessed by the monitoring the HK-2 cells on BM mimics during long-term flow culture. The HK-2 cells were seeded on bioactive UPy-PCL membranes in a sufficiently high cell density to allow instant confluent monolayer formation. The cells were pre-cultured for four days under static conditions to allow formation of a tight monolayer (see Chapter 3). Subsequently, the living bioartificial renal tubule membranes were subjected to a constant flow of culture media inside bioreactors for 21 days. During this culture period, the bioreactors were regularly checked for adequate functionality at several basic criteria, such as leakage, bubble accumulation and sterility. Absence of infection indicated that the separate parts were successfully sterilized and remained sterile during assembly of the system. Absence of media outside the system indicated proper leak-tight assembly. Air bubble formation in the system was expected and observed, but there were no signs of

adverse effects as a result of this. Due to the design and vertical positioning of the bioreactors, air bubbles that entered a flow chamber via the inlet could freely move upward and exit the chamber via the outlet without interfering with the membrane. Cell viability, morphology and phenotype of the HK-2 cells was assessed after three weeks of flow culture inside the bioreactor.

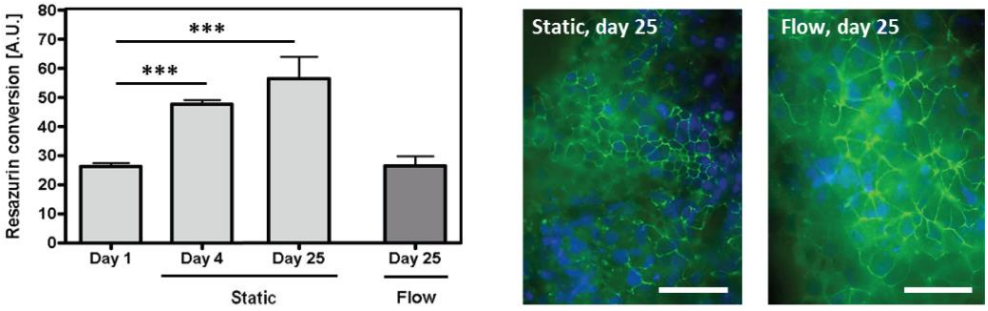

Figure 8. The effect of long-term flow culture on HK-2 cells. HK-2 cells were statically pre-cultured on bioactive UPy-PCL membranes for 4 days, followed by a culture period of 21 days, either under flow in the bioreactor or prolonged static culture in a well plate. Cell viability was monitored throughout the experiment via a non-invasive mitochondrial activity assay based on the conversion of resazurin (left). Error bars indicate standard error of mean. The increase in resazurin conversion during the static pre-culture (day 1 – day 4) and prolonged static culture (day 4 - day 25) was found to be significant (ANOVA, $p < 0.001$ are indicated by ***), whereas there was no difference measured between flow cultured membranes at day 25 and the initial culture at day 1 (two-tailed P value is 0.952, two-sample unpaired t-test). After the total culture period of 25 days, the cells were stained for ZO-1 (green, cell nuclei are in blue). The fluorescence micrographs show the presence of tight-junctions in both the static and flow culture. Scale bars represent 50 µM.

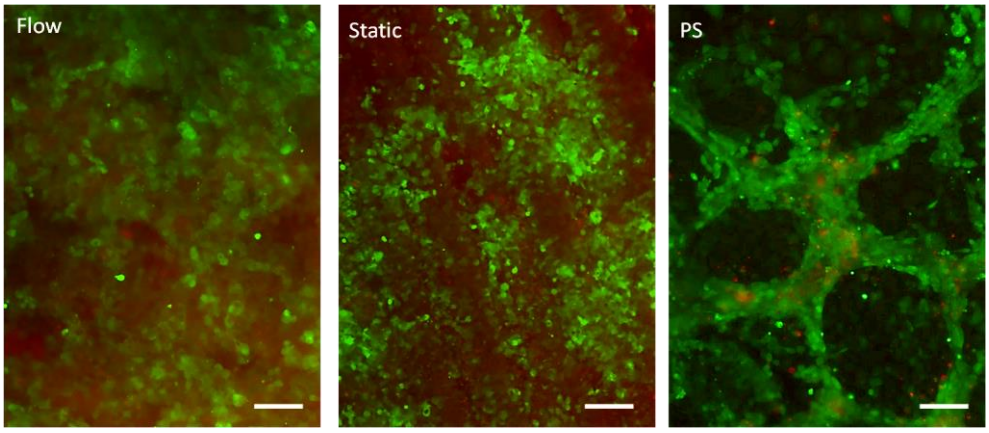

Figure 9. Cell viability after long term flow and static culture. Fluorescence micrographs of live/dead stained HK-2 cells cultured on bioactive UPy-PCL membranes for 21 days under flow conditions (preceded by 4 days static culture) (left), for 25 days under static conditions (middle), or on tissue culture treated polystyrene. Scale bars represent 100 µm. The red background staining for the membrane cultures is caused by remnant resorufin from the resazurin assay that was performed prior to the live/dead staining.

Cell viability was indicated by both a mitochondrial activity assay at set time points during the experiment (Figure 8) and a live/dead staining after the flow culture of 21 days inside the bioreactor ended (Figure 9). The mitochondrial activity assay provided quantitative information. This assay is based on the uptake and mitochondrial conversion of non-fluorescent resazurin to fluorescent resorufin by viable cells. The fluorescent analyte is secreted by the cells to the culture media. This allows non-invasive readout of the total mitochondrial activity of a culture via fluorescence intensity of the culture media at a given time. The assay could hence be repeated on the same cultures at different moments during the experiment to monitor the development of the cultures. Equal fluorescence signals were observed between the different bioartificial kidney membrane cultures one day after seeding of the HK-2 cells on the bioactive UPy-PCL membranes (Figure 8). This indicated equal seeding densities and cell adhesion throughout the cultures. After the static pre-culture period of four days, the assay was repeated prior to subjection of part of the cultures to flow. Although sufficient cells were seeded for instant confluent monolayer formation, overall elevated total mitochondrial activity was observed indicative for elevated cell numbers, compared to day one. After 21 days of flow culture in the bioreactor average total mitochondrial activity returned to the level as measured at day one after cell seeding, whereas the activity for static cultured membranes after 21 extra days remained elevated (Figure 8). Increased mitochondrial activity in time was also observed for static control cultures of HK-2 cells seeded in tissue culture treated polystyrene 24-well plates (data not shown; the data of the resazurin assay is not directly comparable between the membrane and the polystyrene cultures, since the culture area was not equal). After reaching a maximum at five days after seeding the activity remained at a constant level until termination of the experiment at day 25. At this plateau, observations by transmitted light microscopy revealed unstructured, multilayered growth. This indicates the tendency of these cells to lose their typical epithelial phenotype when cultured *in vitro*, if not lost already.

The unstructured, multilayered growth of HK-2 cells seeded on polystyrene 24-well plates was also observed in the live/dead staining (Figure 9). From this staining no quantitative data on live/dead cell ratio was not obtained as separate living cells were hard to distinguish due to the confluent cell density in all cultures. Furthermore, the identification of dead cells stained red by propidium iodide suffered from background staining of the UPy-PCL membrane. When comparing the flow cultured membranes with the static cultures qualitatively, no clear differences in cell viability were observed. A remarkable difference that could be distinguished from these micrographs was the size of the cells. The cells appeared bigger, at least in x-y plane, on the flow cultured membranes. The cells on the membranes, both cultured under static and continuous flow conditions, were more homogeneously distributed compared to static cultures on polystyrene (Figure 9). HK-2 cells cultured for long time on tissue culture treated polystyrene did not stop proliferating when 100% confluence was reached. This resulted in unstructured, multilayered growth. The absence of this severely unstructured growth on the membranes

indicated a positive effect of the bioactive UPy-PCL membrane on the HK-2 cells. This confirmed the findings described by Dankers *et al.*[14]

To examine in more detail the morphology of the epithelial cell-layer that formed on the bioactive UPy-PCL membranes during the long culture period, immunofluorescent staining of zona occludens-1 (ZO-1) protein was performed. The typical fine lined ZO-1 organization at cell-cell borders, which is indicative of a confluent, tight and polarized epithelial cell layer, was observed for cells cultured both under flow and static culture conditions (Figure 8). The cells that were exposed to a continuous flow of medium for 21 days appeared again larger than those on the statically cultured control membranes. This was also indicated by the live/dead staining.

The combined result of lower total mitochondrial activity and apparent bigger cells for flow cultures compared to static cultures is in agreement with previous experiments using primary renal epithelial proximal cells and a different flow culture bioreactor setup.[14] On similar membranes mitochondrial activity was also found to be lower for primary proximal tubule epithelial cells in a commercial flow culture setup, compared to static cultures. The observation that cells cultured under flow conditions appear bigger, at least in the x-y plane, indicate that fewer cells are present on the same surface area, while confluency is maintained. This is in agreement with the lower total mitochondrial activity observed for these flow cultures, since total mitochondrial activity is an indirect measure for the amount of cells. The implication of these results on the active transport capacity of static and flow cultured bioartificial kidney membranes remains unclear so far. However, HK-2 cells have shown the tendency of abundant overgrowth into undesired multilayers on tissue culture treated polystyrene. Furthermore, the seeded cell density on the membranes was high enough to form an instant monolayer. Hence, the presented results might indicate that flow culture either helps to establish a stable cell turnover of continuously proliferating HK-2 cells, or that HK-2 cells cultured under flow conditions are less prone to abundant and unrestricted proliferation as compared to static cultures. The loss of contact inhibition and subsequent overgrowing from a monolayer to multilayer morphology was mentioned by Saito *et al.* as the main cause for suboptimal functioning of a bioartificial renal tubule device.[18] This tendency to overgrow is attributed to the loss of epithelial-specific phenotype of the cells.

Gene expression was assessed to gain insight into loss or preservation of characteristic renal epithelial phenotype when comparing static and flow cultures of our bioartificial kidney membranes. The transcript levels of genes encoding for specialized membrane transporter proteins were measured by quantitative RT-PCR. HK-2 cells showed modulated expression levels when comparing the cultures under flow conditions and static culture conditions (Figure 10). Gene expression analysis implied a tendency towards enhanced expression of renal transporters SGLT2, Na^+/H^+ ATPase, Pept 2, and OAT 3, but not Pept1 and OCT1, under flow conditions compared to static controls. From these results we cannot distinguish between down-regulation under static or up-regulation

under flow conditions. Nevertheless, the results do indicate preserved or even regained renal epithelial phenotype under flow culture conditions in our bioreactor setup.

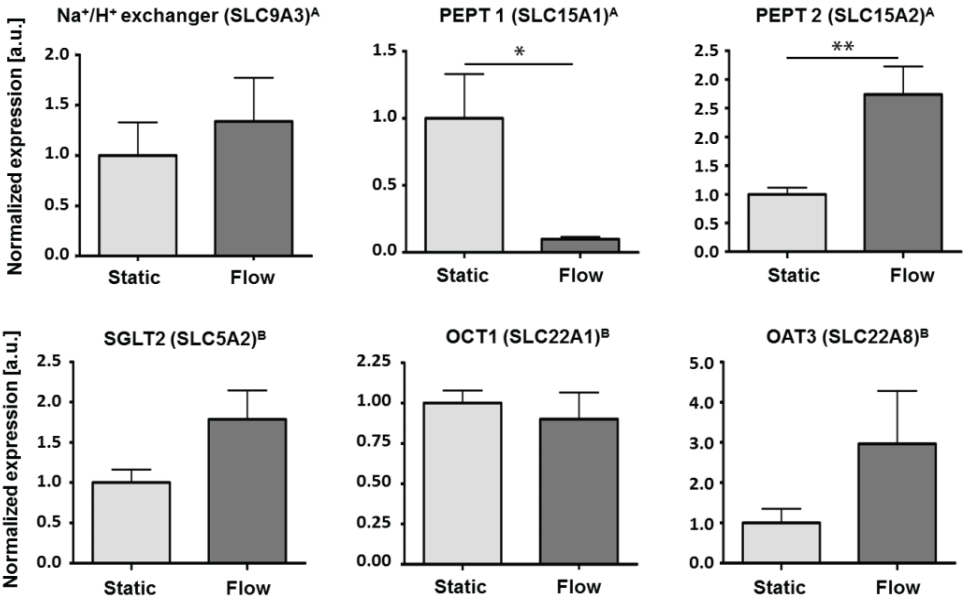

Figure 10. HK-2 phenotype after long-term culture. RT-PCR expression levels of specific apical[A] and basolateral[B] membrane transporter proteins at the mRNA level (corresponding genes are indicated in brackets), determined in HK-2 cells cultured on bioactive UPy-PCL membranes. The expression levels for flow cultures (4 days static pre-culture + 21 days flow culture inside the bioreactor) were compared to levels for static cultures at day 25 after cell seeding. Significant differences are indicated by *($p<0.05$) and **($p<0.01$).

Taken together the results of the long-term flow culture inside the bioreactor demonstrate the successful applicability of this culture device. Here, it was demonstrated with bioartificial renal tubule membranes consisting of UPy-PCL based BM mimics and HK-2 cells. However, in future experiments employing the bioreactor new BM mimics can be combined with other cell sources, in a continuing exploration towards bioartificial renal membranes with *in-vivo* like functionality.

III. The design of the 3x3 flow culture bioreactor

The single membrane bioreactor proved to be effective in the culture and assessment of bioartificial kidney membranes. However, for the screening of different BM mimics or multiple culture conditions, a multichannel system would be beneficial. For this purpose a second bioreactor flow culture system was developed. This 3x3 bioreactor was designed to culture samples in triplicate, with up to three conditions at once (Figure 11). Primary design criteria were similar as for the single membrane bioreactor; the possibility to apply

any flat culture support, culture under continuous flow of media, visual and microscopic accessibility to the membrane, leak-free assembly and re-useable and thus endurable materials that withstand sterilization procedures.

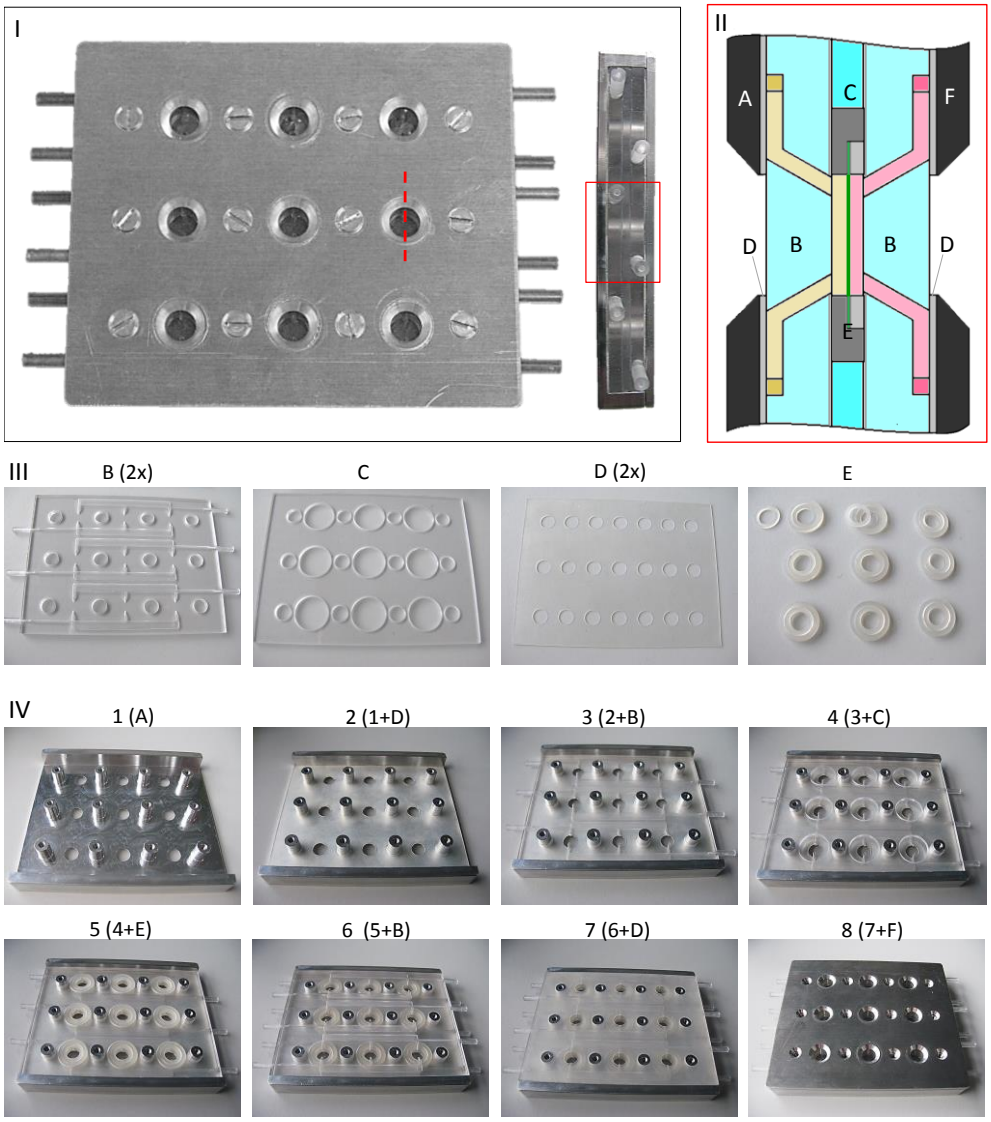

Figure 11. The 3x3 bioreactor. I) Photographs of the assembled bioreactor, front and side-view. II) A schematic partial cross-section (section indicated in red in I). The membrane is indicated in green, the apical and basal fluid in the chambers and flow channels are indicated in pink and yellow, respectively. III) Photographs of the inner body parts constructed from polycarbonate (B & C, indicated in light blue in II) and silicone rubber (D &E, indicated in gray II). IV) Photographs that demonstrate the stepwise assembly of the bioreactor.

Compared to the single membrane bioreactor, the flow chambers at each side of the nine membranes in the 3x3 bioreactor were down-sized to minimize the size of the device. The housing of the bioreactor, consisting of a base with 12 poles (A) and a lid (F), was constructed from aluminum. The poles provided both alignment of components during assembly and pressure-points for tight closing of the lid using 12 screws. The symmetric design of the inner body parts, all provided with 12 holes to fit the poles, facilitated easy assembly. The three main body parts were constructed from polycarbonate (PC) plates. This material is transparent and easily machinable by milling. These properties were required since the outer plates (B) were designed to enclose the flow channels and function as windows at the same time. In the disassembled state the flow channels in the PC plates are open channels at the plate's surface, which facilitates thorough cleaning. In the assembled state, the open channels are closed off by a 0.5 mm thick silicone rubber sheet (D). The middle PC plate (C) was provided with holes to fit the membrane holders (E). As for the single membrane bioreactor, compliant silicone rubber holders were applied that had the dual function of both clamping membrane supports with varying thickness and provide a watertight seal. Additional compliant sheets of 0.1 mm thick thermoplastic polyurethane (TPU) were placed between the PC plates (B and C) to improve the leak-free assembly of the bioreactor.

The assembled bioreactor allowed application of separate media to the apical and basal side of each triplicate of membranes through the six inlets and six outlets. Each triplicate of flow chambers was connected through channels in the PC plates in a parallel fashion (Figure 12a). This arrangement was chosen, rather than an arrangement in series, to provide each membrane with the exact same composition of media. Furthermore, the composition of the outflow media of each triplet would then represent the average, not the accumulative result. However, this arrangement caused problems in flow distribution as it relies on equal resistance through each separate flow pathway. The length and width of each pathway was equal by design. Once filled with media, flow of liquid was observed to be distributed over the three chambers (Figure 12a). However, when air bubbles entered the system, problems arose. In the wide chambers of the single membrane bioreactor air had the freedom to move upward (or liquid downward) and exit via the outflow channel trough application of flow of media. In the design of the 3x3 bioreactor, the volume of the chambers was limited. In combination with different contact materials, air tended to get stuck within the chambers. By the parallel connection of the chambers, air bubbles on one hand caused unequal distribution of flow, while on the other hand flow could not be used to remove air from all the flow chambers. Measures were explored to limit incorporation of air in the system and to eliminate incorporated air in the system. Assembly of the bioreactor while submerged in a bath of media allowed elimination of encapsulated air in the system at first instance. The application of hydrostatic pressure on the bioreactor system reduced the formation of air bubbles in the closed flow system that partially consisted of air-permeable silicone rubber tubing. In addition, it provided an opportunity to even slowly remove air from the bioreactor over time (Figure 12b).

However, from a practical point of view these measures were not considered to provide a workable solution. Hence, for future successful application of the 3x3 bioreactor, the design requires adjustment. A possible consideration could be to change the parallel placement of samples to an arrangement in series. This would ensure exposure of each sample to equal flow. Application of bubble traps[19] could prevent air from entering the bioreactor. Increase of hydrophilicity of the contact surfaces, either by choice of material or application of surface treatment, would reduce air to stick. Furthermore, enlarged chambers would prevent air from interfering with the membranes. However, the latter would result in an increased size of the bioreactor. This might require more fastening points to assure leak-tight assembly by even distribution of pressure upon closing the assembled system. In the current design *in-situ* visualization of fluorescently labelled cells seeded on opaque membranes was successful using low aperture objectives (Figure 12c). This was possible by the limited distance (<4 mm) between the membranes placed inside the bioreactor and the outside of the windows.

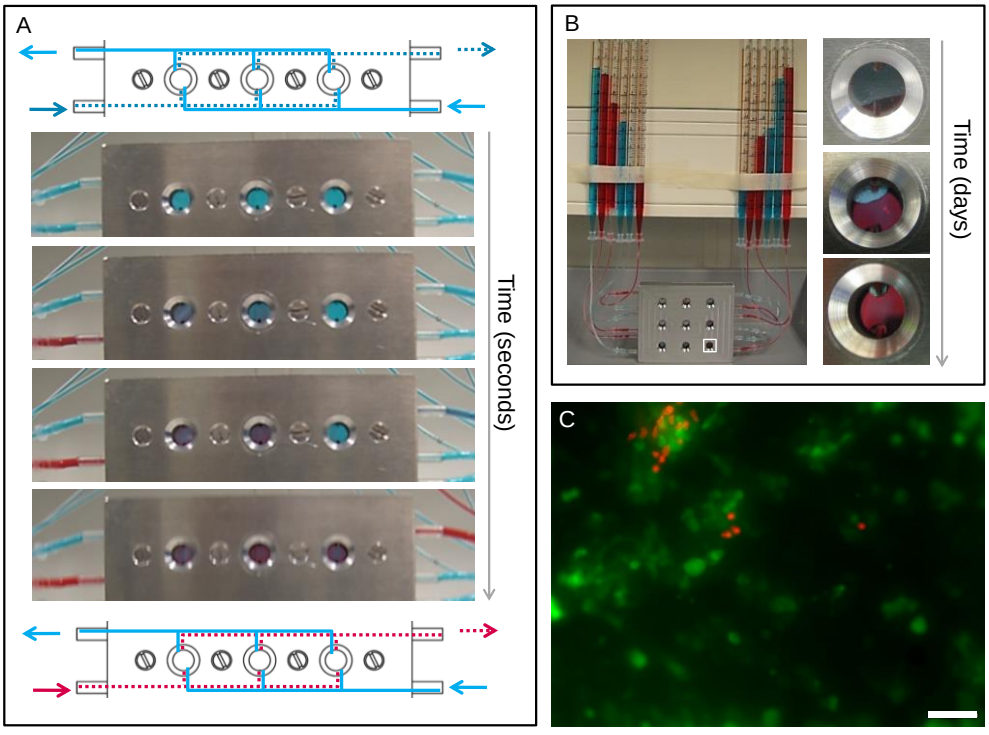

Figure 12. Initial tests with the 3x3 bioreactor. A) The distribution of flow through the tree parallel chambers is demonstrated by replacement of blue media by red media at one side of three transparent membranes. B) Encapsulated air inside a bioreactor chamber can be slowly removed in time by making use of the air permeable silicone rubber parts in the bioreactor body via the application of hydrostatic pressure. C) Fluorescence micrograph recorded of a live/dead stained culture of HK-2 cells on a UPy-PCL membrane inside the 3x3 bioreactor, employing a 20x magnifying LD objective with a 7.9 maximum working distance. The scale bar represents 50 µm.

3. Conclusions and discussion

To create a bioartificial renal membrane an *in-vitro* mimic of the renal tubular epithelial cells natural environment is needed. This environment is composed of the BM and surrounding organotypical factors. In this chapter three devices that provide an organotypical compartmentalized culture environment were described. Both a static system and two flow culture bioreactors were designed, manufactured and tested for basic requirements such as sterile and leak-tight assembly, and compatibility with a diversity of culture supports. Each culture system was determined to have its own advantages and limitations. The static system was based on Transwell inserts and as such allows alike experiments, but is however non-restricted to the commercially attached membranes. The culture system is user friendly and provides a facile system to test and screen different membranes in their function as BM mimic. However, this system is limited to static tests, i.e. flow of culture media is not possible. The system does provide visual access to the cultures. Accessibility by (fluorescence) microscopy is limited to low aperture objectives due to the distance of the culture insert from the bottom of the well plate. Furthermore, in the case of opaque membranes only the bottom side is accessible for visualization, whereas cells would normally be cultured on the upper side of the culture support. Both flow culture bioreactors allowed *in-situ* microscopy imaging of both sides of membrane cultures placed inside the bioreactor. The single membrane bioreactor was furthermore tested for a diversity of key features in cell-employed tests. Transmembrane diffusion studies inside the bioreactor enabled identification of tight epithelial cell barrier formation, although the latter could less elaborately be performed in the new compartmentalized static system. The true beneficial effect of the single membrane bioreactor system was demonstrated during a 21 day flow culture of HK-2 cells on bioactive UPy-PCL membranes. Results from these long term culture studies indicated a positive effect of the culture under flow conditions inside the bioreactor compared to static culture conditions in terms of preserved or regained characteristic renal epithelial phenotype. A disadvantage of the single membrane bioreactor is that it is relative labor intensive to assemble and hence might be impractical to use for experiments in which many membranes are cultured simultaneously. The 3x3 bioreactor was designed to overcome this impracticality. It was intended for more screening type of experiments under flow conditions, allowing the culture of samples in triplicate, up to three triplicates at the same time. However, the adjustments in the basic design compared to the single membrane bioreactor induced new shortcomings that made the intended use not yet possible. This bioreactor requires further development and optimization to facilitate the intended user friendly application. So far, both the static culture system and the flow bioreactor system can readily be applied. When employed in combination with new variants of BM mimics and relevant cells, these culture systems will help the formation, study and screening of living bioartificial kidney membranes for future *in-vitro* clinical applications.

4. Acknowledgements

We acknowledge Anthal Smits for useful discussions on the single membrane bioreactor design and Peter Neerincx for his help with the initial designs for the single membrane bioreactor prototype. We thank our partners from the BMM BioKid consortium for useful discussions and feedback on the static culture system and 3x3 membrane bioreactor. Patrick de Laat is gratefully acknowledged for his ideas and work concerning the technical aspects and the actual realization of all three culture systems. The research leading to these results has received funding from the European Research Council (FP7/2007-2013) ERC Grant Agreement 308045 and 246829. Part of this research forms part of the Project P3.01 BioKid of the research program of the BioMedical Materials institute, cofounded by the Dutch Ministry of Economic Affairs. The financial contribution of the Dutch Kidney Foundation is gratefully acknowledged.

5. Experimental section

Static culture system design and fabrication. Commercial Transwell systems formed the basis of the design. The prefixed membrane could simply be removed to yield only the transparent polystyrene holder. These are designed to fit standard well plates and have one or more openings on their side, depending on the well-size that it fits, that allows accessibility of the bottom media compartment using standard pipet tips. A cap was designed to clamp a membrane of choice at the place where the original membrane was attached. Such cap was constructed for two of the different available Transwell sizes. The one that fits 24-wells plates (referred to as small) and the one that fits 12-wells plates (referred to as big), which have a culture surface of 0.33 cm^2 and 1.12 cm^2, respectively. The cap was constructed from an endurable material to allow reusability. PEEK was chosen for its excellent thermal and chemical resistance which allows repeated sterilization by steam and chemicals, and furthermore for its stiff mechanical properties that allow exact manufacturing via milling and hence a tight fit with the Transwell insert. The shape of the cap was inspired by the Minusheet system (Minucells and Minutissue); a ring with an L-shaped cross-sectional profile. Since the space underneath the commercial Transwell in a standard well is already limited to ~ 2 mm, the lower rim of the cap was minimized to 0.5 mm thickness. Spacer-rings of 0.5 mm thick were made that could be placed under the rim of the Transwell with which it rests on the well plate. This allows adjustments of the space underneath the membrane and the cap as desired when the assembled insert is placed in a well of a culture plate. These rings were manufactured from polyprolylene. This material also enables sterilization by steam and ethanol, but is softer than PEEK. This allowed simple manufacturing via punching from 0.5 mm thick PP sheet material using custom-made metal punching-molds.

Single membrane bioreactor design and fabrication. The bioreactor was designed to hold a single biomaterial membrane, free of choice. The bioreactor was assembled from separate custom-made components (Figure 3). Two central body-parts (1) were constructed from polyether ether ketone (PEEK). PEEK was chosen for its excellent thermal and chemical resistance, to allow repeated sterilization by steam and chemicals. Together the central parts fit a silicone rubber membrane carrier (2), which was inspired by Minusheet carrier (Minucells & Minutissue, Bad Abbach, Germany). This membrane carrier fits a single round 13-11 mm Ø membrane and leaves 8.9 mm Ø of the membrane available for cell seeding. In addition it functions as a silicone rubber O-ring between

the two central parts to facilitate watertight, leak-free assembly. The membrane placed inside the bioreactor divides the system into two separate chambers. These chambers, each provided with an inlet and outlet (1 mm I.D.), allowed separate flow of media on both membrane sides. Each chamber was closed with a 0.7 mm thick, 27 mm Ø glass window (4), which provides visual access to the membrane and the chamber. Rings cut from 1.0 mm thick silicone rubber sheet (3), were placed between the central parts and the glass windows to provide leak tight assembly. PEEK lids (5) were applied to hold the glass windows in place. Twelve stainless steel screws were used for assembly of the bioreactor; four to fix the two central parts, and four to fasten each lid. A closed flow system was formed by connecting the bioreactor inlets and outlets via silicone rubber tubing (2 mm I.D.; Rubber BV, The Netherlands), polypropylene luer and barbed tubing connectors (Qosina, USA) and a polycarbonate medium reservoir. The medium reservoir was equipped with three openings that fit male luer slip connectors, one in the lid to fit a standard 0.2 µm pore syringe filter for sterile ventilation and two to connect medium inflow and outflow tubing. Medium flow was driven by a tubing pump, resistant against the humid environment (IP65 rated, Ismatec MCP process, equipped with MS/CA 4-12 pumphead and extension blocks, and 1.02 mm ID Pharmed Ismaprene tubing with 3 welded stoppers, Inacom) inside a cell incubator. Up to twelve separate bioreactor flow systems could be attached to this pump simultaneously. All unassembled bioreactor and flow circulation parts were sterilized by steam autoclaving for 20 minutes at 121 °C prior to use in any cell experiment.

Preparation of living bioartificial renal membrane models. The preparation of non-bioactive and bioactive microfibrous meshes by electrospinning of bare UPy-PCL (batch 2-I) and UPy-PCL with UPy-ECM-peptides, respectively, as well as the culture of renal epithelial HK-2 cells on these membranes, was described in chapter 3.

Monitoring cells inside the bioreactor: In situ microscopy. *In situ* cell viability inside the bioreactor was visualized via a live/dead assay (L3224, Invitrogen). Cells, statically cultured on a non-bioactive UPy-PCL membrane, were incubated for 15 minutes at 37 °C in complete medium supplemented with 10 µM calcein AM and 10 µM ethidium homodimer and washed with PBS. The membrane was placed inside the bioreactor which was then filled with complete culture medium and incubated further under static conditions at 37 °C and 5% CO_2. Imaging of the cells inside the bioreactor was performed using an inverted fluorescence microscope using a Zeiss Axio observer D1, AxioCam Mrm camera and Zeiss Axiovision software (Carl Zeiss) at different times after staining. Objectives that have working distances (WD, based on standard 0.13 mm thick glass cover slip and air as barrier between the objective and specimen) larger than 3.9 mm were tested for imaging (A-Plan 10x (NA 0.25, WD4.4), LD A-Plan 20x (NA 0.30, WD 4.3), LD plan neofluar 20x korr (NA 0.40, WD 7.9), all from Zeiss).

Transmembrane fluorescent-inulin diffusion: Cell monolayer integrity. Porous electrospun bare UPy-PCL membranes were first sterilized and thoroughly pre-wetted by submersion in PBS for at least 3 days. The membranes (n = 13) were first placed inside the bioreactors and tested without cells, prior to testing the same membranes with cells. The chambers were filled with separate media. The chamber on the side of the membrane to which cells will be seeded, referred to as 'apical side', was first filled with complete culture medium. The chamber on the side of the membrane to which no cells will be seeded, referred to as 'basal side', was filled with complete culture medium supplemented with 5 mM inulin-FITC (FI-100mg, M_w 4.5 kDa, TdB Consultancy AB, Uppsala, Sweden). The bioreactors were placed in a humidified atmosphere for 4 h at 37 °C and 5% CO_2. Then, media from both chambers was collected separately, vortexed and three samples of 200

uL were transferred to a black 96-well plate (Thermo Scientific) and fluorescence was measured (λ_{ex} = 495, λ_{em} = 515) with a fluorescence microplate reader (Safire 2, Tecan). The membranes were washed with PBS and the procedure was repeated at three later times points on the same membranes; first with an incubation time of 24 h, then with cells seeded on the membranes and subsequent incubation times of 4 h and 24 h. For the experiment with cells, 3×10^5 HK-2 cells were seeded per membrane, at the apical membrane sides. The cells were allowed to form a confluent monolayer during a pre-culture period under static conditions for 2 days before the diffusion test was repeated. The 5 mM FITC-inulin in medium that was applied to the basal membrane side was chosen such that it was within the linear regime of concentration dependent fluorescence intensity. The percentage of diffused FITC-inulin was calculated from the measured fluorescence signals (fluorescence apical × 100 % / (fluorescence basal + fluorescence apical)) for each membrane at each time point; 4 and 24 h, and for each condition; without and with cells. From those percentages, the averages and standard errors were determined. The diffusion in presence and absence of cells was compared for both incubation times separately via an unpaired two-sample t-test. The error bars represent standard error of mean. A $p < 0.05$ was considered statistically significant.

Long term cell-culture under flow conditions inside the bioreactor. Bioactive UPy-PCL membranes with HK-2 cells were pre-cultured under static conditions for 4 days before subjection to a continuous flow inside separate bioreactors for 21 days. Each bioreactor was attached to a separate container with 9 mL complete medium. Medium was circulated through the closed system by the peristaltic tubing pump and flowed over the membrane through both the apical and basal chamber at a 6 mL/h flow rate. The bioreactors were arranged vertically, with the outflow of both chambers pointing upward to allow facile removal of any air bubbles that might enter the chambers. The setup was placed as a whole in a cell incubator (Thermo Scientific), which maintained 37 °C, 5% CO_2 and a humidified atmosphere. As a control, membranes were further cultured in 24-well plates under static culture conditions with complete medium refreshment every 2-3 days.

Cell viability: Mitochondrial activity assay. To assess cell viability a mitochondrial activity assay was used based on the mitochondrial conversion of non-fluorescent resazurin to fluorescent resorufin. Resazurin salt (Sigma Aldrich) was dissolved in complete medium in a 4.4×10^{-5} M concentration. The HK-2 cells cultured on membranes were incubated at 37 °C and 5% CO_2 in a humidified atmosphere with 800 µL of the resazurin solution for 2 h. Per membrane three samples of 200 µL resazurin solution were then transferred to a black 96-well plate (Thermo Scientific) and fluorescence was measured (λ_{ex} = 550, λ_{em} = 584) with a Fluoroscan plate reader (Thermo Fisher Scientific). All data were expressed as mean ± standard error of mean. The average total mitochondrial activity for static cultures in time (n=5 for day 1 and 4 and n=3 for day 25) was evaluated using ANOVA, comparison of the flow samples (n=2) with static samples at day 1 and day 25 was performed via separate two-sample t-tests. A $p < 0.05$ was considered statistically significant.

Cell morphology: Fluorescent immunostaining of tight junctions. The formation of tight junctions between cells was evaluated via the immunofluorescent zona occludens 1 (ZO-1) protein, combined with a nuclei counter stain. After the culture period, the cells were washed twice with PBS and fixed with 2% formaldehyde (Fluka)/PBS for 10 minutes and again washed twice with PBS. The fixed cells were stored in PBS at 4 °C until further use. To block non-specific binding sites, the samples were incubated with 5% (w/v) BSA in PBS for 30 min at room temperature. The cells were incubated with mouse anti ZO-1 antibody (1:200; 610966, DB Biosciences Pharmingen) for 1 h and sequentially with rabbit anti-mouse-fluorescein isothiocyanate (RAM-FITC; 1:100; Dako) and 4,6-diamidino-2-phenylindole (DAPI; 1:1000; Sigma Aldrich) in PBS with 5 w/v% BSA for 30 min at room

temperature. The stained membranes were embedded in CitiFluor (Agar Scientific) between glass microscopy slide and cover slip and visualized with fluorescence microscopy using a Zeiss Axio observer D1, AxioCam Mrm camera and Zeiss Axiovision software (Carl Zeiss).

Gene expression: Real-time PCR. The gene expression levels of specific membrane transporters were determined in HK-2 cells cultured on bioactive UPy-PCL membranes. Flow cultures (4 days static pre-culture + 21 days flow culture) were compared to static cultures at day 25 after cell seeding on the bioactive UPy-PCL membranes. Total RNA was isolated using High Pure RNA isolation kit (Roche) according to the manufacturer's instructions and cDNA was synthesized. Transcript levels for SGLT2, Na^+/H^+ ATPase, Pept 1, Pept 2, OCT 1 and OAT 3 (primers were designed using free software from PubMed/NCBI, sequences are listed in Supporting information Table SI-1) were detected with the MyIQ Single Color Real-Time PCR detection System (Bio-Rad, Hercules, CA, USA) using SYBR Green. All expression levels after 40 amplification cycles were presented relative to glyceraldehydes-3-phosphate dehydrogenase (GAPDH) and normalized to static culture conditions. All data were expressed as mean ± standard error of mean. A $p < 0.05$ was considered statistically significant.

Table 1: Real-Time PCR primers for human membrane proteins

Gene	Protein	Sense	Anti-sense	T_{anneal} (C°)	Product (bp)
SLC5A2	SGLT2	5'-gtggtgttcatcgtggtagt-3'	5'-cacaatggcgaagtagaggt-3'	57	309
SLC9A3	Na^+/H^+ ATPase	5'-gaggtccatgtcaacgaggt-3'	5'-gatgatacgcacatgcttgg-3'	60	252
SLC15A1	PEPT1	5'-ccttcagcagcctctgttat-3'	5'-cctgcattgatggacaggta-3'	57	319
SLC15A2	PEPT2	5'-agagctgatctcctccacct-3'	5'-aaaattagggccatcagtcc-3'	57	267
SLC22A1	OCT1	5'-gggaacctctacctggattt-3'	5'-attcaccaggcagatcattt-3'	57	243
SLC22A8	OAT3	5'-gggcgtaagtaacctgtgga-3'	5'-tgcctggctaggatcagtct-3'	57	344

3x3 membrane bioreactor design and fabrication. The bioreactor was designed to hold nine biomaterial membranes, three triplicates free of choice. The bioreactor was assembled from separate custom-made components (Figure 11). Three central body-parts (B&C) were constructed from polycarbonate (PC). PC was chosen for its transparency, machinability by milling and possibility to sterilize by autoclaving. Each of the outer PC plates were constructed with 6 separate open flow channels and equal numbers of inlets and outlets. Together the central parts fit nine silicone rubber membrane carriers (E), as described for the single membrane bioreactor, but with adapted dimensions. These membrane carriers each fit a single round 9-11 mm Ø membrane and leaves 7.0 mm Ø of the membrane available for cell seeding. The membranes placed inside the bioreactor divide each of the nine chambers into two separate chambers. Three chambers are connected in parallel to an inlet and outlet (1 mm I.D.) via flow channels. Sheets cut from 0.5 mm thick silicone rubber (D), were placed between the outer PC plates and aluminum housing. These close of the open side of the flow channels in the outer PC plates. The aluminium base-plate was constructed with 12 equidistant poles. These, together with corresponding holes through all bioreactor body parts, provide alignment during assembly. Twelve stainless steel screws secure the aluminum top plate and press all layers in between tightly together. A closed flow system could be formed by connecting the bioreactor inlets and outlets via silicone rubber tubing (2 mm I.D.; Rubber BV, The Netherlands), polypropylene luer and barbed tubing connectors (Qosina, USA) and a polycarbonate medium reservoir, as described for the single membrane bioreactor. All unassembled bioreactor and flow circulation parts could be sterilized by steam autoclaving for 20 minutes at 121 °C.

6. References

(1) Fujita, Y.; Kakuta, T.; Asano, M.; Itoh, J.; Sakabe, K.; Tokimasa, T.; Saito, A. Evaluation of Na+ Active Transport and Morphological Changes for Bioartificial Renal Tubule Cell Device Using Madin-Darby Canine Kidney Cells. *Tissue Eng*. **2002**, *8*, 13–24.

(2) Ozgen, N.; Terashima, M.; Aung, T.; Sato, Y.; Isoe, C.; Kakuta, T.; Saito, A. Evaluation of Long-Term Transport Ability of a Bioartificial Renal Tubule Device Using LLC-PK1 Cells. *Nephrol. Dial. Transplant.* **2004**, *19*, 2198–2207.

(3) Urban, J.; Parczyk, K.; Leutz, A.; Kayne, M.; Kondor-Koch, C. Constitutive Apical Secretion of an 80-kD Sulfated Glycoprotein Complex in the Polarized Epithelial Madin-Darby Canine Kidney Cell Line. *J. Cell Biol.* **1987**, *105*, 2735–2743.

(4) Matlin, K. S. Ammonium Chloride Slows Transport of the Influenza Virus Hemagglutinin but Does Not Cause Mis-Sorting in a Polarized Epithelial Cell Line. *J. Biol. Chem.* **1986**, *261*, 15172–15178.

(5) Miller, C.; George, S.; Niklason, L. Developing a Tissue-Engineered Model of the Human Bronchiole. *J. Tissue Eng. Regen. Med.* **2010**, *4*, 619–627.

(6) Kim, S. S.; Penkala, R.; Abrahimi, P. A Perfusion Bioreactor for Intestinal Tissue Engineering. *J. Surg. Res*. **2007**, *142*, 327–331.

(7) Baudoin, R.; Griscom, L.; Monge, M.; Legallais, C.; Leclerc, E. Development of a Renal Microchip for in Vitro Distal Tubule Models. *Biotechnol. Prog.* **2007**, *23*, 1245–1253.

(8) Jang, K.-J.; Suh, K.-Y. A Multi-Layer Microfluidic Device for Efficient Culture and Analysis of Renal Tubular Cells. *Lab. Chip* **2010**, *10*, 36–42.

(9) Sciancalepore, A. G.; Sallustio, F.; Girardo, S.; Gioia Passione, L.; Camposeo, A.; Mele, E.; Di Lorenzo, M.; Costantino, V.; Schena, F. P.; Pisignano, D. A Bioartificial Renal Tubule Device Embedding Human Renal Stem/Progenitor Cells. *PLoS ONE* **2014**, *9*, e87496.

(10) Sun, T.; Donoghue, P. S.; Higginson, J. R.; Gadegaard, N.; Barnett, S. C.; Riehle, M. O. A Miniaturized Bioreactor System for the Evaluation of Cell Interaction with Designed Substrates in Perfusion Culture. *J. Tissue Eng. Regen. Med.* **2012**, *6*, s4–s14.

(11) Ferrell, N.; Desai, R. R.; Fleischman, A. J.; Roy, S.; Humes, H. D.; Fissell, W. H. A Microfluidic Bioreactor with Integrated Transepithelial Electrical Resistance (TEER) Measurement Electrodes for Evaluation of Renal Epithelial Cells. *Biotechnol. Bioeng.* **2010**, *107*, 707–716.

(12) Minuth, W. W.; Denk, L.; Roessger, A. Gradient Perfusion Culture-Simulating a Tissue-Specific Environment for Epithelia in Biomedicine. *J. Epithel. Biol. Pharmacol.* **2009**, *2*, 1–13.

(13) Dankers, P. Y. W.; Boomker, J. M.; Huizinga-van der Vlag, A.; Smedts, F. M. M.; Harmsen, M. C.; van Luyn, M. J. A. The Use of Fibrous, Supramolecular Membranes and Human Tubular Cells for Renal Epithelial Tissue Engineering: Towards a Suitable Membrane for a Bioartificial Kidney. *Macromol. Biosci.* **2010**, *10*, 1345–1354.

(14) Dankers, P. Y. W.; Boomker, J. M.; Huizinga-van der Vlag, A.; Wisse, E.; Appel, W. P. J.; Smedts, F. M. M.; Harmsen, M. C.; Bosman, A. W.; Meijer, E. W.; van Luyn, M. J. A. Bioengineering of Living Renal Membranes Consisting of Hierarchical, Bioactive Supramolecular Meshes and Human Tubular Cells. *Biomaterials* **2011**, *32*, 723–733.

(15) Smith, H. W. *The Kidney: Structure and Function in Health and Disease*; Oxford University Press, 1951.

(16) Madara, J. L.; Dharmsathaphorn, K. Occluding Junction Structure-Function Relationships in a Cultured Epithelial Monolayer. *J. Cell Biol.* **1985**, *101*, 2124–2133.

(17) Schophuizen, C. M. S.; Wilmer, M. J.; Jansen, J.; Gustavsson, L.; Hilgendorf, C.; Hoenderop, J. G. J.; van den Heuvel, L. P.; Masereeuw, R. Cationic Uremic Toxins Affect Human Renal Proximal Tubule Cell Functioning through Interaction with the Organic Cation Transporter. *Pflüg. Arch. Eur. J. Physiol.* **2013**, *465*, 1701–1714.

(18) Saito, A.; Sawada, K.; Fujimura, S. Present Status and Future Perspectives on the Development of Bioartificial Kidneys for the Treatment of Acute and Chronic Renal Failure Patients. *Hemodial. Int*. **2011**, *15*, 183–192.

(19) Minuth, W. W.; Strehl, R.; Schumacher, K. Tissue Factory: Conceptual Design of a Modular System for the in Vitro Generation of Functional Tissues. *Tissue Eng*. **2004**, *10*, 285–294.

Summary

Supramolecular biomaterials based on ureido-pyrimidinones

- Development of a synthetic basement membrane for a bioartificial kidney -

Kidney patients who depend on hemodialysis and hemofiltration face decreased quality of life and high morbidity and mortality rates. These artificial renal replacement therapies are incapable of complete replacement of kidney function. They could potentially benefit from supplementation with the active functions of human renal proximal tubular epithelial cells (HPTC). Initial attempts have been undertaken to implement such an approach in the clinic in the form of tissue engineered living bioartificial kidneys. These consist of conventional hemofilters with HPTC seeded inside the hollow fibers of these filters. To improve adhesion of the HPTC to the non-adhesive filter material a cell adhesive coating is applied. The desired clinical benefits were however not achieved as a consequence of insufficient preservation of natural cell function. To improve this, a biomaterial that allows better mimicry of the natural substrate of these cells, the basement membrane (BM), was desired.

The objective of the research described in this thesis is to explore the potential of a relative new class of biomaterials in the formation of a synthetic BM mimic. The applied biomaterial system is based on molecular building blocks functionalized with ureido-pyrimidinone (UPy); a supramolecular, self-complementary moiety, that functions as 'molecular Velcro'. Chapter 2 introduced the building blocks of the UPy-biomaterial toolbox applied in this research. This toolbox comprised UPy-polymers with varying physical properties, bioactive UPy-peptides and UPy-model compounds. In chapter 3 the processing and structure of established UPy-biomaterials based on telechelically functionalized polycaprolactone (UPy-PCL) was discussed. Both pristine UPy-PCL and a mixture with 4 mol% UPy-peptides was augmented by electrospinning from a single solvent. Characterization of resultant membranes by atomic force microscopy (AFM) and wide angle x-ray scattering (WAXS) confirmed the presence self-assembled nanofibrous structures in the electrospun microfibers. This confirmed the postulated ability of UPy end-functionalized polymers to form hierarchical fibrous structures, when processed by electrospinning. This opens possibilities to form new biomaterial scaffolds with better BM mimicking structures. Human kidney-2 cells (HK-2), the HPTC applied in this research, were able to form a tight confluent cell layer within three days on such electrospun UPy-PCL BM mimicking membranes.

Before application in cell-studies, ultraviolet (UV) irradiation is applied to sterilize the UPy-biomaterials. The observation of UV-induced fluorescence prompted us to investigate the effect of UV-irradiation on dynamic UPy-biomaterials in more detail, as described in chapter 4. Besides the anticipated effect of some UV-induced crosslinking, the fluorescence was evidenced to be related to phototautomerization of the UPy-moiety.

This was hypothesized to occur via an excited state intermolecular double proton transfer in the UPy-dimer, leading to transition of UPy-keto to a UPy-enol. Despite these UV-induced changes, UPy-biomaterials were successfully sterilized and applied in cell-culture studies.

Chapter 5 and 6 elaborate on the possibility to mix-and-match UPy-biomaterial building blocks. In chapter 5 this was employed to form a small library of UPy-biomaterials based on UPy-PCL. This supramolecular polymer was used pure, or mixed with telechelically UPy-modified poly(ethylene glycol) (UPy-PEG) or UPy-functionalized integrin-binding peptide (UPy-RGD). A variant with the scrambled peptide was included in the library as negative control. The ability of 3T3 fibroblast cells to adhere to the different biomaterials in absence of serum was assessed using two distinct techniques. Fluorescence microscopy was applied to monitor the number of adhered cells and morphology of these cells on electrospun meshes of the UPy-biomaterials. The optical tweezers technique was used to determine the adhesion probability of single electrosprayed microbeads to the cells and the force required to disrupt the bead/cell interaction. Although most data showed the expected trends of reduced cell adhesion in presence of UPy-PEG and increased cell-adhesion in presence of UPy-RGD, no clear black-and-white results were acquired. A high-throughput screening, or materiomics approach, is expected to provide opportunities in the future for improved UPy-biomaterial read-outs and identification of desired properties.

The possibility to use UPy-based biomaterial building blocks in a combinatorial approach to make BM mimicking scaffolds with tailorable properties was explored in chapter 6. A membrane applied for the bioartificial kidney would be placed in contact with blood at one side, and would require renal epithelial cells to adhere at the other side. UPy-PCL, UPy-PEG and UPy-RGD were applied in a ‘mix-and-match’ approach. Via layered electrospinning two bilayered microfibrous scaffolds were successfully formed: A) A scaffold with one hydrophobic cell-adhesive and one hydrophilic non-cell-adhesive side and B) a completely hydrophilic scaffold with one cell adhesive and one non-cell-adhesive side. This demonstrated that telechelic UPy-polymers could be mixed to benefit from the specific properties of each. Furthermore, the effect of bioactivation by introduction of UPy-RGD peptide was unequivocally shown in anti-cell-adhesive UPy-PCL/UPy-PEG copolymer assemblies.

In chapter 7 a different approach was developed to form a completely hydrophilic scaffold with cell adhesive properties. Chain-extended UPy-PEG (CE-UPy-PEG), a hydrogelator with multiple UPy-moieties along its macromolecular chain, was applied. This molecular design provides superior mechanical properties. It allowed for the formation of microfibrous hydrogel scaffolds by electrospinning. These scaffolds maintained morphology under physiological conditions without the need of chemical crosslinking. Addition of gelatin induced a cell-adhesive character in this non-cell-adhesive hydrogel. This facilitated renal tubular epithelial cell adhesion and formation of the desired tight confluent cell layer. These hydrogel meshes displayed elastic properties with

moduli of ~0.63 MPa, which is a relevant stiffness for soft tissue engineering. These properties prompted the exploration of applicability of these scaffolds in other tissue engineering applications, such as in a cardiac patch. An open-pore scaffold was successfully applied as 3D interstitial ECM mimicking scaffold. The cardiomyocyte progenitor cells seeded inside the scaffold maintained high viability up to at least one week and displayed deposition of ECM already after one day. The extraordinary combination of highly interesting material properties of CE-UPy-PEG and promising performances as 2D BM and 3D interstitial ECM mimic exemplify what molecular design can offer to expand the UPy-biomaterial portfolio.

To perform relevant cell-screenings on new BM mimicking scaffolds, organotypical culture environments were developed as described in chapter 8. A static culture setup allowed compartmentalization of culture media at each side of the scaffold. This enabled read-out of leakage and transport functions over the tissue engineered bioartificial kidney membranes. In addition, two bioreactor systems were designed to allow the same compartmentalization. Furthermore, these bioreactors enabled the culture of either one or multiple membranes under continuous flow of media, while providing the opportunity for *in-situ* visualization of the culture. The multi-membrane bioreactor required further optimization, but the single membrane bioreactor was successfully applied for the flow culture of bioartificial renal tubular membranes for 21 days.

In conclusion, the research described in this thesis provides insight into the possibilities and challenges within the UPy-biomaterial system. Progress has been made towards the identification of interesting biomaterial candidates for the formation of a BM mimic relevant for application in bioartificial renal membranes.

Epilogue

In endeavors to create bioartificial kidneys the materials that have been applied to support renal epithelial cells were primarily based on commercial hemodialysis filters coated with extracellular matrix (ECM) components. However, this approach did not lead to the desired clinical benefits as a consequence of suboptimal renal tubular epithelial cell function *in vitro*. Better mimicry of these cells' natural environment could improve the maintenance of their natural functions. Supramolecular biomaterials based on UPy-functionalized building blocks were hypothesized to enable better mimicry of the natural substrate of renal epithelial cells, the basement membrane (BM). As described in the introduction, the UPy-based biomaterial tool box can in principle be expanded with virtually any UPy-functionalized building block, not solely limited to UPy-polymers and UPy-peptides. The questions formulated at the beginning of the work described here were therefore: *What biomaterial properties do we need to improve the functions of renal epithelial cells in vitro? Can we achieve these properties using UPy-based biomaterials?* And hence the final question was: *What are the possibilities and challenges of UPy-based biomaterials?* This journey included both quests for answers on material-based inquiries, as well as questions from the application point of view. In this epilogue we will discuss the implications of the main findings described in this thesis and place these in a broader perspective towards future developments and applications.

1. *Material requirements for a bioartificial renal tubular BM mimic*

The basic requirements for the BM mimics to be applied in bioartificial renal tubules involve: (1) a relevant morphology, i.e. hierarchical fibers that form a porous but dense mesh, (2) sufficient mechanical stability to function as freestanding membrane, (3) a hydrophilic property to heighten permeability for water and provide hemocompatibility, and (4) a bioactive character to interact with the renal tubular epithelial cells and ultimately maintain their natural functional behavior.

2. *UPy-biomaterial possibilities: A modular system encompassing all relevant properties*

A mayor advantage of the supramolecular UPy-based biomaterial system is the ability to form new biomaterials without the need of synthesis for every new material composition. With the building blocks at hand, endless variations can be made. The currently available UPy-biomaterial toolbox encompasses building blocks that in principle are able to fulfill the formulated requirements for the formation of a bioartificial renal tubular BM mimic.

Hierarchical fibrous morphologies have been shown to result from self-assembled nano-structures within electrospun microfibers for bifunctional UPy-modified polycaprolactone (UPy-PCL). This property is expected to be attributed to all electrospinnable telechelic UPy-modified thermoplastic elastomers within the UPy-biomaterial platform. For chain-extended UPy-building block designs, with multiple UPy-moieties in their macromolecular backbone, the self-assembled structures are likely less well-defined. On the other hand, these chain-extended building blocks provide enhanced mechanical properties compared to their bifunctional counterparts. Nevertheless, both designs allow the formation of free-standing scaffolds, depending on the polymer backbone. As exemplified for poly(ethylene glycol) (PEG) the bifunctional UPy-PEG displays poor mechanical properties, whereas chain-extended UPy-PEG (CE-UPy-PEG) gives rise to exceptionally stable and elastic hydrogels. The latter can be processed by electrospinning to form free-standing hydrogel scaffolds. Bifunctional UPy-PEG was shown useful to introduce a hydrophilic character when used as supplementing element in a supramolecular copolymer biomaterial with another bifunctional UPy-polymer. The introduction of bioactivity via UPy-functionalized peptides has been well-established for UPy-biomaterials based on single bifunctional polymers.[1] This was now also shown successful for supramolecular copolymers that contain UPy-PEG, by application of an appropriate linker to the peptide.[2] For the chain-extended polymers, the bioactivation by UPy-peptides still needs to be assessed. The aspect of required bioactivity should be further explored and defined to enable the development of specific UPy-peptide building blocks.

3. Supramolecular biomaterial challenges: towards control of dynamics and complexity

The dynamic behavior of the supramolecular UPy-biomaterial system provides possibilities, but on the other hand introduces extra complexity. It requires a certain awareness when working with these materials. External factors can alter the material at the molecular level and hence induce unforeseen changes at scales relevant for the application. An example was given by the observed effects of UV irradiation applied to sterilize UPy-biomaterials. In this case the UV-induced effects did not cause direct adverse implications for the use of UPy-based materials as biomaterial. With an eye on future clinical applications, it remains unclear whether industry-scale sterilization methods, such as gamma-irradiation, have similar or other effects on UPy-based biomaterials. This should be subject of careful investigation before application of UPy-biomaterials in the clinic.

The dynamic behavior of supramolecular biomaterials also implies an enlarged chance on varying results. For example as encountered in the experiments described in chapter 6. The introduction of UPy-PEG in electrospun UPy-PCL membranes resulted in varying suppressing effects of renal epithelial cell adhesion. In general working with living, dynamic entities such as cells can cause non-black-and-white and varying results.

However, in this case also unforeseen variations in the multi-component dynamic material might have caused fluctuating results. For example, the distribution of components at the biomaterial surface could have changed by something as simple as the humidity at the day of electrospinning or small contaminations of water in the solvent used. The challenge is to handle the materials in a similar way each time to heighten reproducibility of results and eliminate possible causes for variation. Furthermore, careful registration of material history and surrounding parameters, when working with these biomaterials, will help to gain control over possible varying results by finding rationale in possible causes. Influences of external stimuli might also be used towards an advantage for application, once identified and under control. An example is given by the pH switchability of the bifunctional high molecular weight PEG. The supramolecular hydrogel was switched into a liquid at pH>8.5, with a viscosity low enough to enable passage through a 1 meter long catheter while rapidly forming a hydrogel in contact with tissue.[3]

The advantage of the supramolecular biomaterial approach is the possibility to make new biomaterials without the need of synthesis. This is based on the self-assembling capacity of the building blocks. Currently, we have no or little control over this supramolecular synthesis in multicomponent UPy-materials. For example in a bi-component system with a UPy-polymer and a UPy-peptide, we can only aid in optimized representation of the peptide at the biomaterial surface by design of the linker. The induced cell adhesion by addition of UPy-RGD to the non-cell-adhesive UPy-copolymer material in chapter 6 verified the presence of the peptide at the surface. However, it is unknown how much of the added peptide is responsible for this effect. Part of the mixed-in peptide might be buried in the bulk of the material. So far we still lack proper analysis tools to study and verify: (1) the exact distribution of components, (2) their *in-situ* dynamic behavior and (3) the presumable influence of environmental factors. Current limitations in this matter are accuracy to detect subtle changes and the possible influence that the analysis method has on the subject we attempt to study. Even so, detailed understanding of the biomaterial system, starting at the molecular level, does not yet provide insight into the interaction of a living cell with the material. Further on, the interaction at single cell level might be difficult to translate to scales relevant for the application. Hence for now, the successful formation of a UPy-biomaterial with a specific set of properties can be based on rational design. However, combination of different building blocks and trial and error based testing will continue to play a significant role. To aid in the latter, we foresee big opportunities for a materiomics biomaterial screening approach as discussed in chapter 5.

In conclusion, UPy-based biomaterials encompass specific properties that make them eminently suitable as ECM or BM mimicking synthetic scaffold material. Furthermore, the UPy-biomaterial system entails broad possibilities towards biomaterial scaffold diversification: by molecular design of UPy-biomaterial building blocks, by mix-and-matching of components and by modular formation of the scaffold. These properties

make UPy-biomaterials also interesting for other applications in the field of regenerative medicine, such as for example in drug delivery or cell-therapy applications. However, applications in the clinical field require strict control over material properties and predictable behavior inside or in contact with essentially a non-predictable environment; the human body. The supramolecular interactions within the UPy-biomaterial system are relatively strong and display low dynamics in terms of non-covalent interactions; UPy-dimerization constants of model-compound were determined to exceed 10^6 M^{-1} in organic solvents (K_{dim} of $6 \cdot 10^7$ M^{-1} in chloroform, $1 \cdot 10^7$ M^{-1} in chloroform saturated with water, and $6 \cdot 10^8$ M^{-1} in toluene).[4,5] The strength and dynamics of the supramolecular interactions under physiological conditions still remain to be determined and will be highly influenced by the material surrounding in which they reside. Pristine, well-studied UPy-polymers, such as UPy-PCL might be applied in clinical applications already. However, complex multi-component UPy-biomaterials, require more investigation before sufficient levels of control are reached. Hence, before we can freely apply the total UPy-material system to our advantage, we first need to gain more fundamental insight into the dynamic behavior of components and identify the factors of influence. However, at the end of the day the real question is perhaps: What is the level of control that we should really have and which part should we leave for 'Nature' to control. Because after all, we are trying to mimic natural materials…

The remarks made here for the UPy-based biomaterial system are essentially translatable to other supramolecular and/or dynamic material systems as well, enclosing both the possibilities and challenges. Ultimately, all biomaterials based on supramolecular interactions can only exist when the (collective) stability of the dynamic bonds are sufficiently high. Thus, in terms of non-covalent, supramolecular interactions the dynamics should be relatively low. However, compared to conventional covalent materials, supramolecular materials display a high degree of dynamics. It is for exactly this reason that supramolecular biomaterials have gained high interest in the development of biomaterials for tissue engineering and regenerative medicine applications. It enable better mimicry of their natural, dynamic counterparts. Up to now covalent synthetic materials have dominated the field of biomaterials, but the desire for 'smart' materials demands for a new approach. To achieve successful implementation in the field, researchers will have to gain control over the dynamics of supramolecular materials. Before or during the transition from covalent to supramolecular biomaterials, the dynamic systems might already be applied in the advantage of biomaterial screening. Supramolecular building blocks could be applied for fast biomaterial diversification, screening and identification of optimal combinations of material components. This composition can be translated to a covalent system if high control over material properties are required for the application. Either way, supramolecular biomaterials are expected to cause a paradigm shift in the development of biomaterials for tissue engineering and regenerative medicine applications.

4. Implications for the bioartificial kidney tubular membrane

We have discussed the current possibilities and challenges of supramolecular UPy-based biomaterials, but which implications does this have on the development of a BM for the bioartificial kidney? The research described in this thesis focused primarily on the performance of the biomaterials. Basic renal epithelial cell functions such as adhesion and maturation to form a tight, confluent and polarized cell layer were monitored to assess this. For this aim, the human kidney-2 (HK-2) cell line was applied in the experimental work described in this thesis. However, ultimately the performance of the cells should be optimized, via application of new and optimized biomaterials. Hence research should be continued with more relevant cell sources. An interesting candidate could be conditionally immortalized proximal tubule epithelial cells of human origin (ciPTEC).[6,7] These cells have shown to have maintained expression of relevant transporter proteins and transporter functions. Nevertheless, researchers were unable to isolate cells which maintained expression of specific organic anion transporters (OAT1 and OAT3).[8] These transporters have been observed in primary isolated cells, but their expression levels dramatically decrease during the first days of in vitro culture, and are completely lost after cell passaging.[9] It would be interesting to see whether an optimized organotypical environment could establish maintenance of this difficult to capture cell function *in vitro*. Such environment would comprise both an appropriate BM mimic and a culture environment capable of applying flow and a compositional gradient of media over the membrane, as discussed in chapter 8. Concerning the most appropriate UPy-based BM mimic at hand at this moment, we think that the CE-UPy-PEG, introduced as biomaterial in chapter 7, will be very interesting for further research. This supramolecular hydrogel biomaterial showed very promising results in initial experiments. The physical appearance of the hydrogel, combined with processing into relevant microfibrous structures, enables mimicry of natural BM in ways unmet by the 'solid' PCL-based UPy-biomaterials which we have applied thus far in our research.[10,11] Also the materials that have been applied by other research groups, as discussed in chapter 1, were based on 'hard' polymer materials commonly used in commercial hemofilters, combined with ECM coatings. The work with those materials so far has shown potential of renal epithelial cells for improvement of current renal replacement therapies. However, their natural potential has not yet been met *in vitro*. Those studies also indicated the potential effects of biomaterial surface morphology, charge and bioactivity. CE-UPy-PEG might function as biomaterial platform to introduce and explore the effect of different parameters. The material allows for processing into relevant morphologies. Stiffness can be tuned at the molecular level or by mixing with other UPy-biomaterial components. This mixing with other UPy-polymer components might also provide an opportunity to mimic the heterogeneous composition of natural BM. Bioactivity was in the current study introduced by hybridization with gelatin. This approach can be continued using selected natural components based on presence in natural BM and prior shown positive effects *in vitro*, such as collagen IV and

laminin. However, with future clinical applications in mind, a purely synthetic approach would provide substantial advances and is hence highly interesting to pursue. Bioactivation with UPy-peptides, as achieved and demonstrated in this thesis for telechelic UPy-biomaterials, is worthy to investigate for CE-UPy-PEG. In a similar fashion charges might be introduced into the biomaterial. This could be valuable given the shown positive effect of charged 3,4-dihydroxy-L-phenylalanine (DOPA) on human primary renal proximal tubule epithetlial cells (HPTC) [12] and ciPTEC (unpublished results by R. Masereeuw *et al.*) DOPA itself could be UPy-functionalized and introduced to the material. This could furthermore be used as crosslinking moiety[13] and could be employed to establish improved capturing of for example collagen IV onto the UPy-biomaterial.[12] Furthermore, the introduction of negative charges and/or additional sulphate groups dangling to the CE-UPy-PEG chains might facilitate mimicry of negatively charged proteoglycans. Proteoglycans are a major BM component imperative for BM hydration and of influence to transport functions over the BM.[14] Other essential features to address in future research are hemocompatibility of the UPy-biomaterials and their stability in an environment relevant to the application. Nevertheless, if the aim is to speed up successful implementation of natural cell functions in a bioartificial renal tubular device, it is wise to make use of the knowledge and expertise available in this specific field. Research so far has focused on seeding cells in or on the hollow fibers of commercial hemofilters, coated with ECM components. Possibly the potential of UPy-based biomaterials in this field is most simplest shown by applying them as alternative coating. This would probably allow the assessment of UPy-based biomaterials in a setting most close the application much faster, rather than building a bioartificial renal tubular device based on cells and UPy-based biomaterials alone.

5. References

(1) Dankers, P. Y. W.; Harmsen, M. C.; Brouwer, L. A.; Van Luyn, M. J. A.; Meijer, E. W. A Modular and Supramolecular Approach to Bioactive Scaffolds for Tissue Engineering. *Nat. Mater.* **2005**, *4*, 568–574.

(2) Mollet, B. B.; Comellas-Aragonès, M.; Spiering, A. J. H.; Söntjens, S. H. M.; Meijer, E. W.; Dankers, P. Y. W. A Modular Approach to Easily Processable Supramolecular Bilayered Scaffolds with Tailorable Properties. *J. Mater. Chem. B* **2014**.

(3) Bastings, M. M. C.; Koudstaal, S.; Kieltyka, R. E.; Nakano, Y.; Pape, A. C. H.; Feyen, D. A. M.; van Slochteren, F. J.; Doevendans, P. A.; Sluijter, J. P. G.; Meijer, E. W.; Chamuleau, S. A. J.; Dankers, P. Y. W. A Fast pH-Switchable and Self-Healing Supramolecular Hydrogel Carrier for Guided, Local Catheter Injection in the Infarcted Myocardium. *Adv. Healthc. Mater.* **2014**, *3*, 70–78.

(4) Beijer, F. H.; Sijbesma, R. P.; Kooijman, H.; Spek, A. L.; Meijer, E. W. Strong Dimerization of Ureidopyrimidones via Quadruple Hydrogen Bonding. *J. Am. Chem. Soc.* **1998**, *120*, 6761–6769.

(5) Söntjens, S. H. M.; Sijbesma, R. P.; van Genderen, M. H. P.; Meijer, E. W. Stability and Lifetime of Quadruply Hydrogen Bonded 2-Ureido-4[1H]-Pyrimidinone Dimers. *J. Am. Chem. Soc.* **2000**, *122*, 7487–7493.

(6) Wilmer, M. J.; Saleem, M. A.; Masereeuw, R.; Ni, L.; Van Der Velden, T. J.; Russel, F. G.; Mathieson, P. W.; Monnens, L. A.; Van Den Heuvel, L. P.; Levtchenko, E. N. Novel Conditionally Immortalized Human Proximal Tubule Cell Line Expressing Functional Influx and Efflux Transporters. *Cell Tissue Res.* **2010**, *339*, 449–457.

(7) Jansen, J.; Schophuizen, C. M. S.; Wilmer, M. J.; Lahham, S. H. M.; Mutsaers, H. a. M.; Wetzels, J. F. M.; Bank, R. A.; van den Heuvel, L. P.; Hoenderop, J. G.; Masereeuw, R. A Morphological and Functional

Comparison of Proximal Tubule Cell Lines Established from Human Urine and Kidney Tissue. *Exp. Cell Res.* **2014**, *323*, 87–99.

(8) Jansen, J.; Fedecostante, M.; Wilmer, M. J.; van den Heuvel, L. P.; Hoenderop, J. G.; Masereeuw, R. Biotechnological Challenges of Bioartificial Kidney Engineering. *Biotechnol. Adv.* **2014**, *32*, 1317–1327.

(9) Brown, C. D. A.; Sayer, R.; Windass, A. S.; Haslam, I. S.; De Broe, M. E.; D'Haese, P. C.; Verhulst, A. Characterisation of Human Tubular Cell Monolayers as a Model of Proximal Tubular Xenobiotic Handling. *Toxicol. Appl. Pharmacol.* **2008**, *233*, 428–438.

(10) Dankers, P. Y. W.; Boomker, J. M.; Huizinga-van der Vlag, A.; Smedts, F. M. M.; Harmsen, M. C.; van Luyn, M. J. A. The Use of Fibrous, Supramolecular Membranes and Human Tubular Cells for Renal Epithelial Tissue Engineering: Towards a Suitable Membrane for a Bioartificial Kidney. *Macromol. Biosci.* **2010**, *10*, 1345–1354.

(11) Dankers, P. Y. W.; Boomker, J. M.; Huizinga-van der Vlag, A.; Wisse, E.; Appel, W. P. J.; Smedts, F. M. M.; Harmsen, M. C.; Bosman, A. W.; Meijer, E. W.; van Luyn, M. J. A. Bioengineering of Living Renal Membranes Consisting of Hierarchical, Bioactive Supramolecular Meshes and Human Tubular Cells. *Biomaterials* **2011**, *32*, 723–733.

(12) Ni, M.; Teo, J.; Ibrahim, M. S.; Zhang, K.; Tasnim, F.; Chow, P. Y.; Zink, D.; Ying, J. Y. Characterization of Membrane Materials and Membrane Coatings for Bioreactor Units of Bioartificial Kidneys. *Biomaterials* **2011**, *32*, 1465–1476.

(13) Umanah, G. K. E.; Son, C.; Ding, F.; Naider, F.; Becker, J. M. Cross-Linking of a DOPA-Containing Peptide Ligand into Its G Protein-Coupled Receptor. *Biochemistry (Mosc.)* **2009**, *48*, 2033–2044.

(14) Boron, W. F.; Boulpaep, E. L. *Medical Physiology:a Cellular and Molecular Approach*; 2nd edition.; Saunders Elsevier, 2012.

List of publications

Articles:

B.B. Mollet, M. Comellas-Aragonès, A.J.H. Spiering, S.H.M. Söntjens, E.W. Meijer, P.Y.W.Dankers
A modular approach to easily processable supramolecular bilayered scaffolds with tailorable properties.
J. Mater. Chem. B., **2014**, 2, 2483-2493.

B.B. Mollet, I. L. J. Bogaerts, G.C. van Almen, E.W. Meijer, P.Y.W. Dankers
The development of a bioartificial environment for kidney epithelial cells through a supramolecular polymer basement membrane mimic and an organotypical culture system.
(submitted)

B.B.Mollet, Y. Nakano, P.C.M.M. Magusin, A.J.H. Spiering, J.A.J.M. Vekemans, P.Y.W. Dankers, E.W. Meijer. The effect of ultra violet light irradiation on ureido-pyrimidinone based biomaterials.
(submitted)

G.C. van Almen, H. Talacua, M. Ramaekers, B.B. Mollet , M. Simonet, A.I.P.M. Smits, J. Kluin, P. Y.W. Dankers
The development of mechanically strong, supramolecular grafts with reduced cell adhesion for vascular tissue engineering.
(submitted)

B.B. Mollet, P. Goodarzy Fard, S. Spaans, E.W., N.A.M. Bax, E.W. Meijer, C.V.C. Bouten, P.Y.W. Dankers
Elastic microfibrous hybrid hydrogel scaffolds of chain-extended ureido-pyrimidinone functionalized PEG and gelatin for 2D and 3D tissue engineering.
(manuscript in preparation)

Y. Nakano, K. Berghoff, A.C.H. Pape, B.B. Mollet, H. Kress, E.W. Meijer, P.Y.W. Dankers.
Determination of the cell-supramolecular biomaterial interaction using optical tweezers.
(manuscript in preparation)

Book chapter:

B.B. Mollet, A.C.H.Pape, R.P. Félix Lanao, S.C.G. Leeuwenburgh, P.Y.W. Dankers
Materiomics using synthetic materials; metals, cements, covalent polymers and supra-molecular systems.
In Materiomics: High-Throughput Screening of Biomaterial Properties, Edited by. J. de Boer and C. A. van Blitterswijk, Cambridge University Press, **2013**.

Curriculum vitae

Björne Mollet werd geboren op 16 april 1985 te Oirschot. Na het behalen van het atheneum aan het Jacob Roelands Lyceum te Boxtel, begon zij in 2003 aan de studie Biomedische Technologie aan de Technische Universiteit Eindhoven (TU/e). Tijdens haar master liep zij in de zomer van 2008 stage binnen de onderzoeksgroep van prof. dr. Craig J. Hawker aan de universiteit van Californie, Santa Barbara (UCSB). Zij werkte daar aan de formatie van in water oplosbare nanodeeltjes, gevormd uit enkele polymeerketens gebaseerd op supramoleculaire zelf-assemblage. Tijdens een tweede stage bij Fujifilm in Tilburg in 2009 lag de focus op het creëren van controleerbare poreuze structuren uit recombinante gelatines. Björne studeerde zij af aan de TU/e met een onderzoek naar de ontwikkeling van synthetische membranen uit supramoleculaire bouwstenen welke gefunctionaliseerd zijn met ureido-pyrimidinon. In januari 2010 zette zij dit werk voort in de vorm van een promotieonderzoek. Hierbij werd dieper ingegaan op de modulaire toepasbaarheid van de supramoleculaire bouwstenen met als centraal doel de formatie van een functioneel synthetisch basaal membraan voor humane nier epitheelcellen. Dit met het oog op behoud van functionaliteit van deze cellen *in vitro* ten behoeve van potentiële verbetering van huidige artificiële nier vervangende therapieën. Binnen dit onderzoek opereerde zij op het grensvlak tussen chemie, biologie en engineering. De belangrijkste resultaten van dit promotieonderzoek, uitgevoerd onder leiding van prof. dr. E.W. (Bert) Meijer en dr. dr. Patricia Y.W. Dankers, staan beschreven in dit proefschrift. In september 2013 startte Björne naast de afronding van haar promotie met een onderwijsfunctie binnen de faculteit Biomedische Technologie aan de TU/e, waarin zij voltijds aan de slag is sinds december 2014.

Björne Mollet was born on April 16th, 1985 in Oirschot, the Netherlands. After she obtained her atheneum (pre-university) degree at the Jacobs Roeland Lyceum in Boxtel in 2003, she started her studies at the Eindhoven University of Technology (TU/e) in Biomedical Engineering. The Masters program of her study included an international research internship in summer 2008. She worked on the development of single chain supramolecular polymer nanoparticles in the group of prof. dr. Craig J. Hawker at the Materials Research Laboratory of the University of California, Santa Barbara. During a second research internship at Fujifilm Tilburg in 2009 she developed recombinant gelatin scaffolds with controlled porosity and interconnectivity for tissue engineering purposes. Björne's Masters program was completed with a research project on the development of synthetic basement membrane mimics from supramolecular building blocks based on ureido-pyrimidinone. In January 2010 she continued to work on this project as a PhD student. Her research focused on the modular applicability of the supramolecular biomaterial building blocks towards the formation of suitable synthetic basement membrane mimics for human renal epithelial cells. This was done with the aim to preserve the functionality of these cells *in vitro* to benefit current artificial renal replacement therapies. During this research Björne was active at the interface of chemistry, biology and engineering. The main results of this research, performed at the TU/e under supervision of prof. dr. E.W. (Bert) Meijer and dr. dr. Patricia Y.W. Dankers, are presented in this thesis. Since September 2013 she was, next to finishing her PhD, active within the faculty of Biomedical Engineering at the TU/e as supporting educational staff. She continued in this function full-time since December 2014.

Samenvatting voor niet biomedisch technici

Supramoleculaire biomaterialen gebaseerd op ureido-pyrimidinon

- De ontwikkeling van een synthetisch basaal membraan voor het gebruik in een biologische kunstnier-

Onze nieren maken ons bloed schoon door het verwijderen van schadelijke (afval)stoffen. Verder houden ze de waterhuishouding op pijl via de productie van urine. Urine wordt gevormd via een tweevoudig proces dat plaatsvindt in elk van de ~miljoen nephronen waaruit een enkele nier bestaat. Elk nephron is opgebouwd uit een glomerulus en een tubulus. Het bloed wordt eerst gefilterd over het glomerulaire membraan. Dit membraan is een soort zeef. Kleine moleculen zoals water en zouten gaan er doorheen en vormen de pre-urine, terwijl bloedcellen en grote eiwitten achterblijven in het bloed. Vervolgens stroomt de pre-urine door het buizenstelsel van de tubulus. Voordat deze uitmondt in de blaas, wordt de samenstelling van de pre-urine nauwkeurig aangepast. Water en bruikbare voedingsstoffen worden teruggewonnen. Afvalstoffen die in het bloed zijn achtergebleven worden actief overgedragen aan de pre-urine. De nierepitheelcellen die de tubulus bekleden, zijn verantwoordelijk voor dit actieve transport. Deze niercellen groeien in een enkele laag dicht tegen elkaar aan en vormen zo een barrière, waarover stoffen tussen bloed en urine uitgewisseld kunnen worden.

Nierpatiënten, wiens leven afhangt van belastende niervervangende therapieën zoals hemodialyse, ervaren een sterk verminderde kwaliteit van leven. Bovendien is de kans op complicaties groot en heerst er een hoog sterftecijfer onder deze patiënten; nog steeds sterft jaarlijks ongeveer 1 op de 5 patiënten. Dit komt doordat deze therapieën enkel gebaseerd zijn op passieve filtratie en diffusie processen. Hierdoor zijn zij niet in staat om de functies van de nier volledig te vervangen.

Tegenwoordig zijn wij in staat menselijke nierepitheelcellen te isoleren, buiten het lichaam in leven te houden en te vermeerderen. Het implementeren van deze cellen in de huidige niervervangende therapieën, als 'biologische kunstnier', biedt mogelijkerwijs een veelbelovende verbetering voor patiënten. Tijdens initiële pogingen om dit te bewerkstelligen, werden de cellen op de membranen van hemodialyse filters gezaaid met als doel zo de actieve functies van deze cellen aan de hemodialyse therapie toe te voegen. Klinische tests lieten echter niet de gewenste resultaten zien. Het probleem is dat deze nierepitheelcellen hun specifieke functies verliezen zodra zij uit hun natuurlijke omgeving gehaald worden. Dit maakt ze dus onbruikbaar voor de gewenste therapieverbetering. Men verwacht dat dit probleem opgelost kan worden door de natuurlijke omgeving van deze cellen heel zorgvuldig na te bootsen.

In het lichaam groeien deze nierepitheelcellen op een basaal membraan (BM). Dit membraan bestaat uit vezelachtige eiwitstructuren die samen een dicht netwerk vormen. Het BM ondersteunt de cellen niet alleen maar geeft ook signalen aan de cellen (is bioactief) en kan zich aanpassen aan de cellen (heeft een dynamisch karakter). De kunststof materialen waaruit de hemodialyse filters gemaakt worden lijken in geen enkel opzicht op het BM. Hier valt dus veel winst te behalen.

Het doel van het onderzoek, beschreven in dit proefschrift, is om betere synthetische materialen te ontwikkelen die het natuurlijke BM wel kunnen nabootsen, om zo samen met de cellen een biologisch kunstniermembraan te vormen. Hiervoor gebruiken we moleculaire bouwsteentjes gebaseerd op het ureido-pyrimidinon molecuul, of kortweg UPy. Een UPy kan een binding aangaan met een andere UPy, zoals twee lego-steentjes die op elkaar passen. Dit noemen we dimerizatie. De binding tussen UPy-UPy dimeren is niet-covalent, ook wel supramoleculair

genoemd, wat wil zeggen dat de binding tussen de twee moleculen niet permanent is. In feite kan de binding 'aan' of 'uit' staan en het switchen hiertussen gebeurt spontaan en continu. Een supramoleculair materiaal, opgebouwd uit moleculaire bouwstenen die allemaal voorzien zijn van een of meerdere UPy-moleculen, bezit hierdoor dynamische eigenschappen. Dit biedt mogelijkheden tot het nabootsen van het BM, omdat het BM zijn karakteristieke eigenschappen ook te danken heeft aan niet-covalente bindingen tussen diens natuurlijke bouwstenen.

Hoofdstuk 2 beschrijft de moleculaire blokkendoos, die in de overige hoofdstukken gebruikt wordt om nieuwe biomaterialen mee te bouwen en om specifieke eigenschappen van deze materialen te onderzoeken. Deze blokkendoos is gevuld met drie verschillende categorieën UPy-bouwsteentjes. Ten eerste zijn er de UPy-model moleculen om gericht en in detail naar specifieke eigenschappen van UPy-materialen te kunnen kijken. Ten tweede hebben we diverse soorten lange polymeerketens (bouwstenen van kunststoffen) voorzien van twee of meer UPy-moleculen. Dit noemen we de UPy-polymeren. Ten derde hebben we kleine, specifieke stukjes eiwit gelinkt aan een UPy; de UPy-peptiden. De geselecteerde peptiden komen van nature ook voor in het BM en hebben de bioactive eigenschap dat ze een specifieke bindingsplaats voor cellen vormen. Eerder werk heeft laten zien het mengen van kleine hoeveelheden UPy-peptiden in een UPy-polymeer erin resulteert dat de UPy-peptiden in het kunststof materiaal 'geklikt' worden via de UPy-UPy interactie. Daar dragen zij bij aan een goede hechting van cellen aan het materiaal.

Hoofdstuk 3 beschrijft hoe een UPy-polymeer, UPy-PCL (PCL staat voor polycaprolactone), verwerkt wordt tot een membraan dat morfologisch gezien het BM nabootst. Door middel van een speciale verwerkingstechniek genaamd electrospinnen kunnen zeer dunne vezels gemaakt worden met een diameter van een micrometer (duizendste millimeter) of zelfs dunner. Wanneer er genoeg lagen van dergelijke dunne vezels willekeurig worden opgevangen, ontstaat er een membraan opgebouwd uit microvezels met daartussen poriën die klein genoeg zijn om te voorkomen dat de nier epitheelcellen het membraan binnendringen. Hierdoor kunnen de cellen in een aaneengesloten laag op het membraan groeien. De UPy-bouwsteentjes hebben de eigenschap zichzelf op moleculair niveau te ordenen in nette stapels UPy-dimeren. Dit leidt tot de spontane vorming van vezelachtige structuren op de nanoschaal (miljoenste millimeter). In hoofdstuk 3 geven we bewijs van de aanwezigheid van deze nanovezels, binnen de electrogesponnen microvezels. Dit wil zeggen dat er een hiërarchische vezelachtige structuur wordt gevormd door het electrospinnen van het UPy-polymeer. Dit bootst de hiërarchische structuren na die ook in het natuurlijke BM aanwezig zijn. We laten zien dat nierepitheelcellen in staat zijn om een mooie dichte cellaag te vormen wanneer zij gezaaid worden op deze electrogesponnen UPy-PCL membranen.

Voordat materialen worden toegepast in experimenten met levende cellen, dienen zij eerst gesteriliseerd te worden om de ongewenste groei van andere levende organismen, zoals bacteriën, te voorkomen. De techniek die hiervoor in het laboratorium wordt toegepast is het blootstellen van de materialen aan ultraviolet (UV) licht. UV licht veroorzaakt veranderingen in DNA op moleculair niveau. Hoofdstuk 4 beschrijft observaties waaruit blijkt dat het UV licht ook veranderingen in de UPy-materialen teweeg brengt. Dit leek in eerste instantie niet zo vreemd, gezien de gelijkenis op moleculair niveau tussen het UPy-bouwsteentje en de bouwstenen waaruit DNA bestaat. UPy-model moleculen vormen na UV-bestraling slecht oplosbare producten. Dit duidt op de vorming van covalente (dus permanente) bindingen tussen de moleculen. Daarnaast verkrijgen de UPy-materialen fluorescente eigenschappen door het bestralen met UV licht. Onderzoek met diverse analysetechnieken aan verscheidene UPy-model moleculen laat zien dat deze fluorescentie afhankelijk is van een subtiel verschil in de organisatie van de bindingen tussen de atomen van het UPy-molecuul. Op basis van deze resultaten werd de hypothese opgesteld dat het absorberen van

UV licht een verschuiving in de verbindingen van een UPy-dimeer teweeg brengt. Dit fenomeen is nooit eerder beschreven voor de goed bestudeerde UPy-moleculen. De exacte implicatie van dit fenomeen op UPy-materialen is nog onduidelijk, maar er wordt niet verwacht dat deze bepalend zullen zijn voor hun functie als synthetisch BM.

Een gewenste eigenschap van het synthetisch BM is het kunnen controleren van celhechting. Hiervoor is diepgaand begrip van de interactie tussen cellen en materialen belangrijk. In hoofdstuk 5 onderzoeken we het effect van een aantal verschillende supramoleculaire UPy-materialen op de hechting van fibroblastcellen. Er wordt gekeken naar deze hechting op twee lengte- en tijdschalen. De sterkte van de binding die binnen 1 minuut ontstaat tussen een microbolletje gemaakt van deze materialen en één enkele cel, wordt gemeten door middel van een optische pincet. Hiermee kan het microbolletje heel nauwkeurig worden gemanipuleerd en kunnen de hiervoor benodigde krachten worden bepaald. De binding van een populatie (enkele duizenden) cellen aan het oppervlak van een electrogesponnen membraan van deze materialen wordt onderzocht met behulp van microscopie. De hoeveelheid gehechte cellen binnen 4 uur en de vorm van deze cellen geeft inzicht in de mate van celhechting. Ondanks het toepassen van twee totaal verschillende technieken, bleek het moeilijk om statistische verschillen in het hechten van cellen op deze materialen vast te stellen. Het verzamelen en analyseren van grote hoeveelheden data, een zogenaamde 'materiomics' aanpak, zal in de toekomst helpen om meer inzicht te krijgen tussen specifieke materialen en hun effecten op celgedrag.

Doordat alle moleculaire bouwsteentjes via het UPy-blokje aan elkaar 'klikken', kunnen er gemakkelijk nieuwe materialen gevormd worden. In hoofdstuk 6 laten we zien dat we door de bouwsteentjes slim te kiezen, de eigenschappen van het samengestelde supramoleculaire materiaal kunnen beïnvloeden. Drie bouwstenen worden gebruikt; twee UPy-polymeren die beiden voorzien zijn van een UPy-molecuul aan de uiteinden van de polymeerketen, en een UPy-peptide. Het eerste UPy-polymeer, UPy-PCL, is hydrofoob (stoot water af) en kan, zoals gezien in hoofdstuk 3, verwerkt worden door middel van electrospinnen tot een membraan waar cellen aan hechten. Het tweede UPy-polymeer, UPy-PEG (PEG staat voor poly(ethyleen glycol)) is hydrofiel (trekt water aan) en is mechanisch te zwak om te worden verwerkt tot een membraan met electrospinnen. Dit polymeer werkt te hechting van cellen tegen. Wanneer 30% van het UPy-PEG gemengd wordt in het UPy-PCL, ontstaat er een nieuw materiaal met gecombineerde eigenschappen. Het vormt door electrospinnen een membraan dat water aantrekt en waaraan cellen niet of slecht kunnen hechten. Het toevoegen van een kleine hoeveelheid UPy-RGD, een UPy-peptide dat als bindingsplaats voor cellen werkt, zorgt ervoor dat cellen toch kunnen hechten op dit membraan. Door het spinnen van de verschillende combinaties UPy-bouwstenen in lagen, kan er een dubbellaags hydrofiel membraan gevormd worden, waarop cellen slechts aan één van beide zijden kunnen hechten. Dit is gewenst voor het maken van een biologisch kunstniermembraan om de hemodialyse therapie te verbeteren. Immers, één zijde zal in contact staan met bloed, terwijl de andere zijde de cellen moet dragen. Het principe om bouwstenen te mengen en materialen met gecombineerde eigenschappen te vormen, is een groot voordeel van het supramoleculaire UPy-systeem. De methode is echter nog niet robuust genoeg om ervoor te zorgen dat bij het mengen van diverse bouwstenen het eindresultaat altijd de gewenste eigenschappen heeft. Dit komt doordat we de verdeling en locatie van de afzonderlijke bouwstenen in het eindmateriaal nog niet volledig onder controle hebben. De intrinsieke dynamische eigenschappen van de materialen bieden vele voordelen en mogelijkheden, maar kunnen er ook toe leiden dat er door invloeden van externe factoren veranderingen optreden die we nu nog niet kunnen controleren.

In een ander soort UPy-PEG polymeer (CE-UPy-PEG), beschreven in hoofdstuk 7, zijn meerdere UPy-moleculen in de polymeerketen gekoppeld. Hierdoor kan iedere keten interacties aangaan met meerdere andere ketens en wordt er een netwerk gevormd. Hierdoor bezit CE-UPy-PEG bijzonder sterke mechanische eigenschappen in vergelijking met het zwakke UPy-PEG, dat enkel een UPy aan beide uiteinden van de polymeerketen heeft welke daardoor beperkt is tot het vormen van langere ketens. CE-UPy-PEG kan hierdoor wel verwerkt worden tot membranen middels electrospinnen. In contact met water zwelt dit overwegend hydrofiele materiaal en vormt het een hydrogel. De vezelachtige hydrogelen zijn elastisch en hebben mechanische eigenschappen die vergelijkbaar zijn met diverse zachte weefsels in ons lichaam. Dit maakt deze materialen interessant om bijvoorbeeld nier, hart, spier of long weefsel mee te reconstrueren. Echter, omdat het materiaal zeer hydrofiel is, kunnen er geen cellen op hechten. Daarom voegen we een biologische component toe waaraan cellen wel kunnen hechten. We hebben gekozen voor gelatine. Gelatine wordt gemaakt uit collageen, een veelvoorkomend eiwit in ons lichaam dat ook in het BM terug te vinden is. Doordat er celhechtingsplaatsen zoals onder anderen het RGD-peptide in zitten, kunnen cellen goed hechten aan gelatine. Mechanisch is gelatine echter zwak. Het toevoegen van 20 % gelatine in CE-UPy-PEG blijkt voldoende om celhechting mogelijk te maken, zonder verlies van mechanische eigenschappen. Op een electrogesponnen membraan met dunne vezels en kleine poriën kunnen nierepitheel cellen een perfecte dichte cellaag vormen, zoals gewenst is voor de biologische kunstnier. Deze resultaten laten zien hoe het ontwerp van de UPy-bouwsteentjes van grote invloed is op de eigenschappen van het materiaal, wat waardevol kan zijn voor de vorming van een synthetisch BM. Vervolgonderzoek moet nog uitwijzen of celhechting in het CE-UPy-PEG ook bereikt kan worden door het inmengen van synthetische UPy-RGD peptiden, in plaats van het biologische gelatine.

Zoals eerder besproken is uiteindelijk de functie van de nier epitheel cellen van belang voor de verbetering van niervervangende therapieën. Naast een geschikte ondergrond welke het BM nabootst, vereist dit ook een kweekomgeving die vergelijkbaar is met de natuurlijke situatie. Dit vraagt om een tweecompartimentensysteem waarin het membraan tussen een bloed en urine volume geplaatst kan worden. Een dergelijke verdeling is ook nodig om de functie van het biologische kunstniermembraan, actief transport, te kunnen evalueren. Hiertoe zijn drie verschillende systemen ontwikkeld, welke beschreven worden in hoofdstuk 8. In het eerste systeem wordt een membraan eenvoudig tussen twee stilstaande vloeistoffen geplaatst. Dit noemen we een statisch kweeksysteem, welke de mogelijkheid biedt om eenvoudige tests uit te voeren. De andere twee systemen, zogenaamde bioreactoren, maken het mogelijk om de volumes langs het membraan te laten stromen, zoals in de nier en tijdens hemodialyse ook gebeurt. In de eerst ontwikkelde bioreactor kan één membraan geplaatst worden. Initiële tests laten zien dat een biologisch kunstniermembraan tot wel drie weken lang in leven blijft wanneer het geplaatst wordt in de bioreactor en door de vloeistofstroom van voedingsstoffen voorzien wordt. In het andere bioreactorsysteem kunnen negen membranen tegelijkertijd geplaatst worden, zodat er verschillende condities in één enkele test vergeleken kunnen worden. Dit systeem vereist echter nog verdere optimalisatie.

Samengevat verschaft het wetenschappelijke werk dat beschreven is in dit proefschrift nieuwe inzichten in de mogelijkheden en uitdagingen omtrent de toepassing van de UPy-materialen in biomedische applicaties. Ook zal het beschreven werk helpen bij de identificatie van potentieel interessante materiaalcombinaties die het basale niermembraan kunnen nabootsen om uiteindelijk de vorming van een functioneel biologisch kunstniermembraan te bewerkstelligen.

Dankwoord

Nu ik toch echt op het punt ben aangekomen dat mijn promotie tot een einde komt, kan ik terugblikken op een mooie, ontzettend waardevolle periode. Hiervoor wil ik graag mijn dankbaarheid uiten aan eenieder die hier op zijn of haar manier een aandeel in heeft gehad.

Om te beginnen Bert. Hoewel ik al die jaren terug nog een onzekere, soms zelfs liefst onzichtbare studente was, heb jij iets gezien wat ik misschien zelf nog niet zag. Alle mogelijkheden en kansen die je mij geschonken hebt, hebben er absoluut aan bij gedragen dat er vandaag de dag een andere Björne staat. Hier ben ik je ontzettend dankbaar voor. Bert, ik waardeer het ontzettend hoe je, na al zoveel bereikt te hebben, je nog altijd bescheiden, kwetsbaar en toegankelijk opstelt naar hen die tegen je opkijken. Jouw vaak herhaalde uitspraak tegen mij: 'Als het niet kan zoals het moet, dan moet het zoals het kan', is een waardevol advies gebleken dat me zal bijblijven en welke ik nog vaak zal toepassen. Ik wens je nog vele mooie, vreugdevolle jaren in de wetenschap en daarbuiten.

Patricia, mijn copromotor die de UPy-*bio*materialen op de kaart zette. We begonnen ongeveer tegelijk aan een nieuw hoofdstuk. Jij als kersverse universitair docente, ik toen nog als afstudeerstudente. Inmiddels ben jij benoemd tot universitair hoofddocente en ben ik bijna gepromoveerd. Met beiden dus de nodige extra ervaring en wijsheid op zak, zijn er ongetwijfeld dingen waarvan we het nu anders zouden aanpakken. Desalniettemin ben ik ontzettend tevreden met de behaalde resultaten en het proefschrift dat hier nu voor je ligt. Tijdens de reis van de afgelopen jaren heb ik mogen ervaren hoe waardevol jouw passie en aanstekelijke enthousiasme voor de wetenschap is voor de soms worstelende PhD student; elk resultaat weet jij een positieve wending te geven. Patricia, dank hiervoor en het vertrouwen dat je me steeds gegeven hebt. Hier wil ik ook meteen mijn dankbaarheid uiten voor het feit dat we in het digitale tijdperk leven. Lang leve email! Deze tegenwoordige vanzelfsprekendheid hebben wij goed weten te benutten tijdens je verblijf in Chicago en tweemaal zwangerschapsverlof, dan wel tijdens nachtelijke conversaties (het was altijd weer fijn om te weten niet de enige te zijn die bij voorkeur meters maakt achter de computer tijdens die heerlijke onverstoorde late/vroege uurtjes). Patricia, ik wens je een succesvolle carrière in de wetenschap en daarnaast heel veel geluk en tijd met je mooie gezinnetje.

Graag wil ik alle leden van mijn promotiecommissie bedanken voor het plaatsnemen in de commissie en het kritisch beoordelen van mijn werk. Bedankt voor de feedback en, omdat ik ben er vrij zeker van dat ik dat tijdens de verdediging op een zeker punt ga vergeten te zeggen, nu alvast voor de mooie woorden. In het bijzonder wil ik mij richten tot extern commissielid prof. dr. Marianne Verhaar van het UMC Utrecht; mijn dank is groot dat u afgelopen zomer de uitnodiging accepteerde toen wij u op nogal korte termijn benaderden. Dr. Roos Masereeuw van de Radboud Universiteit Nijmegen wil ik tevens bedanken voor de fijne contacten binnen het BMM BioKid project.

Ook de andere partners binnen het BioKid project wil ik bedanken, in het bijzonder Carolien, Jitske, Saskia, Saed en Sandra voor de fijne samenwerkingen.

Hoewel ik me tijdens mijn promotie met mijn nier-project in een behoorlijke niche bevond binnen de vakgroep, heb ik gelukkig toch het genoegen gehad om samen te werken met een verscheidenheid aan mensen aan diverse (helaas niet altijd even succesvolle) projectjes. Maartje en Roxanne, de allereerste pogingen met de UPy-hydrogelen en cellen hebben helaas nooit tot baanbrekende resultaten geleid. Gelukkig hebben jullie het daar niet bij opgegeven. Bram Pape, de maandag ochtend bezoekjes aan de GTD hebben we toch redelijk lang volgehouden. Ik ben blij dat

je me hierbij, en tijdens de trip naar Amsterdam, vergezeld hebt. Hoewel onze inspanningen nooit geresulteerd hebben in een werkend high-throughput screening platform voor de UPy-biomaterialen, zijn we er in ieder geval in geslaagd onze zogenaamde 'materiomics-dromen' op papier te zetten als boekhoofdstuk, deels ook terug te vinden in hoofdstuk 5 van dit proefschrift. Je bezoekjes aan STO vloer 3 heb ik altijd als welkome afleiding ervaren, ook al was een stop bij mijn kantoor wellicht meer bijzaak dan hoofdzaak, onderweg van/naar het biolab of in afwachting van Patrcia ;-). Yoko Nakano, thank you for the initial photoluminescence measurements on my UV-irradiated polymers. I admire the disciplined way you performed the elaborate experiments with the optical tweezers. Pieter Magusin, bedankt voor je hulp en het delen van je kennis over vaste stof NMR. Marc Simonet, thank you for sharing your knowledge on electrospinning. Unfortunately, that gradient electrospinner never really worked out for us. Patrick de Laat (en collega's), bedankt voor de prettige samenwerking en realisatie van mijn kweeksystemen. Anthal Smits, bedankt voor het delen van jouw eigen kweeksysteemontwerpervaringen en kennis over biaxiale trektesten aan onhandelbare membranen. Tina Thakkar, thank you for showing me how to use the biaxial tensile tester. Marc van Maris, bedankt voor het introduceren en onderhouden van misschien wel mijn favoriete 'speeltje' binnen het brede scala aan analysetechnieken: de rasterelectronenmicroscoop (overigens nooit geweten, tot nu, dat dit de Nederlandse benaming is voor de SEM).

Met name in het begin hebben vele Spinozastudenten een steentje bijgedragen om 'het nierproject' een vliegende start te geven: Bas R, Benjamin, Jibbe, Jules, Lenny, Loes, Man Teng, Marloes, Olga, Parinaz, Samantha en Ruben. Leuk om te zien dat velen van jullie inmiddels ook begonnen zijn aan een promotieproject. Ik wens jullie allen veel succes hierin en in jullie verdere carrière. Ook heb ik diverse studenten direct of vanaf de zijlijn mogen begeleiden bij een bachelor eindproject, interne stage of zomerstage. Bas M, Nicky, Loes, Sam, Berly, Adrien, Tijmen en Parinaz, Ik wens jullie allemaal veel succes in jullie verdere (wetenschappelijke) carrière. Iven, jij was (bent?) mijn enige afstudeerstudent. Er is veel gebeurt de afgelopen jaren, maar ik hoop van harte dat ik je op een dag nog mag feliciteren met je afstuderen. Hoe dan ook, jij hebt mijn Belgische woordenschat iets verrijkt en ik hoop op mijn beurt iets te hebben bijgedragen aan jouw wetenschappelijke, dan wel niet wetenschappelijke kennis. Sergio, wat fijn dat je bent begonnen aan je promotie. Hoewel ik geen begeleider was in jouw afstudeerproject, heb ik je werk met grote interesse gevolgd. Ik denk dat het, samen met het werk van Parinaz en dat van mezelf, een mooi hoofdstuk in dit proefschrift is geworden en wellicht een mooi paper gaat zijn. Parinaz, bedankt voor je stage en Spinozawerk aan de chain extended UPy-PEG. Rudy, bedankt voor het voorwerk om dit materiaal te verwerken tot membranen doormiddel van electrospinnen.

Gedurende mijn promotie heb ik ontzettend genoten van de open een aangename sfeer binnen SMO, het ICMS, op de labs en op kantoor. Hiervoor wil ik iedereen bedanken die hier een aandeel in heeft gehad. Het kleine cel lab was 'mijn domein', waarvan ik blij ben dat ik het met steeds meer mensen heb kunnen delen. Sascha 'de Vos', it was always a lot of fun having you around. As 'the original' cell-lab habitants (after Maëlle) we saw the 'cell-lab-family-tree' with nicknames grow taller and taller, until it did not fit one sheet of paper anymore. It was nice to also welcome and introduce people, or should I say ladies, from 'the chemists side' to the cell lab; Ewelina, Roxanne, Maartje, Samaneh and Mellany (apparently the cell lab attracts women. So, single male chemists, use this information wisely and go bio...)

Hoewel ik aan de start van mijn promotie kort een privé kantoor had, heb ik daarna het kantoor mogen delen met een grote diversiteit aan kantoorgenoten: AIO's, post-docs, vaste staf, mannen, vrouwen, koppels (hoewel nooit met beiden helften tegelijkertijd), een vader, moeders, kinderen

(incidenteel), Nederlandssprekend, non-Dutch, and a little bit of beiden. I thank all my (old)officemates for their pleasant company in STO 3.47 or 3.27, scientific and non-scientific conversations and joint walks upstairs for coffee: Christian & Andrea (und 'die kleine Haasen') Ralf & Olga, Parisa, Debarshi, Salman, Annemie, Peggy en Stijn. Mijn huidige kantoorgenoten, Olga, Peggy en Stijn wil ik in het bijzonder bedanken voor de afgelopen maanden, voor de mentale steuntjes in de rug en succeswensen als ik nog wat langer op kantoor bleef om 'even iets af te maken'. Peggy ook bedankt voor de goede zorgen voor het biolab. Stijn en Olga beiden heel veel succes met jullie eigen promotieonderzoek. En al klinkt dit een beetje als een afscheid, voorlopig zal ik het bureau bij het raam nog wel bezet houden, zolang ik in het onderwijs werkzaam ben. Verder wil ik ook iedereen bedanken met wie ik nooit een kantoor gedeeld heb, maar die toch met zekere regelmaat even binnenwandelden voor een welkome korte afleiding. The sisters Goodarzy Fard, thank you for the non-scientific talks we had about the truly important things in life. I wish you both a lot of happiness and success for the future. Brian, Ralf en Bram, jullie ook veel succes met de laatste loodjes.

De 'supramolecular biomaterials' subgroep wil ik graag bedanken voor alle waardevolle discussies tijdens onze tweewekelijkse meetings en daarbuiten. Het was mij een genoegen om deze meeting ruim twee jaar te organiseren en voor te zitten. Toch is het fijn om nu het stokje over te kunnen dragen, samen met de verantwoordelijkheid voor het cel lab. Ik heb er het volste vertrouwen in dat jij, 'Maarten de 1^{e}', hier op geheel eigen wijze invulling aan zult geven. Ook tijdens de algemene groepsmeetings, in al haar verschijningsvormen en onder verschillende namen, heb ik veel geleerd uit de wetenschappelijke discussies en ook zelf de nodige bruikbare feedback mogen ontvangen. Mijn dank daarvoor aan alle huidige en oud-groepsleden. Peter, ik geloof niet dat onze collega's ons graag samen over vloer 4 zagen lopen, omdat dit meestal betekende dat er een presentatie gemaakt moest worden voor de Academisch Genootschap meeting. Des al niet te min was het mij een genoegen om deze meeting samen met jou te organiseren en voor te zitten.

Ook het ICMS heeft vele mogelijkheden tot wetenschappelijke ontwikkeling, verdieping en verbreding geboden. Onlosmakelijk verbonden met het succes van het ICMS, weerspiegeld in de overgang van het 'huiskamertje' in het hoofdgebouw tot het huidige, prachtig ruime ICMS gebouw, is natuurlijk Sagitta. Chapeau hoe je dit alles voor elkaar gekregen hebt. Iedereen betrokken bij het ICMS, bedankt voor alle mogelijkheden, interessante lezingen en discussie meetings die ik door de jaren heen heb kunnen bijwonen. Koen en collega's van de ICMS animatiestudio, bedankt voor het maken van het niermembraanfilmpje, waardoor ons onderzoek naamsbekendheid kreeg tijdens de World Expo 2010 in Shanghai, en het knappe staaltje digitale art-work dat een mooie frontcover opleverde voor mijn eerste paper.

Jolanda, met jouw jarenlange ervaring, ordelijke manier van werken en 'fingerspitzengefühl' voor synthese, was het mij een genoegen om in ieder geval de basiskneepjes van het vak van jou te mogen leren. Hoewel ik vervolgens zelf nauwelijks nog op een organisch synthetisch lab heb gestaan om moleculen te maken, blijft het me fascineren dat, door te 'kokerellen met chemicaliën', het mogelijk is stoffen te maken die nooit eerder iemand maakte. Zonder jouw synthetische vaardigheden en inspanningen had ik niet zoveel bouwstenen gehad om mee te spelen. Mijn dank daarvoor. Daarnaast ben jij iemand die niet bang is om de handen uit de mouwen te steken, of om mensen aan te sporen hetzelfde te doen. Ik hoop dat je nog heel lang met veel plezier die constante factor in de groep zult blijven.

Henk bedankt voor de goede zorgen, broodnodige koffie, gezellige babbels en vakkundige inpakservice van mijn pakketjes. Alle huidige dames van de diverse secretariaten, Nora, Martina,

Jolanda, Marjo, Cindy, Carla, en alle dames die daarvoor deze functie op voortreffelijke wijze vervuld hebben, hier wil ik in het bijzonder Joke even noemen, wil ik bedanken voor alle zaken die jullie geregeld hebben; het merendeel achter de schermen waar ik niet eens weet van heb. Hans, bedankt voor het regelen van al mijn bestellingen en het op pijl houden van de algemene voorraden, zodat ik (haast) nooit mis hoefde te grijpen. De mannen van het analytisch team; Thank you. Despite the fact that I did not perform any synthesis during my PhD, I did make use of your knowledge and services a few times. Joost, ik wil jou tevens bedanken voor de einde-van-de-werkweek-wake-up-call-aan-kantoor-service (Björne je mag naar huis, het is weekend!!!) tijdens het afgelopen jaar en je uitstekende invulling van de rol als steevaste quizmaster als antwoord op iedere vraag die ik je maar durfde te stellen.

Mijn paranimfen Geert en Mellany wil ik bedanken, niet alleen alvast voor de mentale steun op 29 januari. Geert, als collega in het kwadraat, in onderzoek en onderwijs, hebben we de nodige tijd met elkaar opgetrokken. Jouw pogingen om me enigszins in muziek en ander 'cultureel erfgoed' bij te scholen waren wellicht tevergeefs, maar jouw kennis en kunde als 'bioloog' in deze chemische groep was voor mij zeer waardevol. Daarnaast hoop ik dat er iets van jouw bijzondere sociale kwaliteiten op mij hebben afgegeven. Ik dank je ook voor de regelmatige, zeer welkome koffie-en-klets-momentjes. Ik ben ervan overtuigd dat de docentenrol je op het lijf geschreven is en wens je heel veel plezier in je verdere loopbaan en veel geluk samen met Leanne.

Mellany, van lieve collega tot goede vriendin; je was er voor me. Van onze vitamine D synthese buiten in het zonnetje tijdens een zomerse wandeling in de pauze, fijne gesprekken, gewoon een goeie knuffel op zijn tijd, mooie ervaringen en leuke herinneringen (o.a. de decaan stalken voor een handtekening op formulier 1, Mundial, Linsey, Londen, en het mooiste moet waarschijnlijk nog komen: Costa Rica en een prachtige bruiloft!); het was fijn om dit allemaal te kunnen delen met jou. Ik wens je een voorspoedige afronding van je eigen promotie, een mooie baan en veel geluk voor jou en Niek.

Isja, het was fijn om bijna synchroon te lopen in de afronding. Londen samen met jou en Mellany als beloning voor al het harde werk was echt te gek en hoewel we daar geen promotieoutfits gescoord hebben, weet ik zeker dat je er geweldig zult staan in februari. Ik vind het jammer dat ik er dan niet bij kan zijn. Ik wens je heel veel plezier en succes met je droombaan. De volgende citytrip wordt Kopenhagen?

Naast academische vorming heb ik de afgelopen jaren ook de nodige 'persoonlijke vorming' genoten. De trainingen 'Mastering your Excellence' en 'Mastering your Leadership' hebben daar een groot aandeel in gehad. Ik dank al mijn mede MYE-ers en MYL-ers voor de ervaringen die we gedeeld hebben, jullie openheid en vertrouwen. Het was mij een waar genoegen deze bijzondere ontdekkingsreis met jullie te delen. Ook trainers Nico, Ayala en anderen, thank you for the possibilities you created. In dit rijtje hoort zeker ook Yvonne thuis. Zonder jouw inbreng en betrokkenheid had ik deze prachtige ervaringen nooit opgedaan.

Naast de vele uurtjes in het lab en achter de computer, waren de uurtjes op het volleybalveld over het algemeen een zeer welkome afwisseling. Ik wil al mijn teamgenootjes en trainers/coaches van de afgelopen jaren bedanken voor de welkome ontspanning door inspanning en gezelligheid buiten het veld. Chantal, als Oirschotse 'veteranen' was het fijn om samen met jou de overstap naar Nuenen te maken. Ik hoop nog steeds dat je terugkomt; we kunnen een extra spelverdeler goed gebruiken. Mijn huidige team, Caro, Inge, Linda, Mariska, Marloes, Martine, Merel, Patty, Sanne, Tineke en Eric bedankt ook voor jullie begrip voor de nodige trainingen en zelfs wedstrijden die ik dit

seizoen heb gemist en nog zal gaan missen (na werk volgt vakantie…). Maar wat er ook gebeurt, ik heb er absoluut vertrouwen in dat de beste seizoenshelft nog gaat komen.

Ik wil alle familie, vrienden, kennissen en (over)buren bedanken voor de interesse die jullie getoond hebben in mijn werk.

Stan en Imke, bedankt voor de gezellige (film)avondjes en ski/snowboard (val)partijen. Jullie bruiloft en de jaarwisseling 2012-2013 in Londen waren onvergetelijk. Yvette, dank voor de sportieve, creatieve of culinaire afleiding en uitstekende vakantietips. Ik blijf me erover verbazen hoe we op zoveel vlakken exact dezelfde smaak hebben, behalve als het over muziek en kledingstijl gaat ;)

Oma, Ik heb U veel te weinig gezien, zeker het afgelopen jaar. Gelukkig verleren we het rikken nooit. Ik verheug me erop dat u er de 29e januari bij zult zijn. Astrid en Peter, inspirerend hoe jullie in 100 dagen naar Santiago de Compostella liepen; echte doorzetters en wereldreizigers pur-sang. Ik hoop ooit ook nog eens zoveel van de wereld te zien als jullie.

Mijn lieve broertje en zus; als enige van ons drieën die voor de wetenschap heeft gekozen, ben ik altijd wel een beetje jaloers geweest op jullie creatieve werkzaamheden. Sebastian, ik wens het beste voor je en hoop dat je spoedig daar bent waar je zou willen zijn. Kirsten, wat fijn om een zus te hebben die wel op de hoogte is van de modetrends, weet wanneer er leuke concerten zijn en die verstand heeft van grafische programma's (zonder jouw korte tutorial had het me ongetwijfeld veel meer moeite gekost om de kaft van dit proefschrift in elkaar te zetten). Ik kijk uit naar ons volgende concert of middagje shoppen. Ik wens jou en Marlo veel geluk. En Marlo, sorry, ik moet je teleurstellen; mijn promotie is klaar, maar die nier nog steeds niet. Angela, Dennis en Florian, ook jullie bedankt voor de fijne momenten. Hoe heerlijk is het om met je kleine neefje weer even kind te kunnen zijn! Ik wens jullie veel geluk samen. Carla en Henk, ik kan me geen lievere of meer zorgzame schoonouders wensen en ik kan jullie niet genoeg bedanken voor alles wat jullie voor Michael en mij gedaan hebben de afgelopen jaren! Pap en mam, ik ben dankbaar dat jullie mij alle ruimte hebben gegeven om mezelf te ontwikkelen en mij altijd vrij hebben gelaten om mijn eigen keuzes te maken.

De één na laatste paragraaf is voor jou, Michael. Gedurende de jaren (alweer bijna 13!) hebben we al veel samen meegemaakt en overwonnen. Een promotie kunnen we nu op dat lijstje erbij zetten. Jij hebt me gedurende al die tijd door dik en dun gesteund, soms met een 'schop onder m'n kont', gelukkig vaker een lieve knuffel, maar altijd met precies dat wat ik nodig had. Dank je wel dat je er altijd voor me bent. Ik hou van jou! Nu is het tijd voor ons, om te beginnen met een welverdiende lange vakantie.

Het laatste is misschien wat ongebruikelijk. Wellicht ook doordat het gemakkelijk vergeten of voor lief genomen wordt. Ik wil het, misschien juist daarom ook wel, graag hier benoemen: Ik ben ontzettend dankbaar voor mijn goede gezondheid, lichamelijk en geestelijk, nu en in het verleden, en voor iedere nieuwe dag die nog komen gaat, waardoor ik niet alleen mag dromen, maar ook de kans krijg om mijn dromen waar te maken.

Allemaal bedankt!

Björne